COMPOSITE BEAMS INCORPORATING CELLULAR STEEL FLOOR

by

IVAN WAYNE WALLACE, B.Eng.

A Thesis

submitted to the Faculty of Graduate Studies

in Partial Fulfilment of the Requirements

for the Degree of

Master of Engineering

McMaster University

April, 1969

MASTER OF ENGINEERING (1969) McMASTER UNIVERSITY

(CIVIL ENGINEERING) Hamilton, Ontario

TITLE: Composite Beams Incorporating Cellular Steel Floor

AUTHOR: I. W. Wallace, P.Eng. (McMaster University)

SUPERVISOR: Dr. H. Robinson

Number of Pages: x, 201

SCOPE AND CONTENTS:

This thesis involves the testing and analysing of five full-scale composite beams and sixteen push-out specimens incorporating cellular steel floor. Influence of loss of interaction and other parameters on the elastic and ultimate performance of the beams is studied.

ACKNOWLEDGEMENTS

I would like to thank Dr. H. Robinson for his instruction and guidance during the preparation of this thesis.

Thanks also goes to McMaster University for awarding the teaching assistantship.

Special thanks is due to my wife for her patience.

ABSTRACT

Test results for five full-scale steel-concrete composite beams incorporating cellular steel floor and sixteen push-out specimens are reported. The measured strains and deflections of the beams are compared to those computed assuming complete interaction, to those computed from the C.S.S.B.I. Composite Beam Manual, and to those computed from the A.I.S.C. effective section modulus. The elastic finite difference method is used to analyse the composite beams in the elastic range. The effects of thickness of concrete slab and stud arrangement on composite beam performance are studied. The ultimate flexural capacity of each composite beam is computed on the basis of the inadequate connection model using the average ultimate strengths of the push-out specimens. The computed theoretical ultimate flexural capacity is compared to the measured ultimate moment and reasonable agreement is obtained. The inelastic finite difference method of analysing composite beams through the inelastic region is studied and reported on.

TABLE OF CONTENTS

<u>List of Figures</u>

CHAPTER I

INTRODUCTION

1.1 General

Composite beams have been used in construction for several decades and many research studies have been undertaken on them[17]. Steel-concrete composite beams possess recognized inherent advantages due to the rational disposition of the two materials in respect to their tensile and compressive strength and stability[26]. The steel-concrete composite beam is studied in this report.

Steel-concrete composite beams are composed of a concrete slab and a steel beam, these two components being connected together by means of shear connectors. These shear connectors usually consist of some device welded to the top flange of the steel beam and embedded in the concrete slab. The shear connector can have many forms, but only the stud shear connector is studied in this report.

Conventional steel-concrete composite beams are composed of a solid slab connected to a steel beam. The studs are welded to the steel beam and the slab is cast around and over the headed stud shear connectors. A conventional composite beam is pictured in Fig. 1.1.

In the past decade, a different type of composite beam has become widely used, and is the object of this study. This type of composite beam evolved after the introduction of cellular steel floor to the construction industry. The purposes of the cellular steel floor are to act as "in-situ" formwork for the concrete floor slab, to act as the working surface during construction, and possibly to act as in-floor ducts for mechanical and electrical services. The possibility of obtaining composite action between the cellular steel floor with concrete topping

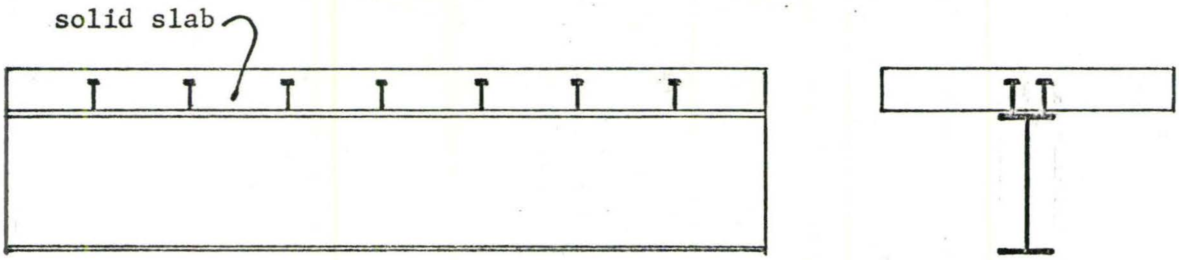

CONVENTIONAL COMPOSITE BEAM

FIG. 1.1

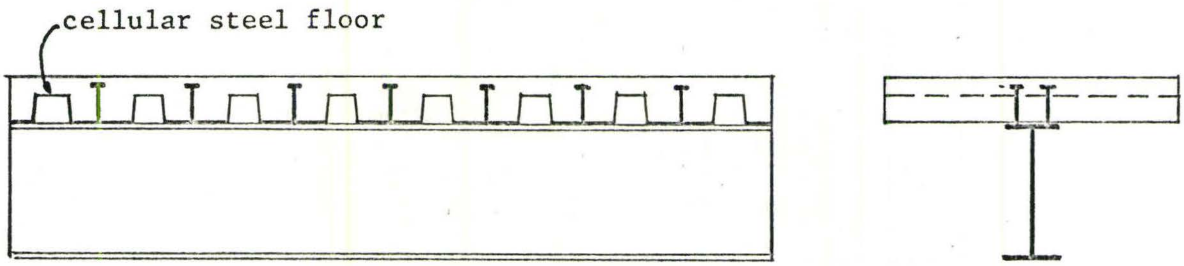

COMPOSITE BEAM INCORPORATING CELLULAR STEEL FLOOR

FIG. 1.2

and the steel beam was suggested[2]. This type of composite beam incorporating cellular steel floor has been studied in subsequent reports (1, 2, 3, 11). Fig. 1.2 shows this type of composite beam.

In this second type of composite beam, the cellular steel floor is laid on top of the steel beams with the cells running transversely to the direction of the span of the steel beams. Headed stud shear connectors may then be welded to the steel beam through the cellular steel floor at points of contact between the upper flange of the steel beam and cellular steel floor. The concrete is then poured on top of the cellular steel floor and around the stud shear connectors. This type of composite beam has a cellular zone between the solid upper part of the slab and the top flange of the steel beam. The cellular zone consists of concrete-filled ribs of the cellular steel floor which may or may not have a stud shear connector embedded in them.

The stud shear connectors extend from the top flange of the steel beam through the concrete-filled rib of the cellular steel floor and into the solid part of the concrete slab above the cellular zone.

The second type of composite beam, described above and pictured in Fig. 1.2, incorporating cellular steel floor and stud shear connectors, is studied in this report.

1.2 Composite Action

Interaction of the concrete slab with the steel beam, under flexural loading, is a function of how the two components are connected together. The connection must resist the shearing force developed along the interface between the slab and beam. The relative horizontal movement between the slab and the beam is called slip. When no slip occurs, the concrete slab and the steel beam are rigidly interconnected and complete interaction is achieved. When the slab and beam are not rigidly interconnected, some slip occurs, and incomplete interaction results.

1.2a Conventional Composite Beams with Solid Slab

Conventional composite beams have a solid slab and no cellular steel floor. Because the shear connection resists slip, it causes a compressive force in the concrete slab and an equal tensile force in the steel beam. This force, called the interaction force because it would not be present if there were no interaction, cannot exceed the sum of the ultimate strengths of the shear connectors. To assure the prevention of premature beam failure due to shear connection failure, the sum of the ultimate strengths of the stud shear connectors must exceed the lesser of A_sF_y (the tensile strength of the steel beam) or $0.85\ f'_c ab$ (the compressive strength of the concrete slab). When the shear connection satisfies this minimum ultimate strength criterion, it is spoken of as an adequate shear connection. An adequate shear connection has enough strength to develop the full steel area in tension or the full concrete area in compression, whichever is least.

For conventional composite beams with adequate shear connection, slip is neglected in their analysis, and a working stress approach based on the transformed section method is applicable [5, 18]. By transforming the area of the concrete slab into an equivalent area of steel, and analysing the beam as if it were composed of only one material, the analysis effectively assumes a rigid shear connection. This assumed rigid shear connection is a good approximation for conventional composite beams[3, 12].

The conventional composite beam with an adequate shear connection has an (idealized) elastic-plastic load-deflection behaviour as indicated in Fig. 1.3. Its elastic load-deflection response is calculated assuming complete interaction. Its ultimate load may be determined from a simplified ultimate stress distribution as outlined in Reference 5.

For a conventional composite beam with an inadequate shear connection, the elastic load-deflection response can be calculated by means of a modified section modulus as proposed for the revised A.I.S.C. code(8), or by more comprehensive methods(9). The ultimate strength of conventional composite beams with an inadequate shear connection can be calculated on the basis of simplified ultimate stress blocks as outlined in Reference 5.

In conclusion, for conventional composite beams with or without adequate shear connection, the design and analysis is specified in structural codes and is reasonably straightforward.

1.2b Composite Beams Incorporating Cellular Steel Floor

Because of the cellular zone separating the solid part of the concrete slab and the upper flange of the steel beam, these beams behave more flexibly than those composite beams having a solid slab. This is because the shear connection is more flexible. Under flexural loading, these composite beams respond with incomplete interaction. Their shear connection is not capable of transmitting as large an interaction force per unit of slip as does the shear connection of a conventional composite beam with the same overall dimensions and connector spacing. The idealized elastic-plastic load-deflection response of a composite beam with incomplete interaction is shown in Fig. 1.3. Fig. 1.3 shows that the idealized elastic load capacity of this type of composite b eam is less than that of the conventional composite beam for the same deflection. For this type of composite beam, Fig. 1.3 shows a lower idealized ultimate strength than the conventional composite beam.

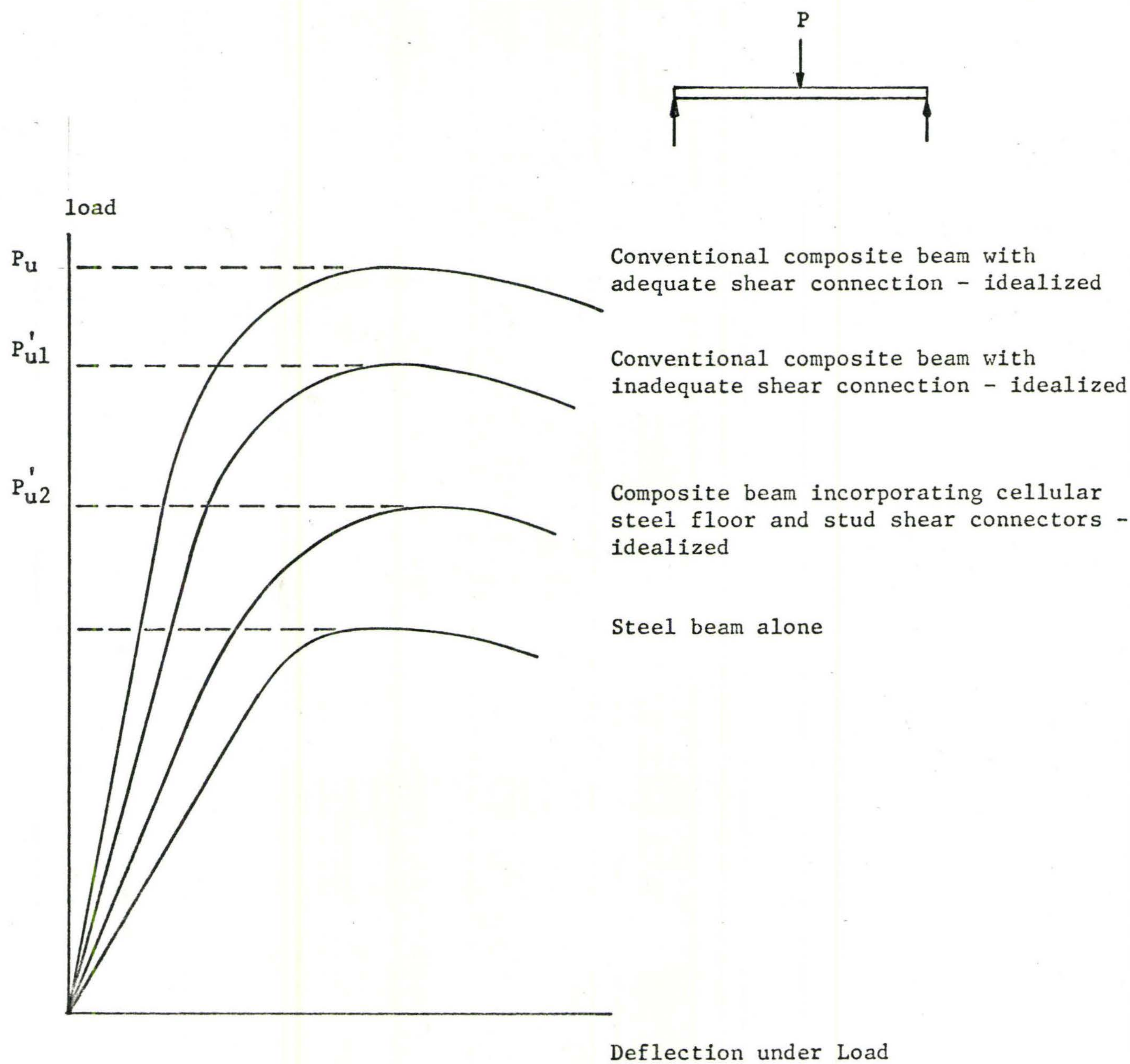

FIG. 1.3

IDEALIZED LOAD-DEFLECTION CURVES

Fig. 1.3 shows that the load-carrying capacity of the conventional composite beam and the composite beam incorporating cellular steel floor is greater than that of the steel beam alone. The load-carrying capacity of the steel beam alone is taken as a reference line because any beam performance over this line reflects the additional contribution of the interaction force on the resisting moment. Clearly, the interaction force, being the compressive force in the slab, cannot exceed the sum of the ultimate strengths of the shear connectors. The ultimate strength of the stud-concrete rib-cellular steel floor shear connection is markedly lower than the ultimate strength of a stud shear connector in a solid slab(2). When the sum of the ultimate strengths of the shear connectors between points of maximum and minimum applied moments is less than either of $0.85f'_c ba$ or $A_s F_y$, the shear connection is spoken of as inadequate.

Composite beams with cellular steel floor and stud shear connectors typically have an inadequate shear connection because the maximum strength of the connections may be much lower than the strength of those in the solid slab.

For instance, a 3/4 in. diameter 3" long steel stud embedded in solid concrete has an ultimate strength of about 2.5 x 11.5 = 28.8 kips(8). The same stud welded through 1-1/2 in. cellular steel floor with concrete topping has an ultimate strength of only 11.3 kips.

The shear connection in composite beams incorporating cellular steel floor may be inadequate for another reason. It may not be possible to place enough shear connectors in the beam because they can only be located in the ribs of the cellular steel floor. In composite beams with a solid slab, the connectors can be spaced very closely.

1.3 Object and Scope

The performance of composite beams incorporating cellular steel floor is markedly different from that of conventional composite beams. No provisions for their design or analysis are incorporated in the North American codes at the time of writing this report. This paper is intended to examine the performance of the composite beam incorporating cellular steel floor and stud shear connectors, and to evaluate the application of some existing theories to their analysis both in the elastic and inelastic ranges.

Since the load-slip relation for the shear connection must be prescribed for theoretical analysis of this type of composite beam, a series of push-out specimens were tested. The construction and testing of these push-out specimens is described in Chapter 2.

The testing and analysis involved the following phases:

1. From push-out tests, the obtaining of representative load-slip relations for the four types of shear connections used in the test beams.

2. The construction of five full-scale composite beams.

3. The testing of these five composite beams, measuring strain, deflection, and slip on each.

4. The comparison of measured performances of the five beams keeping in mind the differences intentionally built into them.

5. The theoretical calculation of the performance of the five beams in the elastic range, using the load-slip relations measured in the push-out tests.

6. The theoretical calculation of the ultimate strengths of the five composite beams tested, using the inadequate connection model of

Reference 5 and using the ultimate strengths of the shear connections from the push-out tests.

7. The theoretical calculation of the complete moment-curvature curve for the five beams tested, following the elastic-plastic extension of the Stüssi finite difference method[9].

Chapter 2 introduces and describes the experimental programme concerned with testing the push-out specimens.

Chapter 3 describes how the beam testing was done, and presents the results of the tests.

Chapter 4 introduces the theoretical methods of analysis and presents the results of the theoretical analyses alongside the measured results both in the elastic range and at the ultimate load.

Chapter 5 describes how the complete moment-curvature curve of a composite beam can be theoretically generated and describes the author's work in this field.

CHAPTER II

PUSH-OUT TESTS

2.1 Introduction

A push-out specimen consists of two concrete slabs and a stub length of steel beam connected together such that each flange of the steel beam abuts one of the largest faces of the slab (see Fig. 2.1). In the tests of this report, the push-out specimens have stud shear connectors welded through cellular steel floor to each flange of the steel beam. A concrete slab is cast around the studs adjacent to each flange of the steel beam. After setting, the two slabs are seated along one edge such that the axis of the steel beam is vertical. By pushing the steel beam out from between the two slabs in a direction parallel to the axis of the steel beam, a shear force is applied to the shear connection on each side of the steel beam. As this shear force is applied, slip develops between the steel beam and the slab. By measuring the applied force and the interfacial slip, a load-slip relation for the particular shear connection can be plotted. This load-slip relation from push-out tests is one measure of the way in which the shear connection will behave in the composite beam.

The load-slip relation is influenced by number and type of shear connectors[4, 12], geometry of ribs[2], strength of concrete[12], flange thickness[12], and length of embedment of the shear connector. The principal variables studied in this report are number of shear connectors in each shear connection, and stud shear connector embedment length.

2.2 Description of Push-Out Specimens

The 16 push-out specimens tested are pictured in Figs. 2.1 and

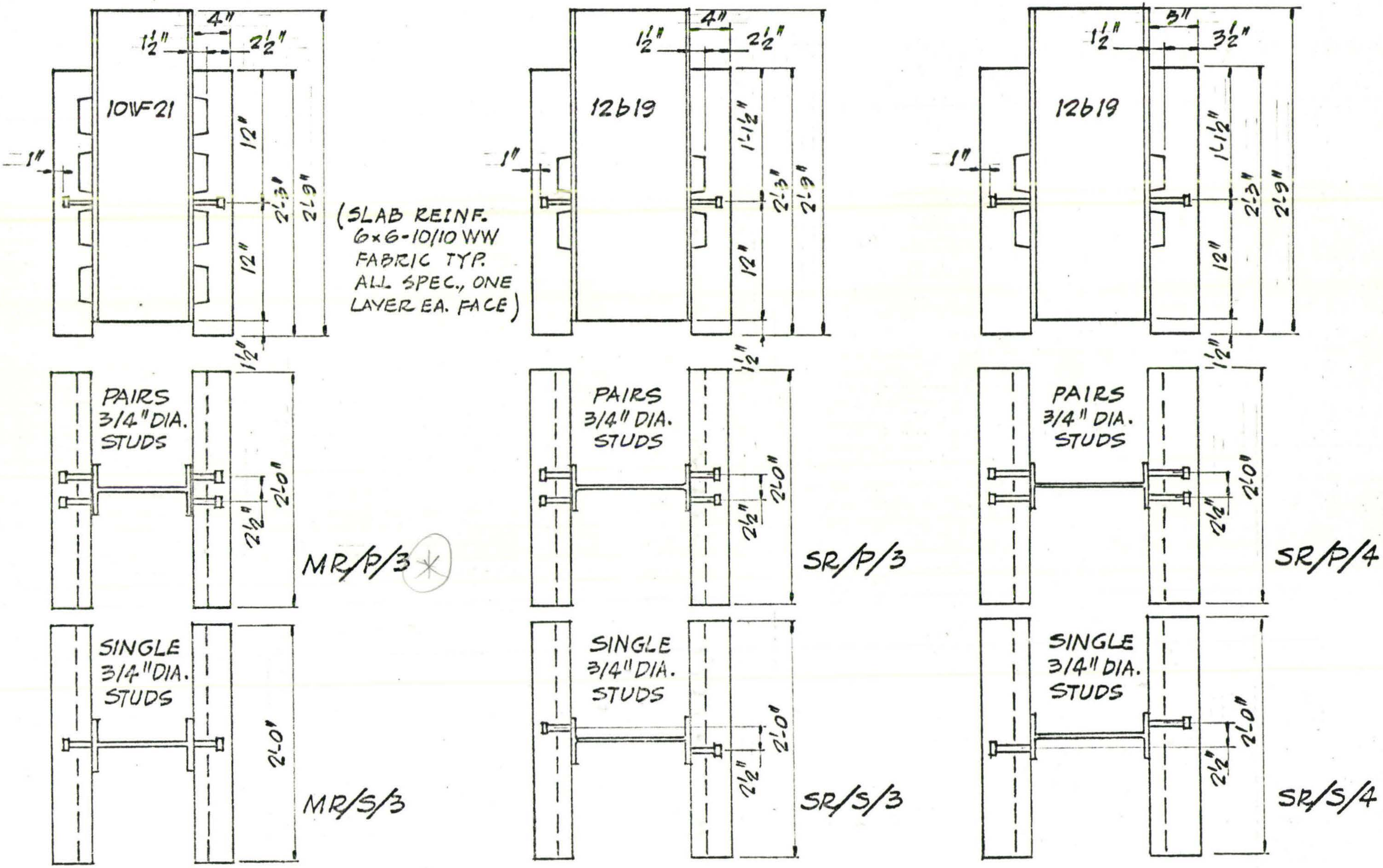

FIG. 2.2

FIG. 2.1

DETAILS OF PUSH-OUT SPECIMENS

2.2. The following items were common to all specimens:

Cellular steel floor; Type T-15, 18 ga., Q-deck

Steel beam ; 12 b 19, or 10WF21

Studs ; 3/4" diameter, steel, 3" and 4" long

Reinforcing for slab; 6 x 6, 10/10 WWF

Twelve specimens incorporated a single rib of the cellular steel floor, while 4 specimens incorporated multiple ribs. In 14 of the specimens, single shear connectors and pairs of shear connectors were offset from the centreline of the flange of the steel beam. In 2 of the specimens, single shear connectors were located directly over the web of the steel beam. The reinforcement of the concrete slabs was the same in all specimens. The concrete strength differed from specimen to specimen, but was not considered as a variable for study.

The 16 push-out specimens incorporated 6 different types of shear connections:

1. Single 3 in. stud on each flange, offset, single rib, 4 in. slab. (3 specimens) SR/S/3

2. Double 3 in. studs on each flange, offset, single rib, 4 in. slab. (3 specimens) SR/P/3

3. Single 4 in. stud on each flange, offset, single rib, 5 in. slab. (3 specimens) SR/S/4

4. Double 4 in. studs on each flange, offset, single rib, 5 in. slab. (3 specimens) SR/P/4

5. Single 3 in. stud on each flange, on centerline, multiple rib, 4 in. slab (2 specimens) MR/S/3

6. Double 3 in. stud on each flange, offset, multiple rib, 4 in. slab. (2 specimens) MR/P/3

The concrete was a commercial "ready-mix" ordered with a maximum aggregate size of 3/4 in. and a nominal 28-day strength of 3,000 p.s.i. The mix was adjusted on delivery to give 1-1/2 in. slump.

The slabs were cast one side at a time, and cylinders from each pour were tested concurrently with the push-outs to determine both the modulus of elasticity and the crushing strength.

Table 2a

Shear Connection Type - See P.12	Crushing Strength Slab I/Slab II	Modulus of Elasticity Slab I/Slab II
1	4290 / 4340	$3.19/3.23 \times 10^6$
2	4290 / 4340	$3.19/3.23 \times 10^6$
3	4050 / 4560	$3.20/3.41 \times 10^6$
4	4050 / 4560	$3.20/3.41 \times 10^6$
5	3350 / 4432	$3.33/3.82 \times 10^6$
6	3350 / 4432	$3.33/3.82 \times 10^6$

2.3 Instrumentation and Testing of Push-Out Specimens

The push-out specimens were instrumented so that the overall slip between the slab and the steel beam, and the applied load, were measured. Fig. 2.3a shows the location of the .0001 in. dial gauges mounted on the first five specimens, while Fig. 2.3b shows those mounted on the remaining 11. The four extra gauges on the first five specimens tested (labelled gauges 1 to 4, Fig. 2.3a) were used to indicate at what load first slip reversal occurred. First slip reversal indicates rotation of the rib of concrete in which the shear connector is embedded. This

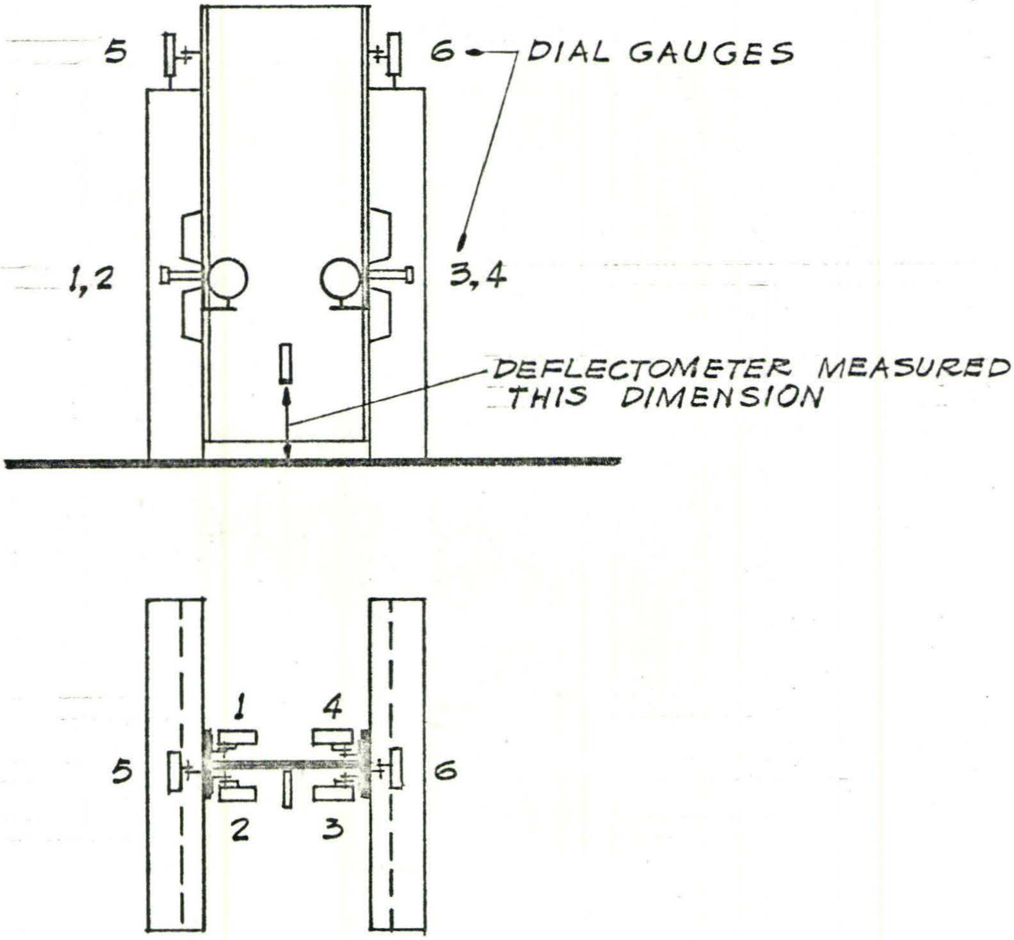

FIG. 2.3. a

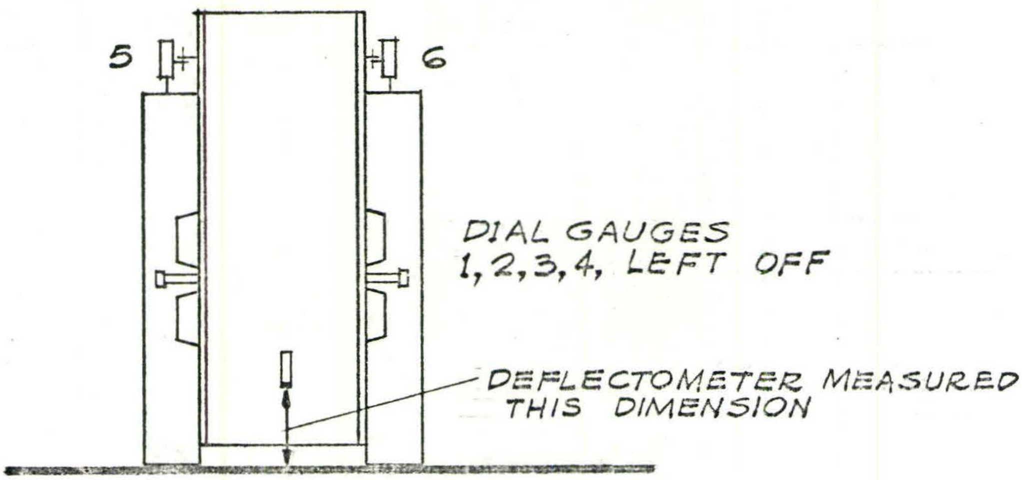

FIG. 2.3. b

rotation shows up on the dial gauges because the indicating angle bracket (see Fig. 2.3a) begins to rotate. When the bracket rotates, it compresses the dial gauge shaft causing a reduction in the reading of the dial gauge. This reduction in the magnitude of slip being recorded on the dial gauge is referred to as slip reversal.

Since the load at first slip reversal was found to be approximately coincident with that load at which sudden jumps of slip appeared on dial gauges 5 and 6 (see Fig. 2.3b), only the latter two were mounted on the remaining 11 specimens.

In addition to the dial gauges, an electronic deflectometer was installed to measure the change in distance between a bracket on the web of the steel beam and the test bed. The bracket was mounted on the centreline of the web so that small rotation of the deformed specimen during the test would not influence the deflectometer reading. The signal from the deflectometer was used as the abcissa drive for a drum plotter, the ordinate being driven mechanically from a load indicator.

The push-out specimens were tested in a 120,000 lb. Tinius-Olsen Universal testing machine. Before testing each specimen, the bond between beam flange and concrete slab was gently broken by jacking the slabs apart.

Load was increased in 2,000 lb. increments up to first cracking, pausing at each increment. Thereafter, the load was increased in finer increments, after a steady state had been reached at each load level.

2.4 Results and Observations

The load-slip curves as measured for each of the 6 shear connection types (see Section 2.2) are presented in Figs. 2.4 to 2.8. Where the curve did not end on the page, an ultimate slip greater than that shown was developed. However, every shear connection reached a maximum statically sustainable load within the extent of each load-slip curve presented in Figs. 2.4 to 2.8.

Each load-slip curve demonstrated that the load on the shear connection increases proportionally with slip up to the first cracking load. This is the load at which the concrete rib containing the shear connector cracks across the root of the rib, leaving the shear connector head embedded in the solid slab. The concrete rib appears to suffer a tensile failure in like manner to the development of a tensile crack at the root of a concrete cantilever (see Fig. 2.9b).

After first rib cracking, a drop in load of 5 to 20 percent occurred. This drop can be easily identified on the load-slip curves. Application of more load from this point of reduced capacity after first rib cracking resulted in increased slip and an increased resistance to slip. The modulus of this increased resistance to slip after first rib cracking was in every case lower than the original load-slip modulus. The ultimate load of each shear connection was reached after slip developed to a magnitude approximately six times that at first rib cracking.

The load-slip curve after first rib cracking is erratic because of the effects of the broken concrete teeth binding between the intact part of the slab and the flange of the steel beam, and because of erratic slipping of the cellular steel floor over the concrete.

A summary of the cracking loads and the ultimate loads is presented in Table 2.b.

Figure 2.9a is a picture of the push-out specimen before testing. Figure 2.9b shows the rib cracks fully developed. Figure 2.9c shows the pattern of slab cracking that developed subsequent to rib cracking.

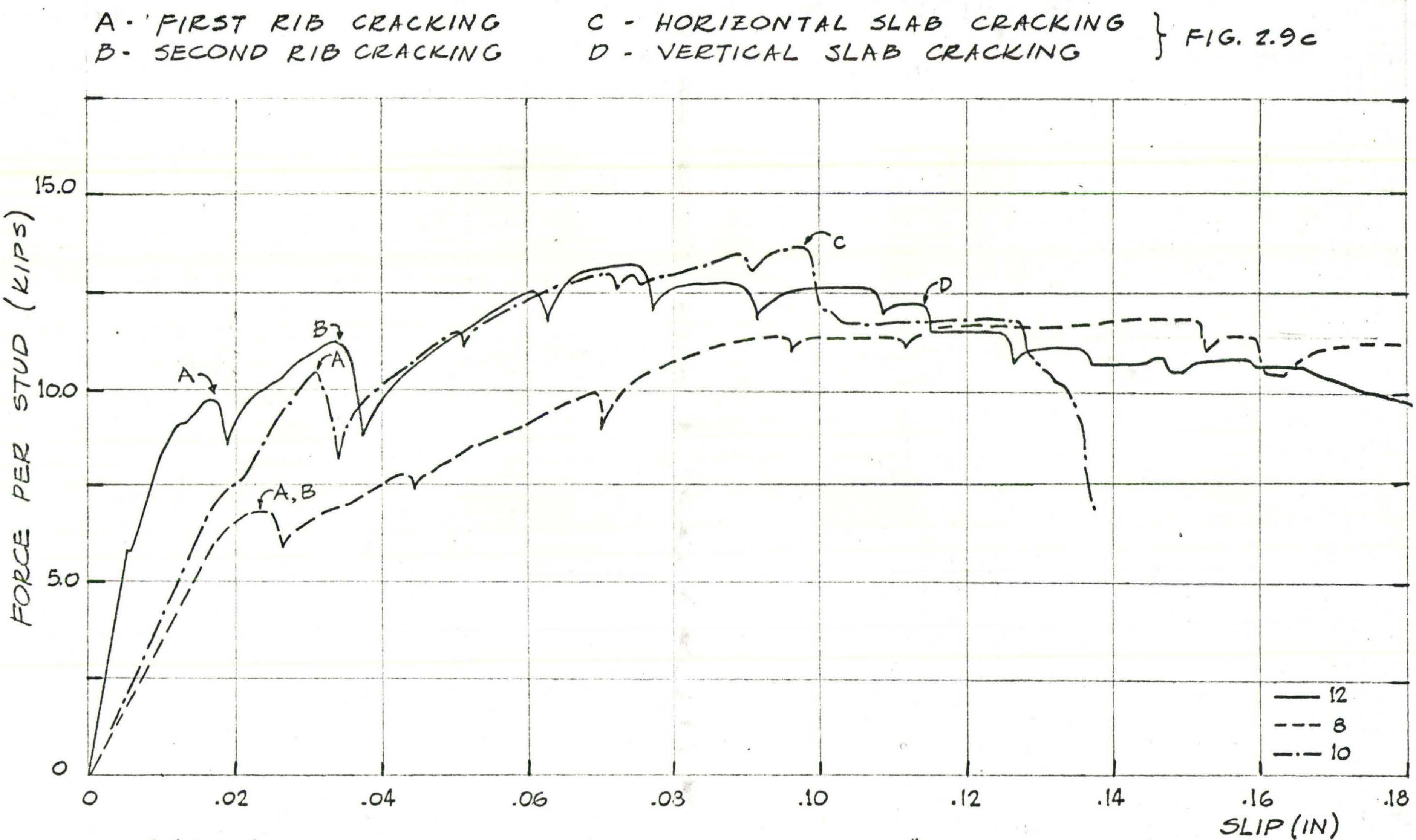

FIG. 2.4 SHEAR FORCE VS SLIP RELATION - 3" SINGLE STUDS SR/S/3

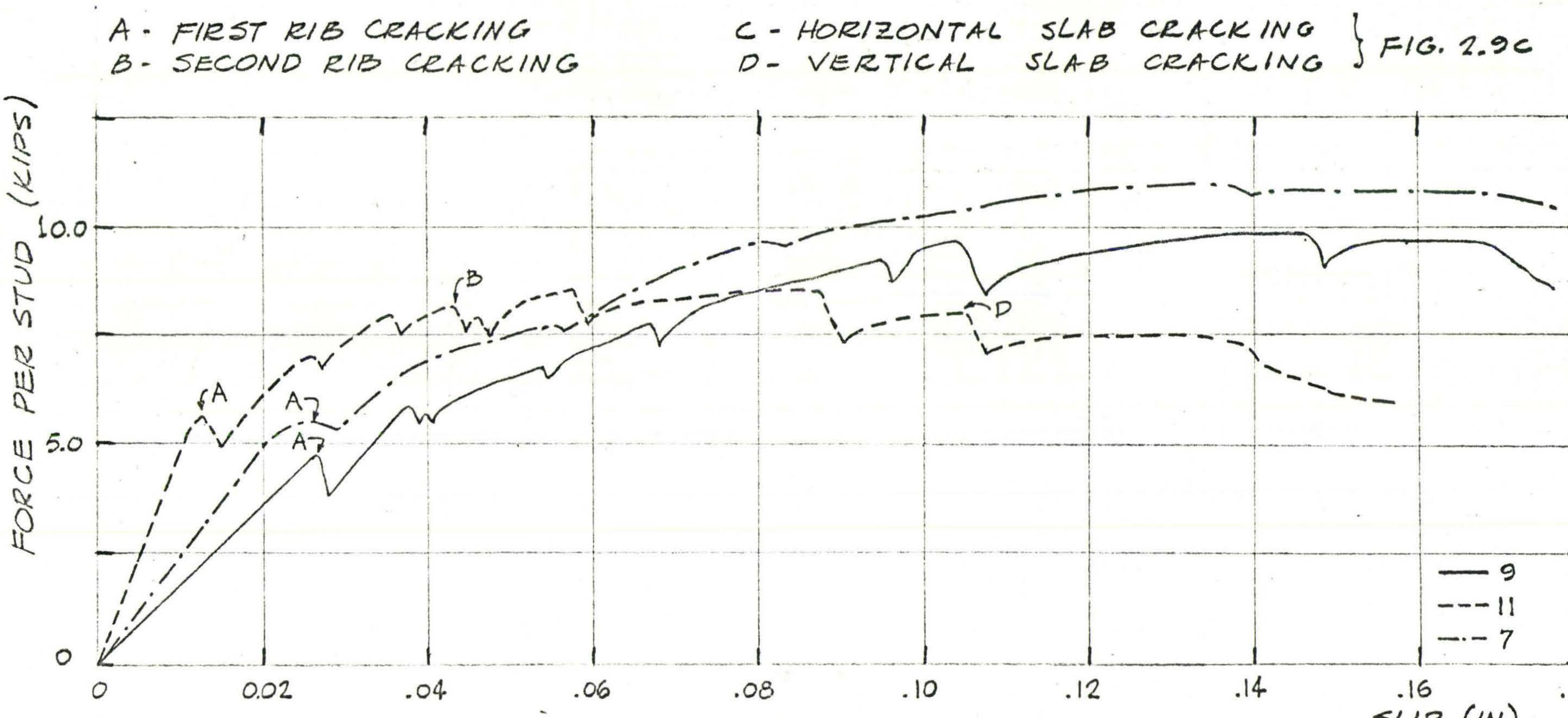

FIG. 2.5 SHEAR FORCE VS. SLIP RELATION - 3' DOUBLE STUDS SR/P/3

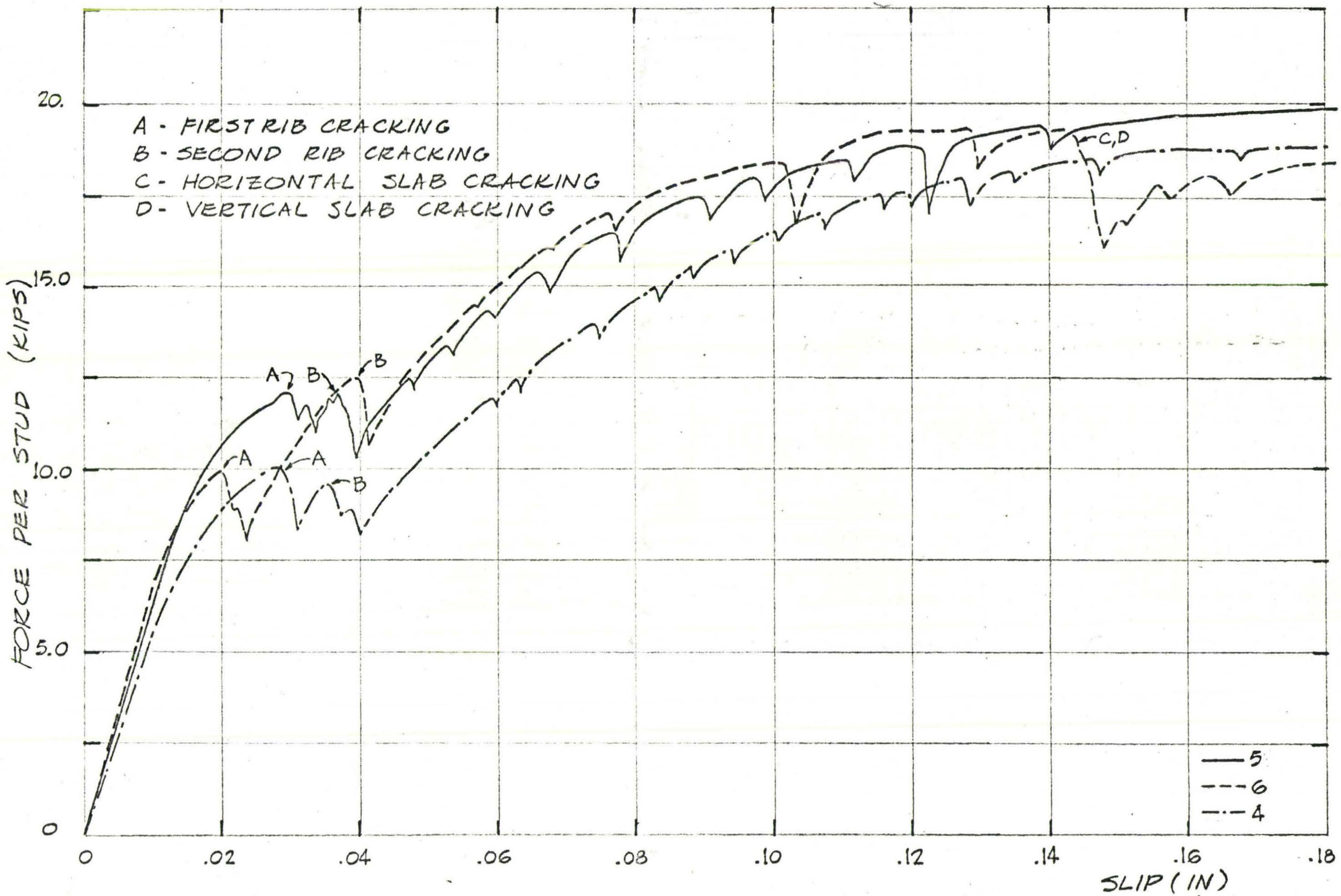

FIG. 2.6 SHEAR FORCE VS. SLIP RELATION - 4" SINGLE STUDS SR/S/4

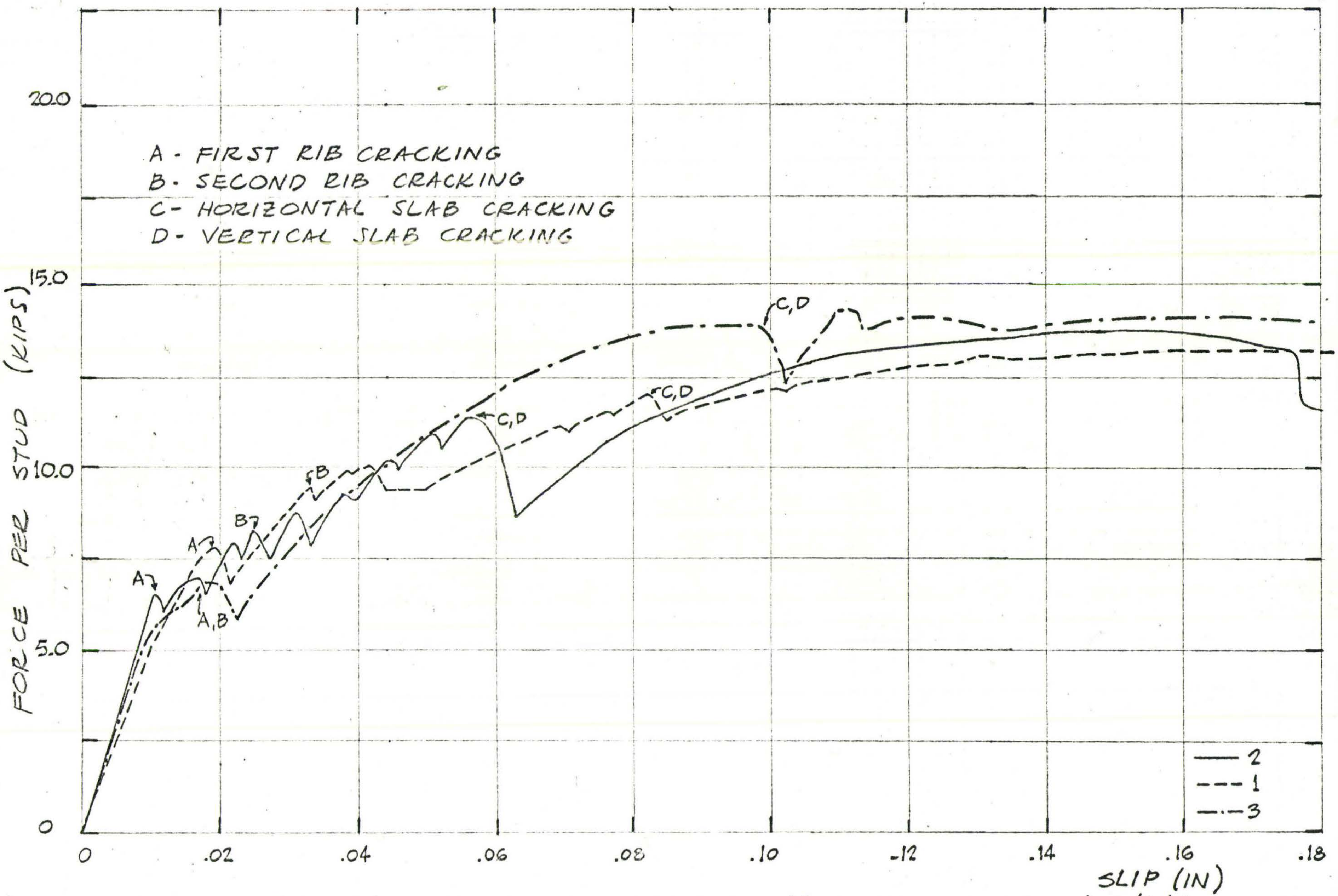

FIG. 2.7 SHEAR FORCE VS. SLIP RELATION - 4" DOUBLE STUDS SR/P/4

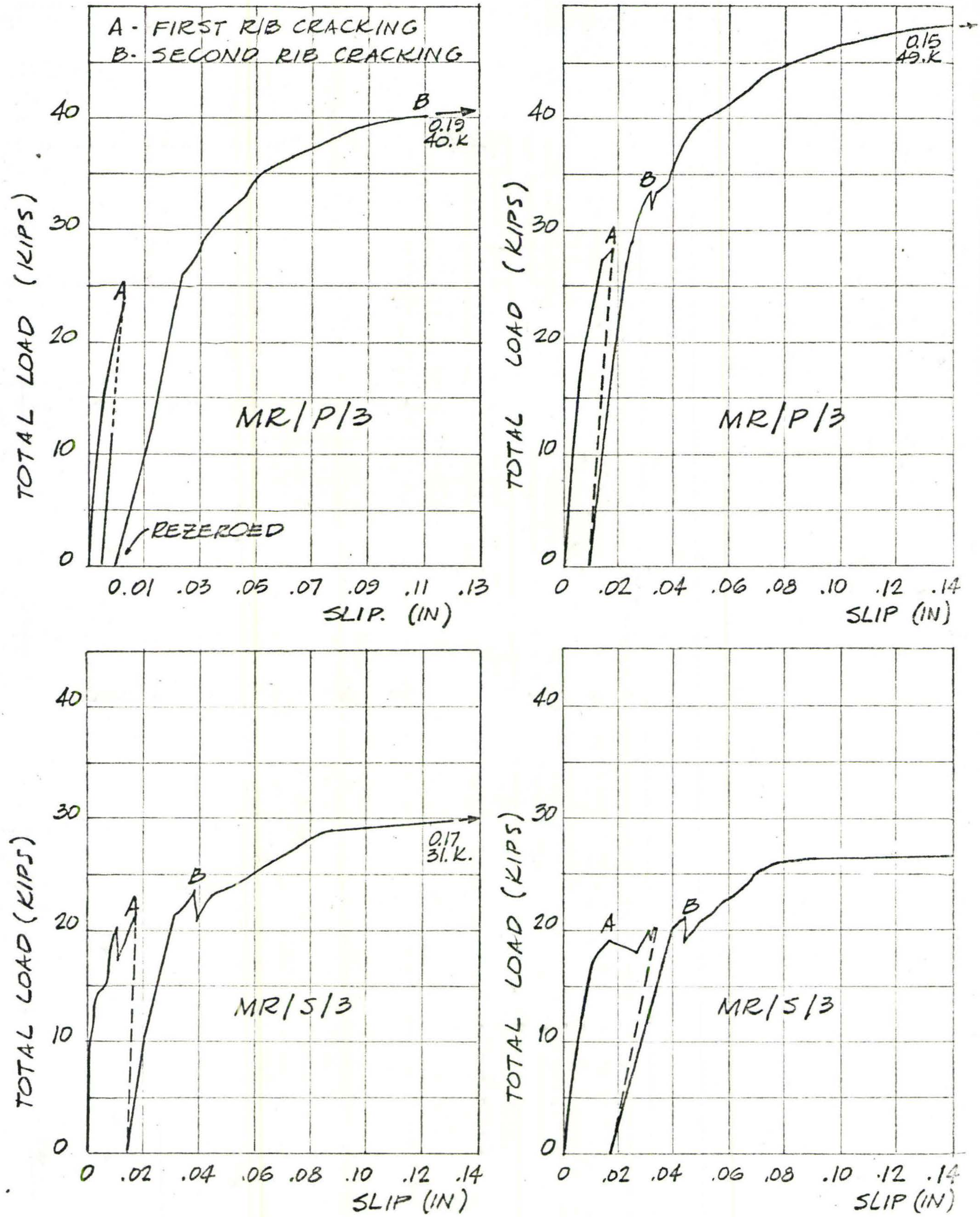

FIG. 2.8 TOTAL LOAD VS. MAXIMUM RECORDED SLIP FOR PUSH-OUT SPECIMENS WITH 3" SINGLE AND DOUBLE STUDS, MULTIPLE RIB

TABLE 2.b SUMMARY OF RESULTS OF PUSH-OUT TESTS

Details of Push-Out Specimens [a]	f'_c p.s.i. Slab I/Slab II	Load at 1st Crack Static Maximum	Maximum Static Load - kips Total	Per Connection	Average per Connection [b]	Ratio of Strength Pairs connectors / Single Connectors
SR/S/3 - OF	4290/4340	0.57	21.0	10.5		
		0.64	24.0	12.0	11.3	
		0.83	23.0	11.5		1.50
SR/P/3 - OF	4290/4340	0.30	40.0	20.0		
		0.74	30.0	15.0	17.0	
		0.59	32.0	16.0		
SR/S/4 - OF	4050/4560	0.57	35.0	17.5		
		0.68	36.0	18.0	17.7	
		0.59	35.0	17.5		1.44
SR/P/4 - OF	4050/4560	0.63	50.0	25.0		
		0.52	52.0	26.0	25.4	
		0.66	50.0	25.0		
MR/S/3 - OC	3350/4432	0.65	31.0	15.5		
		0.68	26.3	13.15	14.3	1.55
MR/P/3 - OF	3350/4432	0.60	40.0	20.0		
		0.57	49.0	24.5	22.2	

[a]MR = Multiple rib; SR = Single rib; P = Pairs of studs; S = Single stud; 3 = 3 in. long studs; 4 = 4 in. long studs; OF = Offset; OC = Over centerline

[b]Connection means overall connection - not individual connectors

2.9a

2.9 b

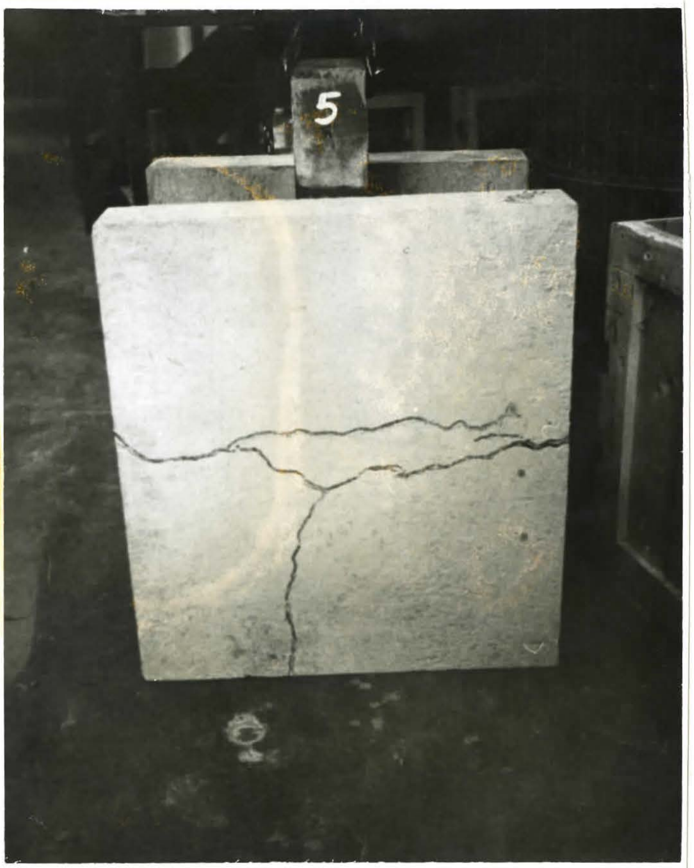

2.9c

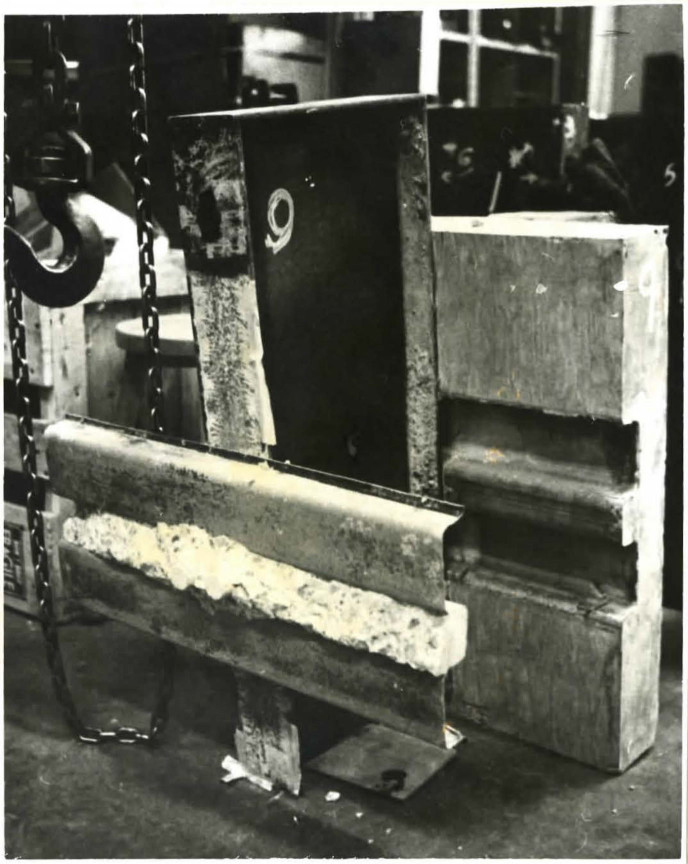

2.9d

FIG. 2.9

Figure 2.9d shows the shear connector pulled out of the concrete slab.

After the ultimate load of the shear connection was reached, the load fell abruptly in the shear connections of the 4 specimens where there was more than one complete rib[4]. In the 12 single rib specimens, the shear connections demonstrated a further ability to sustain load even after the slab had developed the crack pattern of Figure 2.9c. Eight of the 12 tests of single rib specimens were discontinued because of rotation of the steel beam from its originally vertical position due to failure of the shear connection on only one side of the steel beam. Pull-out of the studs from the concrete slab was observed in 3 single rib specimens with 3" studs. One tensile failure of a single 4 in. stud was observed at a slip of 0.90 in.

The load-slip curves of the shear connections incorporating 3 in. studs, both singly and in pairs, showed a greater variation from test to test than did the load-slip curves of the shear connections incorporating 4 in. studs. This is evidently due to the longer embedment length of the 4 in. studs and their greater subsequent dependence on the more uniform tensile properties of the steel stud rather than on the more predictable shear strength of the concrete slab.

Comparing the average static ultimate load for pairs of connectors with that of single connectors from Table 2.b shows that the performance of the connection with pairs of connectors is from 1.44 to 1.56 times that of the connection with single connectors. Therefore, two connectors only develop 1.5 times the ultimate shear resistance of a single connector, for 3/4 in. diameter stud shear connectors spaced laterally at 2-1/2 in. on centre.

The first cracking load from Table 2.b can be compared to the maximum load developed on the shear connection. If the lowest and highest ratios are discarded as being unrepresentative extremes, then the first cracking load is from a minimum of 0.57 to a maximum of 0.74 of the ultimate load.

The increase in load after first cracking was in every case more for pairs of connectors than for singles. The ratio of increase in load after first cracking for pairs of connectors to that for single connectors is:

(a) 2.04 for the multiple rib specimens, 3 in. studs

(b) 1.50 for the single rib specimens, 4 in. studs

(c) 1.20 for the single rib specimens, 3 in. studs.

CHAPTER III

COMPOSITE BEAM TESTS

3.1 Introduction

Five full-scale composite beams incorporating cellular steel floor and stud shear connectors were tested. The principal variables studied were number and arrangement of shear connectors in the shear span (see Fig. 3.1), and embedment length of shear connectors. The slab width and reinforcement, and the beam span and loading were kept constant for all five beams. The slab depth, and number, arrangement and length of shear connectors were varied. The concrete strength varied from beam to beam because separate pours were required, but concrete strength was not a variable for study.

Two types of cellular steel floor were used: 1-1/2" deep rib without bottom cover sheet, and 1-1/2" deep rib with bottom cover sheet (see Fig. 3.1a). The first three beams used only the cellular steel floor without a bottom cover sheet. The last two beams used a blend of the two types of steel floor. Alternate 24" widths of the cellular steel floor on the last two beams had a bottom cover sheet. Since the stud shear connectors were to be welded through the cellular steel floor on all beams, it was not possible to place studs at locations on the last two beams where there was cellular steel floor with bottom cover sheet. This is because it is only possible to weld through the cellular steel floor where the total thickness of metal does not exceed that of 18 ga. material.

The first three beams are detailed in Fig. 3.1 and incorporate one type of cellular steel floor uniformly over their lengths. Six, 9 and 12 studs respectively were evenly spaced throughout their shear spans.

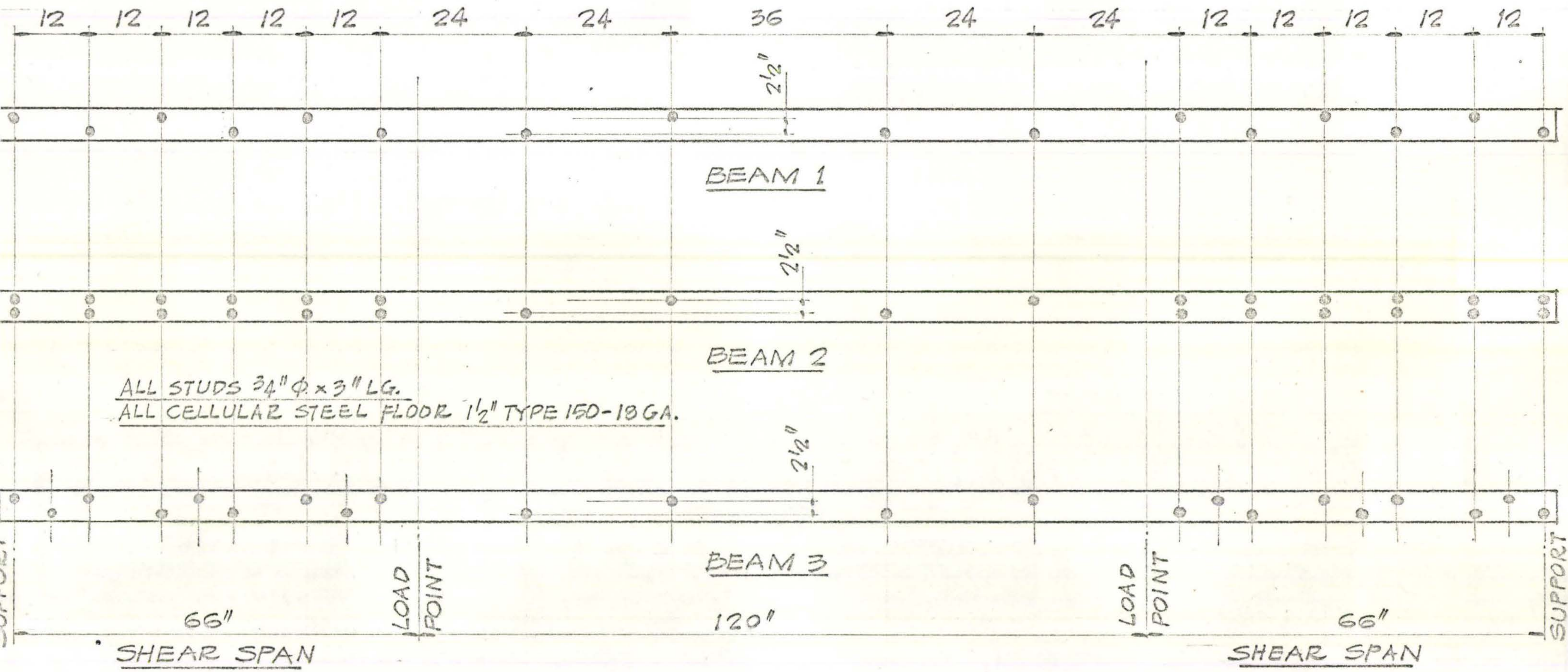

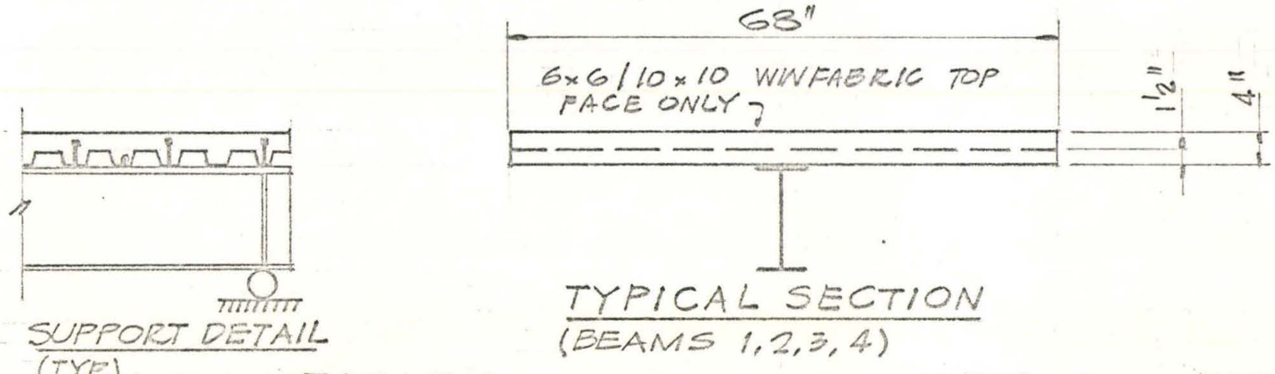

FIG. 3.1
(BEAMS 1, 2, 3)

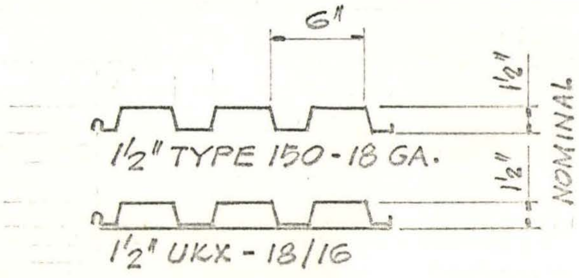

FIG. 3.1a

27

Three in. long studs and a 4 in. deep slab were used in the first three beams. These three beams had a total of 16, 22, and 28 studs respectively, and were identical except for the number of studs in their shear spans.

The fourth and fifth beams tested (Fig. 3.2) both had 12 stud shear connectors in the shear span, and incorporated the blend of two types of cellular steel floor explained above. In both of the beams, the 12 studs in the shear span are situated in two groups of six, separated by a gap of 36 in. where there are no studs. As explained above, the gap of 36 in. between studs in the shear span was necessitated by the presence of a width of cellular steel floor with bottom cover sheet, through which no studs could be welded. The fourth and fifth beams had a total of 30 studs in each. The studs of beam 4 were 3 in. long and the slab was 4 in. thick. The studs of beam 5 were 4 in. long and the slab was 5 in. thick.

The five beams designed in the manner described above permit comparisons to be made between them. The first three beams, because they are identical except for the number of studs, can be compared to show the influence of number of studs. Comparison of beams 2 (12 studs evenly spaced) and 4 (12 studs, groups of 6) is intended to show how large connector intervals affect beam performance. Comparison of beams 4 (4 in. slab) and 5 (5 in. slab) is intended to show how slab depth/stud embedment influences beam behaviour.

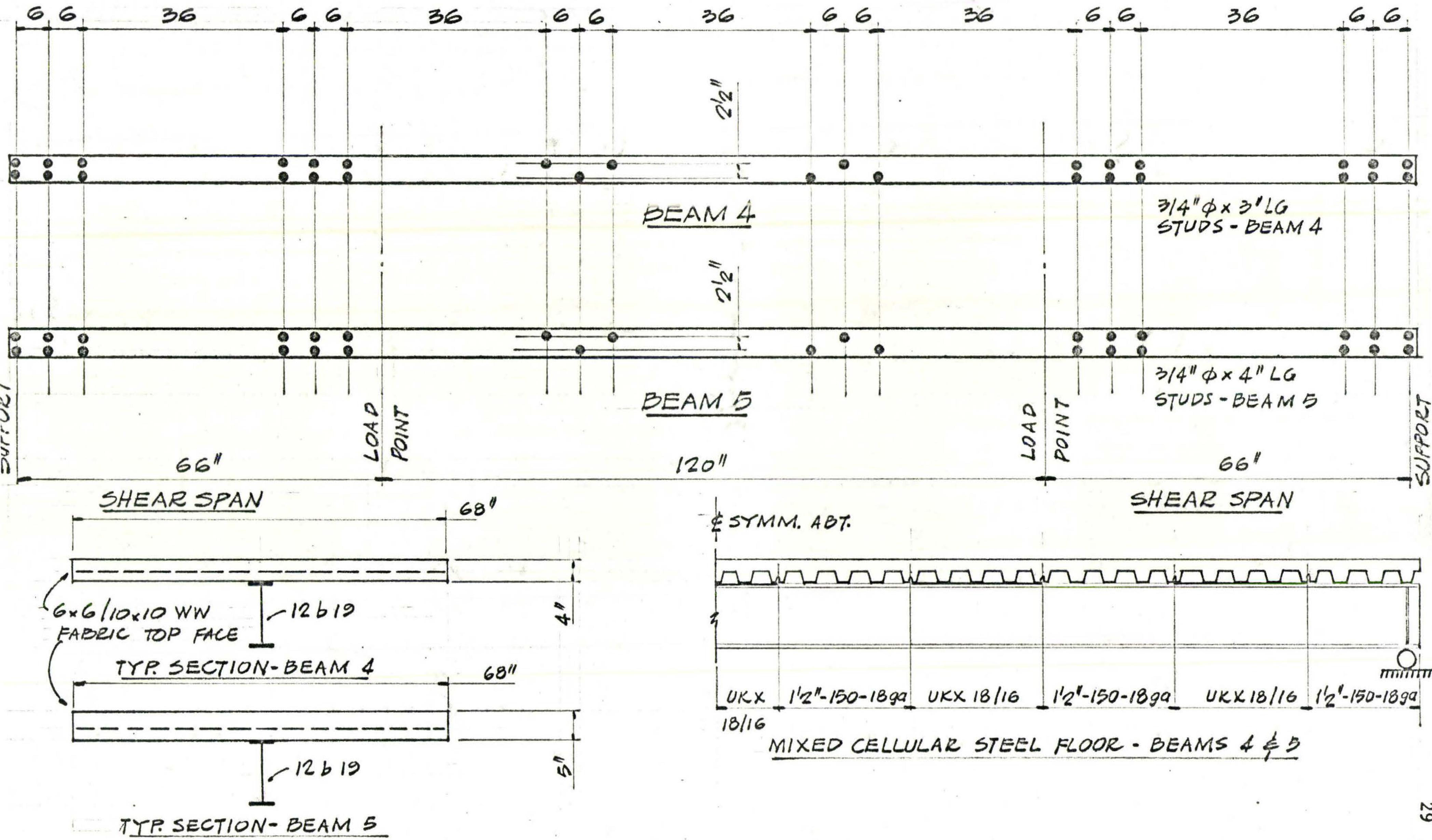

DESCRIPTION OF BEAMS 4, 5

FIG. 3.2

3.2 Description of Specimens and Materials

The five composite beams with cellular steel floor were fabricated by aligning the deck pieces on the steel beam and securing them in place by temporary templates along the underside of the top flanges of the steel beam. The studs were then welded through the deck, and plywood formwork for the concrete slab set in place and secured by tie-rods through the open cells above the steel beam.

Prior to casting the slabs, the partially fabricated assemblies were tilted up on one edge, after which the surfaces of the steel beams were prepared for strain gauging. After the strain gauges were applied and lead wires connected, the beams were lowered flat again, the reinforcing mesh was set in place, and the slabs were cast. Curing for seven days under wet burlap and plastic sheeting followed.

The fabricated properties of the composite beams are listed in Table 3.a.

Table 3.a

Composite Beam No.:		1	2	3	4	5
Deck Used:		Ribbed	Ribbed	Ribbed	Rib/Cell	Rib/Cell
Studs	No. Tot.	16	28	22	30	30
	Shear Sp.	6	12	9	12	12
	Tensile	68,000	68,000	68,000	68,000	68,000
	Length	3"	3"	3"	3"	4"
Steel Beam	Designation	12B19	12B19	12B19	12B19	12B19
	F_y (FLG)	41.6	41.6	40.7	40.7	40.7
	F_y Web	46.7	46.7	46.3	46.3	46.3
Conc. Slab	Dimensions o/A	68 x 4	68 x 4	68 x 4	68 x 4	68 x 5
	f'c	4290	5670	5670	3890	3890

3.3 Instrumentation

The beams were instrumented to measure the following parameters:

1. load applied,
2. deflection,
3. slip between slab and steel beam, and
4. strains over the entire cross-section.

Fig. 3.3 to 3.5 detail the position of strain gauges and slip gauges. From 34 to 49 electric resistance foil strain gauges, each 1/4 in. long, were used on the steel surface of each composite beam. From 1 to 15 paper-backed electric resistance filament strain gauges with 6" gauge lengths were applied to the concrete top surface. The strain gauges were located so as to:

1. measure the strain across the depth of the steel beam midway between studs,

2. measure the complete strain profile of the full composite beam including slab at each load point and at mid-span.

Strain on the steel beam was measured and recorded by a DATRAN automatic digital recorder, typically at the rate of about 3 seconds per gauge. The strain gauges on the concrete were read on a PICO manual strain indicator via a manual switching box.

The load was applied by means of one 100,000 lb. hydraulic ram through a load cell and spreader beam to two point loads located 66 in. from each support. The load cell was connected to a digital-display electronic voltmeter through circuitry that allowed the voltmeter to read 1 millivolt per 10 lb. applied load.

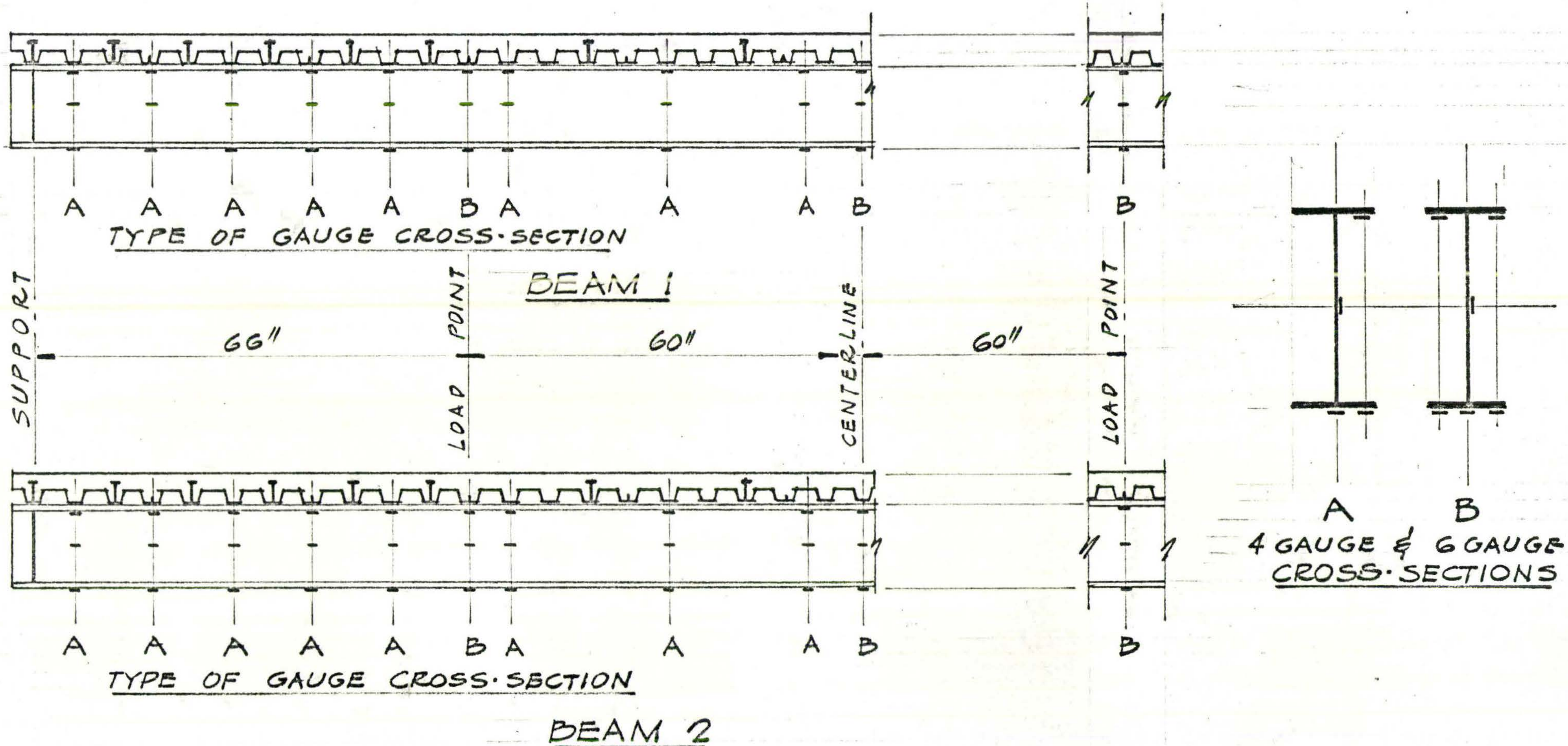

LOCATION OF STRAIN GAUGES

BEAMS 1 & 2

FIG. 3.3

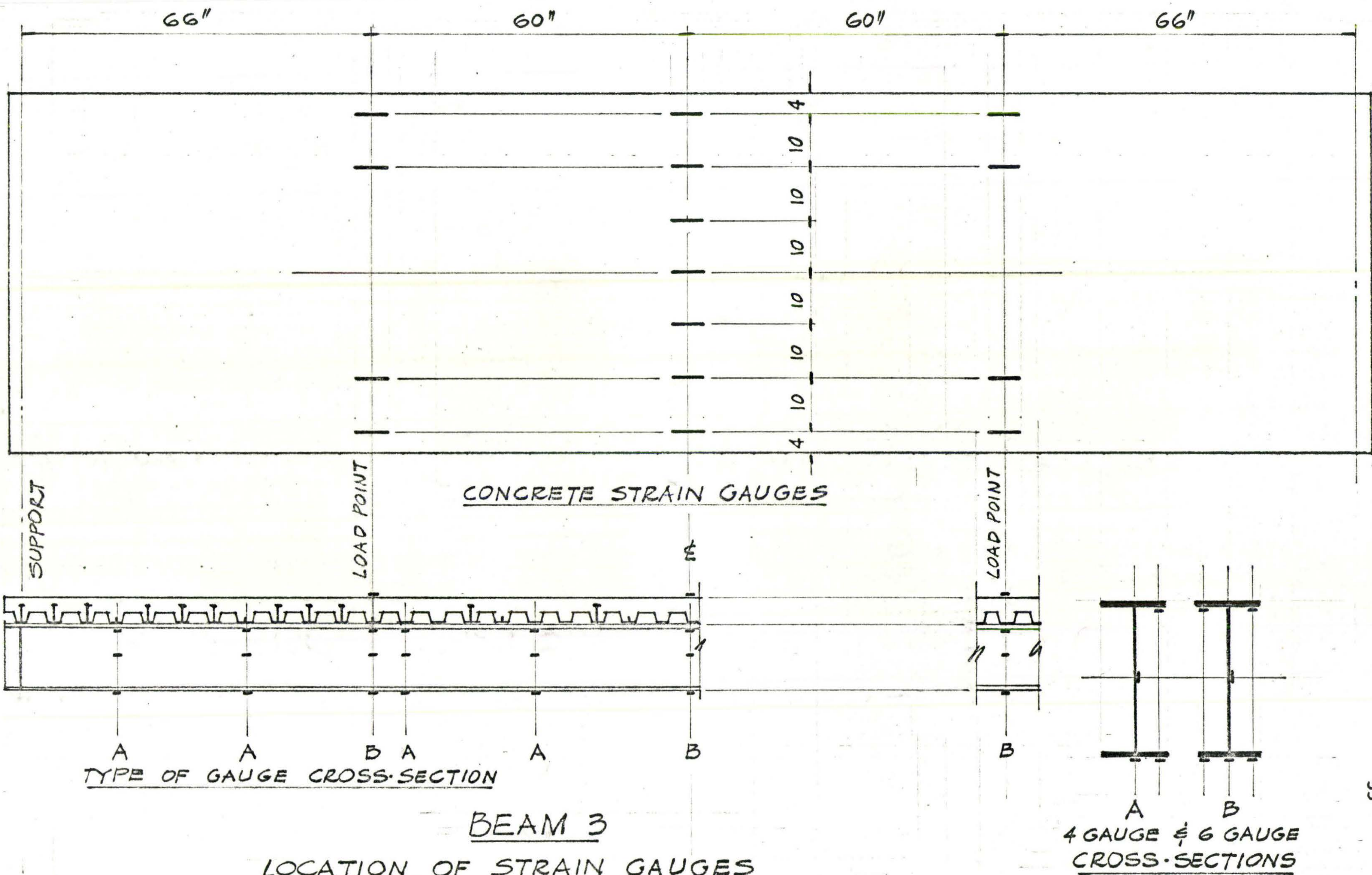

BEAM 3

LOCATION OF STRAIN GAUGES

FIG. 3.4

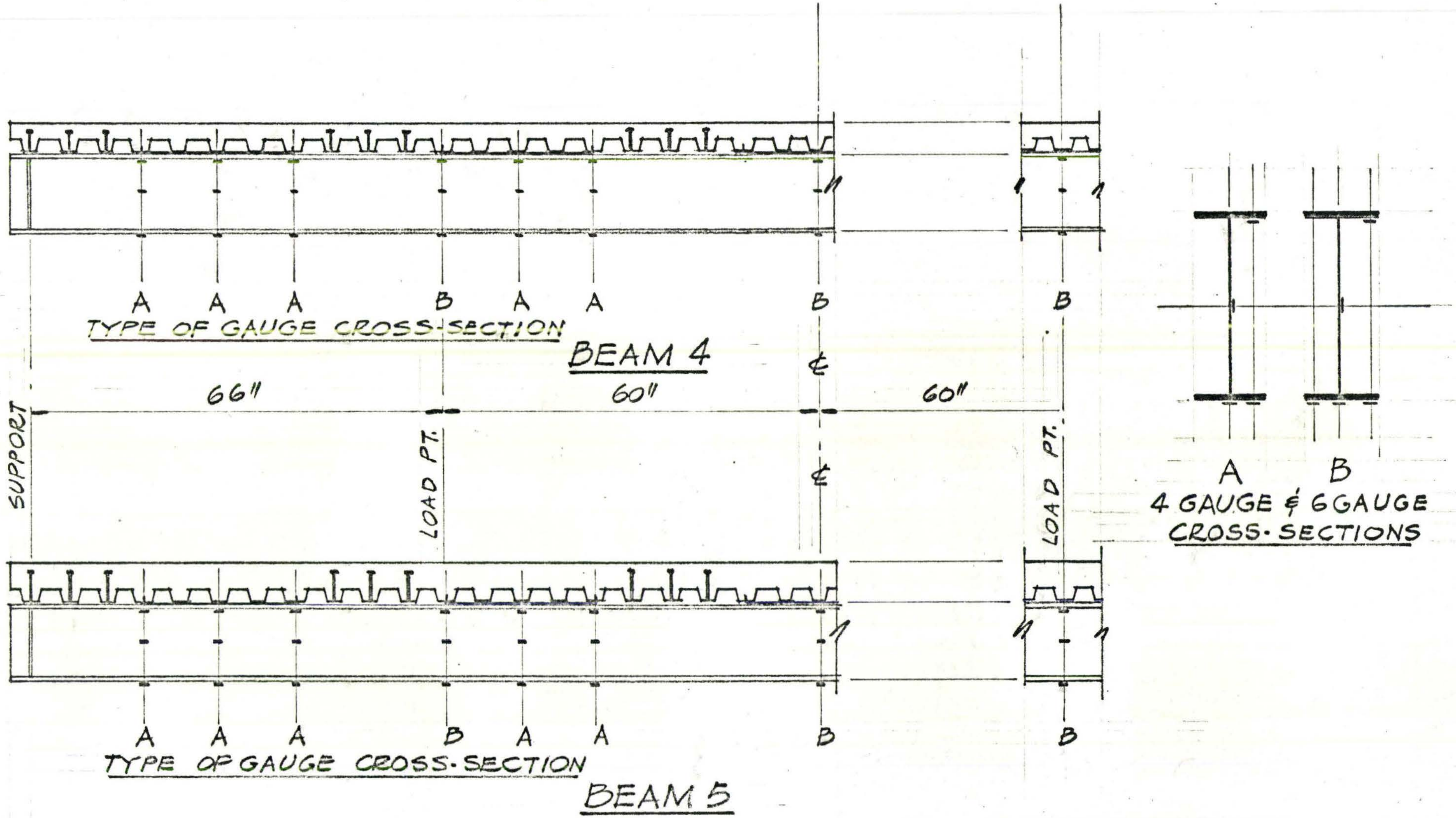

LOCATION OF STRAIN GAUGES

BEAMS 4 & 5

FIG. 3.5

3.4 Test Procedure

Testing the five full-scale composite beams incorporated two phases:

Phase One - Dead load and shrinkage strains were measured in the steel beam while the slab was being poured and then as it was curing.

Phase Two - Live load was applied to the beams, and load, deflection, slip and strain were measured.

For Phase One of the beam test programme, the strain gauges on the steel beam at mid-span were monitored and read before casting the slab, immediately after casting the slab, and then daily subsequent to that. As the concrete cured and shrinkage occurred, the strains in the steel beam were seen to change (see Table 3.b).

Phase Two of the test programme began with lifting the beam into the loading frame. The load was applied by means of one 100,000 lb. hydraulic ram through a load cell and spreader beam to two point loads located 66 in. from each support.

Fig. 3.6 shows the loading frame, the single hydraulic ram, the load cell directly beneath it, and the spreader beam which bears on two points on the top surface of the composite beam. A schematic diagram of the two-point loading arrangement is shown in Fig. 3.6.

The strain recording instrument that had been used to measure dead load and shrinkage strains was re-zeroed before any live load was applied. Load was applied in 2,000 lb. increments while a graphical check was maintained on increasing strains and deflections at mid-span and at the load points. Subsequent to the onset of yielding on the bottom flange, the beam was allowed to relax to a steady state capacity

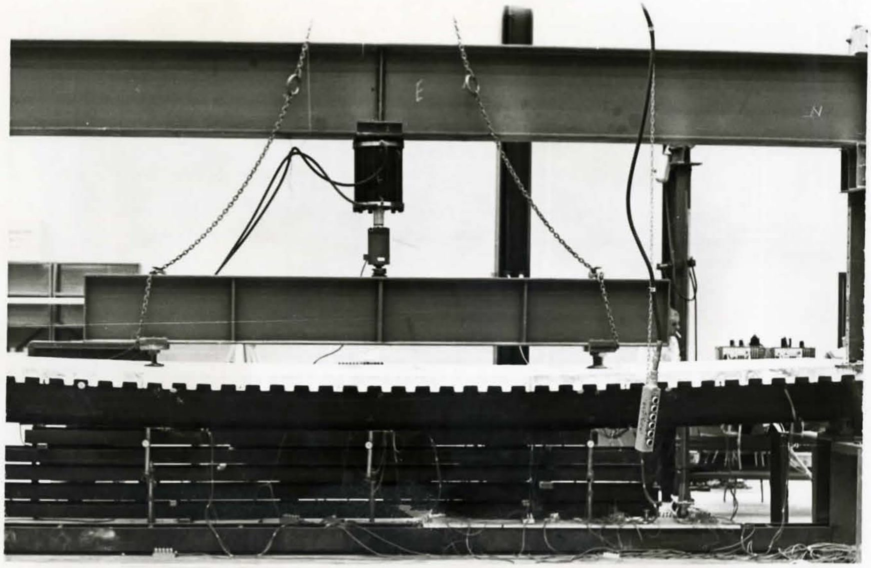

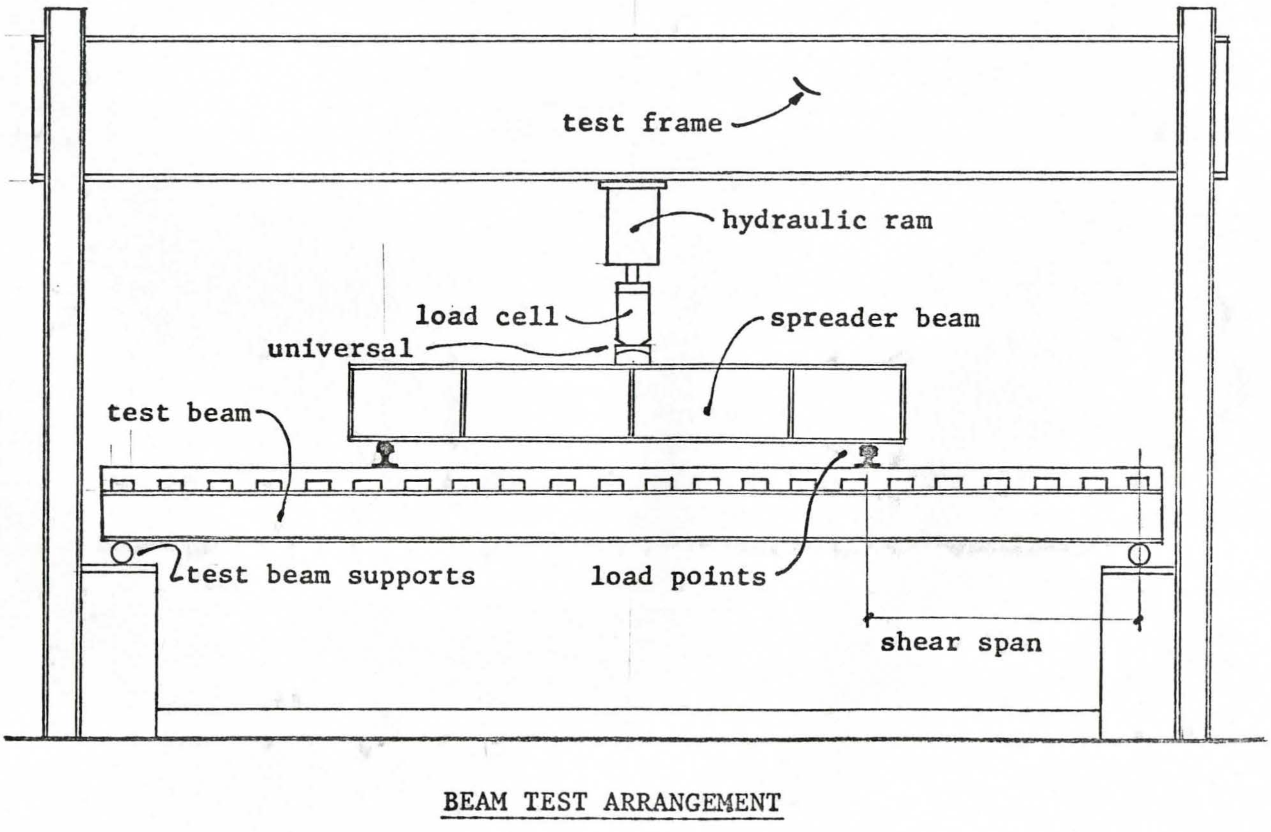

BEAM TEST ARRANGEMENT

Fig. 3.6

before each new load increment was applied. No cycling of the load was carried out intentionally.

After the beam was well into the yield region, loading was controlled by increments in deflection. Testing was discontinued when the deformation resulted in complete collapse or when it became apparent that further deformation presented too great a hazard to personnel. For all five beams, the test continued until at least several points on the falling branch of the load-deflection curve were obtained.

3.5 Results and Observations

In Phase One of the beam testing programme, mid-span strains were monitored before and after pouring of the slab, and during slab curing.

The dead load and shrinkage strains are presented in Table 3.b. In the same table, the strain difference over the depth of the steel beam is listed as a measure of curvature. The curvature is seen to decrease during wet curing, only to increase again during the drying out and shrinking of the slab. By subtracting these dead load and shrinkage-induced strains from the nominal yield strain, a strain difference available for live load is arrived at.

The bottom fibre strains are seen from Table 3.b to increase in tension as curing progressed, narrowing the strain difference between dead load strain and yield. The bottom fibre strain of beam No. 1 increased from +220 micro-inches under the dead load of the wet concrete to +324 micro-inches after 41 days of curing, during which time no live load was applied. This increase of 104 micro-inches is significant when compared to a total allowable strain difference between no load and allowable load of F_y/E = 1,300 micro-inches.

TABLE 3.b

Strains in Steel Beams Due to Dead Load of Wet Concrete and While Concrete is Hardening/Shrinking

BEAM NO.	STRAIN GAUGE	TOTAL DAYS ELAPSED 0 AFTER POURING	7 PLUS 7 DAYS WET CURING	14 PLUS 7 DAYS DRY CURING	41 PLUS 27 DAYS DRY CURING
1	Top	-202	- 81	-103	-182
	Bottom	+220	+263	+281	+324
	Diff.	422	334	384	506
2	Top	-218	-174	-219	n.a.
	Bottom	+242	+275	+305	
	Diff.	460	449	524	
3	Top	-222	-121	-171	n.a.
	Bottom	+239	+357	+388	
	Diff.	461	478	559	
4	Top	-183	-143	n.a.	n.a.
	Bottom	+219	+222		
	Diff.	402	365		
5	Top	-273	-245	n.a.	n.a.
	Bottom	+307	+317		
	Diff.	580	562		

n.a. - not available

Note: Top strains are averaged from two gauges, bottom strains from three gauges, located as shown. Gauges are at mid-span.

In Phase Two of the beam testing programme, applied load, deflection, slip and strains were measured as a two-point live load was applied to the beams. The deflection, slip and bottom and top fibre strains are plotted as functions of position on the beam and applied load in Figs. 3.7 to 3.17. The moment-curvature curves are shown in Fig. 3.18, and the strains across the top surface of the slab of beam 3 are shown in Fig. 3.19.

As explained earlier, the live load was applied by means of a single loading ram acting at the centre of a spreader beam (see Fig. 3.6) which was supported on the top of the test beam at two points. Therefore, the test beam was not forced to deflect equally at the load points, and as a result one load point tended to deflect more than the other. This is the reason that the measured slips and strains plotted in Figs. 3.8 to 3.17 are not symmetrical about the mid-span of the beams.

Fig. 3.7

Mid-Span Deflection as a Function of Total Applied Load - Beams 1 to 5

Beam 1 exhibits a lower load-deflection curve than do the other four beams. Beam 5 exhibits a higher load-deflection curve than do the other four beams. The load-deflection curves for beams 2, 3 and 4 are very close together up to a deflection of 4 in. The shear connection and slab dimensions are as follows for the five beams:

Beam 1: 6-3" single studs in each shear span, 68" x 4" slab

Beam 2: 12-3" studs in pairs in each shear span, 68" x 4" slab

Beam 3: 9-3" single studs in each shear span, 68" x 4" slab

Beam 4: 12-3" studs in two groups of three pairs in each shear span, 68" x 4" slab

Beam 5: 12-4" studs in two groups of three pairs in each shear span, 68" x 5" slab.

Each beam deflected elastically up to a certain load, after which the deflection increased in a smooth curvilinear manner up to the ultimate load of the beam. At the ultimate load, the deflection increased without any increase in load. For beams 1, 2 and 4, this load-deflection plateau lasted through approximately 2 in. of vertical deflection. Beams 3 and 5 did not exhibit any significant post-ultimate load-deflection plateau, but instead began to unload immediately after the ultimate load had been attained.

The unloading of each beam was gradual and no severe or sudden increases in deflection were observed. Except for the test of beam 3, the tests were eventually discontinued because of instability of the loading apparatus, not because of complete breakdown of the beam.

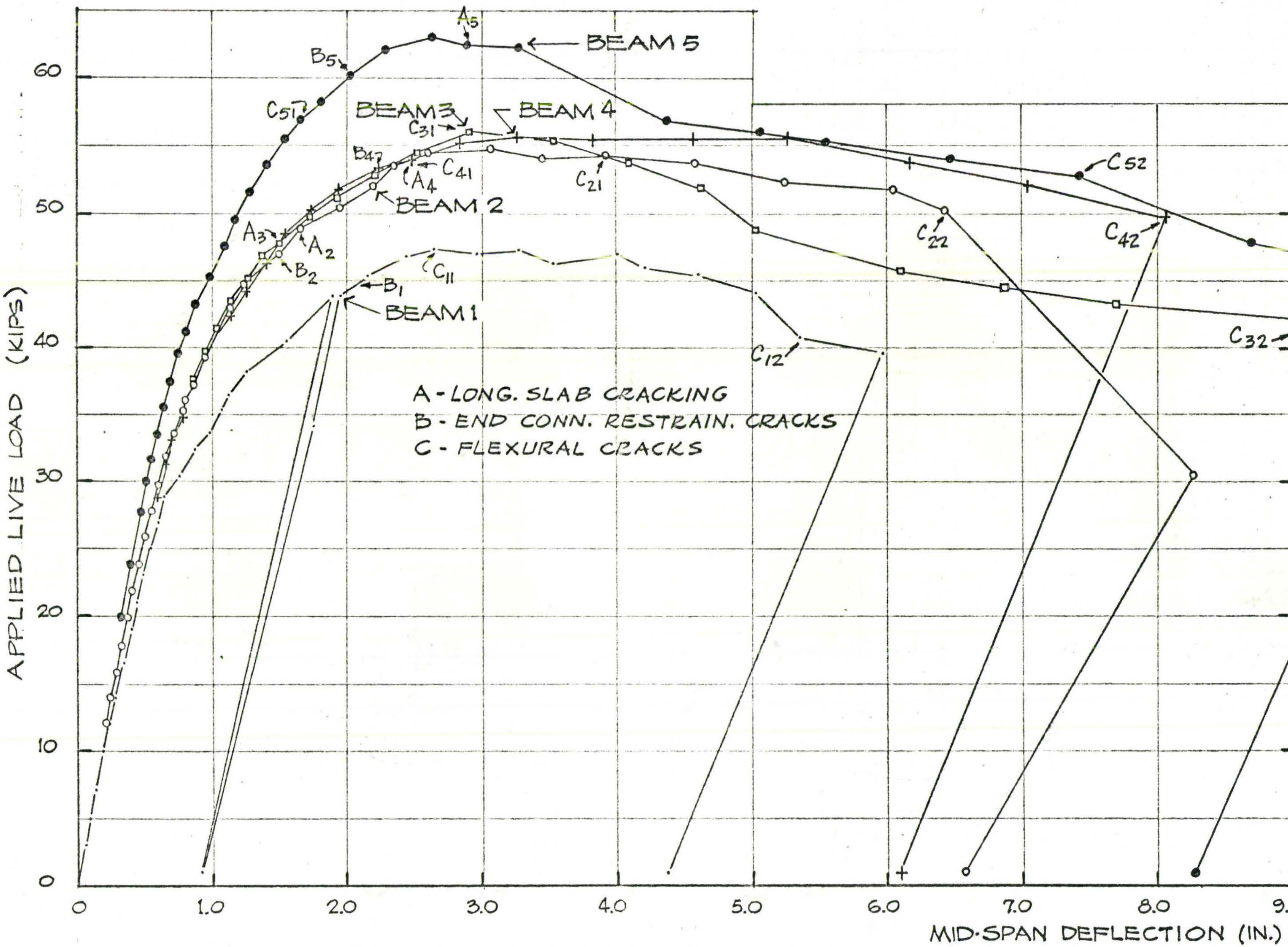

FIG. 3.7 LOAD-DEFLECTION CURVES

After 8 in. deflection of beam 3, the loading ram was unexpectedly forced down too quickly, and catastrophic failure resulted.

From the load-deflection plots (Fig. 3.7), it can be seen that first yielding of the beams occurred at from 60 to 70% of their ultimate loads. Qualitatively, first yielding of the beam is evident when a deflection occurs noticeably greater than the extension of the original linearly elastic load-deflection line would predict.

The concrete slab remained entirely intact according to visual inspection up to a load of from 0.85 to 0.92 of the ultimate load. At this point, the concrete slab began to break down, as evidenced by one or more of three types of cracking.

A. Longitudinal Slab Cracking (see Fig. 3.7a)

This crack began on the top surface of the slab as a hairline separation, probably due to transverse tension, originating under one or both load points at the centreline of the slab. It extended either way longitudinally from the loading pads, becoming longer as the load was increased. Eventually this crack extended from each loading pad to the ends of the beam and through the mid-span area. This longitudinal crack never opened beyond a hairline and so is considered as relatively unimportant. This crack was probably due to transverse tension across the slab caused by anticlastic curvature of the slab. Such an effect would very likely not be present in a complete floor system consisting of several beams with a slab spanning continuously at right angles to them.

Point A on Fig. 3.7 indicates the first indication of longitudinal cracking.

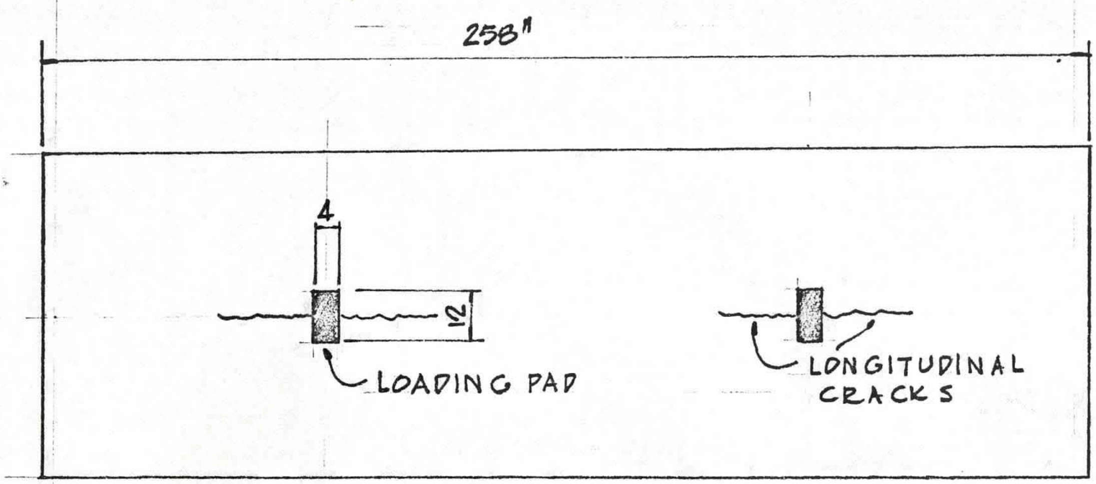

PLAN OF CONCRETE SLAB

FIG. 3.7a

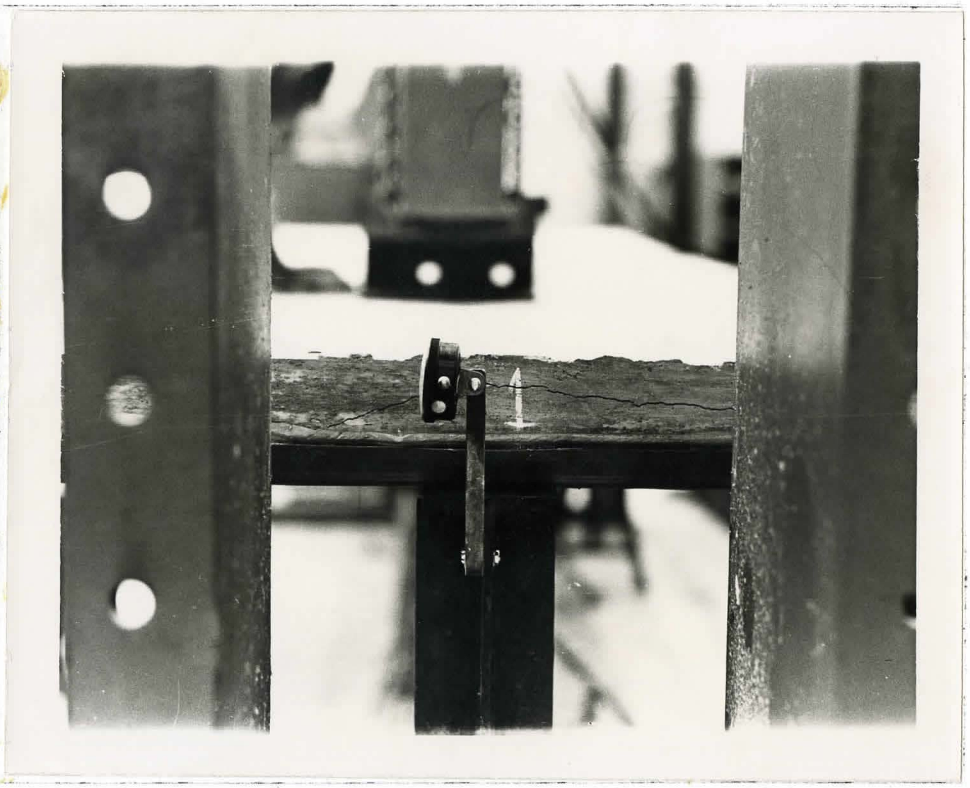

END CONNECTOR RESTRAINING CRACKS

FIG. 3.7b

<u>B. End Connector Restraining Cracks</u> (see Fig. 3.7b)

Because the slip increased towards the supports, the end connectors were deformed to the greatest extent. These end connectors tended to restrain a horizontal lens of concrete below their heads. The part of the slab above their heads tended to ride over these end connectors in a direction parallel to the axis of the steel beam. As a result, cracks of the type pictured in Fig. 3.7b formed.

This crack was originally of a shearing nature but tended to open up to a maximum of about 1/4" very late in the testing. Point B marked on Fig. 3.7 indicates the first indication of these end connector restraining cracks.

<u>C. Flexural Cracks</u> (see Fig. 3.7c)

These cracks in the slab originated on the underside of the solid part of the slab and progressed upward at a decreasingly acute angle to the horizontal, much in the same way as flexural tension cracks propagate in ordinary reinforced concrete beams. Several of these cracks developed in the region of the load points on every beam. Fig. 3.7c shows the form of several of these cracks and indicates that their form is bifurcated.

These flexural cracks in the slab, as apparent from external observation, extended upward and inward to within 1/4 in. of the top surface of the slab before very much unloading had occurred.

As pictured in Fig. 3.7d, these flexural tension cracks ultimately extended through to the top surface of the slab, resulting in a sudden loss of interaction and a steeper unloading. The initial indication of flexural cracking is marked on Fig. 3.7 as C_{11} and $C_{\cancel{22}}$ 12 for beam $\cancel{2}$ 1, etc.

FIG. 3.7c

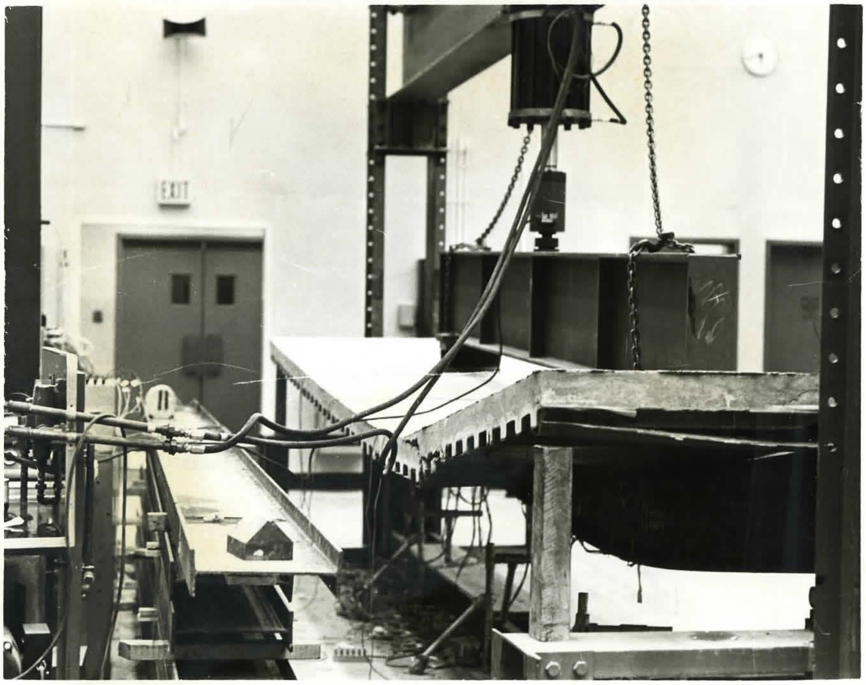

FIG. 3.7d

Fig. 3.8

Bottom fibre strain as a function of position on the beam and as a function of total applied load - Beam 1

Breakdown of interaction between the slab and steel beam was most advanced at the left-hand load point of Fig. 3.8 at the ultimate load of 47.4 kips. However, complete breakdown of interaction occurred at the right hand load point subsequent to the attainment of ultimate load. This is evidenced by the very large bottom fibre strains that developed at the right hand load point.

A solid straight line is drawn at a strain of 1240 micro-inches per inch to represent the yield strain. This was achieved at mid-span at a total applied load of 31 kips. For loads greater than this, the strain is seen to increase very quickly in the regions of the beam where the strain is greater than 1240 micro-inches per inch.

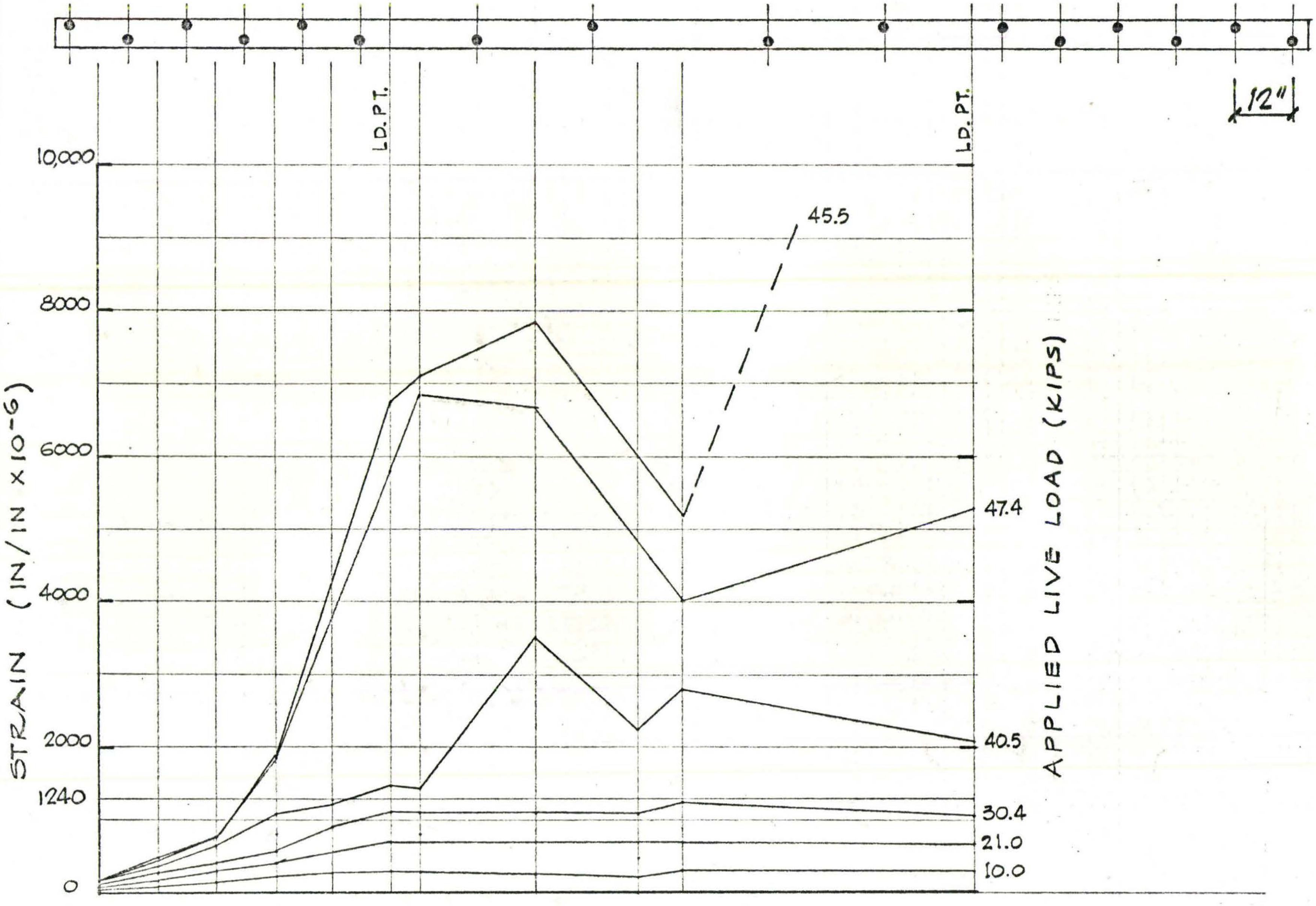

FIG. 3.8 BOTTOM FIBER STEEL STRAINS - BEAM 1

Fig. 3.9

Bottom Fibre Strain as a Function of Position on the Beam and as a Function of Total Applied Load - Beam 2

Breakdown of interaction, as evidenced by the high localized strains under the right-hand load point, was not as far advanced in this beam as it was in beam 1 at an equal total applied load. Therefore, the shear connection of beam 2 (12 studs in the shear span) caused more complete interaction than did the shear connection of beam 1 (6 studs in the shear span).

It can be observed that the strains at ultimate load were very high (about 5 times the yield strain) in a localized region of the shear span directly beneath the load points. This was not the case with the weaker shear connection of beam 1 (Fig. 3.8), where the region of high strains was more extensive and occurred slightly inward from the load points.

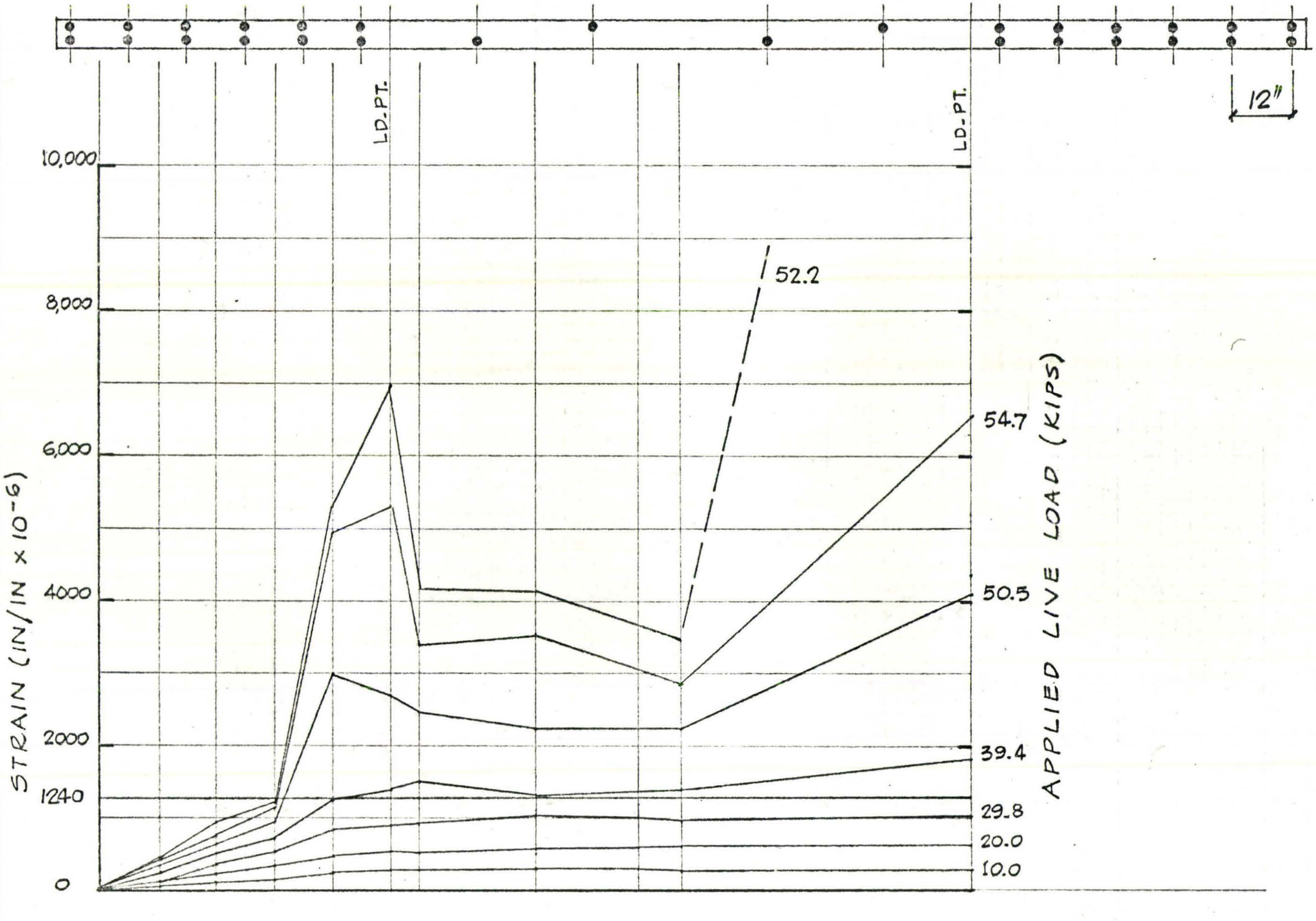

FIG. 3.9 BOTTOM FIBER STEEL STRAINS - BEAM 2

Fig. 3.10

Bottom Fibre Strain as a Function of Position on the Beam and as a Function of Total Applied Load - Beam 3

The strains were higher for the same total applied load than those of beam 2, and lower than those of beam 1. The localized region of high strains at ultimate load occurs inward from the load point, and is more extensive than that of beam 2.

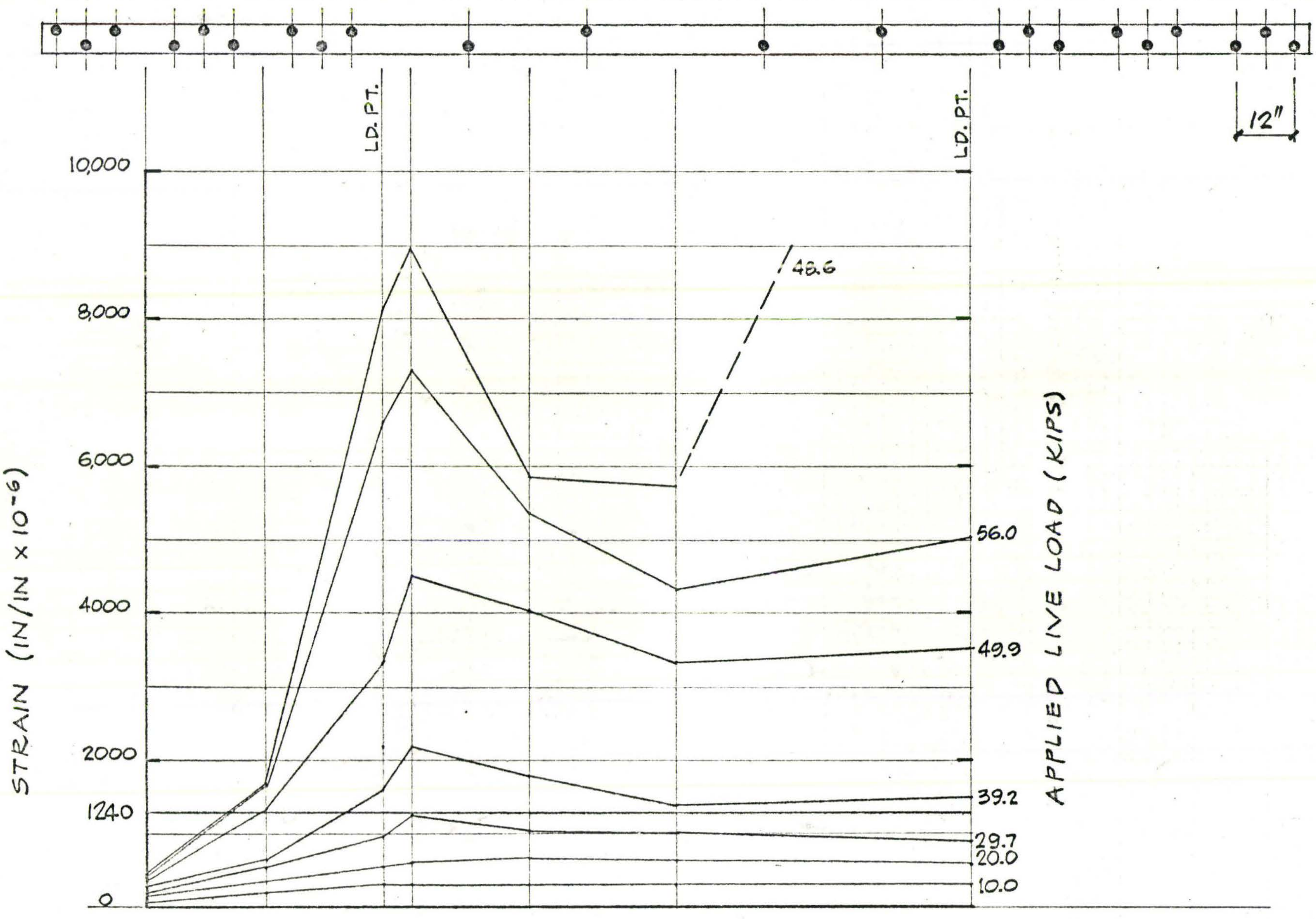

FIG. 3.10 BOTTOM FIBER STEEL STRAINS - BEAM 3

Fig. 3.11

Bottom Fibre Strain as a Function of Position on the Beam and as a Function of Total Applied Load - Beam 4

The strains of beam 4 at ultimate load were about 2.5 times those of beam 2, both beams having 12 studs in their shear spans. The region of very high strains around the load point was much more extensive in this beam than in beams 1, 2, or 3. As evidenced by the higher strains, the breakdown of interaction on beam 4 at ultimate load was much more severe than on any of the beams 1, 2 or 3.

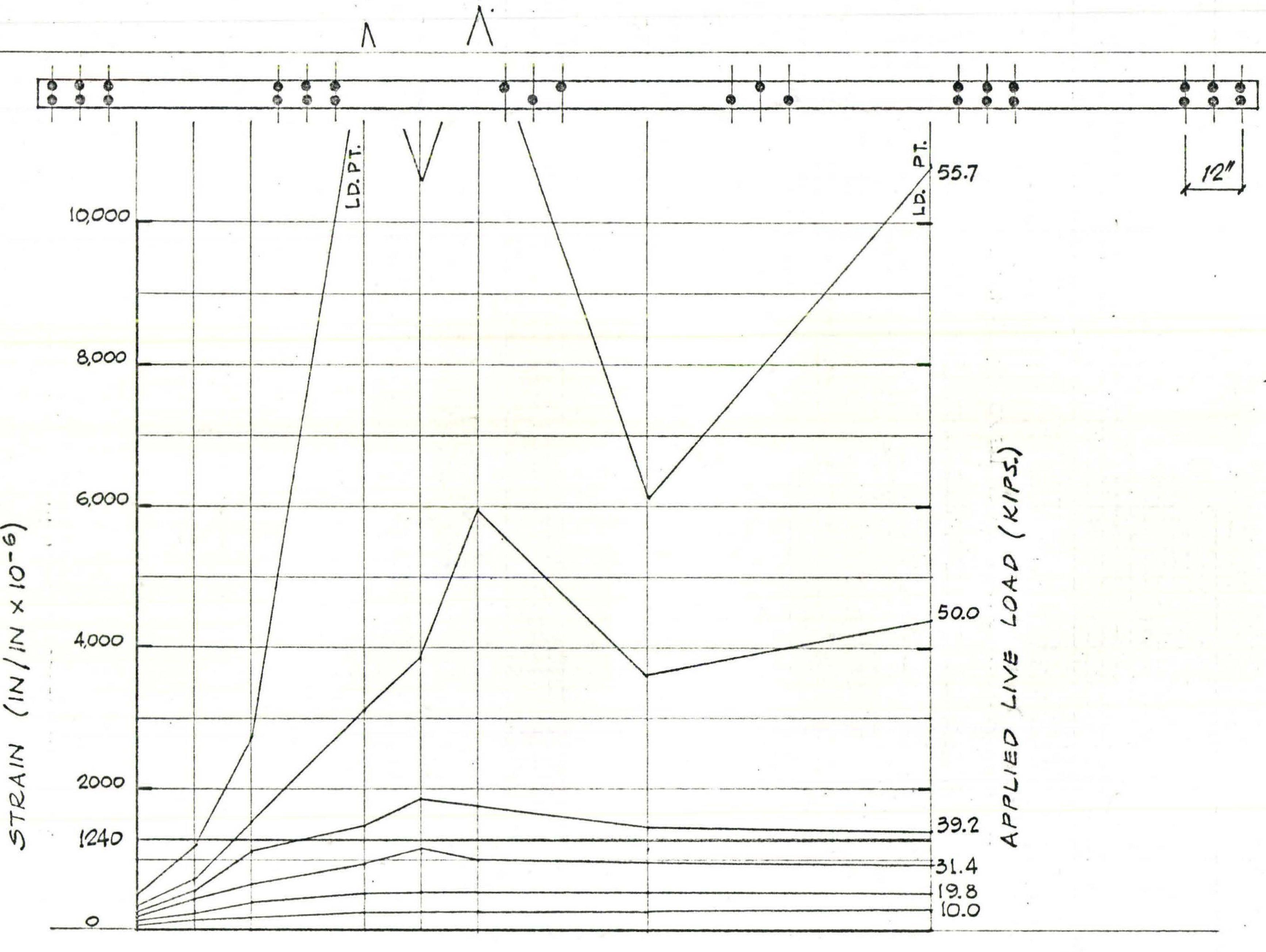

FIG. 3.11 BOTTOM FIBER STEEL STRAINS - BEAM 4

Fig. 3.12

Bottom Fibre Strain as a Function of Position on the Beam and as a Function of Total Applied Load - Beam 5.

The strains of beam 5, for an equivalent total applied load, were very much less than on any of beams 1, 2, 3, or 4. The zone of high strain was as extensive as it was on beam 4, and extended inward from the load point approximately to the same extent as on beam 4. At a total applied load of 50 kips, the strains of beam 4 are twice those of beam 5.

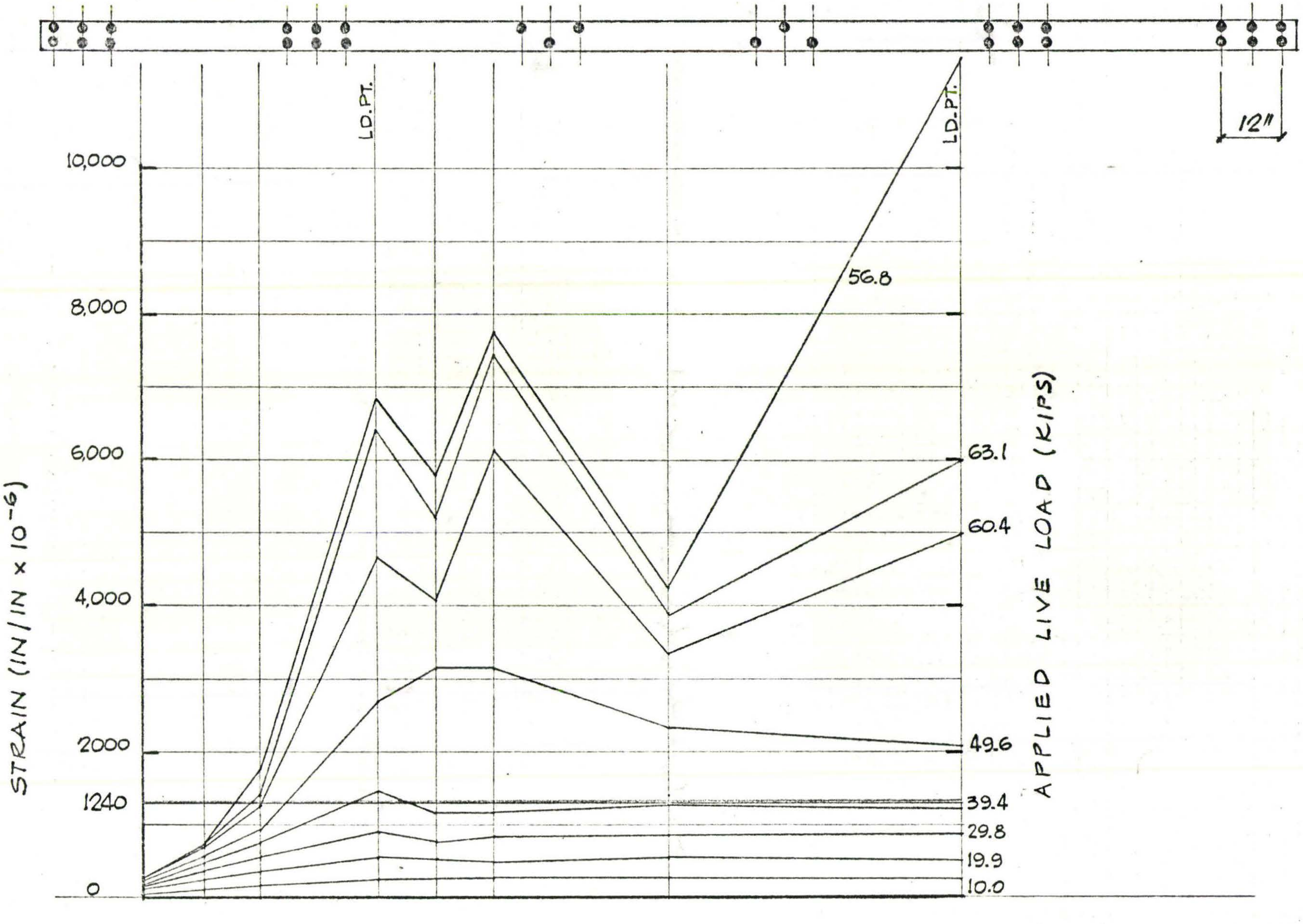

FIG. 3.12 BOTTOM FIBER STEEL STRAINS - BEAM 5

Fig. 3.13

Slip as a Function of Applied Load and as a Function of Position on the Beam - Beam 1

The slip increased from zero at mid-span to a local maximum at the load points, and then to an overall maximum at the support points. The slip is seen to be very low (less than .01 in.) for total applied loads of 25 kips or less. The slip increases very rapidly for loads greater than 25 kips up to 0.2 in. at ultimate load. The figure 25 kips load is significant because in Chapter IV, the working load is shown to be less than 25 kips.

The load-slip curves for the shear connections as measured in the push-out tests (section 2 of this report) indicate that the shear connection reaches a maximum load at a slip of about 0.06 in. A horizontal line at this slip is drawn on Fig. 3.13. The measured slip at each shear connector at a total applied load of 47.4 kips (ultimate) is greater than .06 in., except at one stud in the right-hand shear span. Therefore, at ultimate applied load, each shear connector except one is loaded to its maximum capacity.

Some slip reversal can be noted at a total applied load of 40.5 kips in the left-hand shear span. Slip reversal could be due to the cellular steel floor separating from the concrete rib and the consequent incorrect measurement of slip.

The slip measured at the ends of the beam was thought to be more reliable than the slip measured at points along the underside of the slab. This is because, at the ends of the beam, the mid-height of the slab is exposed and its movement can be measured relative to the steel beam. On the underside of the slab, the differential longitudinal displacement between the underside of the cellular steel floor and the steel beam is measured. If the cellular steel floor separates from the concrete, this slip measurement is no longer accurate. For this reason, no significance is attached to slip reversal.

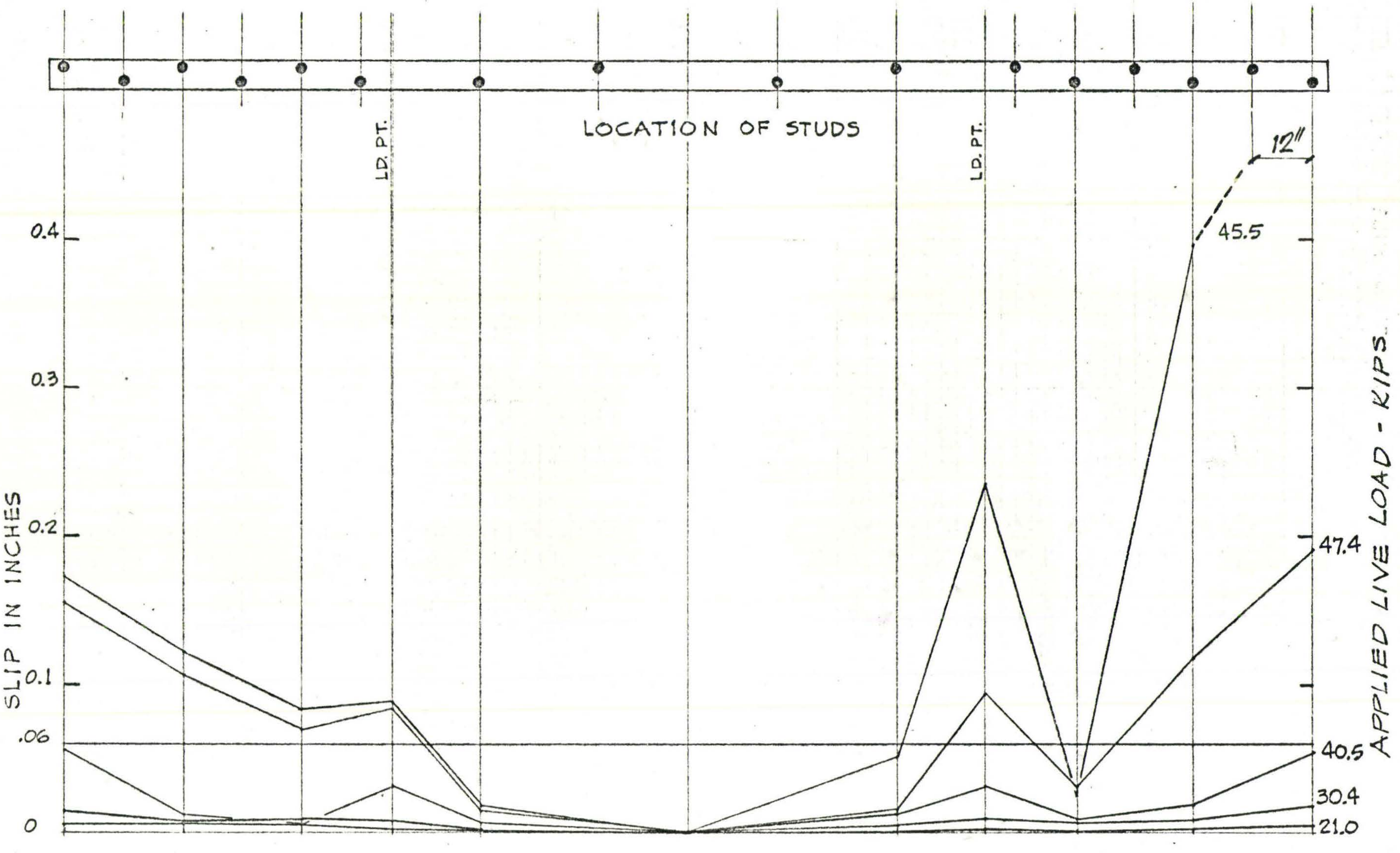

FIG. 3.13 MEASURED SLIPS - BEAM 1

Fig. 3.14

Slip as a Function of Applied Load and as a Function of Position on the Beam - Beam 2

The slip increased from zero at mid-span to a maximum about midway through the shear span, and then decreased slightly towards the support points of the beam. The slips measured on beam 2 were quantitatively about half of those measured on beam 1. All of the studs in the shear spans reached their ultimate shear capacities at the beam's total ultimate applied load, because the slip at each stud is greater than .06 in.

No slip reversal was measured, and the slip remained less than .01 in. for loads less than about 30 kips.

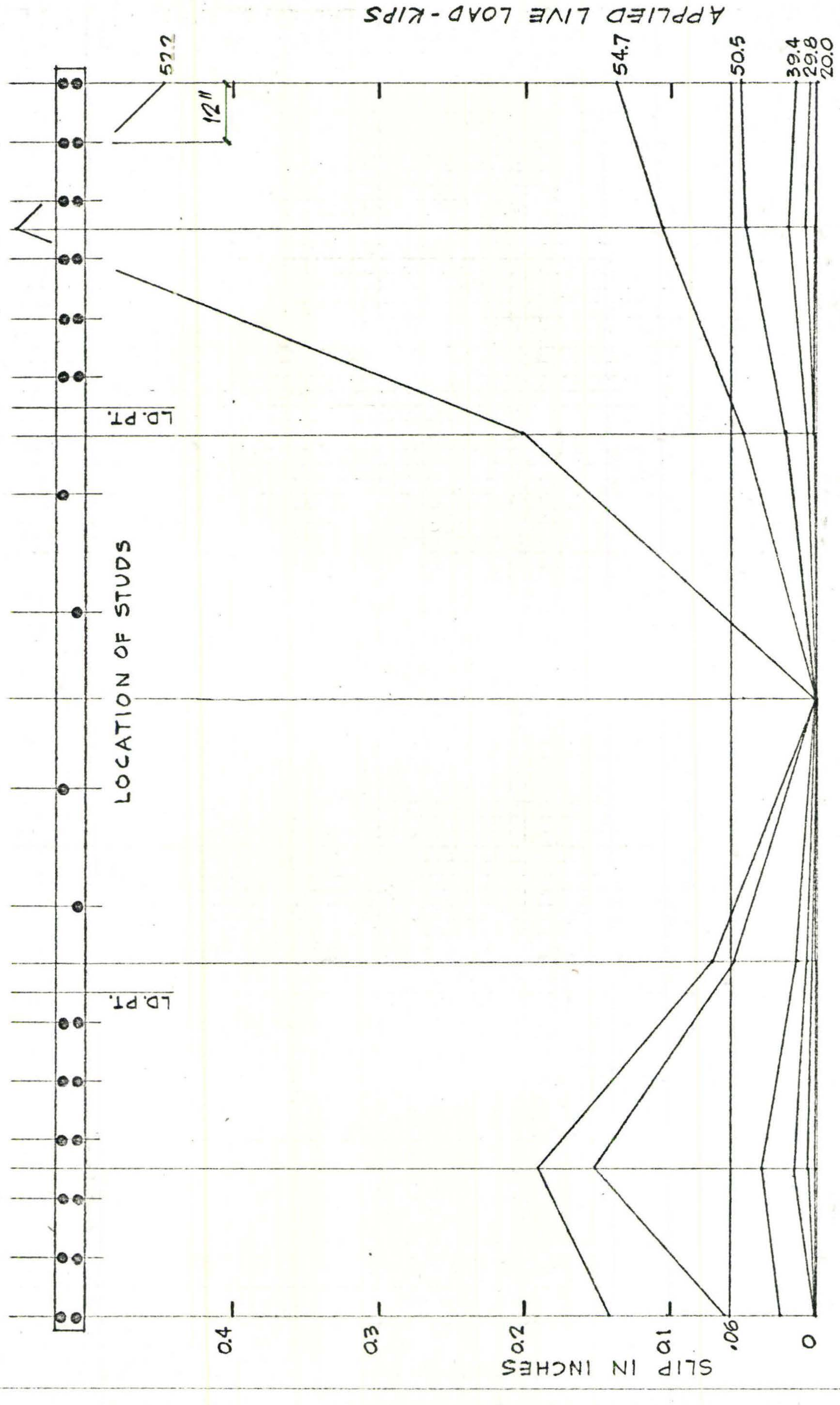

FIG. 3.14 MEASURED SLIPS - BEAM 2

Fig. 3.15

Slip as a Function of Applied Load and as a Function of Position on the Beam - Beam 3

The slip increased from zero at mid-span through a local maximum at the load point and to an overall maximum at the end of the beam. The local maximum at the load point was also observed on beam 1. The slip at one point in the right-hand shear span showed a reversal in direction beginning at a total load of about 45 kips.

At the ultimate total applied load, the slip at all studs was not up to .06 in. This indicates that the maximum possible shear force may not be developed in the shear span at the ultimate load of the beam.

The slips measured on beam 3 were slightly lower than those measured on beam 2, and remained less than .01 in. everywhere on the beam for loads less than about 40 kips.

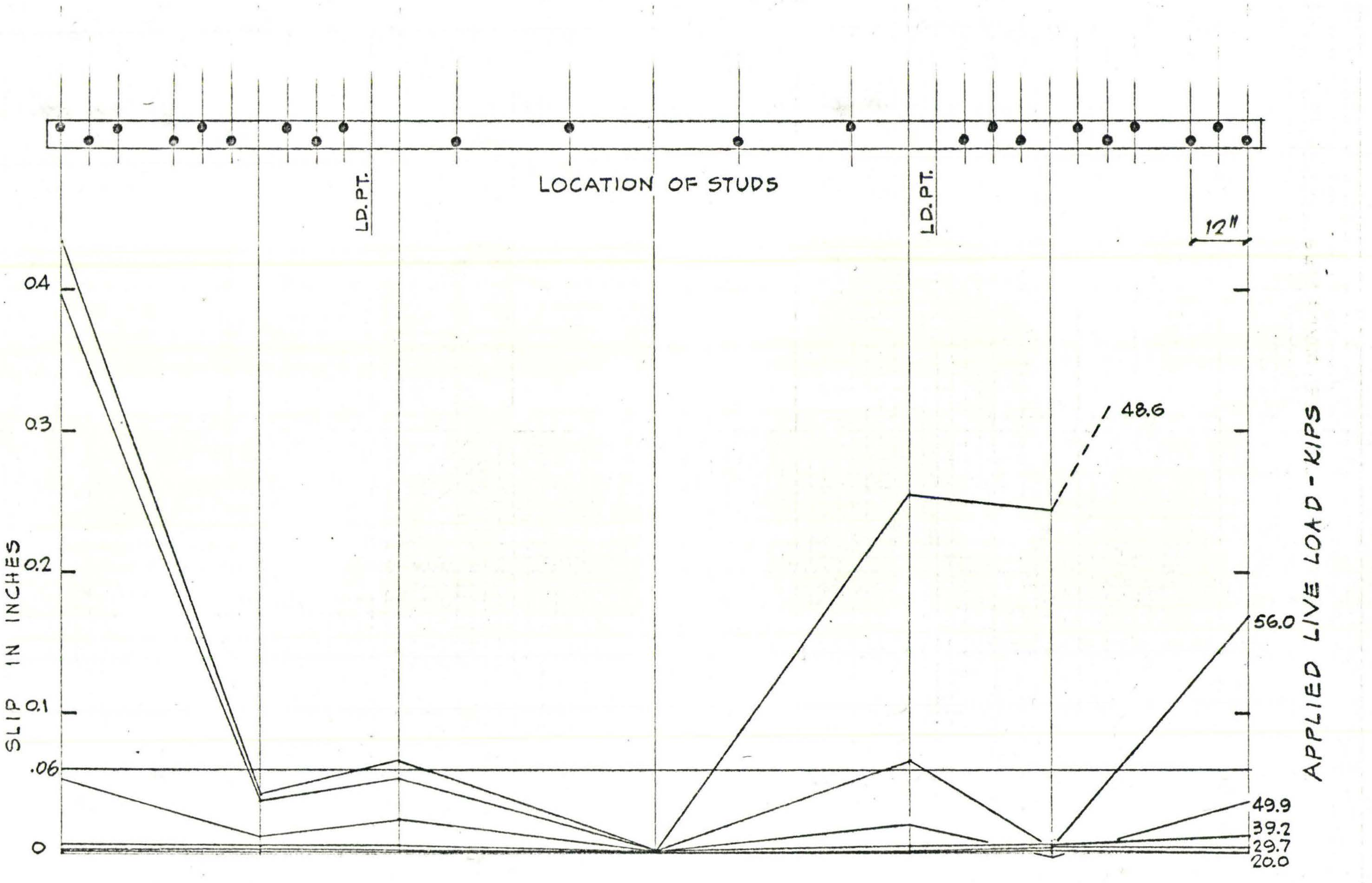

FIG. 3.15 MEASURED SLIPS - BEAM 3

Fig. 3.16

Slip as a Function of Applied Load and as a Function of Position on the Beam - Beam 4

As in beam 2, which also had 12 studs in the shear span, the slip increased from zero at mid-span to an overall maximum in the left-hand shear span. From this point the slip decreased toward the end of the beam.

For loads up to about 50 kips, the slips measured on beam 4 were only slightly greater than those measured on beam 2 for the same applied load. At ultimate load, approximately 55 kips for beams 2 and 4, the slips of beam 4 were about 4 times those of beam 2.

The slip had progressed far enough at ultimate load so that all the studs should have developed their maximum shear forces.

No slip reversals were measured, and at about 30 kips applied load, the slip was in places greater than .01 in.

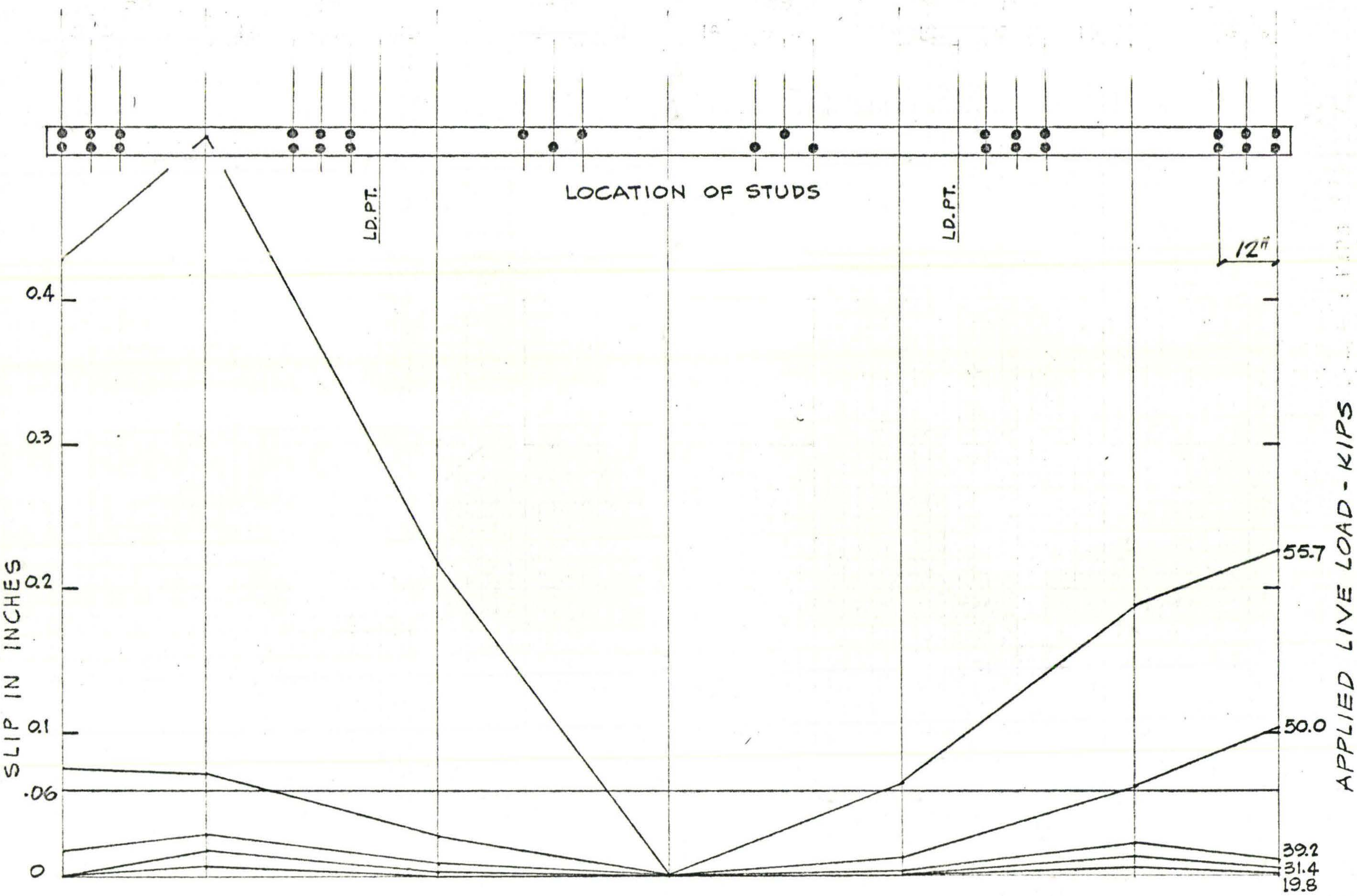

FIG. 3.16 MEASURED SLIPS - BEAM 4

Fig. 3.17

Slip as a Function of Total Applied Load and as a Function of Position on the Beam - Beam 5

As on beam 4, the slip increased from zero at mid-span to an overall maximum at the mid-point of the 36 in. interval between studs in the shear span, for loads up to and including the ultimate load. All measured slips of beam 5 are less than those of beam 4 for the same total applied load.

All of the studs in the right-hand shear span and all but the inntermost pair of studs in the left-hand shear span had reached ultimate shear force at the total ultimate applied load of the beam.

At 30 kips load, the slip approached .01 in. No slip reversals were measured.

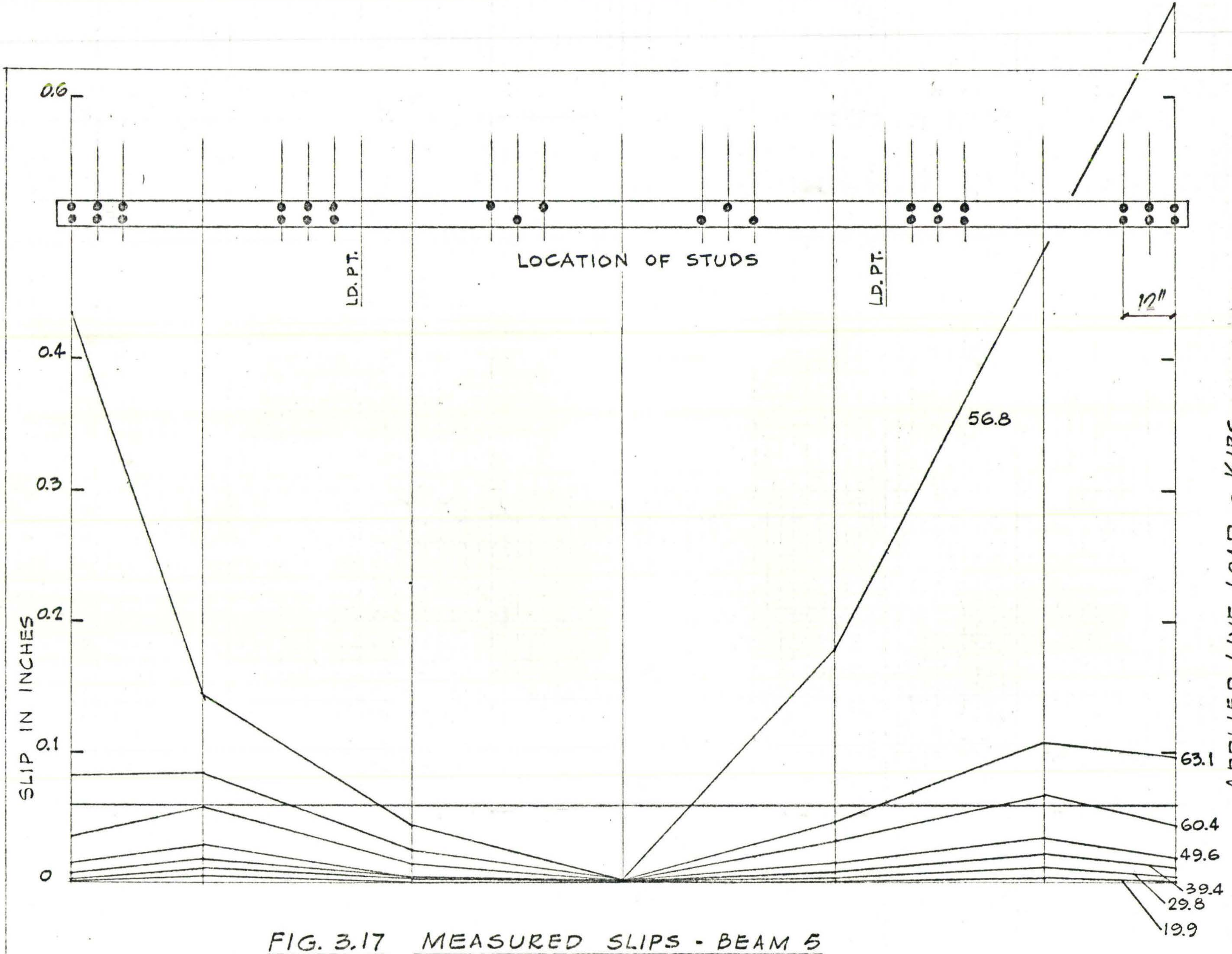

FIG. 3.17 MEASURED SLIPS - BEAM 5

Fig. 3.18

Applied Moment vs. Measured Curvature for the Steel Beam - Beams 1 to 5

Moment vs. curvature curves show the (post-ultimate) ductility of the beams. Curvature is calculated by dividing the strain difference across the depth of the steel beam by the depth of the steel beam.

The ductility factor of a beam is defined[14] as the ratio of the member deformation at unloading to the fictitious elastic member deformation at the ultimate load of the member (see part 4.8 of this report). Unloading is loss of load to below 0.95 of the ultimate member load.

The fictitious elastic member deformation is found by extending the elastic part of the moment-curvative curve up to intersect the horizontal projection of the ultimate load level attained. Calculating the ductility factor on this basis, the following ratios are obtained for the five beams:

Beam 1	-	16.0
2	-	11.7
3	-	6.3
4	-	14.3
5	-	5.7

As can be seen from Fig. 3.18, the moment-carrying capacity of beams 3 and 5 drops off relatively more quickly than do the curves for the other three beams. This is reflected in a lower ductility factor listed above for beams 3 and 5.

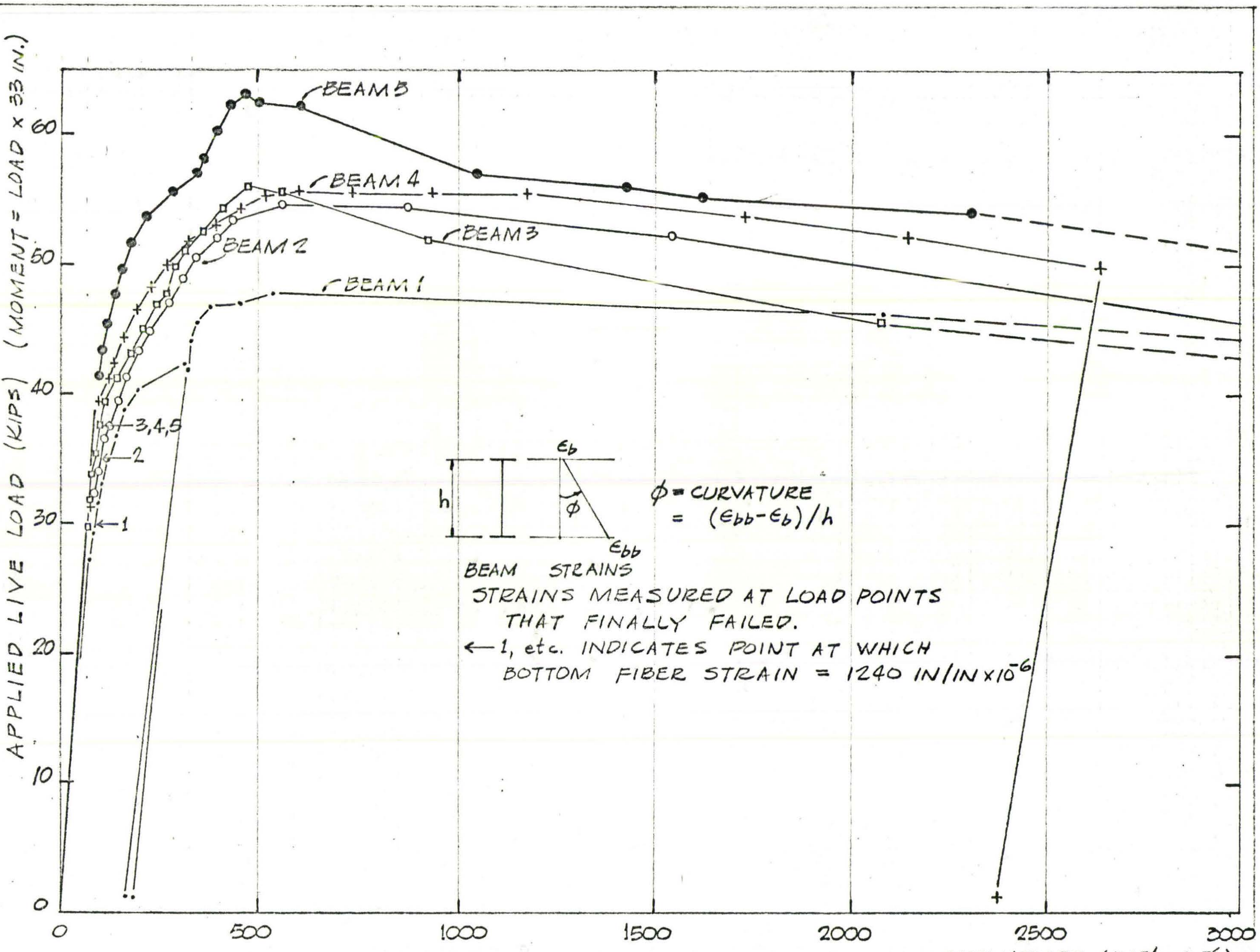

FIG. 3.18 LOAD VS. CURVATURE - ALL BEAMS

Fig. 3.19

Strain in the Top of the Slab as a Function of Total Applied Load for Each Load Point and for Mid-Span - Beam 3

Four strain gauges were attached across the width of the slab at each load point, and 7 strain gauges were attached across the width of the slab at mid-span.

At mid-span, the concrete slab strains were uniform across the width of the slab up to and after ultimate load. At each load point, the strains remained uniform across the slab up to a total load of 40 kips for the east load point, and up to about 30 kips for the west load point.

The strains at the load points were significantly higher than those at mid-span for loads greater than about 10 kips. This is consistent with earlier findings(3), which show that the extreme fibre strains at mid-span do not increase very much after first yielding of the beam, whereas the extreme fibre strains under the load points increase very quickly after first yielding of the steel beam. Yielding of beam 3 began at about 35 kips and progressed until 56.0 kips when the beam was at its ultimate load. At 35 kips, the average slab strain at mid-span was about 250 micro-inches, and at the full ultimate load of 56.0 kips, the average mid-span strain was about 650 micro-inches.

Between the same loads, the strain at the load points increased from about 300 micro-inches to about 1,000 micro-inches. The latter figure is an approximate average of the measured edge strains and the projected centreline strain at the load point.

The measured slab strains for beam 3 show that the full slab

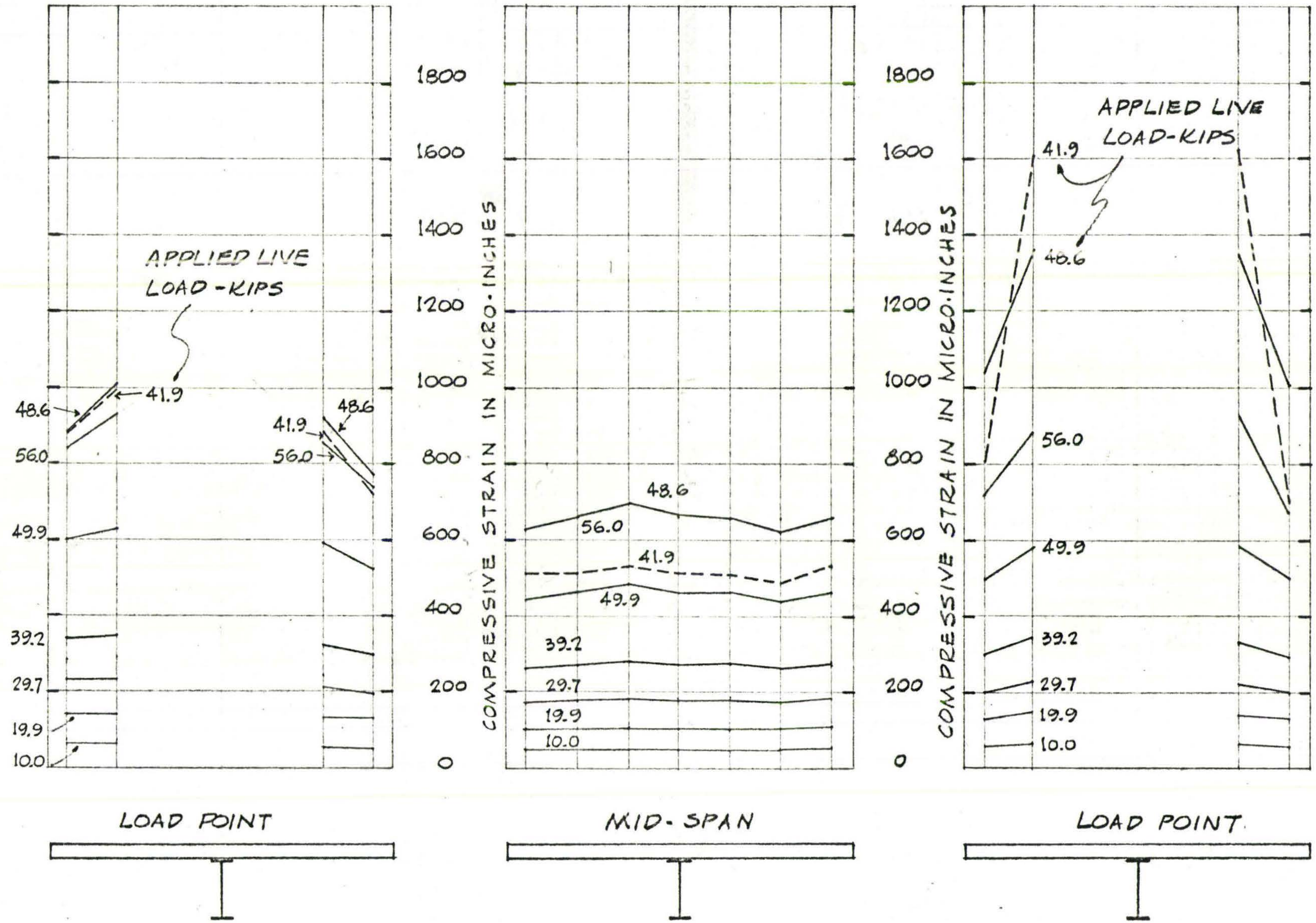

FIG. 3.19 CONCRETE TOP FIBER STRAINS - BEAM 3

width of 68 inches is equally strained and therefore effective at mid-span at the ultimate load. Under the load points, however, at ultimate load, a region of high compressive strains developed close to the centreline of the slab. This strain concentration at the centreline of the slab at the load points was not in evidence at the working load of the beam (less than 25 kips).

General Observations on Beam Testing

As loading of the beams progressed, the steel beam yielded at about 30 kips for beams 1 to 4, and at about 40 kips for beam 5. After yielding of the steel beam, the concrete slab began to crack as indicated on Fig. 3.7. The cracking began and continued gradually and without any sudden effects. As the deflection increased and the ultimate load was approached, concentrated rotations were noticeable at the load points by viewing the beam in elevation. The beams remained structurally sound through the ultimate load. Unloading was in every case gradual, but faster in beams 5 and 3. No web or flange buckling was noticeable on any of the five beams until well after unloading had begun.

The concrete slab continued to provide lateral support for the steel beam, up to an estimated deflection of 13 in. in the case of beam 3, before lateral buckling occurred. Fig. 3.20 shows beam 3 after collapse.

A tendency was observed in all beams for the ribs of the cellular steel floor to deform locally around the base of the individual studs, eventually resulting in ripping of the metal sheet as shown in Fig. 3.21. This ripping did not occur until very late in the test of beam 3, and not at all in the other beams, but the tendency was evident in all tests.

Between locations on the steel beam where the slab was held down by the shear connectors, the slab showed a tendency to lift off the top flange of the steel beam. For beams 1 to 3, the gap that developed between the top flange of the steel beam and the bottom of the cellular steel floor was small, but for beams 4 and 5, the gap increased to an

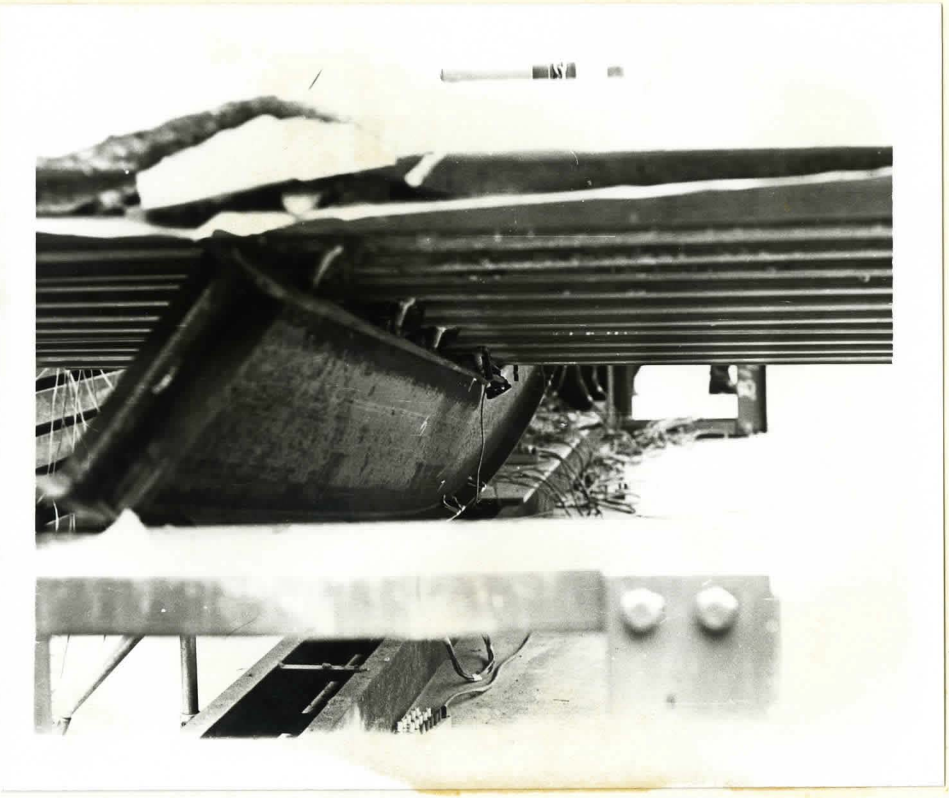

FIG. 3.20

FIG. 3.21

estimated 3/8 in. This gap occurred in the 36 in. interval between shear connectors in the shear span.

The tendency of the slab to lift off the steel beam is the reason that shear connectors must be capable of resisting uplift. Studies have been made[19, 20] of the uplift stresses in shear connectors, but it is now common design practice to neglect any effects of uplift.

CHAPTER IV

ANALYSIS OF TEST RESULTS

4.1 Introduction

Analysis of composite beams incorporating cellular steel floor is accomplished on the basis of certain assumptions. For example, if slip between the concrete slab and the steel beam is assumed to be negligible, then calculation of the strength of the composite beam is made using the transformed section. Analysis on the basis of the transformed section implies that no loss of interaction between the concrete slab and steel beam occurs.

If, on the other hand, loss of interaction is to be taken into account in the analysis of the composite beam, then the shear force vs. slip relation of the shear connection must be known or assumed. If a linear shear force vs. slip relation is assumed, then the continuum analysis due to Newmark et al[12] may be used. If a trilinear shear force vs. slip relation is assumed, then the finite difference analysis of Dai and Siess[9] may be used.

The analysis of test results is done in this paper at two levels of load; working load and ultimate load. Working load is defined as the live load at which the bottom fibre steel strain reaches the elastic allowable strain. Ultimate load is the maximum static live load that the composite beam can carry.

4.2 Determination of Working Load

The elastic allowable strain for the steel beam is 0.66 of the yield strain. Since the working load is the load causing the steel strain to reach the elastic allowable strain, the designer must establish a numerical value for the elastic allowable strain. This can be done if the actual material properties of the steel are known, if the strain in the steel caused by shrinkage of the concrete slab is known, and if the strain in the steel due to the dead load of the wet concrete slab is known.

A designer is usually equipped with only design material properties rather than actual material properties (see Table 4.a). The designer can usually calculate what strain in the bottom fibres of the steel beam is caused by dead load, but he cannot estimate the strain induced in the steel beam due to shrinkage of the concrete.

The difference between design and measured material properties for the G40.12 steel beam used in these tests is as shown in Table 4.a.

Table 4.a

	Design	Measured by Coupon Tests
E	29×10^6 p.s.i.	33×10^6 p.s.i.
f_y	44,000 p.s.i.	40,700 to 46,700 p.s.i. (see Table 3.a)
E_*	1510×10^{-6} IN/IN	1240×10^{-6} to 1410×10^{-6} IN/IN

The shrinkage of the concrete slab, the application of the dead load of the slab to the steel beam alone, and the application of live load to the composite beam, all affect the allowable strain in the bottom

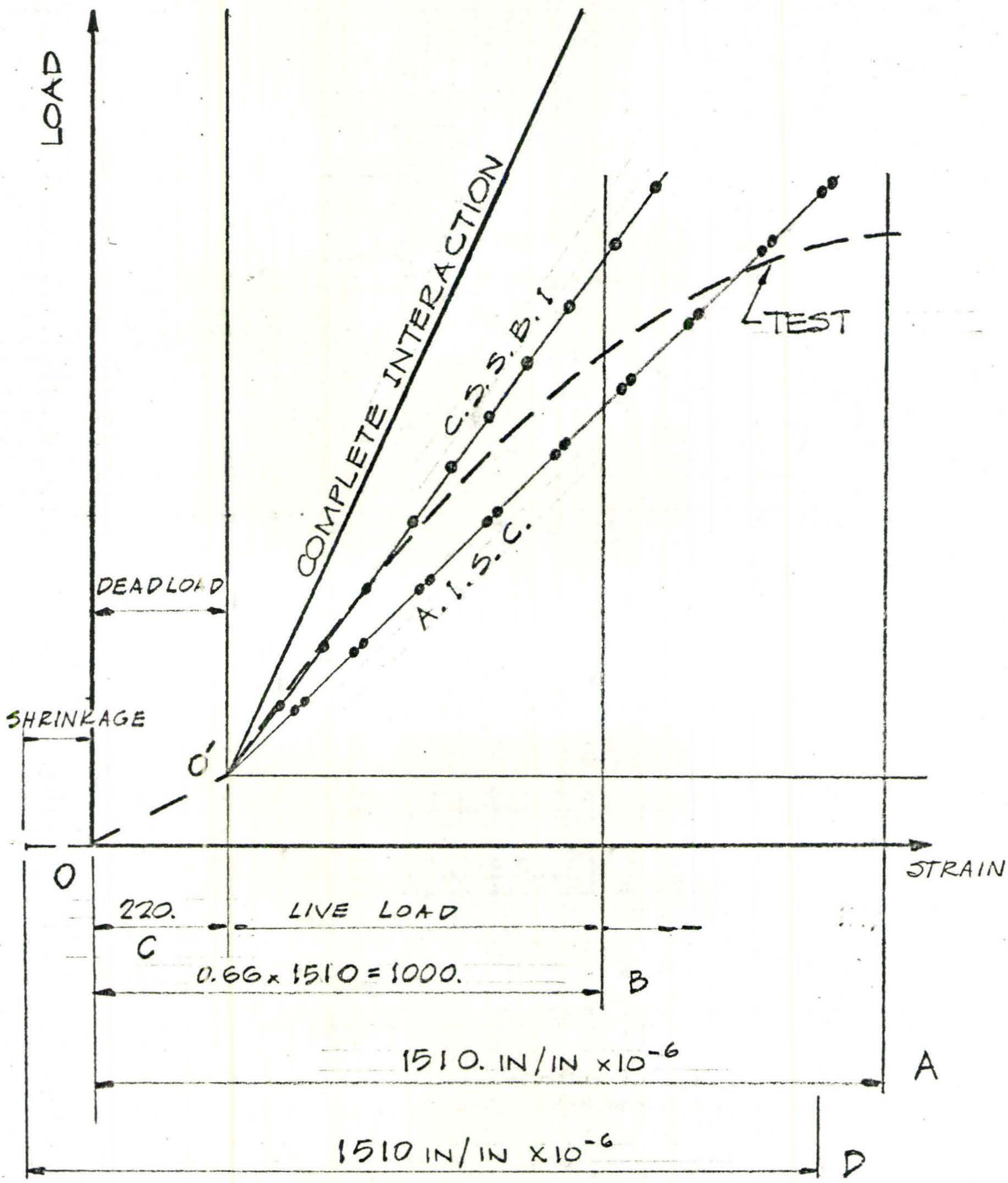

SCHEMATIC LOAD-STRAIN HISTORY OF A TYPICAL COMPOSITE BEAM

FIG. 4.1

fibre of the steel beam. This effect is shown schematically in Fig. 4.1.

The broken line on Fig. 4.1 indicates the beam response to applied load. If shrinkage-induced strains are neglected, the designer has a strain available up to yield for dead and live load of 44,000/ $29 \times 10^6 = 1510 \times 10^{-6}$ IN/IN (abcissa A, Fig. 4.1). A strain of 0.66 of this 1510, or 1000, is allowed to be used under working loads (abcissa B, Fig. 4.1). If the strain caused by dead load is subtracted from the 1000×10^{-6} IN/IN allowable, then only 780×10^{-6} IN/IN is available for live working load (abcissa B minus abcissa C, Fig. 4.1, with the strain due to dead load equal to 220×10^{-6} IN/IN).

If shrinkage strains are included in this discussion, they would reduce the allowable strain by a small amount (abcissa D, Fig. 4.1). In the calculation of working loads to follow, shrinkage strains will be neglected.

The tests of this report were performed in the live load range (labelled on Fig. 4.1), and began at origin O' on Fig. 4.1. The straight solid lines on Fig. 4.1 marked "complete interaction", "C.S.S.B.I." and "A.I.S.C.", are three theoretically-computed load-strain relations. These lines will be referred to again later.

In the live load region, the bottom fibre steel strains are as shown in Fig. 4.2, as measured under one load point during the beam test. The strains of Fig. 4.2 do not demonstrate a definite yield point as did the coupon strains. The absence of a distinct yield point was very likely caused by residual strains present in the steel before testing.

It should be noted that it is not absolutely necessary for the steel to demonstrate a definite yield point as long as an adequate load factor can be obtained on beam failure.

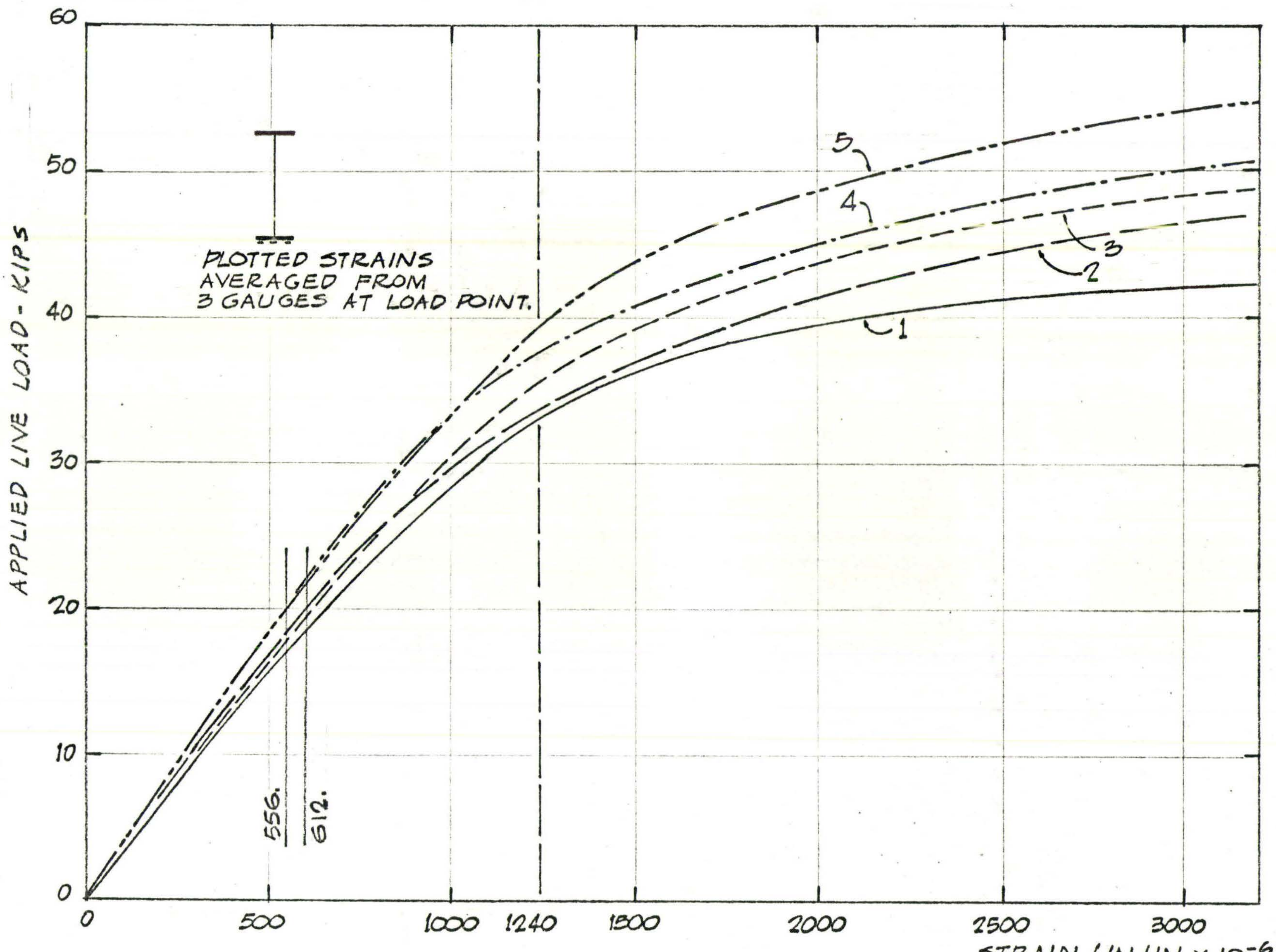

FIG. 4.1a LOAD-STRAIN CURVES FOR FIVE BEAMS

On Fig.4.1a are drawn vertical lines corresponding to line B of Fig. 4.1. These lines would be drawn at the measured allowable strains shown in Table 4.b for each of the beams.

Table 4.b

Determination of Working Load Including Effect of Dead Load Strains

Beam	1	2	3	4	5
lower flange yield strain (static yield from coupons)	1240	1240	1240	1240	1240
0.66 of yield strain	820	820	820	820	820
less strain under load point due to dead load of wet concrete	208	208	208	208	264
measured allowable strain for live load	612	612	612	612	556
working live load from Fig. 4.1a at measured allowable strain	18.5	20.0	19.5	22.0	20.0

From Table 4.b, the measured working total live loads range from 18.5 to 22.0 kips. These measured working loads can be compared to design working loads. Design working loads can be calculated in accordance with:

(a) complete interaction,

(b) C.S.S.B.I. Composite Beam Manual[10], and

(c) A.I.S.C. effective section modulus[8].

The calculations (a), (b), and (c) above can be explained as follows:

(a) Complete Interaction

Using $E_s = 29 \times 10^6$ p.s.i., n = 9, calculate I of transformed section (see Appendix (a)). Using F_y = 44,000 p.s.i., calculate useable strain difference between dead load strain and 0.66 of yield strain. Calculate the live load on the beam which will give this useable strain difference. This is the working live load.

(b) C.S.S.B.I. Composite Beam Manual

Using $E_s = 29 \times 10^6$ p.s.i., n = 9, the procedure given in Reference 10 allows the designer to calculate stress and deflection efficiency factors. These efficiency factors are less than 1.0 and are used to reduce the section modulus and the moment of inertia of the transformed section. Using the reduced section modulus, the designer can calculate what live load will cause the bottom fibre steel strain to equal the strain difference available for live load. This load is the working live load (see Appendix (b)).

(c) A.I.S.C. Effective Section Modulus

The A.I.S.C. effective section modulus is equal to that of the steel beam alone plus a fraction of the difference between the transformed section modulus and the section modulus of the steel beam alone. The section modulus of the transformed section is calculated on the basis of $E_s = 29 \times 10^6$ p.s.i. and n = 9. Using this effective section modulus, the designer can calculate what live load is required to cause the bottom steel fibre strain to equal the strain difference available for live load. This load is the working load (see Appendix (c)).

The measured and computed working loads are shown in Table 4.c.

Table 4.c

Beam	Total Working Live Load (kips)			
	Measured	Complete Interaction 1	C.S.S.B.I. 2	A.I.S.C. 3
1	18.5	25.6	22.6	18.0
2	20.0	25.6	22.6	19.3
3	19.5	25.6	22.6	19.3
4	22.0	25.6	22.6	19.3
5	20.0	26.4	23.2	20.1

1, 2, 3 -
For calculations leading to these working loads, see Appendices (a), (b), and (c) respectively.

Note that the four working loads as listed above for each of the beams are all determined on the same basis. That is, dead load strains are accounted for in each calculation. The measured working load is low compared to the C.S.S.B.I. value because the flange yield stress of the beams was only 41.6 ksi and not 44 ksi.

4.3 Load-Strain Behaviour in the Working Load Range

Fig. 4.1 is a schematic representation of the complete load vs. strain history of a composite beam through dead load, shrinkage, and live load. Figures 4.2 to 4.6 show the measured load vs. strain behaviour as the live load was applied to the five beams during testing. The origin of the measured load vs. strain curves of Figs. 4.2 to 4.6 corresponds to point 0' on Fig. 4.1. The bottom fibre strains plotted in Figs. 4.2 to 4.6 were measured under the load point at which failure finally occurred.

On Figs. 4.2 to 4.6 are drawn four solid load vs. strain lines that can be compared to the measured line. The four load vs. strain lines are determined by:

(a) "complete interaction" ($E_s = 29 \times 10^6$ p.s.i., n=9, transformed area section modulus)

(b) "in accordance with the C.S.S.B.I. design" ($E_s = 29 \times 10^6$ p.s.i., n = 9, reduced section modulus)

(c) "A.I.S.C. effective section modulus"

(d) "steel beam alone".

The calculations leading to (a), (b) and (c) above are briefly explained in section 4.2, and detailed calculations are listed in Appendices (a), (b) and (c) of this report.

The dashed load-strain line on Figs. 4.2 to 4.6 represent the line of complete interaction if the measured values of E_s and E_c are used ($E_s = 33 \times 10^6$ p.s.i., $E_c = 3.19 \times 10^6$ p.s.i.).

In addition to the four theoretical load-strain lines shown in Figs. 4.2 to 4.6 are two horizontal lines at the upper and lower theoretical working loads. These two lines represent the extremes of the theoretical working loads calculated in Table 4.c.

Fig. 4.2

Bottom Fibre Strain at Load Point vs. Applied Load - Beam 1

The efficiency of the beam at a particular load is measured by the increase in strain from that for complete interaction divided by the strain for complete interaction.

Beam 1 demonstrated the lowest efficiency of any of the five beams. This indicated that the shear connection of beam 1 was the weakest of the five beams.

The strain calculated in accordance with the C.S.S.B.I. Manual over-estimated the bottom fibre strain produced at a given load. In other words, the C.S.S.B.I. is conservative in its strain calculation. The C.S.S.B.I. Manual assumes $AsF_y/18.8 = 14$ studs in each shear span. Beam 1 had only 6 studs in each shear span, and therefore had a comparatively weak shear connection. The fact that the C.S.S.B.I. overestimated the strain produced at a given load for a beam with a very weak shear connection speaks in its favour as a design procedure.

The A.I.S.C. effective section modulus overestimated the measured bottom fibre strains by about 30% in the working load range. This error, although on the conservative side, is too great, especially when applied to a beam with a very weak shear connection such as beam 1.

Prediction of strains that are too high results in under-estimation of working load (see discussion of Fig. 4.3).

Fig. 4.2 is somewhat misleading because the measured load-strain curve follows the theoretical load-strain curve labelled "complete interaction". This fact is misleading because the shear connection of beam 1 is known to be very weak, consisting of only 6 single studs in the shear span. Because the shear connection is very weak, some loss

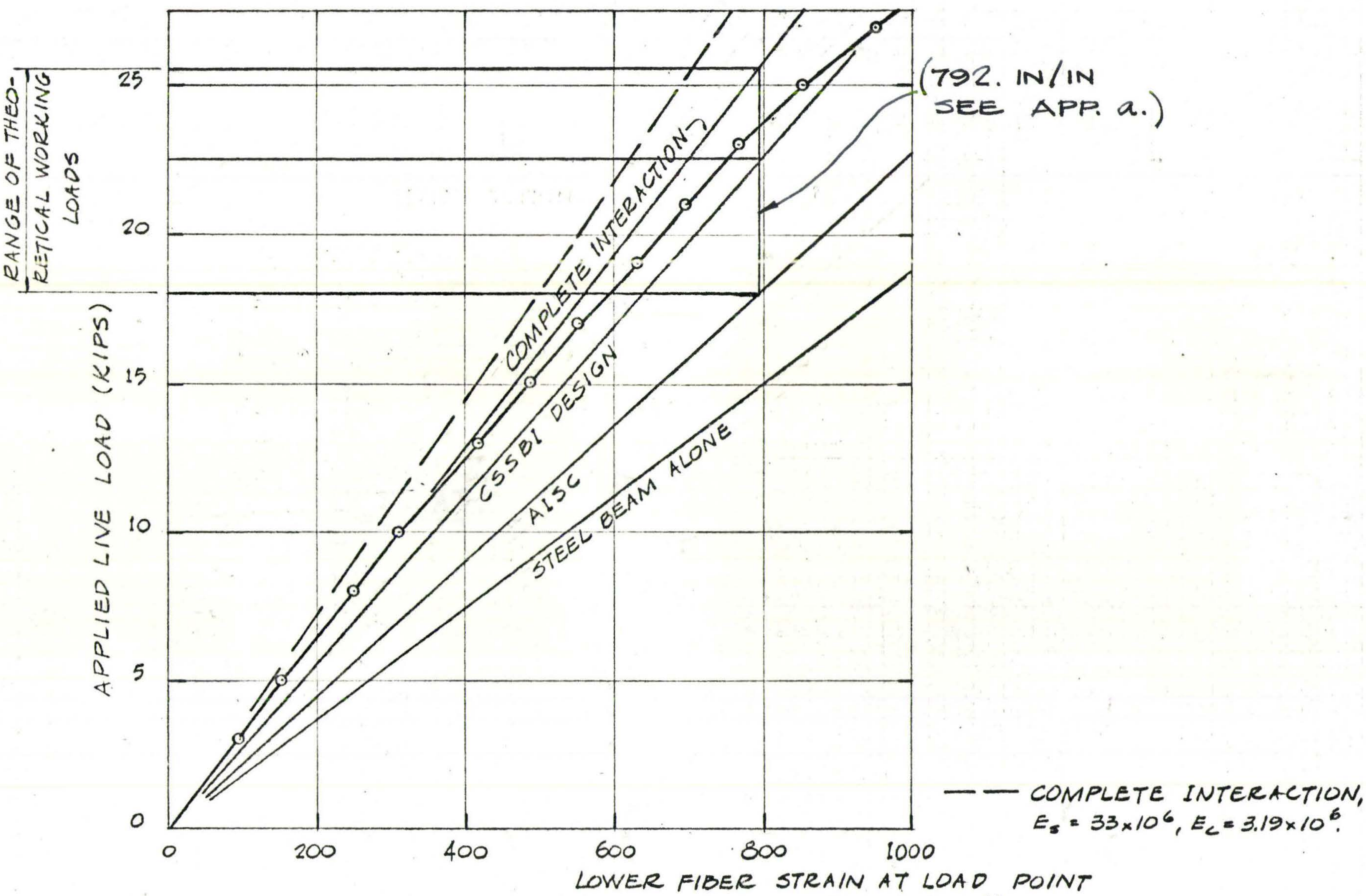

FIG. 4.2 LOAD-STRAIN BEHAVIOR UP TO WORKING LOAD
BEAM 1

of interaction would have been expected for every applied load. Up to a load of 12 kips, however, no loss of interaction was measured.

The true steel and concrete properties may not be equal to those used in calculating the strain predicted by the line labelled "complete interaction". In fact, the measured values for E_s and E_c were quite different from those assumed in calculating the strain of the line labelled "complete interaction" (see Table 4.a). The load-strain line labelled "complete interaction - measured material properties" may in fact be a truer representation of complete interaction. The measured strain is seen from Fig. 4.2 to be greater than the strain of the line labelled "complete interaction - measured material properties", as would be expected.

However, the load-strain line labelled "in accordance with the C.S.S.B.I. design" is derived from the complete interaction line and therefore is based on design material properties. For this reason, the load-strain line labelled "complete interaction" must be shown on Fig. 4.2.

Fig. 4.3

Bottom Fibre Strain at Load Point vs. Applied Load - Beam 2

Beam 2 had 12 studs in the shear span in 6 pairs. Beam 2 demonstrated a greater efficiency than that of beam 1. This is indicated by the tendency for the lower fibre strains to be equal or below those of complete interaction, whereas the strains of beam 1 were equal to or above those of complete interaction.

The calculations based on the C.S.S.B.I. produce bottom fibre strains about 15% greater than the measured strains through the working load range.

The strains calculated using the A.I.S.C. effective section modulus are about 30% greater than the measured strains.

Overestimation of theoretical strain values may lead to an underestimation of working load. The theoretical allowable live load strain difference for beam 2 is 792 x 10^{-6} in/in (see Appendix a.). From Fig. 4.3, the theoretical load at which the strain reaches 792 x 10^{-6} in/in is 25.6 kips for complete interaction, 22.5 kips according to the C.S.S.B.I., and 19.0 kips according to the A.I.S.C. effective section modulus.

The measured allowable live load strain difference, however, was only 612 x 10^{-6} in/in, based on the coupon test yield (see Table 4.b). The measured load producing the bottom fibre strain of 612 x 10^{-6} in/in was 20 kips. Therefore, because the steel used for these tests had a low flange yield stress (41.6 ksi compared to a nominal 44.0 ksi) as measured by coupon tensile tests, the measured allowable live load strain difference was lower than the design value. It happened that the working load calculated by means of the A.I.S.C.

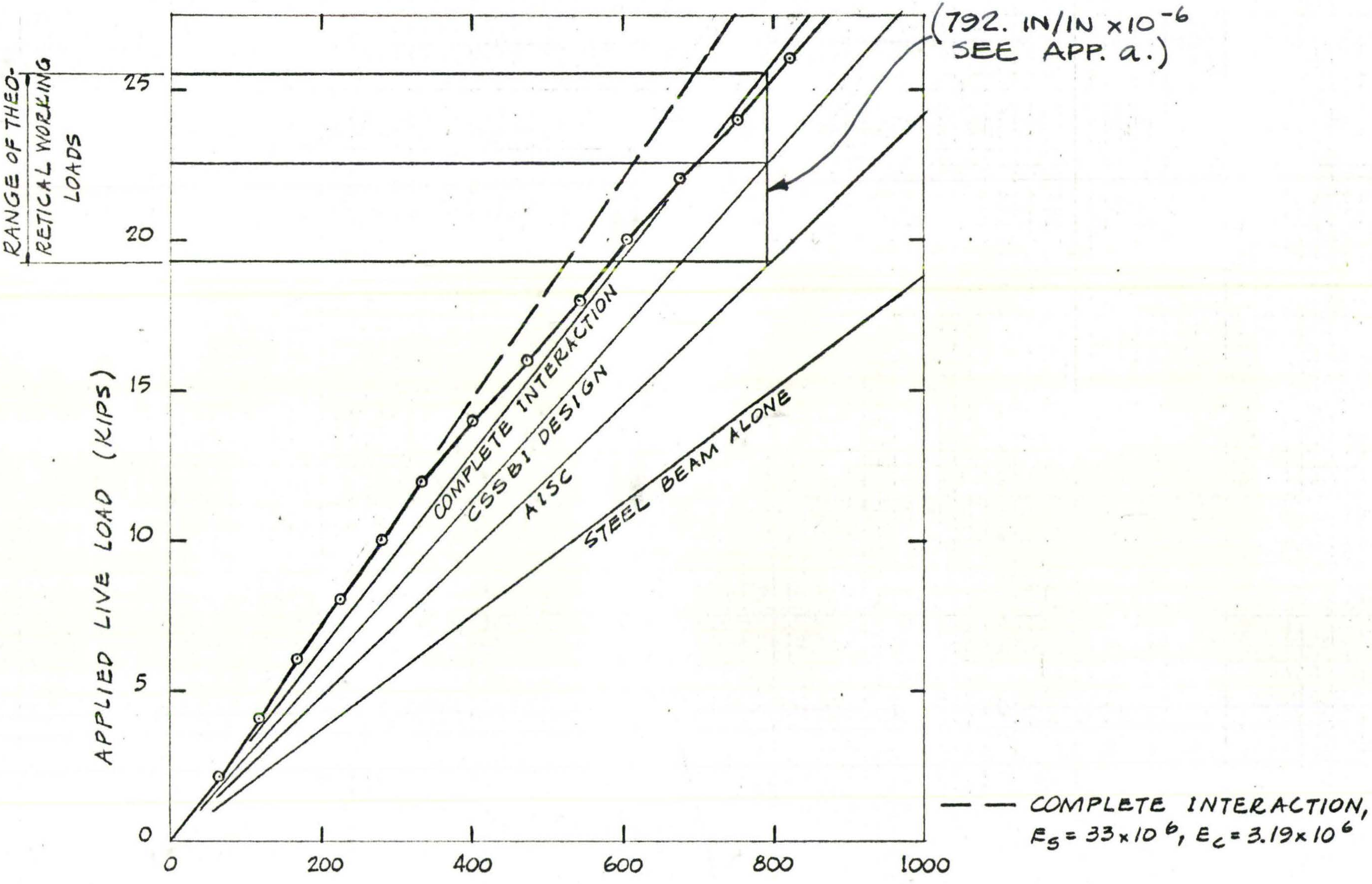

FIG. 4.3 LOAD-STRAIN BEHAVIOR UP TO WORKING LOAD BEAM 2

effective section modulus was the closest approximation to the measured working load determined on the basis of the reduced yield strain.

If, however, the yield of the steel had been 44.0 ksi, then the measured working load would have been about 25.0 kips, and both the A.I.S.C. and C.S.S.B.I. calculations would have underestimated the allowable load by 24% and 10% respectively. For most composite beams, then, the A.I.S.C. and the C.S.S.B.I. methods of analysis would be expected to give very conservative values of working load.

Fig. 4.4

Bottom Fibre Strain at Load Point vs. Applied Load - Beam 3

Beam 3 had 9 single shear connectors in the shear span.

The bottom fibre strains measured on beam 3 are lower than those of beam 1 and higher (very slightly) than those of beam 2.

The shear connection of beam 3 must therefore be stiffer than that of beam 1 and slightly weaker than the shear connection of beam 2.

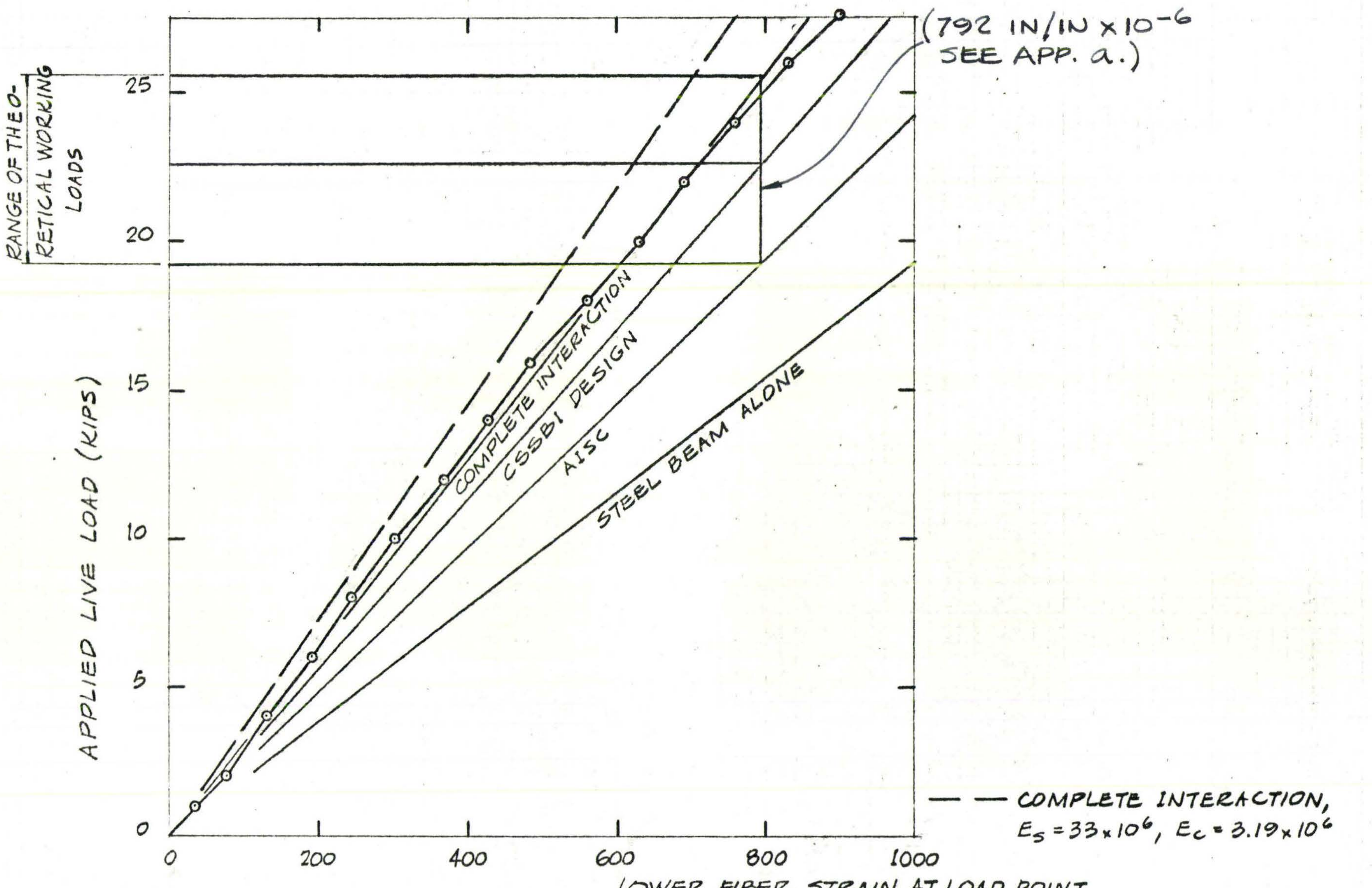

FIG. 4.4 LOAD-STRAIN BEHAVIOR UP TO WORKING LOAD
BEAM 3

Fig. 4.5

Bottom Fibre Strains at Load Point vs. Applied Load - Beam 4

The shear connection of beam 4 consisted of 12 studs in pairs in the shear span, arranged in two groups of 3 pairs. The measured bottom fibre strains of beam 4 are lower through the working load range than the strains measured for beam 2. Beam 2 had an equal number of studs, but more evenly spaced. The bottom fibre strains of beam 4 are seen to be less than those predicted by complete interaction through the working load range. The groups of studs in beam 4, therefore, provide a stiffer shear connection than do the evenly spaced studs of beam 2.

The strains predicted by the C.S.S.B.I. calculation and the strains predicted by the A.I.S.C. effective section modulus are both higher than the strains measured by about 20% and 48% respectively. This leads to an underestimation of working load if the latter is calculated by either of these procedures.

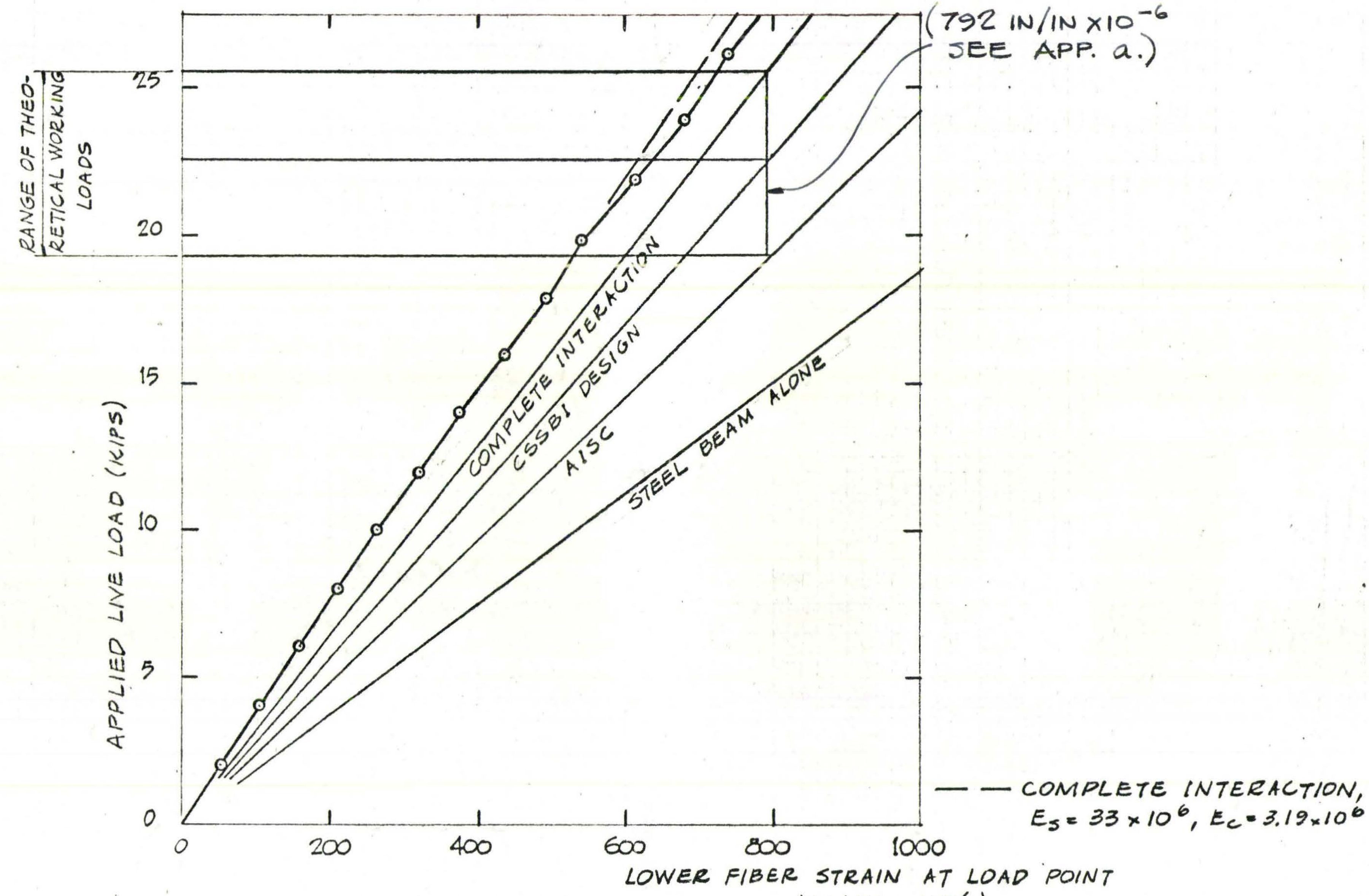

FIG. 4.5 LOAD-STRAIN BEHAVIOR UP TO WORKING LOAD BEAM 4

Fig. 4.6

Bottom Fibre Strains at Load Point vs. Applied Load - Beam 5

The slab of beam 5 is 1 in. deeper than the slabs of the other 4 beams, and the studs are 1 in. longer. The pattern of stud location is the same as that of beam 4. There are 12 studs in the shear span arranged in two groups of 3 pairs.

The strains measured on beam 5 were almost numerically identical with the strains measured on beam 4. At 25 kips, the strain of beam 5 is 730 micro-inches, and of beam 4 is 710 micro-inches. Beam 5 had a transformed area bottom fibre section modulus of 40.7 $in.^3$, whereas the bottom fibre section modulus of beam 4 was 36.9 $in.^3$ (see Appendix a). For this reason, beam 5 would have been expected to demonstrate lower strains by a factor of 36.9/40.7 = 0.907.

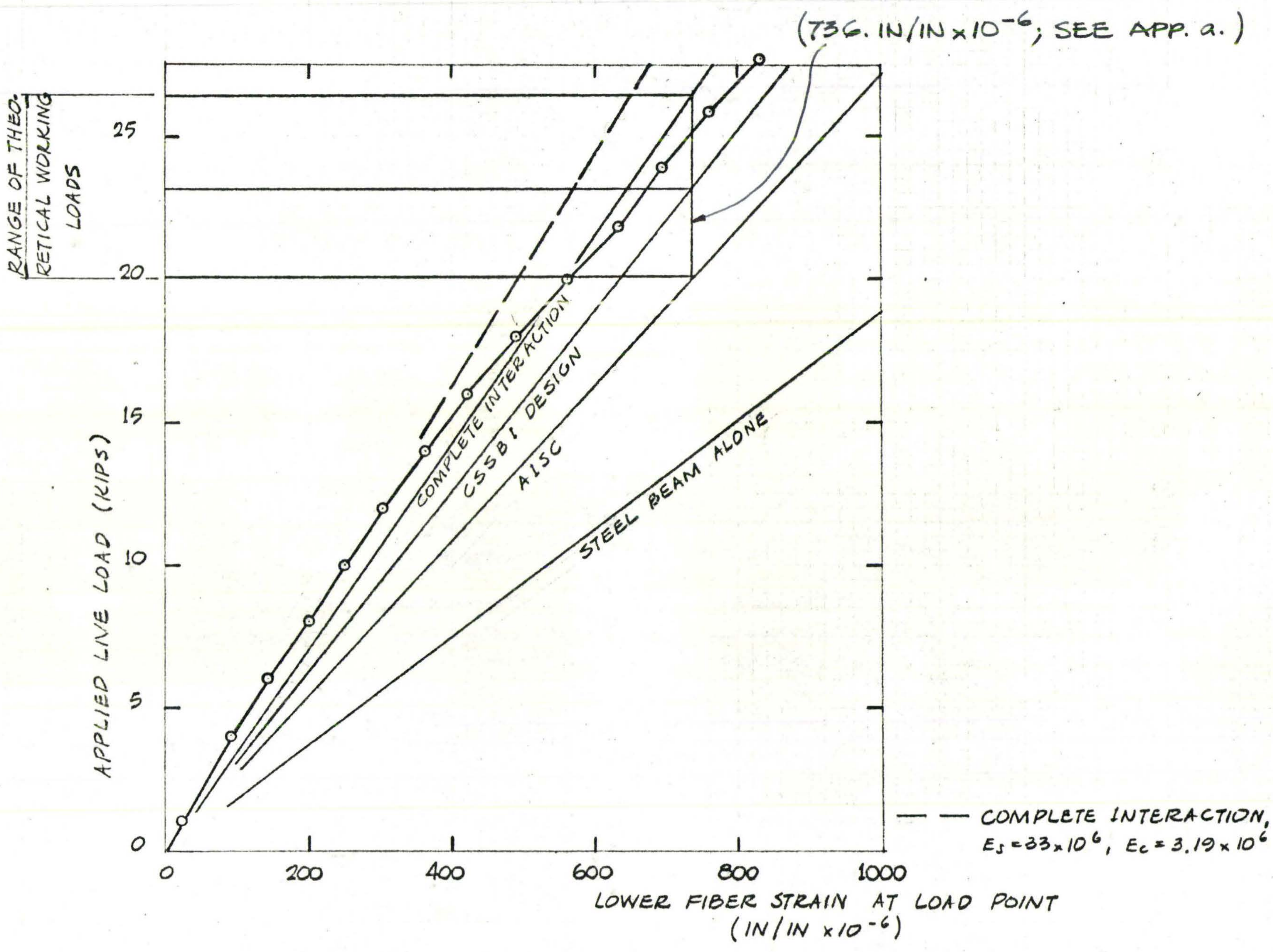

FIG. 4.6 LOAD-STRAIN BEHAVIOR UP TO WORKING LOAD
BEAM 5

Fig. 4.7a

Bottom Fibre Strains at Load Point as Calculated by the Elastic Finite Difference Method - Beams 1 and 3

An elastic finite difference analysis[9] of beam 1 was done using three trilinear shear force vs. slip relations. Interaction force, slab strains, slip, stud forces, and steel fibre strains were calculated by this method. The lower fibre steel strain for beam 1 is plotted in Fig. 4.7a, alongside the measured strains, for the three shear force vs. slip relations of Fig. 4.7b.

Curve 1 of Fig. 4.7b is closest to the push-out curve (Fig. 2.4). Using shear force vs. slip curve 1 of Fig. 4.7 b in the elastic finite difference analysis of beam 1 resulted in strains very close to those measured (see Fig. 4.7a). However, the strains calculated using this method were not sensitive to what shear force vs. slip relation was assumed for the connection. This can be seen by noticing that a doubling of the original modulus of the shear force vs. slip curve of Fig. 4.7b caused only a few percent change in strain (Fig. 4.7a).

The elastic finite difference analysis of beam 3 using the shear force vs. slip relation 2 of Fig. 4.7b resulted in a close prediction of bottom fibre strains at the load point (Fig. 4.7d).

The stud forces calculated by the elastic finite difference calculations at a total live load on the beam of 25 kips were as marked on Fig. 4.7b. Above a load of 25 kips, the composite beam cannot safely be assumed to act elastically. Therefore, the elastic finite difference calculations were not used for loads on the beams greater than 25 kips.

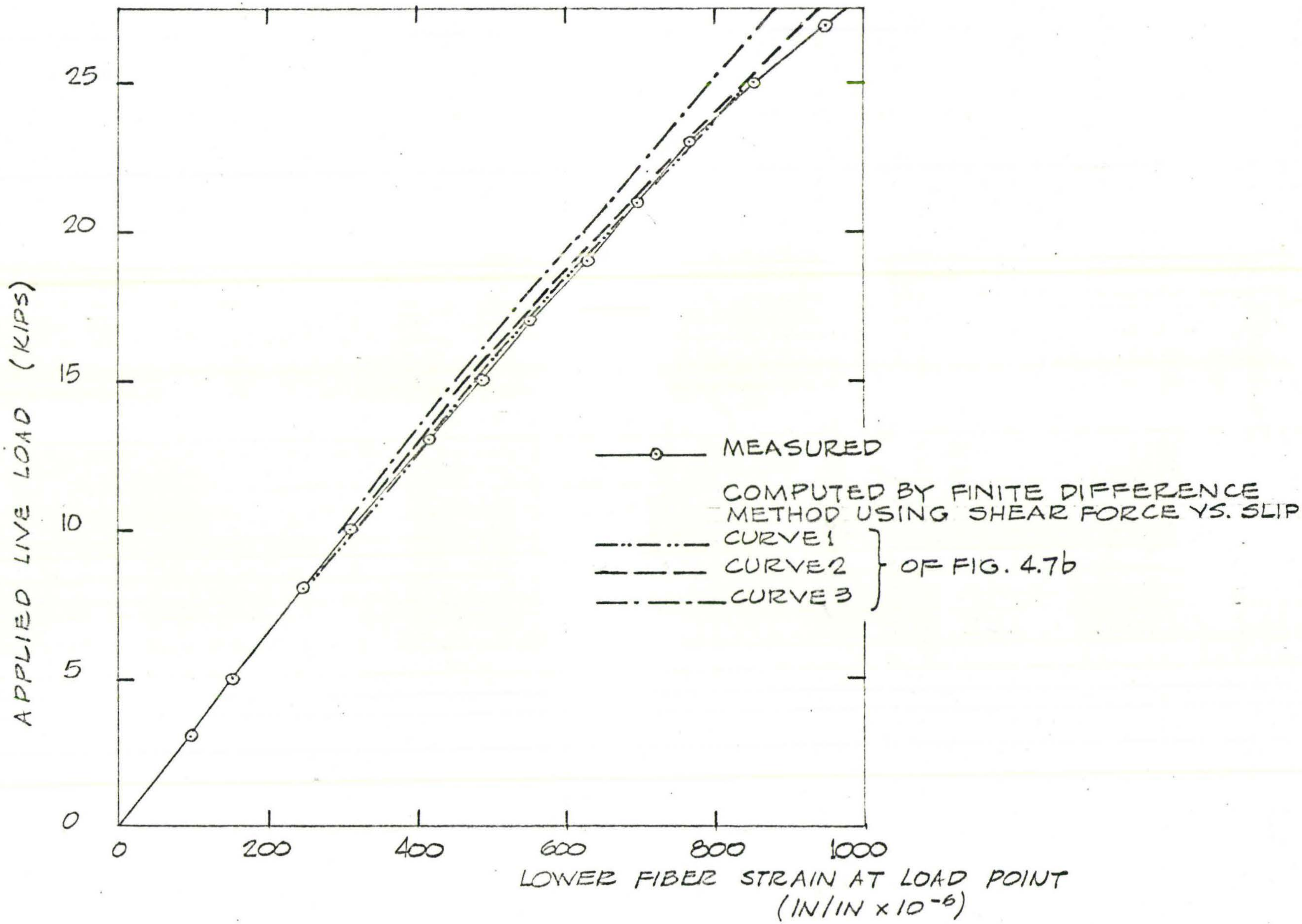

FIG. 4.7a MEASURED AND THEORETICAL LOAD-STRAIN CURVE - BEAM 1

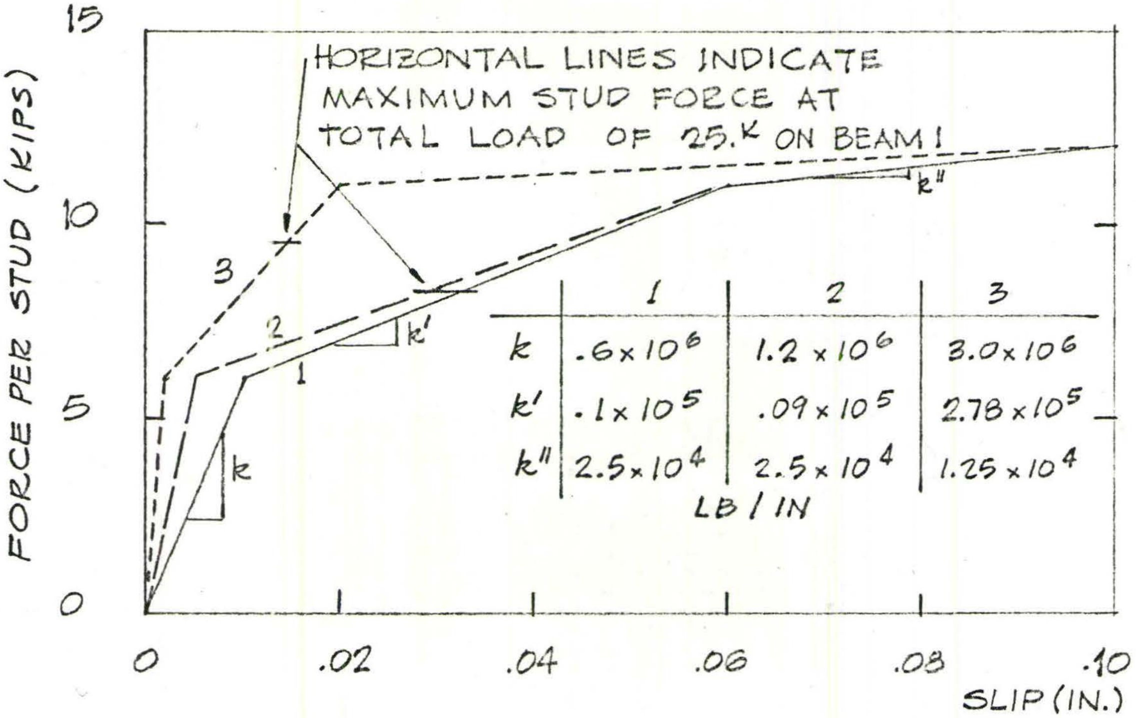

FIG. 4.7b THEORETICAL SHEAR FORCE VS. SLIP RELATIONS FOR SINGLE 3/4"φ - 3" LG. STUD CONNECTION

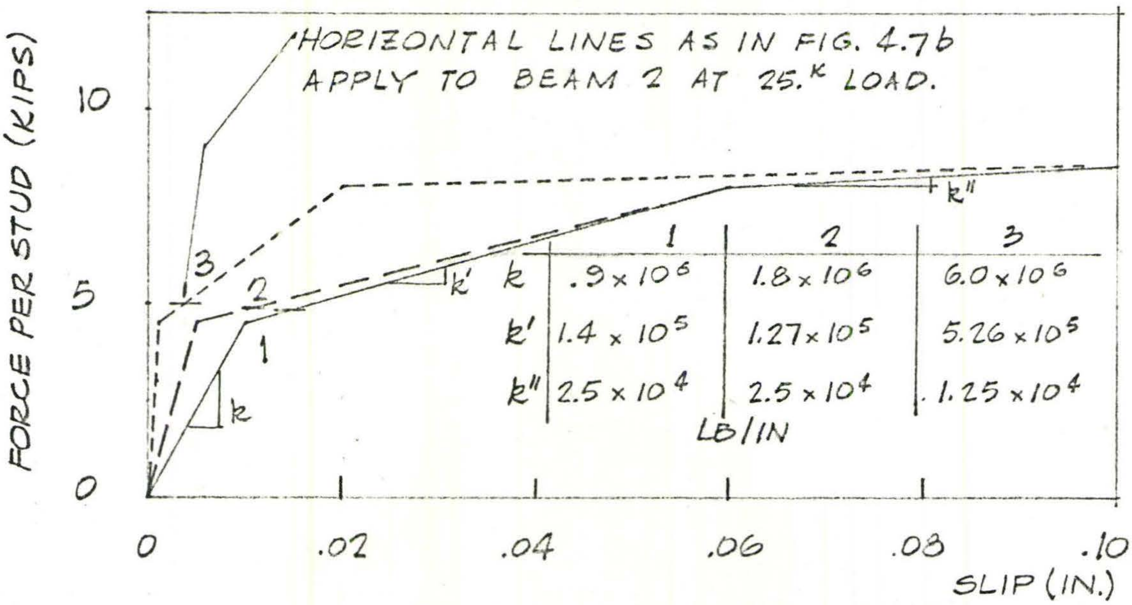

FIG. 4.7c THEORETICAL SHEAR FORCE VS. SLIP RELATIONS FOR DOUBLE 3/4"φ - 3" LG. STUD CONNECTION.

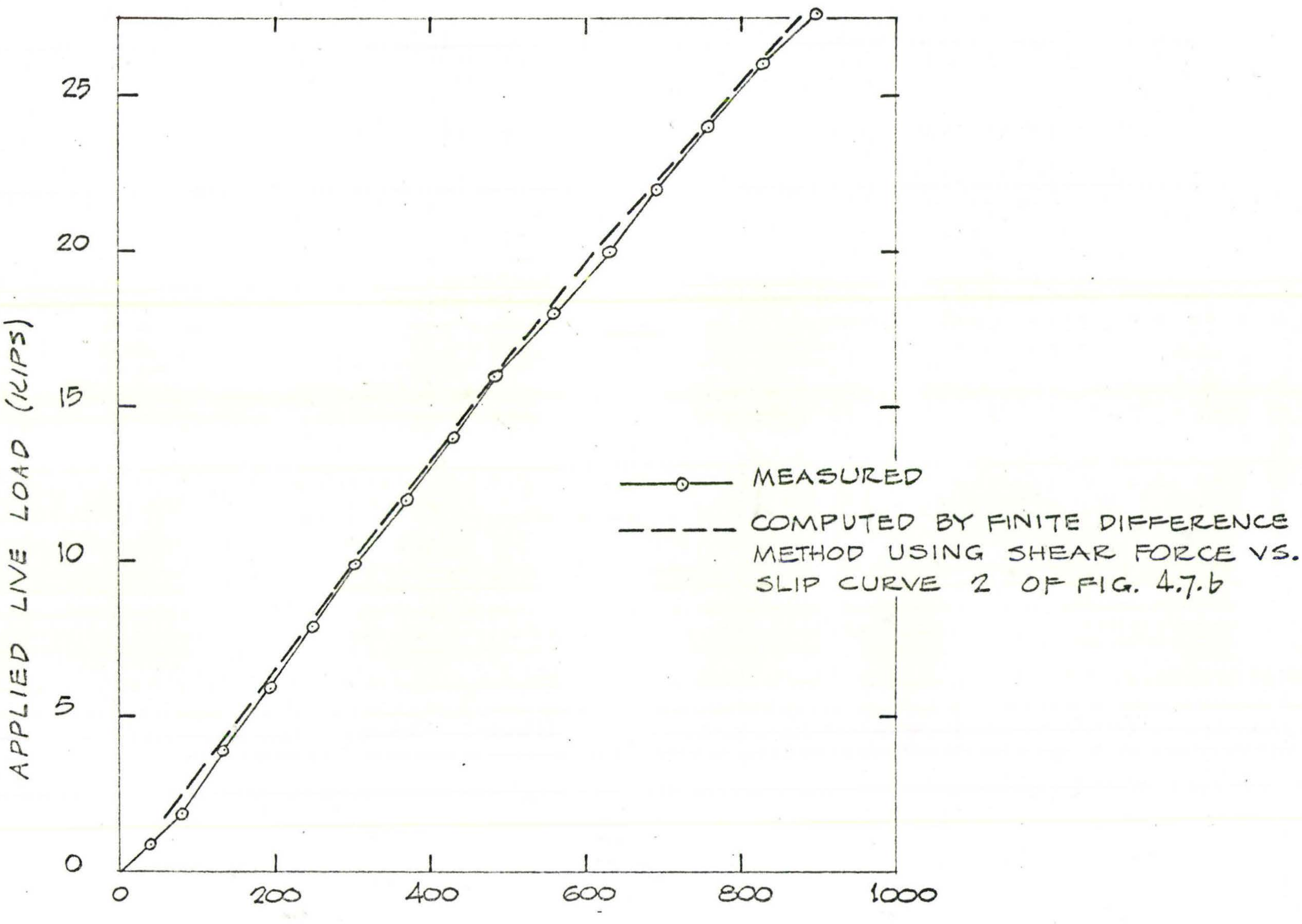

FIG. 4.7d MEASURED AND THEORETICAL LOAD-STRAIN CURVE - BEAM 3

Fig. 4.7e

Bottom Fibre Strains at Load Point as Calculated by the Elastic Finite Difference Method - Beams 2 and 4

The three shear force vs. slip relations of Fig. 4.7c were used in the elastic finite difference analysis of beam 2, resulting in the three theoretical load-strain curves of Fig. 4.7e. In this case, curve 3 of Fig. 4.7c appeared to produce strains very close to those measured. The strains so calculated were again insensitive as to which of the three shear force vs. slip relations of Fig. 4.7c was used in the analysis.

Beam 4 had the same number of studs as did beam 2 (12 in the shear span) but arranged in 2 groups of 3 pairs. Using the shear force vs. slip curve 2 of Fig. 4.7c, an elastic finite difference analysis was made of beam 4.

The strains calculated by this analysis are shown in Fig. 4.7f, and can be seen to be greater than the measured strains by about 10%. Beam 4 was stiffer than beam 2 because the measured lower fibre strains of beam 4 were less than the measured strains of beam 2.

It is evident from Fig. 4.7f that, if the elastic finite difference method of analysis is to produce the measured strains, a much stiffer shear connection will have to be used in the analysis. This is further evidence that grouped pairs of shear connectors act more rigidly than pairs of shear connectors more evenly spaced.

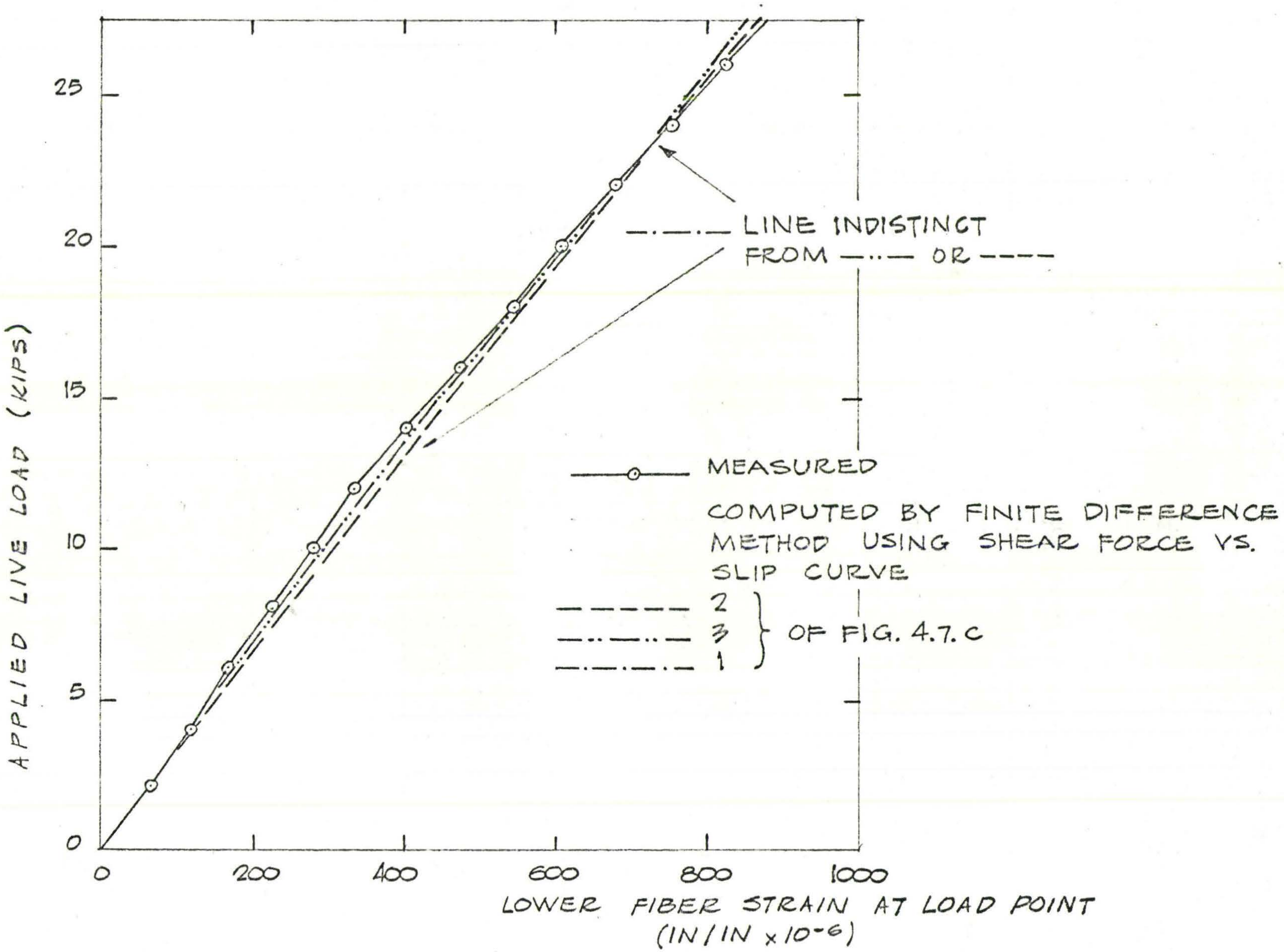

FIG. 4.7e MEASURED AND THEORETICAL LOAD-STRAIN CURVE - BEAM 2

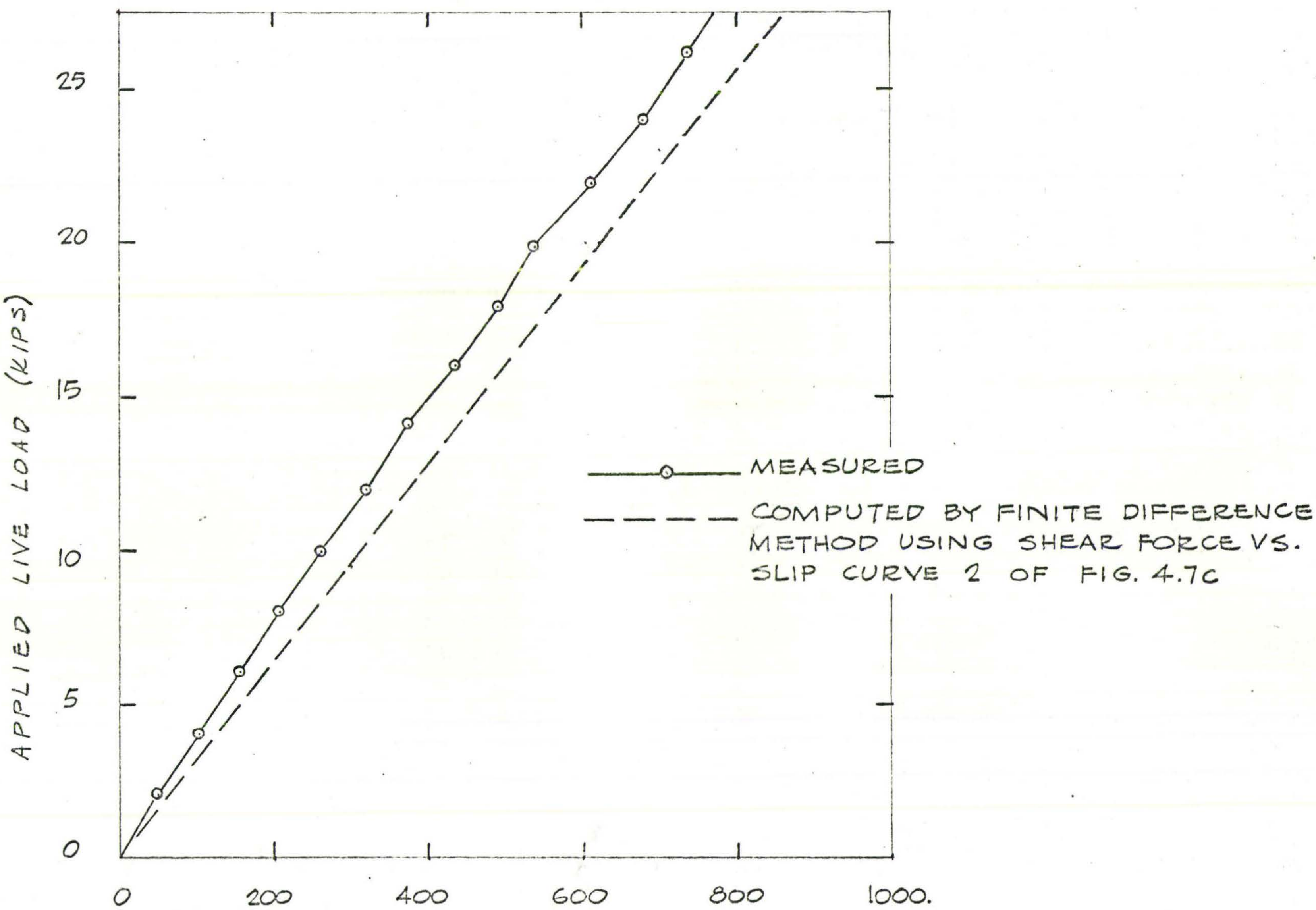

FIG. 4.7 f MEASURED AND THEORETICAL LOAD-STRAIN CURVE - BEAM 4

Fig. 4.7g

Bottom Fibre Strains at Load Point as Calculated by the Elastic Finite Difference Method - Beam 5

The two shear force vs. slip relations of Fig. 4.7h were used in the elastic finite difference analysis of beam 5. The dashed load vs. strain curve shown in Fig. 4.7g resulted from both shear force vs. slip relations shown in Fig. 4.7h.

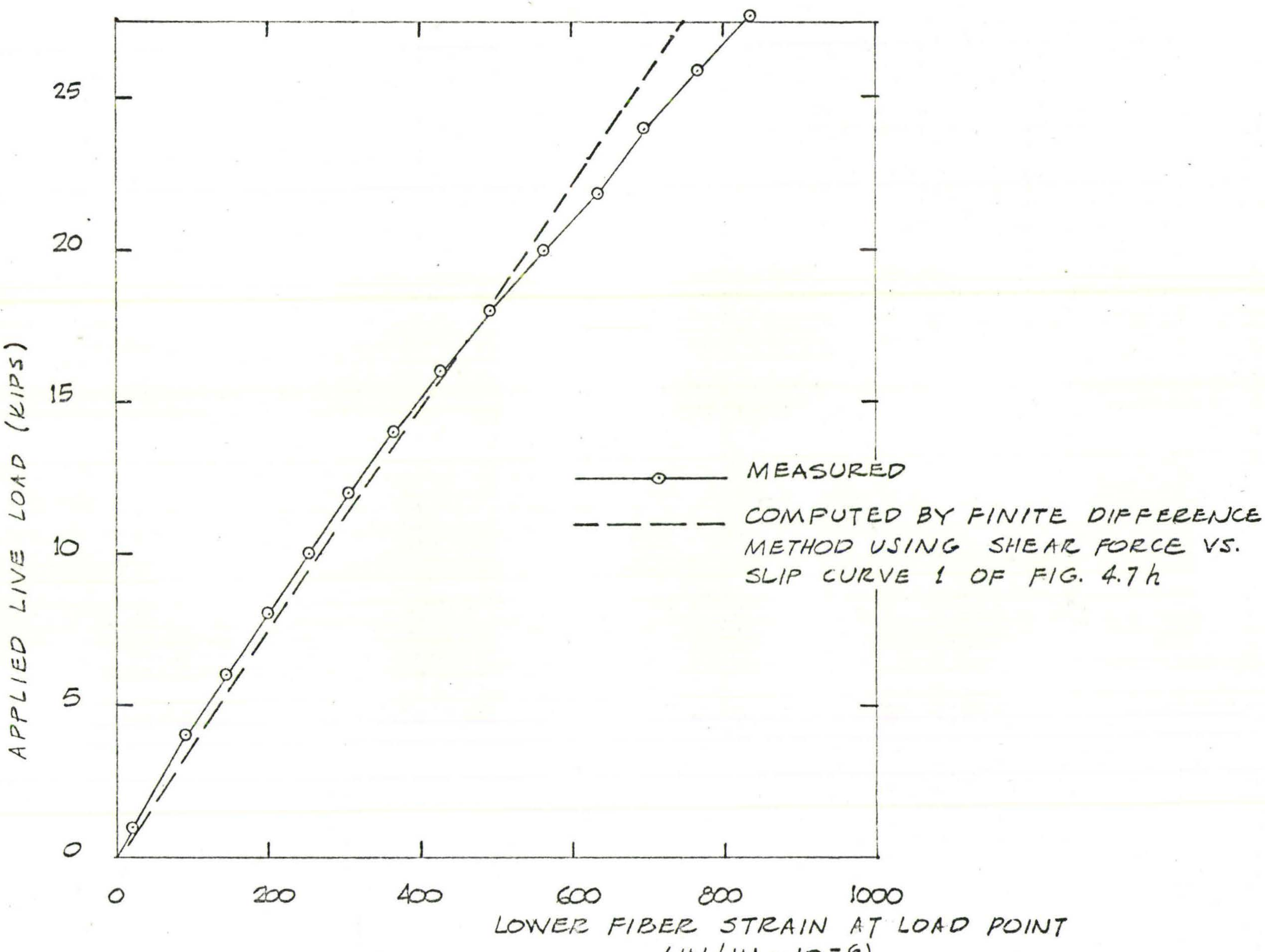

FIG. 4.7g MEASURED AND THEORETICAL LOAD-STRAIN CURVE - BEAM 5

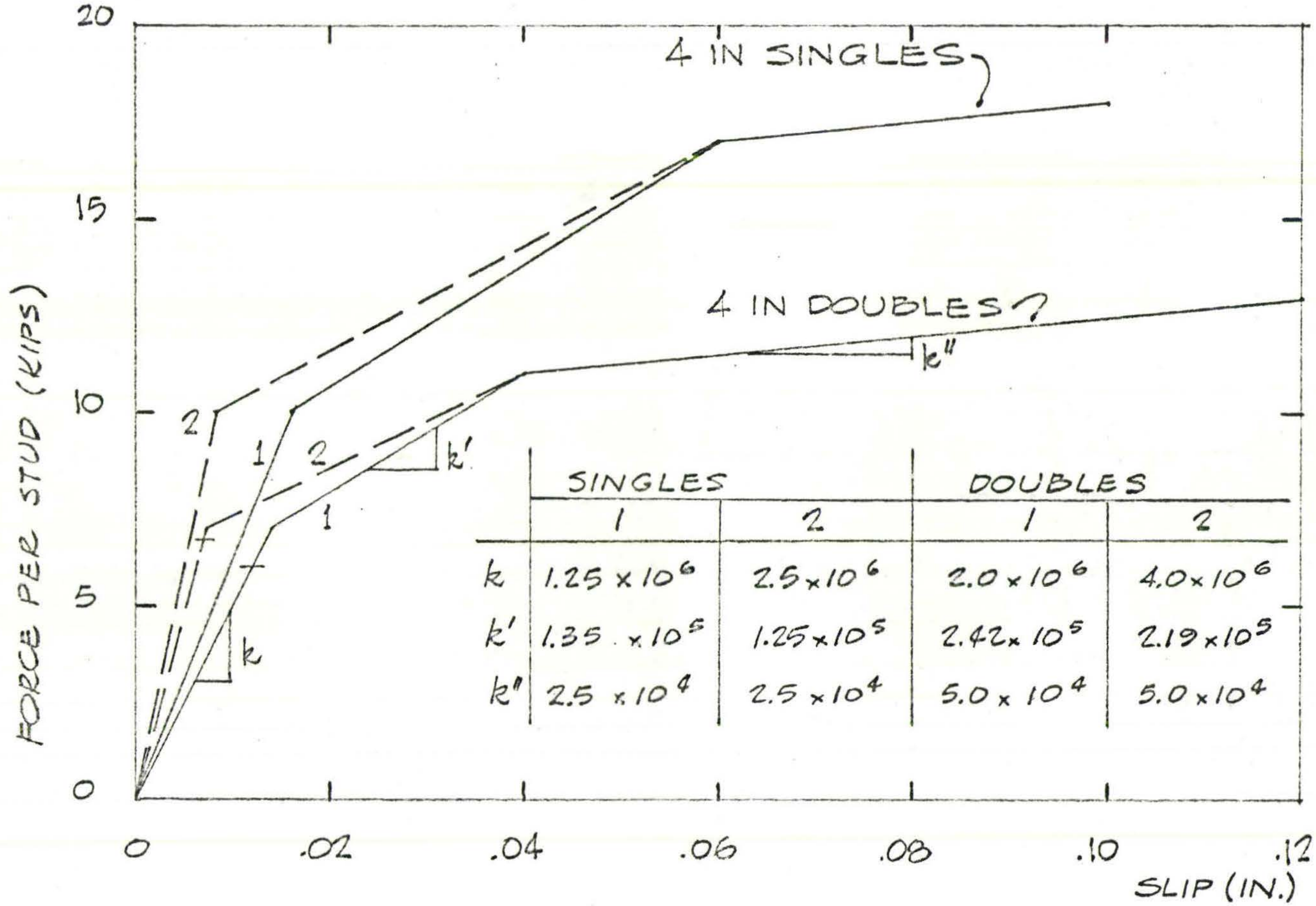

	SINGLES		DOUBLES	
	1	2	1	2
k	1.25×10^6	2.5×10^6	2.0×10^6	4.0×10^6
k'	1.35×10^5	1.25×10^5	2.42×10^5	2.19×10^5
k''	2.5×10^4	2.5×10^4	5.0×10^4	5.0×10^4

FIG. 4.7h THEORETICAL SHEAR FORCE VS. SLIP RELATIONS FOR SINGLE AND DOUBLE 3/4" - 4" LG. STUD CONNECTION

4.4 Load-Deflection Behaviour in the Working Load Range

In Figs. 4.8 to 4.12, the measured mid-span deflections of the five beams tested are presented as functions of the total applied load. On the same figures are three theoretical load-deflection lines. One, labelled "complete interaction", is calculated on the basis of the transformed section ($E_s = 29 \times 10^6$ p.s.i., n = 9). Another theoretical load-deflection line shown in Figs. 4.8 to 4.12 is calculated on the basis of the C.S.S.B.I. Manual for Composite Construction. A third load-deflection line is based on the transformed section calculated using measured material properties ($E_s = 33 \times 10^6$ p.s.i., $E_c = 3.19 \times 10^6$ p.s.i.).

In addition to these three load-deflection lines is one point marked "deflection computed by finite difference analysis". The latter point was calculated by integrating the curvature calculated by the elastic finite difference method of analysis. This was done at a load within the working load range.

Fig. 4.8

Mid-Span Deflection vs. Applied Load - Beam 1

Two load-deflection lines are drawn for complete interaction. One is for E_s equal to 33 x 10^6 p.s.i. and E_c = 3.19 x 10^6 p.s.i., as measured in the coupon tests, and the other is for E_s equal to 29 x 10^6 p.s.i. and n = 9. The latter represents the usual design value of E and n. The two complete interaction lines are drawn to indicate the sensitivity of the transformed section calculations.

The measured deflection is seen to be everywhere greater than the deflection calculated on the basis of complete interaction using either theoretical or measured material properties.

This measured result, when compared with the measured strains of Fig. 4.2 which are approximately equal to those for complete interaction, shows a greater loss of efficiency for deflection than for strains.

The deflection calculated on the basis of the C.S.S.B.I. Manual overestimates the deflection by only about 5%.

The finite difference elastic analysis of beam 1 gives the top and bottom steel fibre strains everywhere along the beam, constant through intervals of beam length between connectors. The curvature of the steel beam was calculated from these steel strains, and piece-wise integrated over half the length of the beam to yield deflection at mid-span. This deflection is shown on Fig. 4.8 as a crossed square at a load of 25 kips, and is seen to be 13% greater (0.61 in. compared to 0.525 in. measured) than the measured deflection at this load. This discrepancy is very likely because the elastic finite difference method does not predict the upper fibre steel strains accurately.

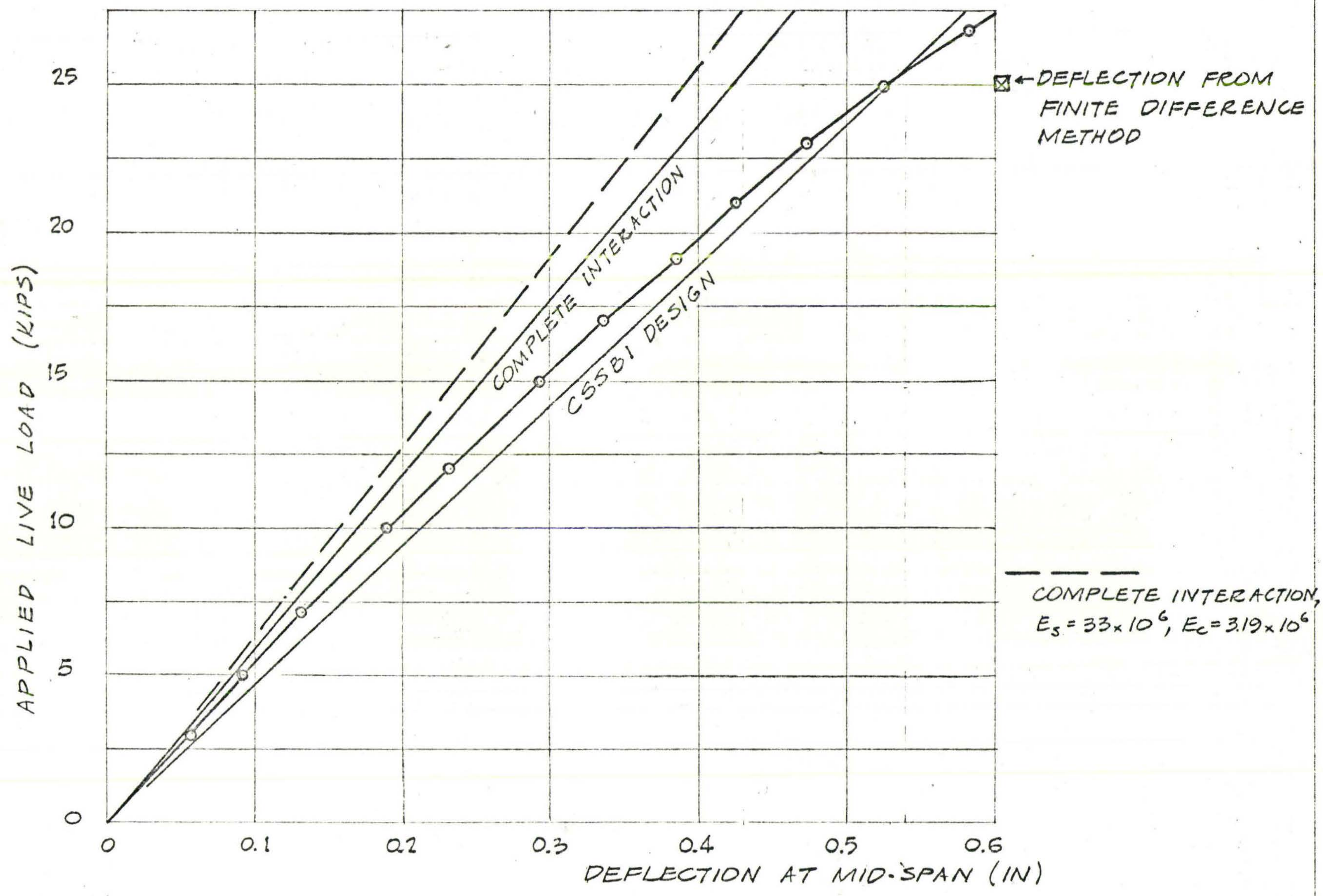

FIG. 4.8 MEASURED AND THEORETICAL LOAD-DEFLECTION CURVES - BEAM 1

Fig. 4.9

Mid-Span Deflection vs. Applied Load - Beams 2, 3, 4, 5

In this figure, and in the figures 4.10, 4.11, and 4.12 to follow, the measured deflections were slightly greater than the deflection predicted by complete interaction. The deflections calculated by the C.S.S.B.I. Manual are about 10% greater than the measured deflections. The deflection calculated using the strains of the finite difference elastic method of analysis agrees very closely with the measured deflection, except for beam 5 where it is lower than the measured deflection.

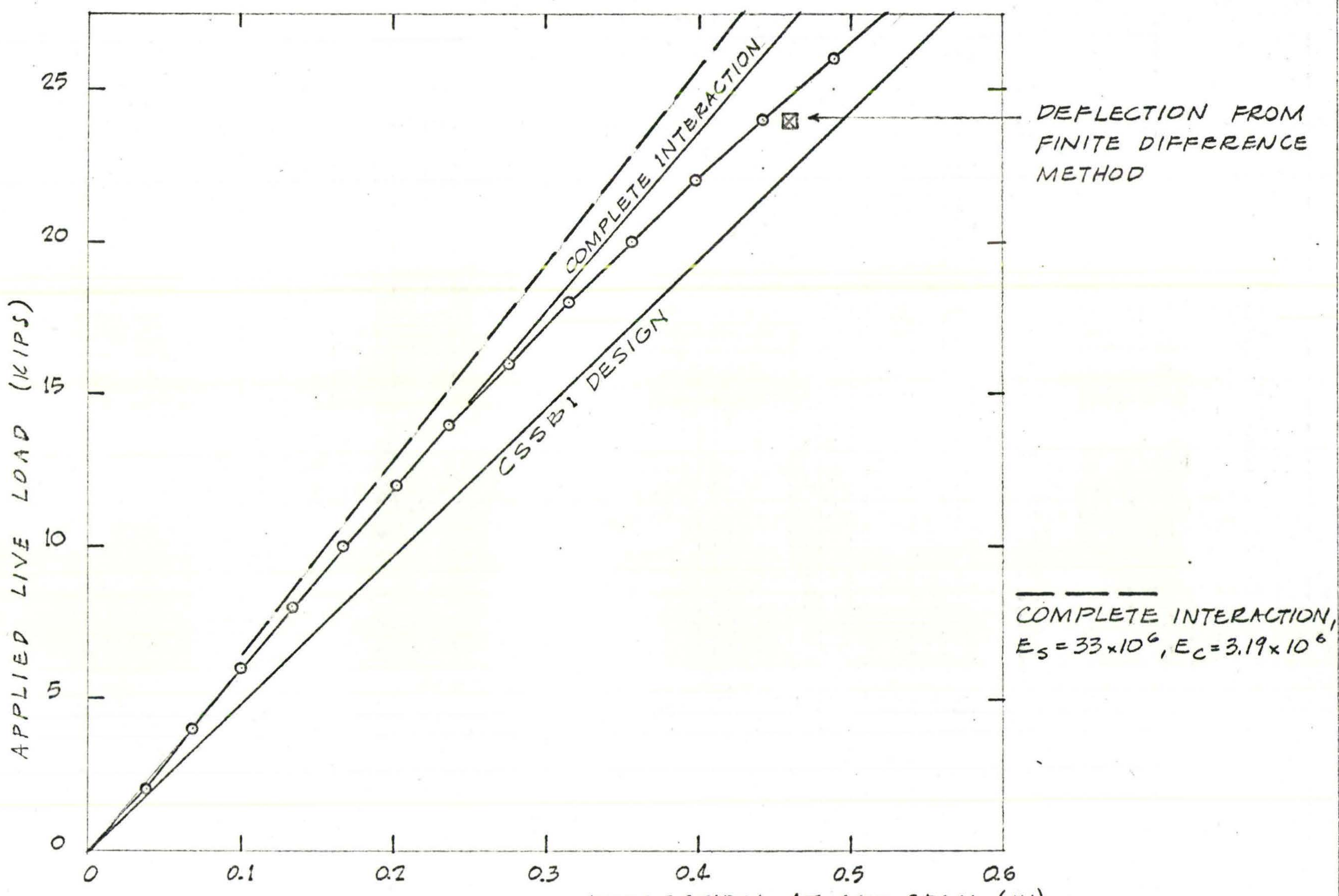

FIG. 4.9 MEASURED AND THEORETICAL LOAD-DEFLECTION CURVES - BEAM 2

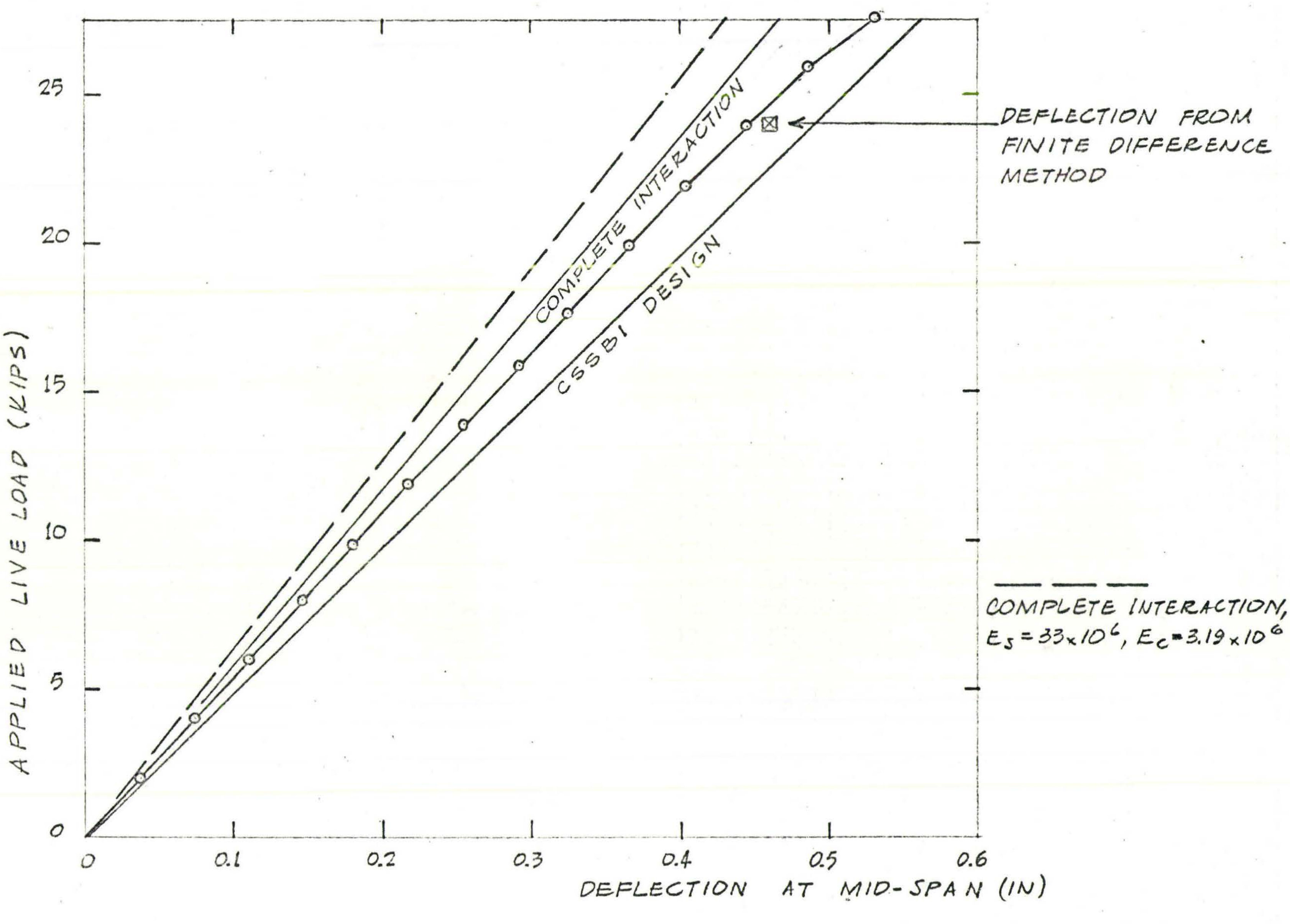

FIG. 4.10 MEASURED AND THEORETICAL LOAD-DEFLECTION CURVES - BEAM 3

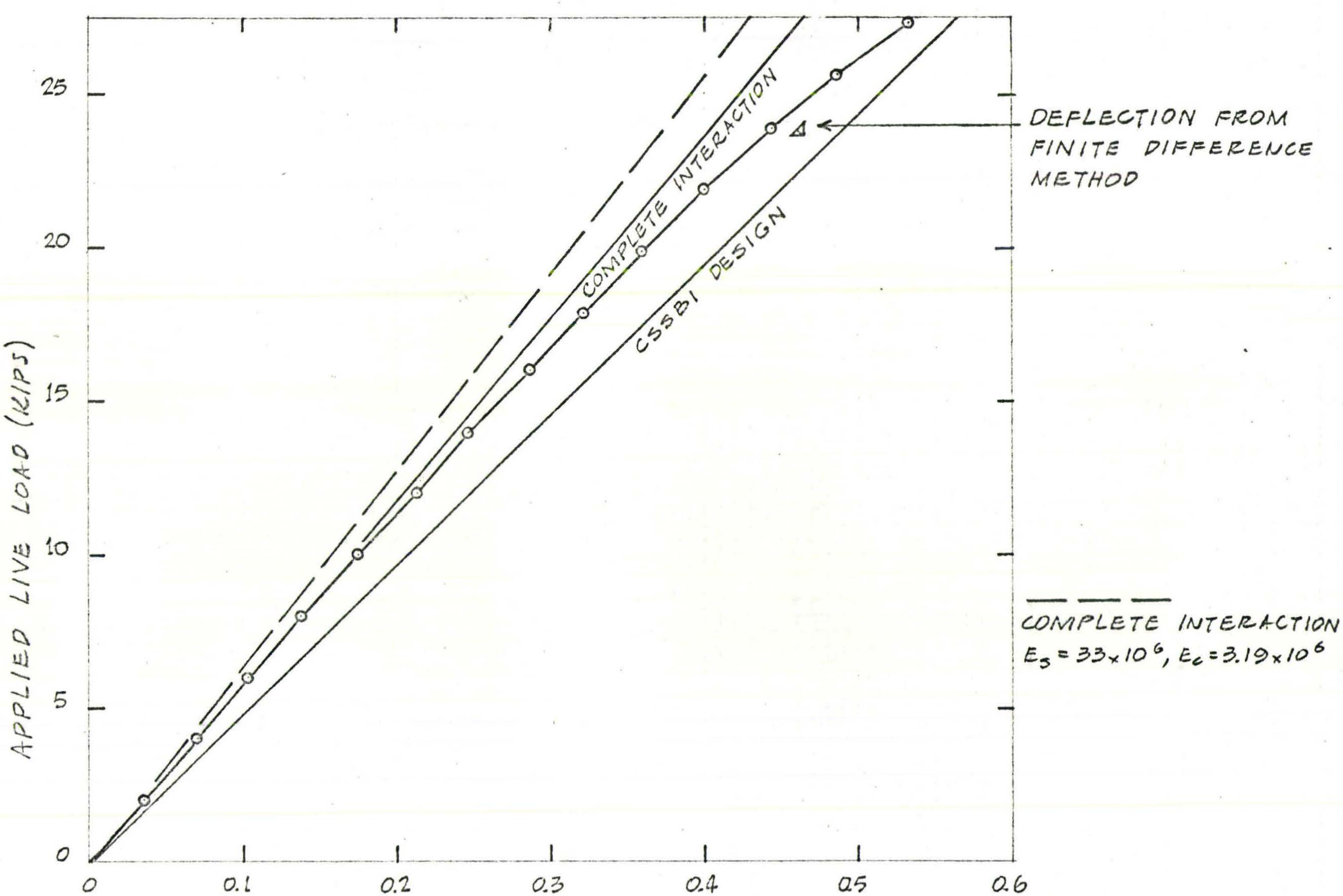

FIG. 4.11 MEASURED AND THEORETICAL LOAD-DEFLECTION CURVES - BEAM 4

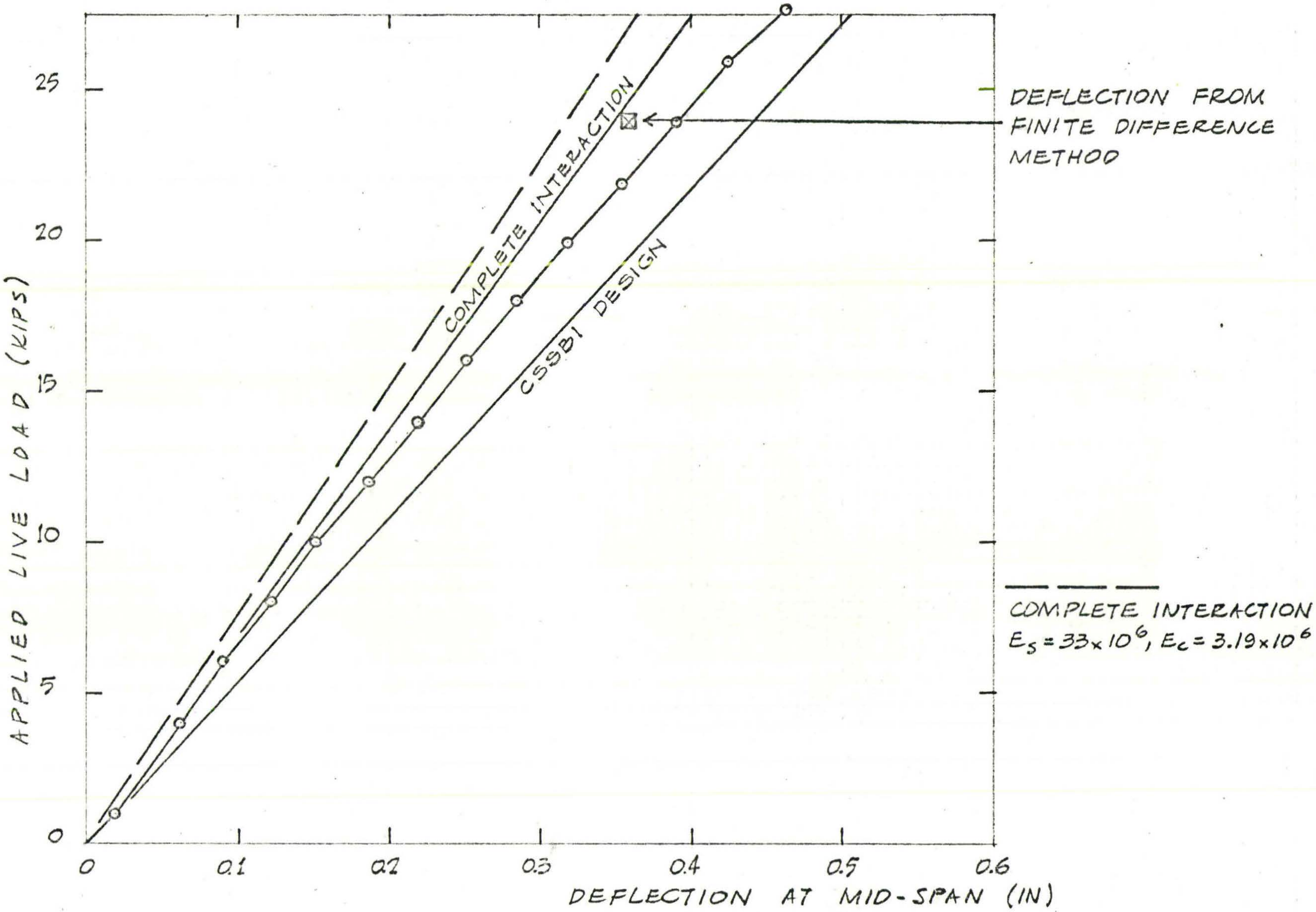

FIG. 4.12 MEASURED AND THEORETICAL LOAD-DEFLECTION CURVES - BEAM 5

4.5 Curvature Along the Beam in the Working Load Range

The measured curvaturesalong the beam are presented for each of the five beams tested in Figs. 4.13 to 4.17 to follow. The measured curvature was calculated from the strain gauge data by dividing the strain difference across the depth of the steel beam by the depth of the steel beam. Therefore, the measured curvatures presented represent the curvatures of the steel beam. However, the curvatures of the steel beam and the concrete slab would be approximately equal, since they deflect equally.

The measured curvatures are presented as broken lines in the following figures.

The curvatures in Figs. 4.13 to 4.17 that are drawn by stepped solid lines are a result of analyses of the beams by the elastic finite difference method. This analysis assumes the curvatures of the steel beam and concrete slab are equal, and that the strains and curvatures remain constant over the intervals of length between studs. Hence, the calculated curvatures presented as solid lines in the following figures are stepped, increasing or decreasing at every stud location.

Fig. 4.13

Curvature along the Beam at a Total Applied Live Load of 25 kips - Beam 1

Curvature of the steel beam is the strain difference across the depth of the steel beam divided by the depth of the steel beam. Curvature is non-dimensional and is plotted as the ordinate of Fig. 4.13 incorporating a multiple of 10^6.

The dashed line connecting circular points represents the curvature measured by strain gauges during testing of the beam. Strain gauges were mounted on the top and bottom flanges of the steel beam at the mid-interval point of every interval between studs.

The stepped solid line represents the curvature as calculated by the finite difference elastic analysis of beam 1 (using the shear force vs. slip relation 2 of Fig. 4.7b). This method assumes constant strains and therefore constant curvature across an interval between connectors.

The calculated curvature gradient through the shear span compares well with the measured curvature gradient. Both the calculated and measured curvatures reach a maximum slightly outward of the load point, although the calculated curvature at the load point is 21% higher than the measured curvature. This difference between calculated and measured curvature in the region of the load point accounts for the discrepancy between calculated deflection and measured deflection in Fig. 4.8.

The discrepancy between calculated and measured curvature in the region of the load point on beam 1 indicates that a stiffer shear-force vs. slip relation could have been used in this region of the beam.

No explanation was found for the sudden variations in measured curvature through the shear span.

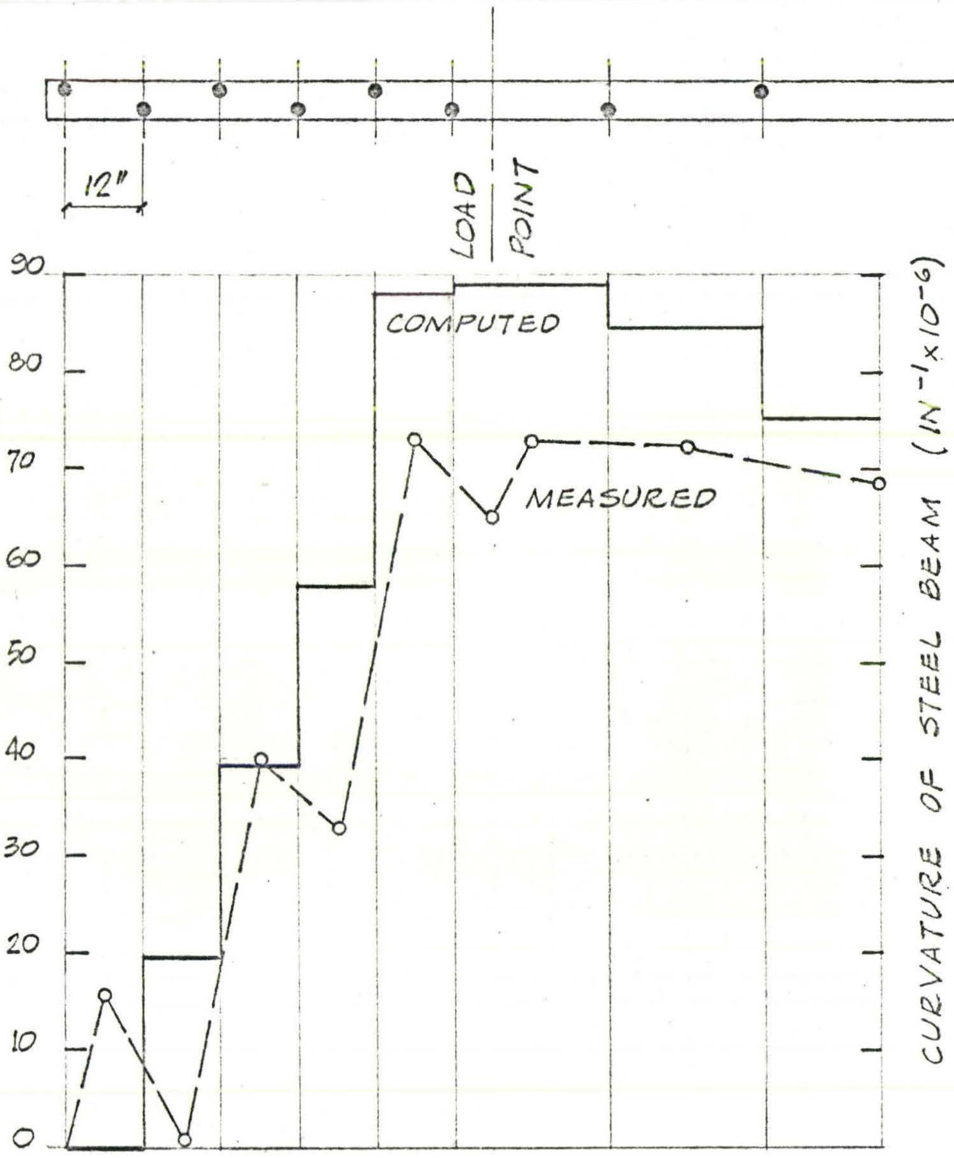

FIG. 4.13 MEASURED AND COMPUTED CURVATURES - APPLIED LOAD OF 25 KIPS - BEAM 1

Fig. 4.14, 4.15, 4.16, 4.17

Curvature Along the Beam at a Total Applied Live Load of 24 kips - Beams 2, 3, 4, 5

The curvatures computed using the elastic finite difference method for these four beams are in better agreement with the measured curvatures than were the curvatures computed for beam 1.

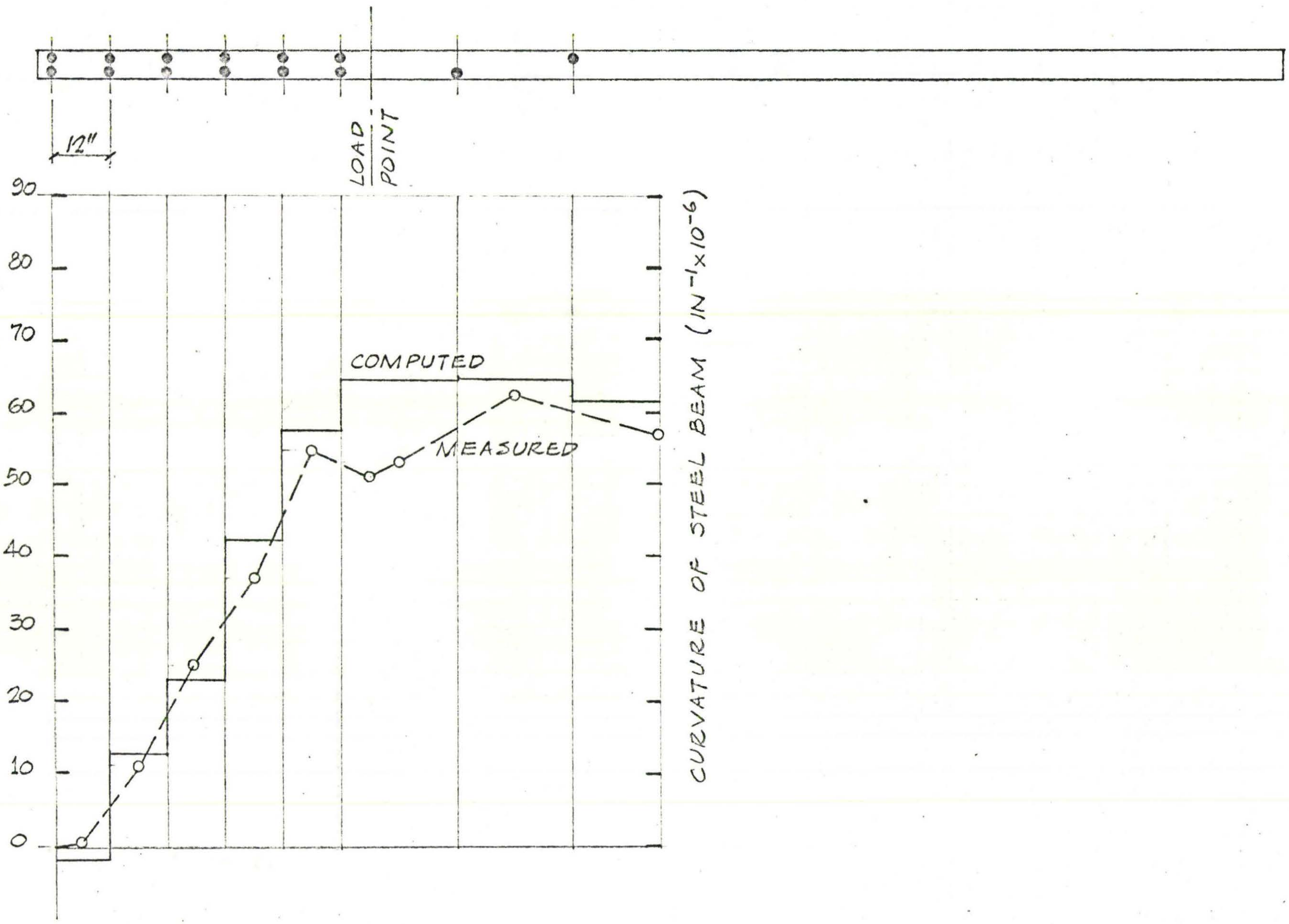

FIG. 4.14 MEASURED AND COMPUTED CURVATURES - APPLIED LOAD OF 24 KIPS - BEAM 2

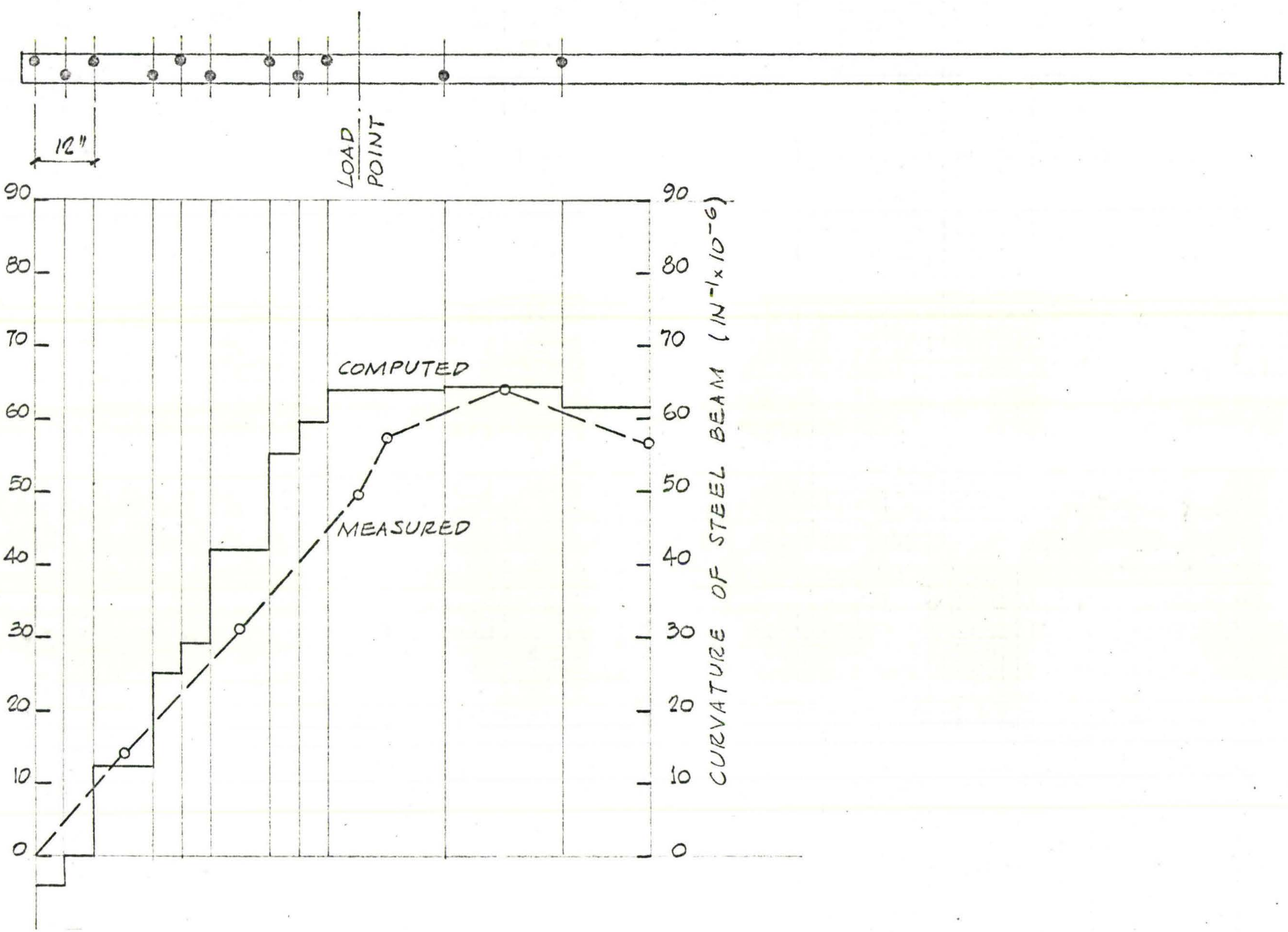

FIG. 4.15 MEASURED AND COMPUTED CURVATURES-
APPLIED LOAD OF 24 KIPS - BEAM 3

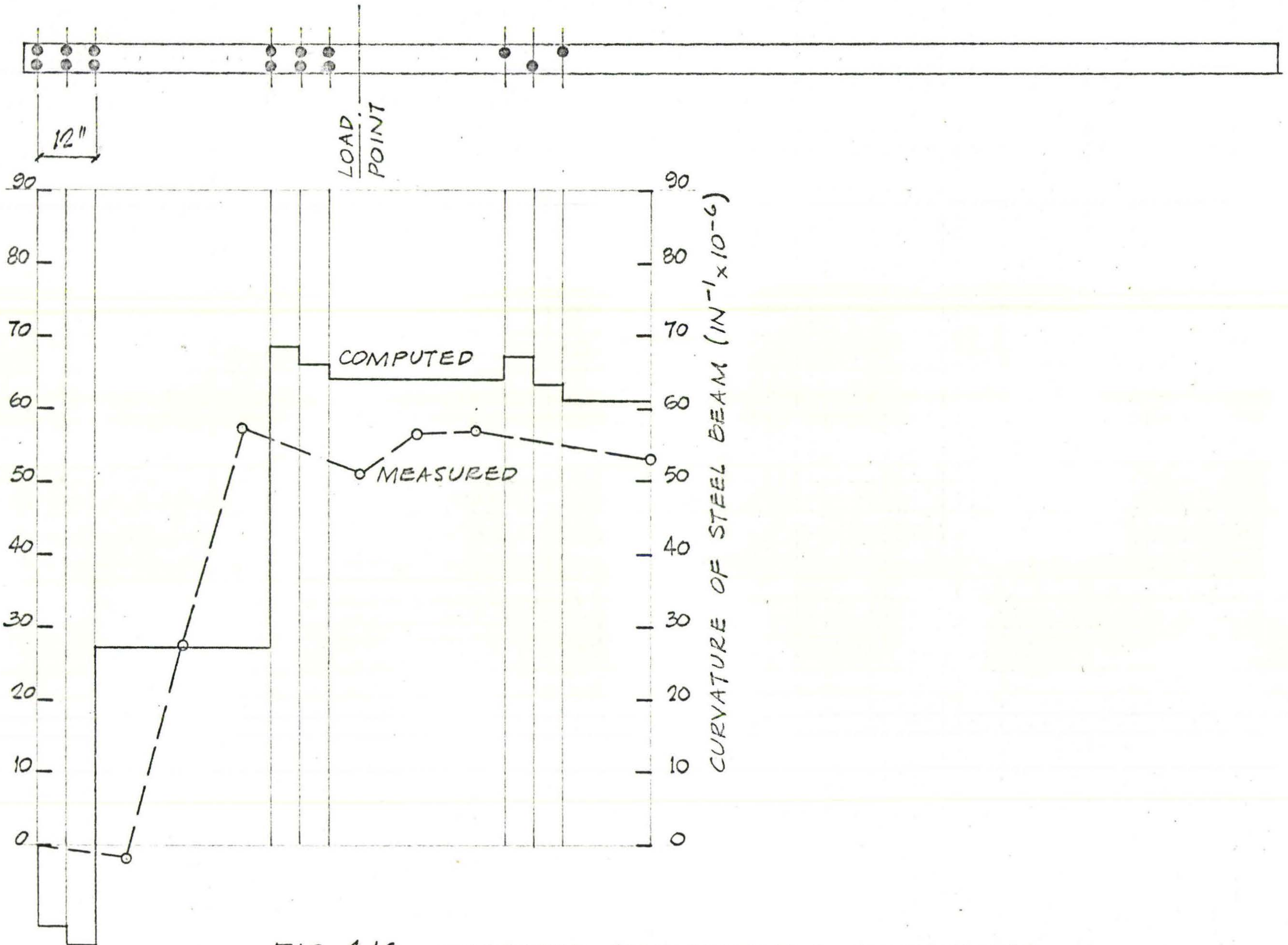

FIG. 4.16 MEASURED AND COMPUTED CURVATURES - APPLIED LOAD OF 24 KIPS - BEAM 4

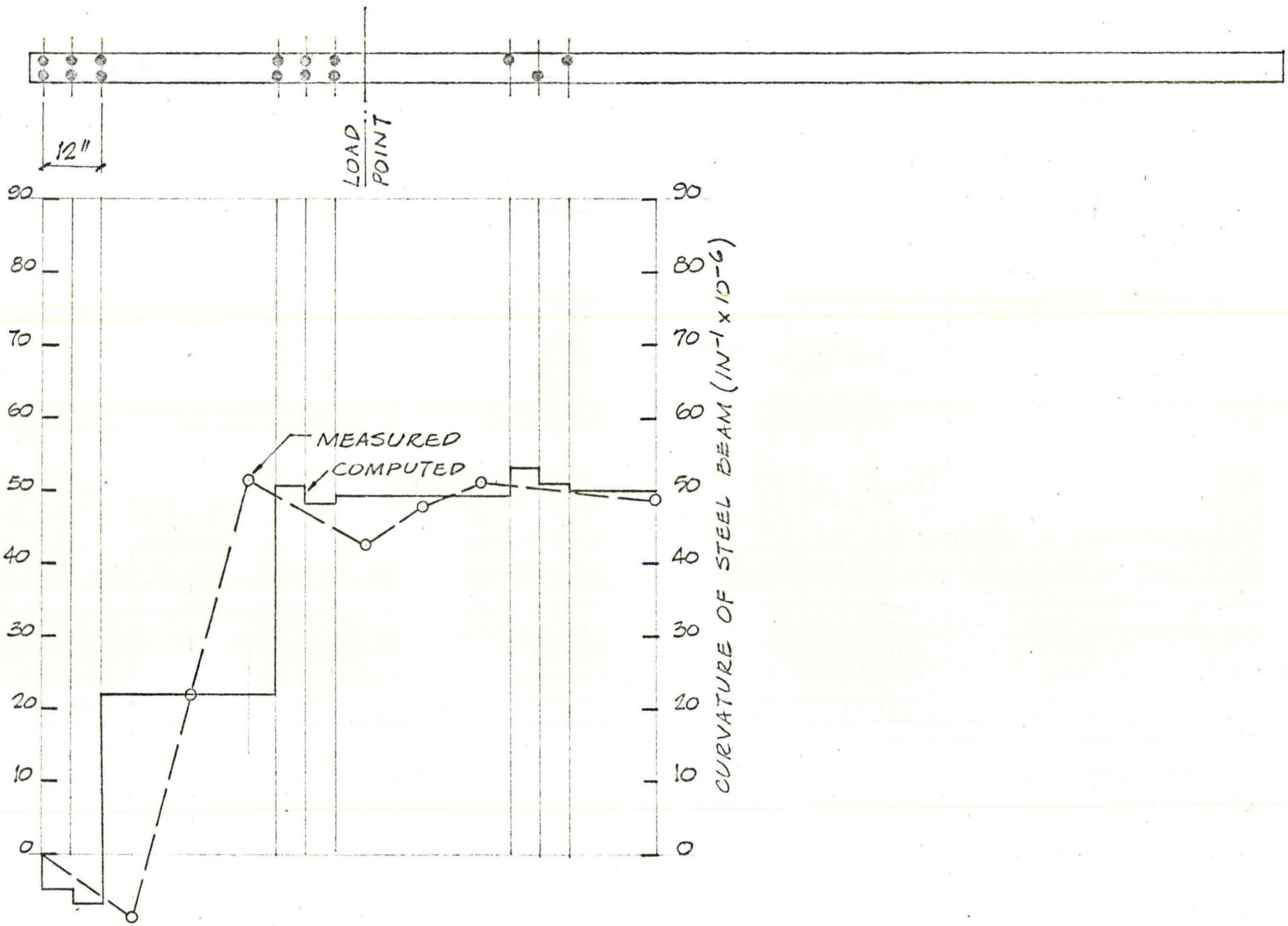

FIG. 4.17 MEASURED AND COMPUTED CURVATURES - APPLIED LOAD OF 24 KIPS - BEAM 5

4.6 Stud Forces in the Working Load Range

The forces acting on the stud shear connectors could not be measured explicitly. However, they can be measured implicitly by measuring the strain profile of the steel beam on each side of the shear connector. The strain profile was measured on each side of each shear connector of beams 1 and 2. The strain gauges of beams 3, 4, and 5 were spaced several studs apart, so for beams 3, 4, and 5 the stud forces could not be calculated from the measured strains.

For beams 1 and 2, the net axial force in the steel beam was calculated from the measured strain data on each side of the shear connectors. This was accomplished by summing the measured strain multiplied by Young's Modulus and the area of the steel beam, and dividing the product by the depth of the steel beam.

At any cross-section, the net axial force in the steel beam must equal the net axial force in the concrete slab. The difference in net axial forces between adjacent cross-sections is the (longitudinal shear) force that must be acting on the stud.

For beams 1 and 2, the stud forces so calculated are written in along the top of each graph (Fig. 4.18, 4.19) and represent forces in kips.

It is possible to calculate the theoretical stud forces by means of the elastic finite difference analysis, taking into account different stud spacing and different connection shear force vs. slip relations.

The stud forces calculated by means of the elastic finite difference method are drawn as solid lines on the following five graphs, Figs. 4.18 to 4.22.

Fig. 4.18

Stud Forces as Calculated by the Finite Difference Elastic Analysis - Beam 1

The stud forces in kips per stud at an applied load of 25 kips on the beam are shown by the solid line. These stud forces were calculated by means of the finite difference elastic analysis using the shear force vs. slip relation for a single 3" stud as shown in Fig. The same shear force vs. slip relation was used to calculate the strain, deflection, and curvature of beam 1, Figs.

The stud forces as calculated at a load of 25 kips on the beam show the force on the stud increases smoothly from zero at mid-span to about 8 kips through the shear span.

The ordinates of the solid curve of Fig. 4.18 can be compared to the stud forces as calculated from the measured steel strain data. This was done by summing the measured strains multiplied by Young's Modulus across the depth of the steel beam (negative for compressive strains, positive for tensile strains). The net axial force so obtained in the steel beam is equal to the axial force in the concrete slab. This strain summation was done at all cross-sections where strain gauges were applied and monitored (see Fig. 3.3).

The compressive force in the concrete slab, when calculated in this manner, varied from cross-section to cross-section. Clearly, the shear connectors cause this change in compressive force. By subtracting adjacent slab forces, the force on the intervening shear connector was derived.

The stud forces, calculated from the measured steel strains, are shown in Fig. 4.18 above the theoretically calculated curve. The

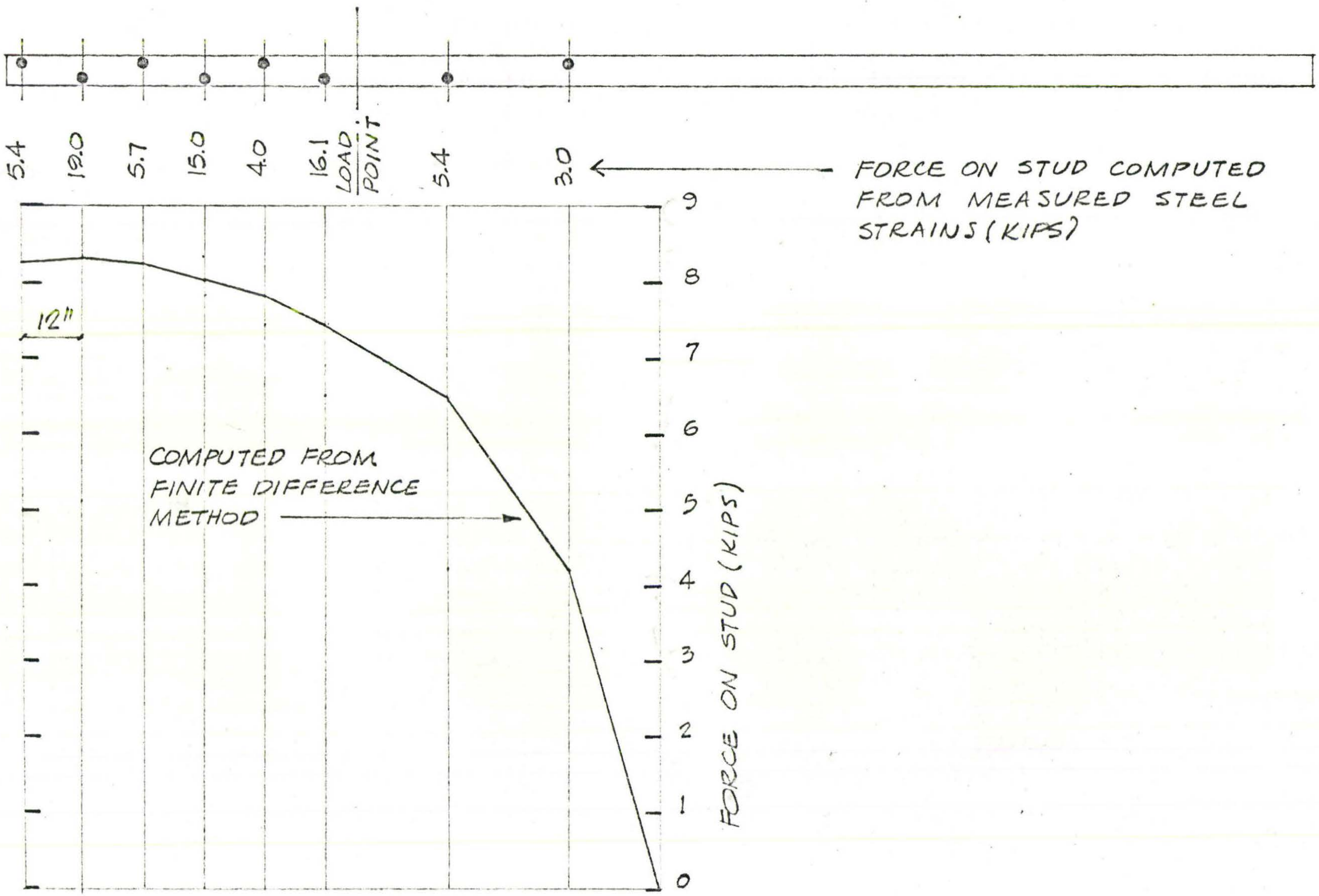

FIG. 4.18 FORCES ON SHEAR CONNECTORS- LOAD OF 25 KIPS, BEAM 1

measured stud forces apparently vary from 4.0 to 19.0 kips in the shear span, while the calculated stud forces vary only from 7.4 to 8.3 kips. Such a scatter in the implicitly measured stud forces probably means the measured strain data is faulty. However, this is not conclusive proof.

Fig. 4.19

Stud Forces as Calculated by the Finite Difference Elastic Analysis - Beam 2

The calculated stud forces for an applied load of 25 kips are shown in Fig. 4.19 as the solid line, while the measured stud forces are plotted as separate points. The measured values of stud forces have some range because the measured strains varied across the bottom flange. The extremes of stud forces were computed from the maximum and minimum possible measured strain differences across the depth of the steel beam.

The agreement between measured and calculated stud forces is very good in beam 2 except in the shear span just outward of the load point. In this area, the measured stud forces are as much as 60% higher than those calculated.

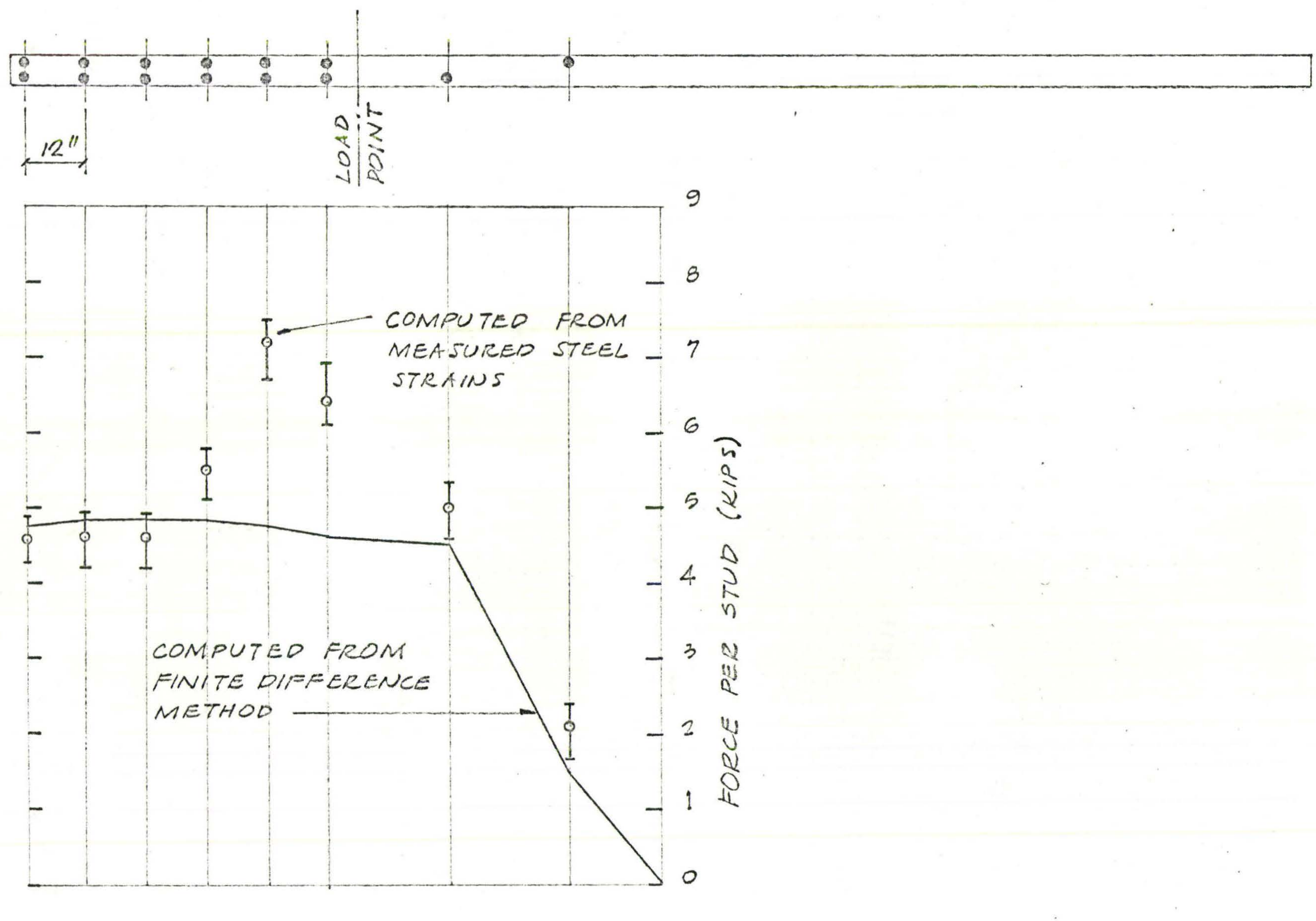

FIG. 4.19 FORCES ON SHEAR CONNECTORS - LOAD OF 25 KIPS, BEAM 2

Fig. 4.20

Stud Forces as Calculated by the Finite Difference Elastic Analysis - Beam 3

The calculated stud forces are almost constant through the shear span at 6.4 kips. This figure can be compared to the shear force of about 8 kips per stud in the shear span of beam 1 at the same applied load on the beam.

The strain profile of the steel beam was measured only in the 12" intervals (see Fig. 3.1), so the measured stud force per group of 3 connectors could only be calculated. These figures are shown on Fig. 4.20 averaged for 3 studs, and are written in above the calculated curve.

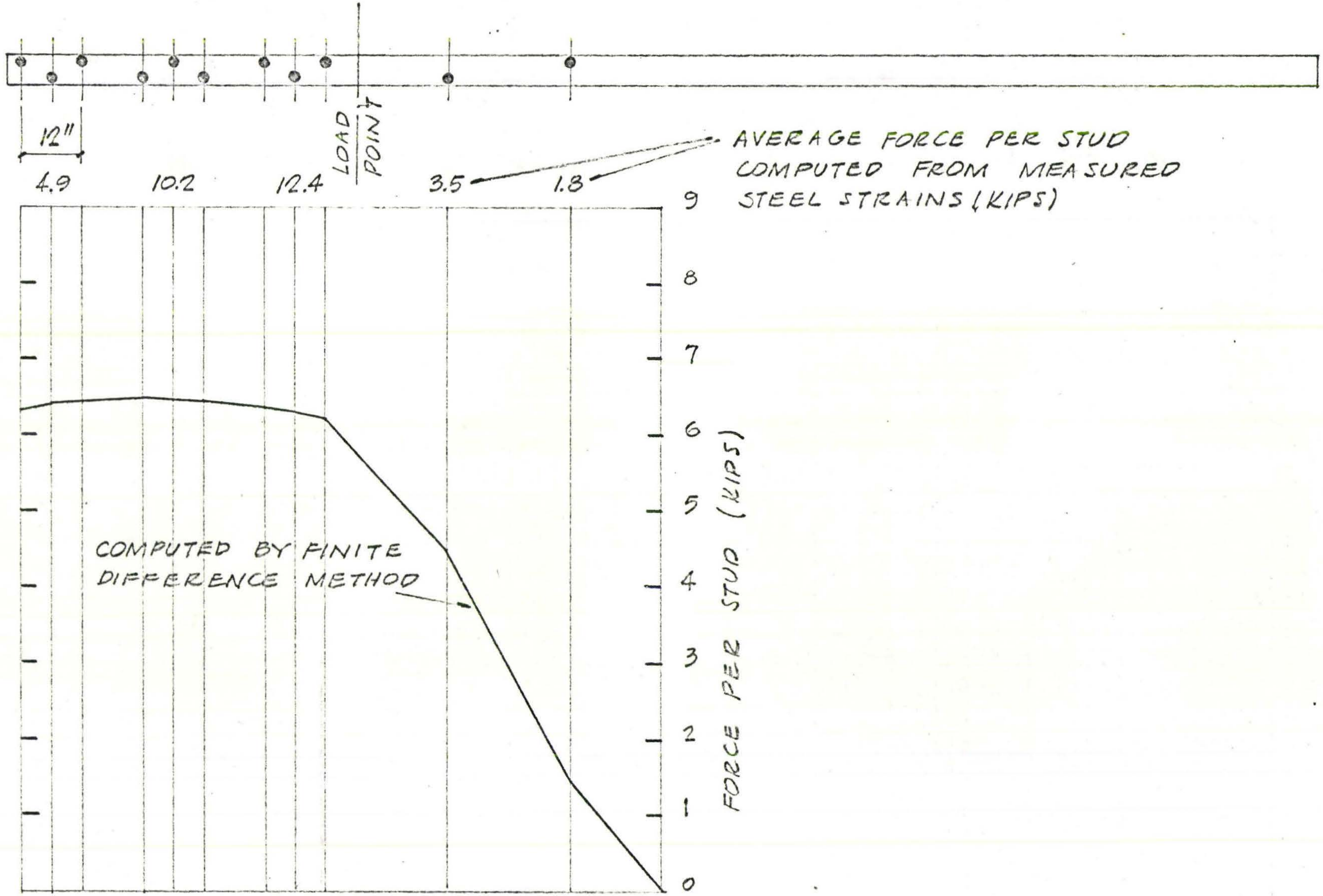

FIG. 4.20 FORCES ON SHEAR CONNECTORS - LOAD OF 25 KIPS, BEAM 3

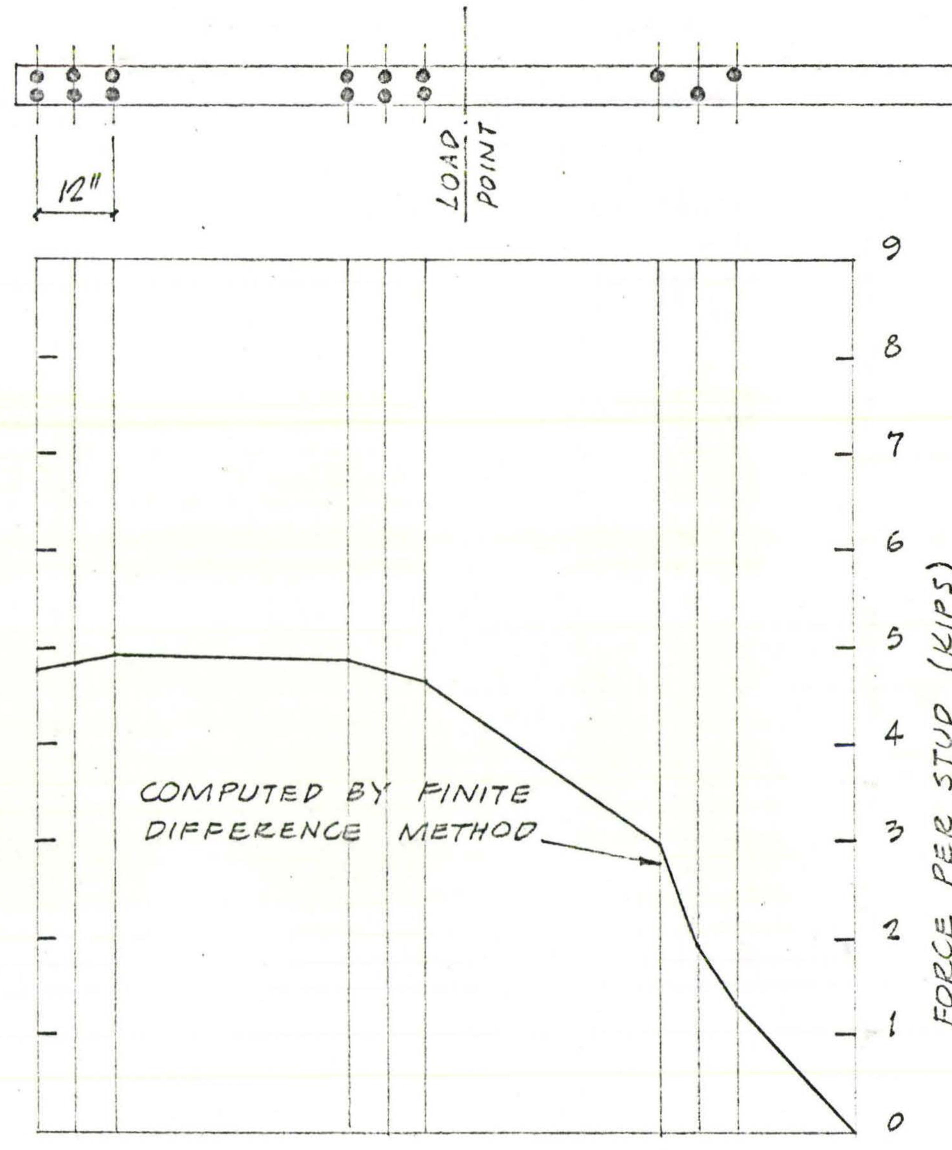

FIG. 4.21 FORCES ON SHEAR CONNECTORS - LOAD OF 25 KIPS, BEAM 4

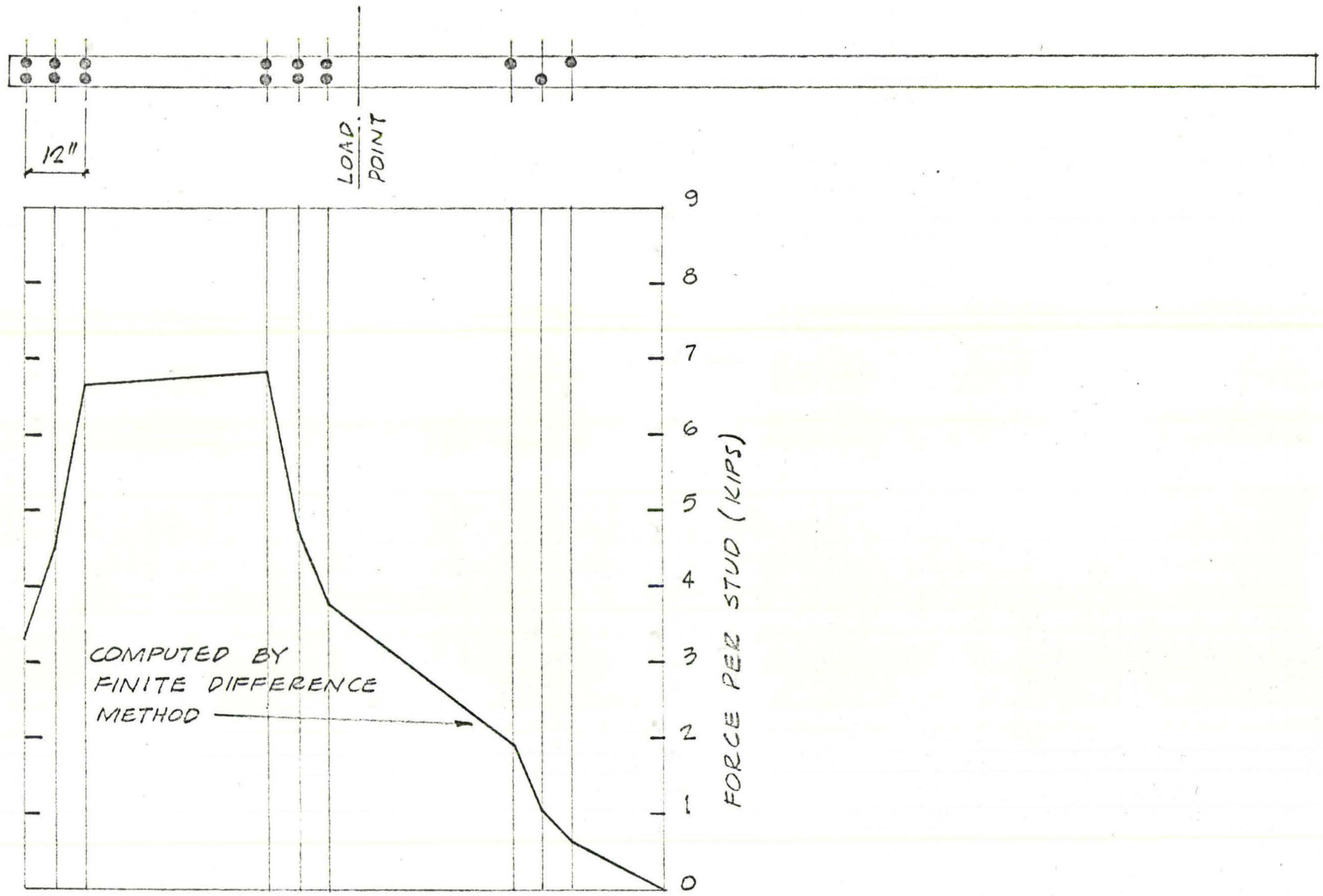

FIG. 4.22 FORCES ON SHEAR CONNECTORS - LOAD OF 25 KIPS, BEAM 5

4.7 Analysis of the Composite Beams at Ultimate Load

The ultimate load is the maximum total load that the beam can sustain. The ultimate load of a composite beam is dependent on the shear force that can be sustained by the shear connection. Using the ultimate shear forces measured on the push-out specimens (Table 2.b), and following the inadequate connection model of Reference 5, the ultimate flexural capacity was calculated at each interval between studs along the length of the five beams. An ultimate moment envelope is the plot of ultimate flexural capacity versus length from one end of the beam. The ultimate flexural capacity envelopes for the five composite beams are shown in Figs. 4.23 to 4.27. On the same figures is drawn the envelopes of maximum applied moment, shown as the sum of moment caused by live load and by dead load.

Fig. 4.23 to 4.27

Ultimate Applied and Ultimate Theoretical Moment Envelopes - Beams 1, 2, 3, 4, 5

The envelope of ultimate flexural capacity is seen to be lower towards the ends of the composite beam. This is because there are fewer connectors between a point in the shear span and the support. During a beam test, the attainment of ultimate load is recognized because it is followed by unloading as the deflection is increased. Flexural failure has occurred at the stage when unloading begins.

Ideally, if the envelope of ultimate moment capacity could be correctly calculated, flexural failure would occur when the applied moment encroached on the theoretical moment capacity anywhere on the envelope.

At the ultimate load of beam 1, the applied moment is seen to be greater than the theoretically calculated flexural capacity between the load point and mid-span. The theoretical ultimate moment is seen to be a conservative estimate of the measured capacity.

In the lower right-hand corner of Fig. 4.22 is shown the measured strain across the depth of the steel beam at ultimate load (dashed line) and at one post-ultimate load (chain line). In addition, the stress blocks used to calculate the theoretical ultimate flexural capacity are shown as solid lines. The measured strain at ultimate load (dashed line, Fig. 4.23) is seen to involve elastic compressive steel strains in the top steel fibres, while the bottom steel fibres are well-yielded. The measured strain at the post-ultimate load (chain line, Fig. 4.23) is in better agreement with the theoretical stress blocks, the top steel fibres having yielded in compression.

The ultimate load of the steel beam was observed to occur before the measured strains could in fact develop the theoretical stress blocks. This shows that it is possible to develop as much flexural capacity from the strain distribution at ultimate load as it is from the strain distribution at the post-ultimate load.

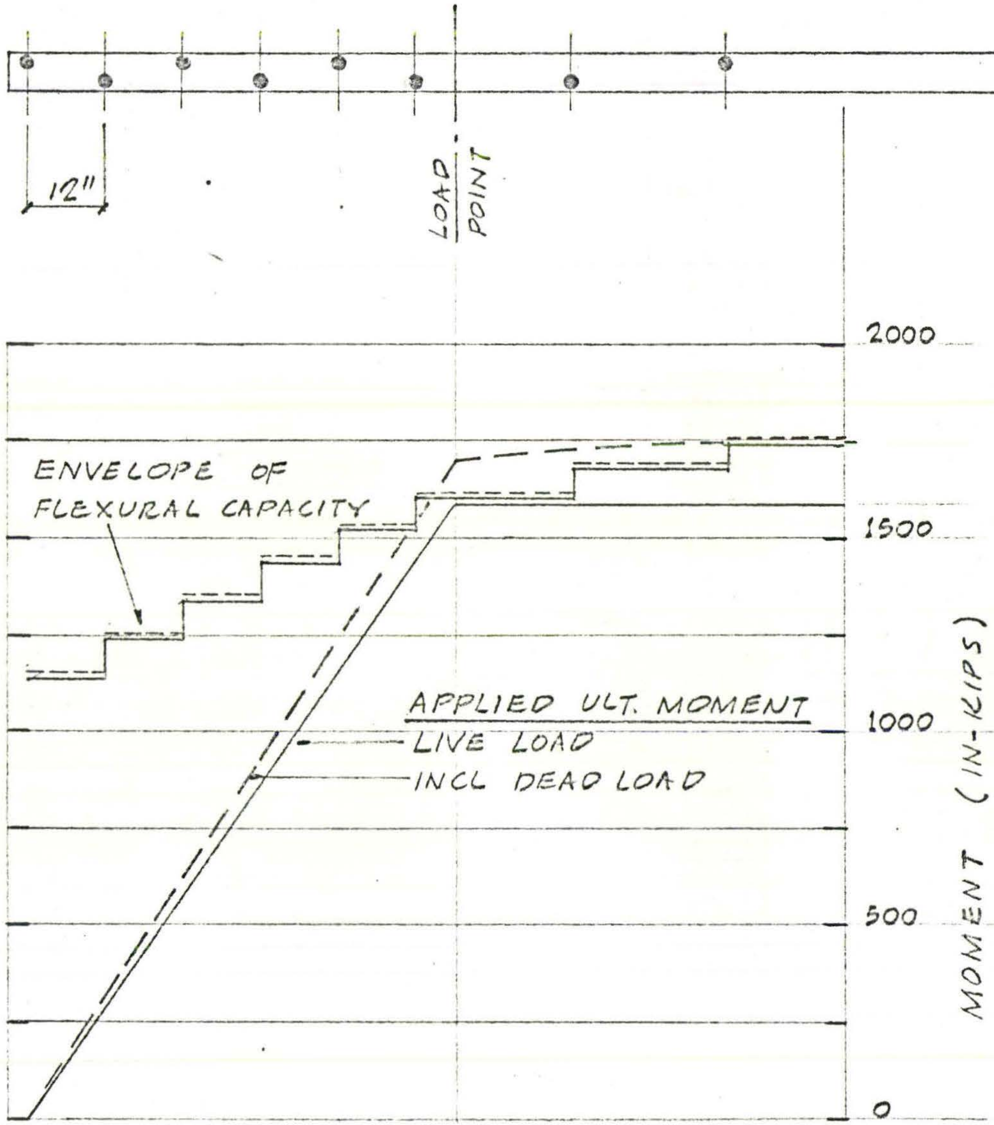

NOTE:
LOWER FLEXURAL CAPACITY ENVELOPE USES MEASURED FLANGE AND WEB YIELD STRESSES.
UPPER FLEXURAL CAPACITY ENVELOPE USES NOMINAL FLANGE AND WEB YIELD STRESSES.

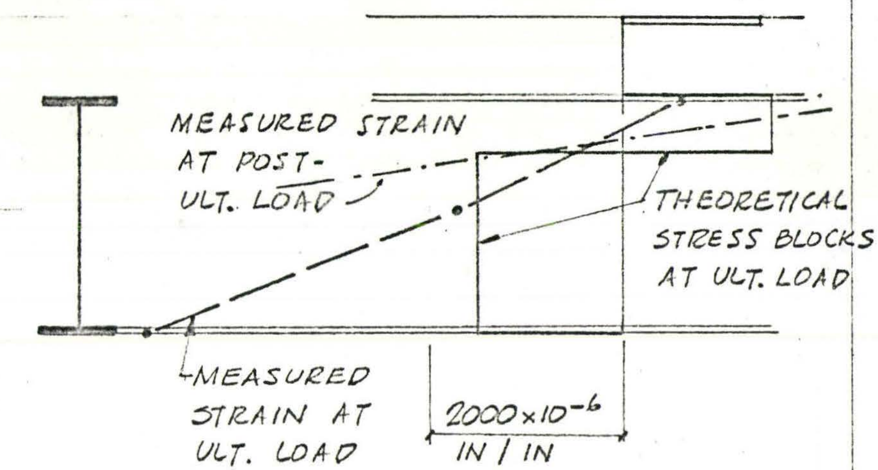

FIG. 4.23 THEORETICAL AND MEASURED ULTIMATE MOMENTS - BEAM 1

THEORETICAL AND MEASURED STRAINS AT ULTIMATE AND POST-ULTIMATE LOAD - AT LOAD POINT

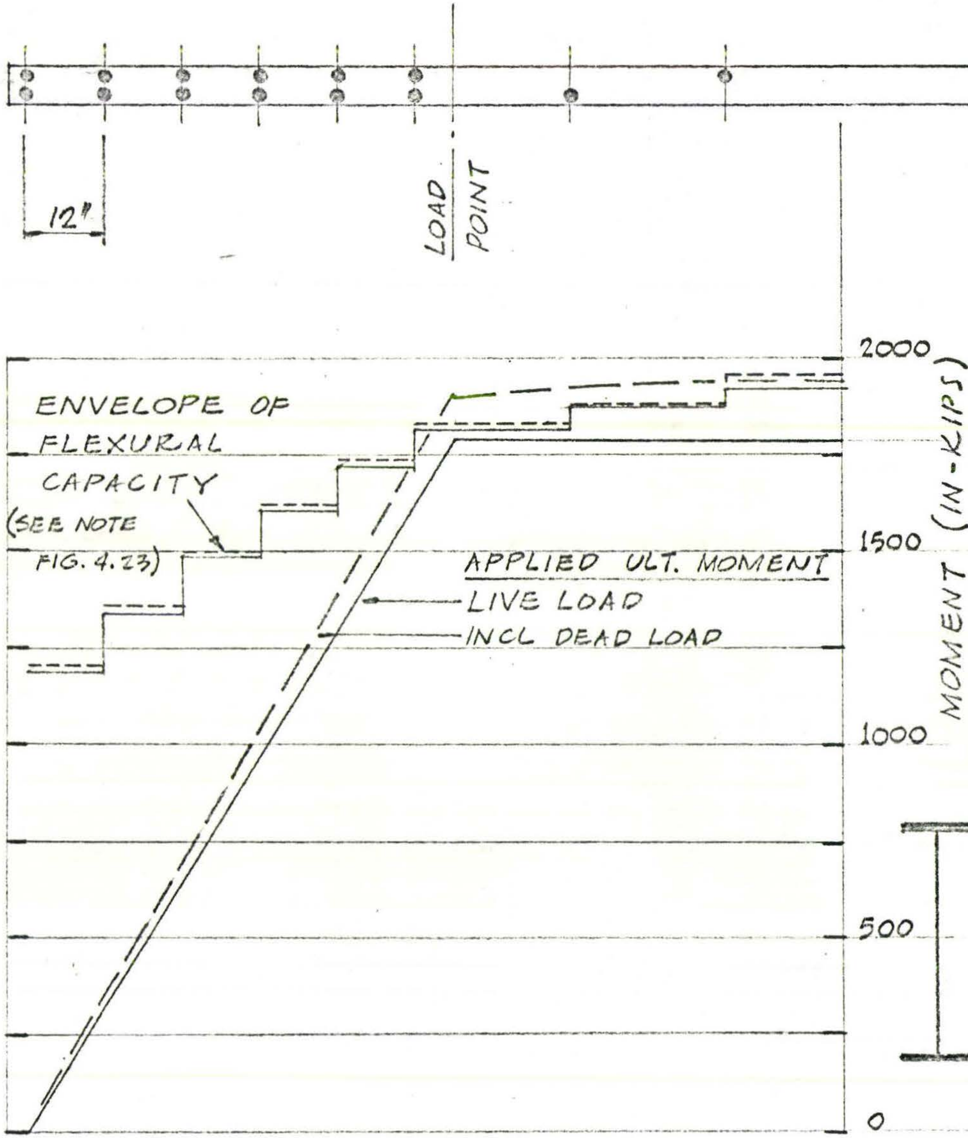

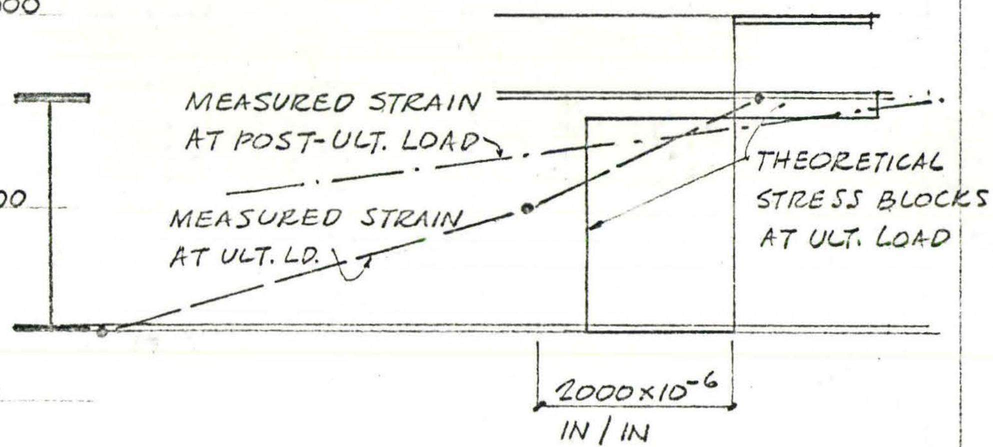

THEORETICAL AND MEASURED STRAINS AT ULTIMATE AND POST-ULTIMATE LOAD - AT LOAD POINT

FIG. 4.24 THEORETICAL AND MEASURED ULTIMATE MOMENTS - BEAM 2

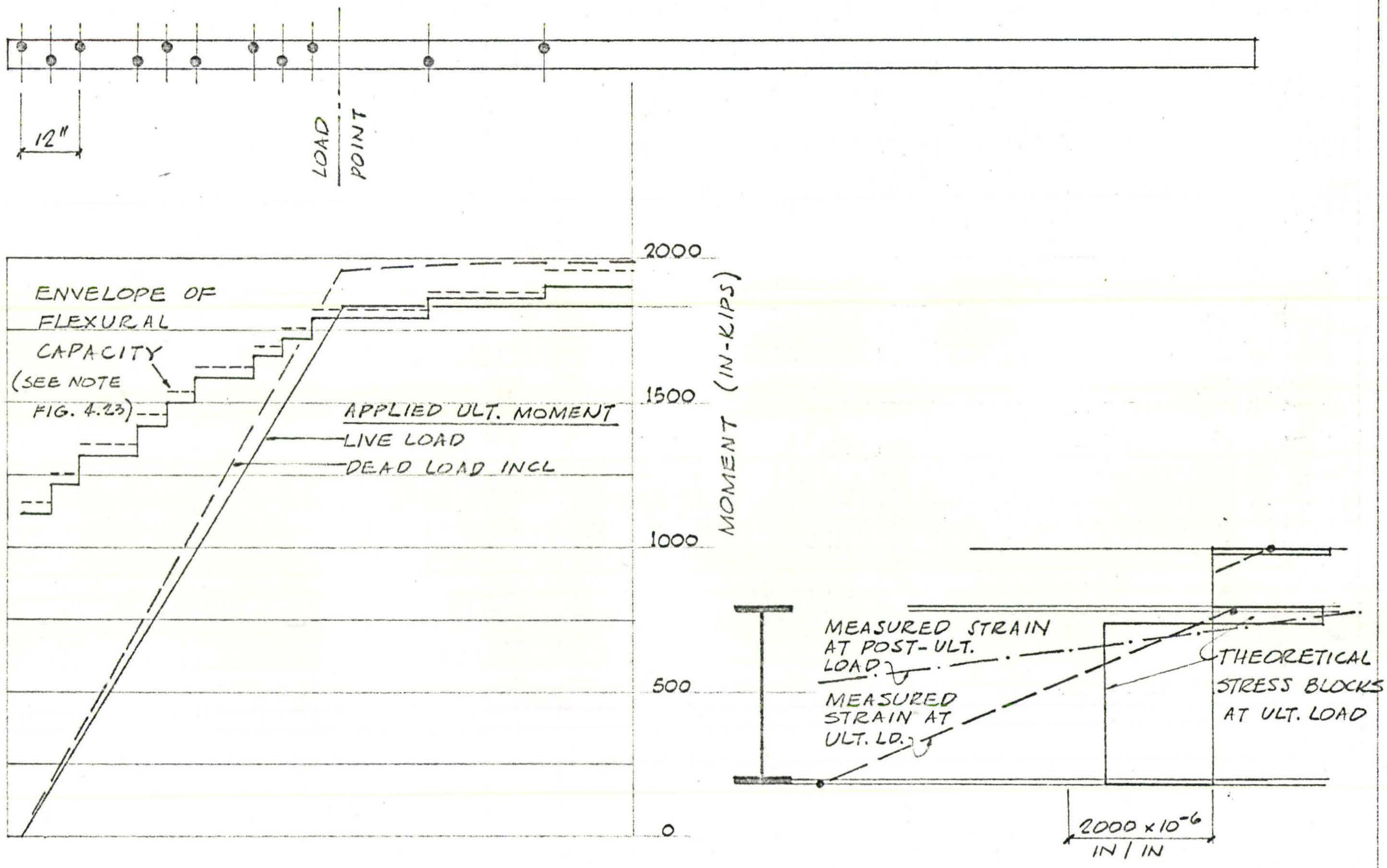

THEORETICAL AND MEASURED STRAINS AT ULTIMATE AND POST-ULTIMATE LOAD - AT LOAD POINT

FIG. 4.25 THEORETICAL AND MEASURED ULTIMATE MOMENTS - BEAM 3

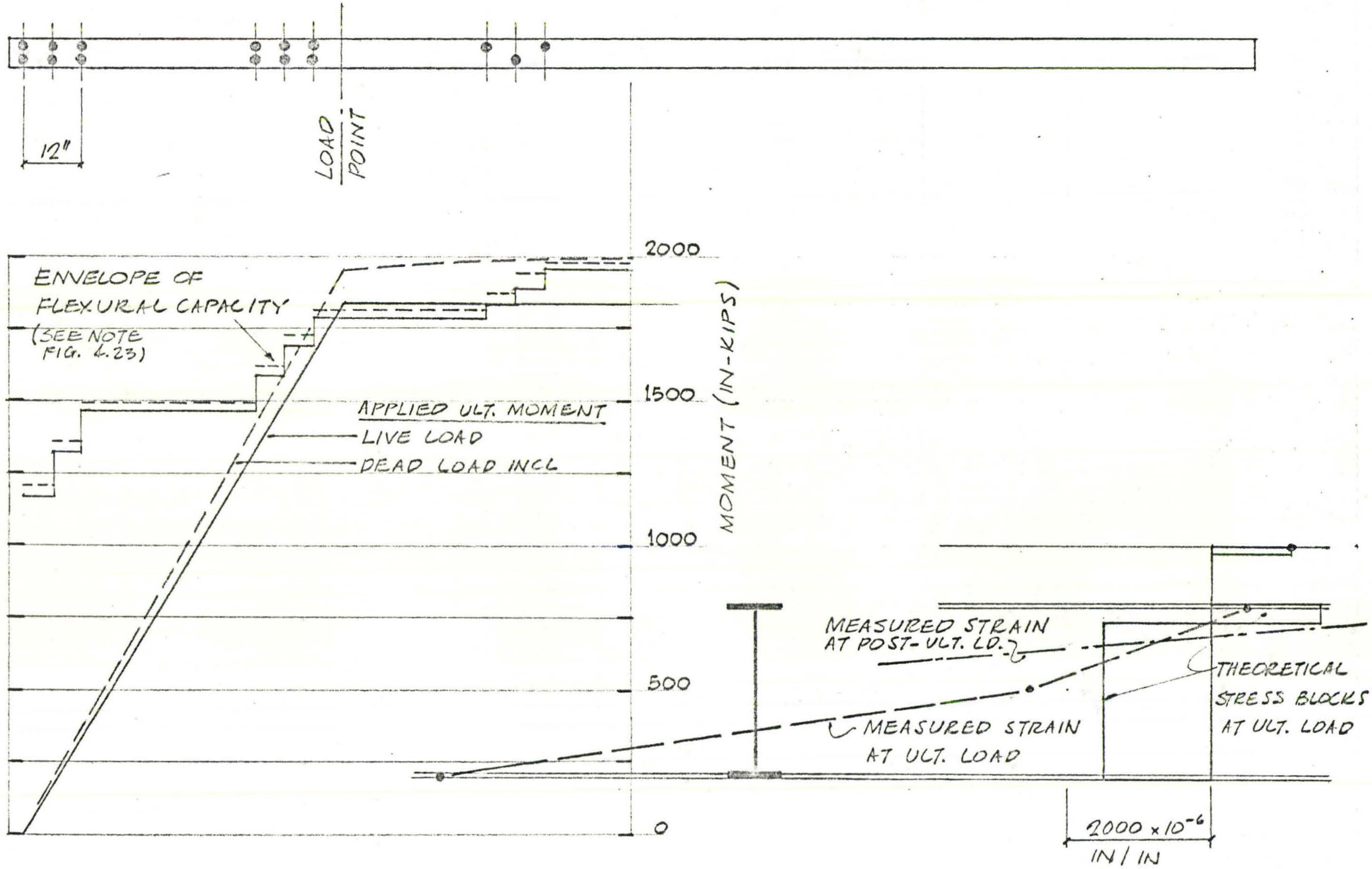

FIG. 4.26 THEORETICAL AND MEASURED ULTIMATE MOMENTS - BEAM 4

THEORETICAL AND MEASURED STRAINS AT ULTIMATE AND POST-ULTIMATE LOAD - AT LOAD POINT

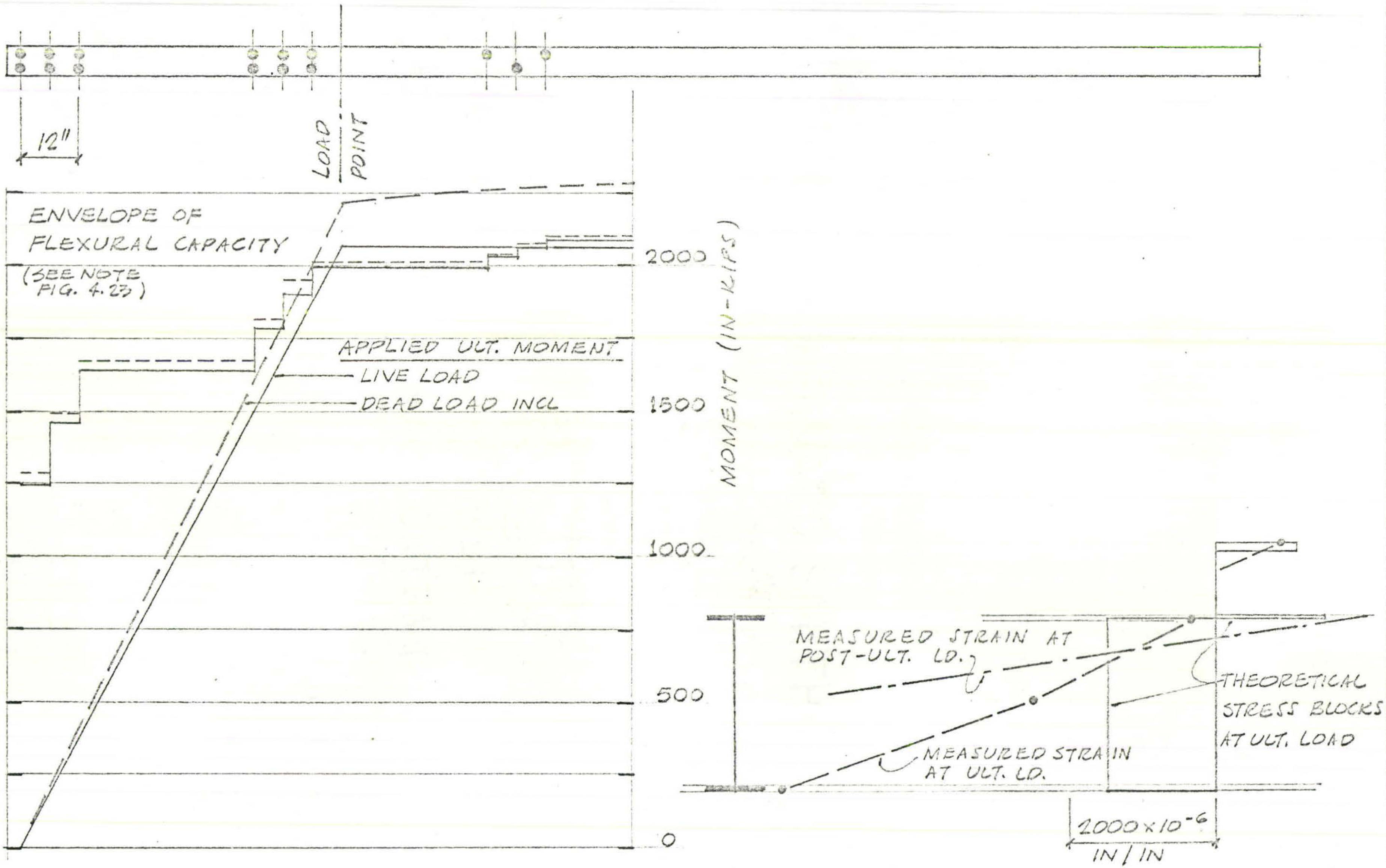

FIG. 4.27 THEORETICAL AND MEASURED ULTIMATE MOMENTS - BEAM 5

THEORETICAL AND MEASURED STRAINS AT ULTIMATE AND POST-ULTIMATE LOAD - AT LOAD POINT

4.8 Ductility of the Composite Beams

As the applied load was increased through the working load range and up to the ultimate load, no secondary failures were observed. Secondary failures would include lateral-torsional buckling and local buckling of the steel beam, and shear lag failure of the concrete slab. Unloading followed the attainment of ultimate load in each case. No secondary failures were observed until very late in the unloading stage.

No out-of-plane deformations occurred during the unloading stage.

Unloading of the composite beams after the attainment of ultimate load could be due to two other influences. The falling branch of the shear force vs. slip relation of the connections could have reduced the shear force transferred across the beam-slab interface. Also, the falling branch of the concrete stress-strain curve could have reduced the capacity of the concrete slab to resist compression[21, 22]. Very likely, unloading was caused by the influence of the falling branch of the shear force vs. slip relation of the shear connection. The influence of the shape of the concrete stress-strain curve on the moment capacity of composite beams has been shown to be small[21] in conventional composite beams with a solid slab. This fact has yet to be established for composite beams with cellular steel floor.

The five beams tested had a large area of concrete relative to the area of steel.

The neutral axis, based on the transformed section, is above the top flange of the steel beam for all five beams. This neutral axis location leads to the condition where yielding of the lower fibres of the steel beam governs the behaviour of the composite beams. The moment-curvature and moment-deflection curves for the five beams (Figs. 3.18 and 3.7) are therefore similar in form to those of an under-reinforced concrete beam. That is, the lower fibres of the steel beams are well into the yielded range at the ultimate load of the beams.

The shape factor is defined as the ultimate moment divided by the moment at first yielding of the bottom fibres. The shape factor, M_u'/M_y, was calculated for each of the beams. M_y is determined from Fig. 4.1 at the yield strain of 1240×10^{-6} in/in. The shape factors of Table 4 can be interpreted correctly only by examining the ratio of M_y/M_w, where M_w is the working load moment. The ratios of Table 4d include the ratio M_y/M_w.

Table 4 d

Beam	M_u'/M_y	M_y/M_w	M_u'/M_w
1	1700/1224 = 1.39	1224/792 = 1.55	2.16
2	1900/1324 = 1.44	1324/858 = 1.55	2.25
3	1950/1339 = 1.45	1339/843 = 1.59	2.31
4	1950/1240 = 1.57	1240/941 = 1.32	2.07
5	2200/1458 = 1.51	1458/906 = 1.61	2.43

It can be seen from Table 4 that the ratios of M_y/M_w are all greater than 1.32. This indicates that if yield strain is taken at 1240×10^{-6} in/in, there is a sufficient margin of safety between working load strain and yield strain.

These shape factors from Table 4, M_u'/M_y, in the range of 1.39 to 1.57, can be compared to a shape factor of 1.15 for a wide-flange beam. Composite beams thus have a much greater reserve of strength than do conventional flanged steel sections.(21)

The ductility of the steel in the lower fibres of the composite beam evidently contributes to its unloading characteristics. Under loading conditions normally associated with simple beams, unloading would not be possible. The applied load would increase to the ultimate load of the beam and the beam would subsequently collapse. It is only for continuous structures that the slope of the unloading curve becomes important.

The ductility factor is a measure of the rate of unloading of a beam. Ductility factor is defined as[14] the deformation (curvature or deflection) at 5% unload ($v_{0.95M_u'}$) divided by the fictitious elastic deflection at ultimate load ($v_{M_u', \text{ elastic}}$). This can be written as: (see Fig. 4.28)

$$\text{Ductility Factor} = \mu = \frac{v\ (\text{at } 0.95\ M_u')}{v\ (M_u',\ \text{elastic})} \quad .$$

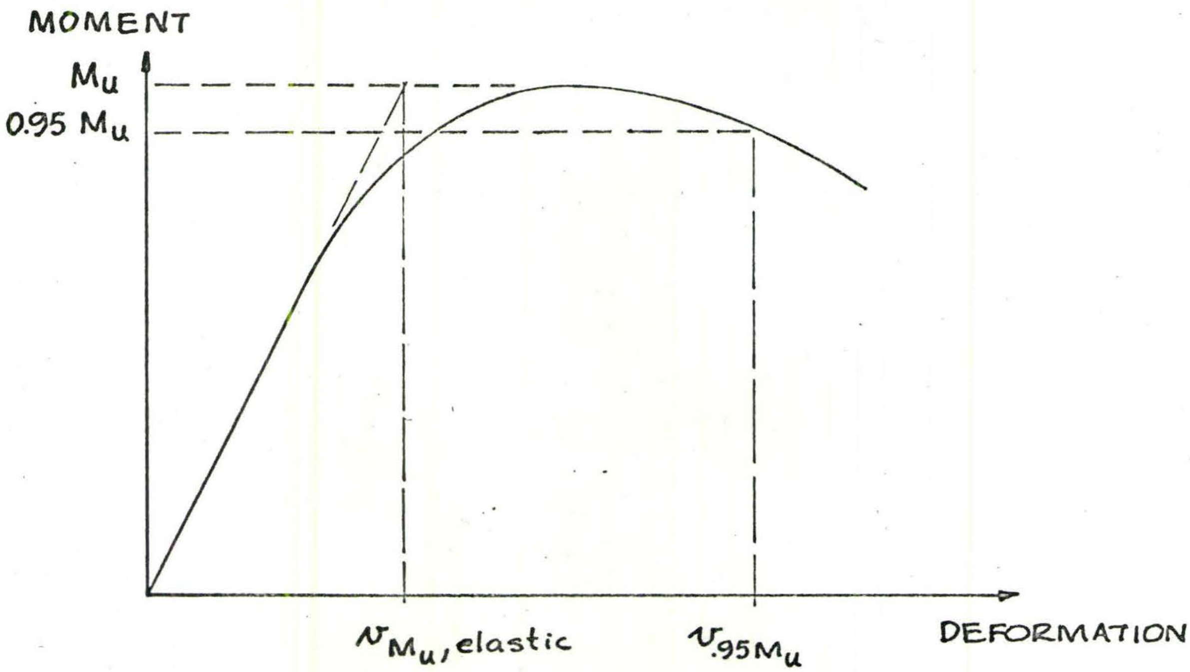

Fig. 4.28

The curvature and deflection ductility factors for the five beams tested are as shown in the following table.

Beam	μ (Curvature)	μ (Deflection)
1	16.0	5.3
2	11.7	5.8
3	6.3	4.0
4	14.3	6.5
5	5.7	3.7

These curvature figures can be compared to a curvature ductility factor of 4 for an A-36 wide-flange compact beam with lateral bracing spaced at 60 r_y, and to a curvature ductility factor of 11.5 for a bracing spacing of 35 r_y[12].

The beams showing the lower values of curvature and deflection ductility factors clearly demonstrate a greater relative rate of unloading.

CHAPTER V

THEORETICAL GENERATION OF THE COMPLETE MOMENT-CURVATURE CURVE

5.1 Introduction

An attempt was made to duplicate the work of Reference 9 and compute the moment-curvature curve of the composite beam from zero load to ultimate load. Up to first yielding of the steel beam, this theoretical analysis has been referred to earlier in this paper as the elastic finite difference method of analysis. After first yielding of the steel beam, the method is referred to as the inelastic finite difference method of analysis.

5.2 The Elastic Finite Difference Method of Analysis

The type of composite beam considered was that shown in Fig. 1.2. The two elements were the concrete slab and the steel beam. These were considered separated by a flexible zone of depth equal to the depth of the cellular steel floor.

The principal assumptions made in the elastic finite difference analysis were as follows:

1. The steel beam and the concrete slab are assumed to deflect equally at all points along their lengths.

2. The steel beam and the concrete slab are assumed to have equal curvatures at any section.

3. The distribution of strains is linear throughout the depth of the slab itself and of the steel beam itself. However, the strains are not, in general, linear through a section of the composite beam.

4. The shear connection between the slab and the steel beam is assumed to be provided by shear connectors placed at discrete points along the length of the beam. The shear-slip curve for a shear connector is approximated by three straight-line segments as shown in Fig. 5.5.

5. The stress-strain relationship for the steel beam is as shown in Fig. 5.1 and for the concrete slab is as shown in Fig. 5.2, both linearly elastic. The stress-strain curves in tension and compression are assumed to be the same.

Assuming that the strain distribution through the depth of the composite beam (Fig. 5.3) can be produced by the three parameters F, M_b, and M_s (Fig. 5.4), Dai and Siess derive the equation of equilibrium

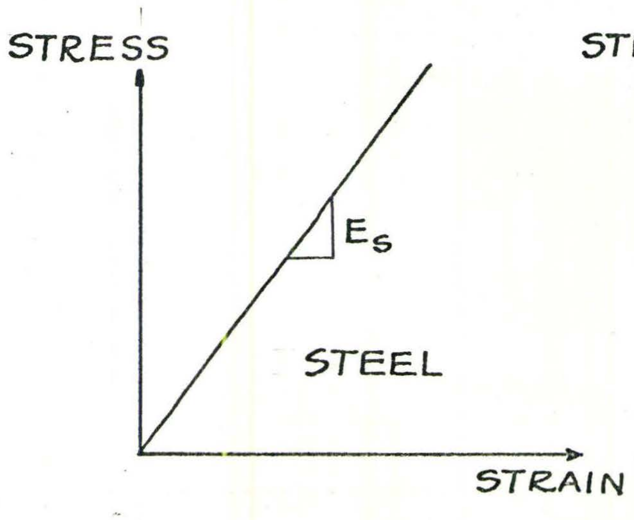

FIG. 5.1

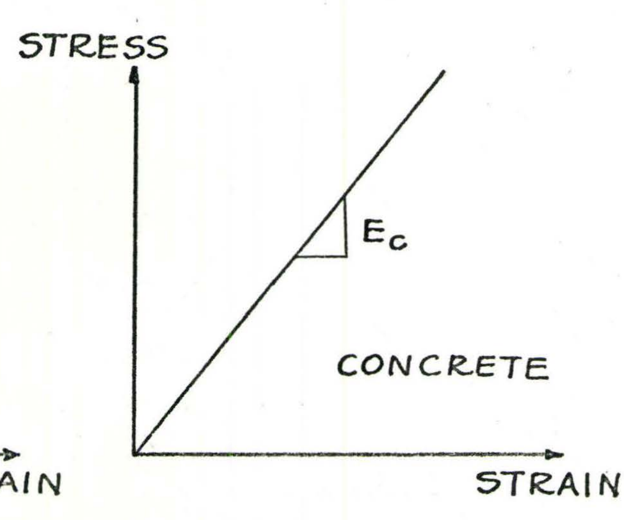

FIG. 5.2

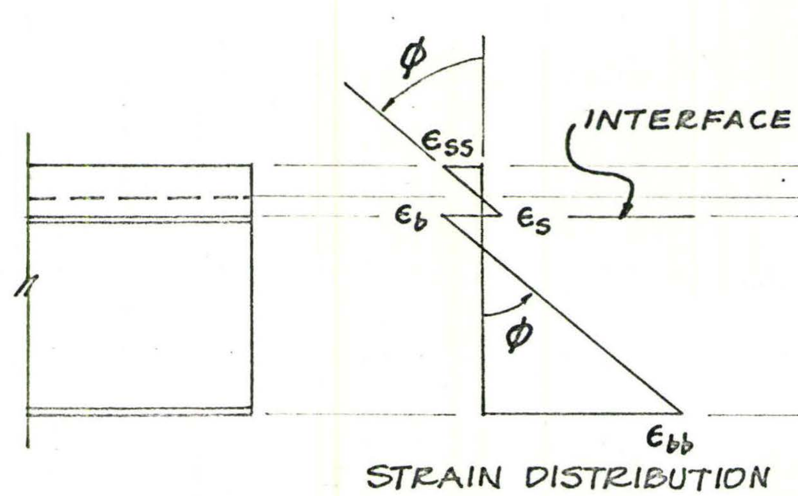

FIG. 5.3

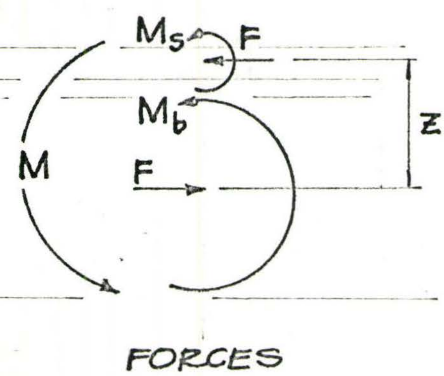

FIG. 5.4

$$M = F.z + M_b + M_s \qquad 5.1$$

where M = the applied moment,

M_b = moment in the beam,

M_s = moment in the slab, and

F = interaction force.

F is assumed to act at the centroid of the steel beam and at the solid part of the concrete slab. z is the vertical distance between centroids.

The interaction force F is assumed to be constant throughout the length of one interval, and so the equilibrium equation 6.1 is satisfied at each mid-interval point along the beam.

Dai and Siess derive the difference equation of compatibility at the interface of the beam and slab, which is

$$\gamma_{i+1} - \gamma_i = \int_{S_i} (\epsilon_b - \epsilon_s)\, dx \qquad 5.2$$

Equation 5.2 states that the difference in slip between one connector and an adjacent connector ($\gamma_{i+1} - \gamma_i$) is equal to the interfacial strain difference (E_b - E_s) integrated over the interval length (S_i).

Assuming the beam to be prismatic, Dai and Siess reduce equations 5.2 and 5.1 to the elastic difference equation of interaction

$$-\frac{F_{(i+1)}}{k_{i+1}} + \left(\frac{1}{k_{i+1}} + \frac{1}{k_i} + a s_i\right) F_{(i)} - \frac{F_{(i-1)}}{k_i} = \frac{z}{\sum EI} \int_{S_i} M(x)\, dx \qquad 5.3$$

where $$a = \frac{1}{E_b A_b} + \frac{1}{E_s A_s} + \frac{z^2}{\sum EI}$$

and where

$$\sum EI = E_b I_b + E_s I_s \,.$$

In equation 5.3, the bracketed subscripts refer to a mid-interval point. The non-bracketed subscripts refer to a connector point. k_i refers to the modulus of the first line of the trilinear shear-slip curve of Fig. 5.5.

A set of equations similar to equation 5.3 is set up for the composite beam with $F_{(i)}$ as the array of unknowns.

Equation 5.3 represents the typical equation for the panel bounded by the i^{th} and $i+1^{th}$ shear connectors. Therefore, the number of panels, or intervals, determines the number of equations to be solved.

Equation 5.3 is applicable until the force on one or more connectors becomes greater than Qp. When this occurs, the elastic difference equations (5.3) for the intervals on each side of the offending shear connector (connector i, say) must be modified. Dai and Siess outline this modification as a substitution of $k_i^{'}$ for k_i in the left-hand side of both equations, and an addition of a term

$$\pm \left(\frac{Q_P}{k'} - \gamma_P \right)_i \qquad 5.4$$

in the right-hand side of both equations. The sign of the correction term 5.4 is determined by whether the increase in rate of slip is tending to shorten (negative corrective term 5.4) or to lengthen (positive corrective term 5.4) the interval.

When the force on the connector i becomes greater than Q_y (Fig. 5.5), corrective terms similar to 5.4 are introduced into the elastic finite difference equations for the intervals adjacent to connector i.

For a composite beam having 4 shear connectors, a set of three elastic finite difference equations shown in Fig. 5.6 can be set up. If the shear force Q on the outside shear connector became greater than Q_p, the three equations of Fig. 5.6 would be modified to read as shown in Fig. 5.7.

In a similar manner, for each of the five beams tested, a set of elastic finite difference equations was set up.

These were put in matrix form and solved for live loads of 4 kips to 40 kips in 1-kip increments. As each connector yielded (the force on the connector became greater than Q_p, Fig. 5.5) suitable corrections were made and the solution re-computed for that load. Similar corrections were made as the force on the connectors became greater than Q_y. (Fig. 5.7).

The computer programme that was used for the elastic finite difference analysis is shown in Appendix (d) of this report. The theory and assumptions used in setting up the computer programme were due to Dai and Siess[9], and others[12, 13, 25] originally. Computed results of the elastic finite difference analysis have been presented earlier in this report.

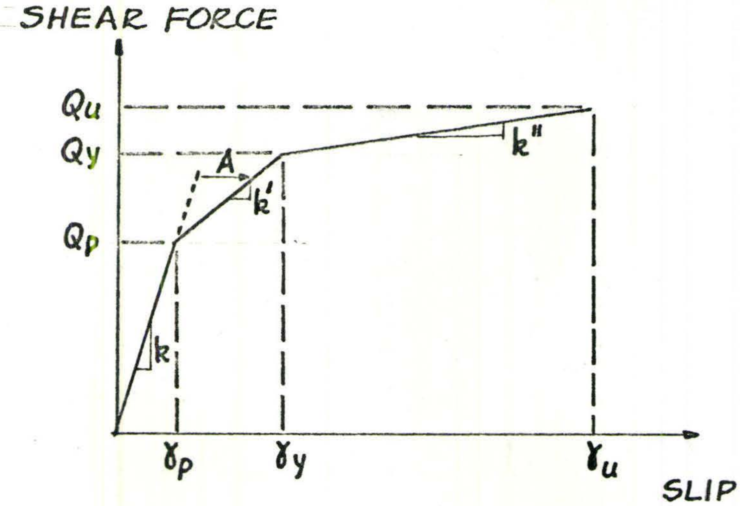

IDEALIZED TRILINEAR
SHEAR FORCE VS. SLIP RELATION
FIG. 5.5

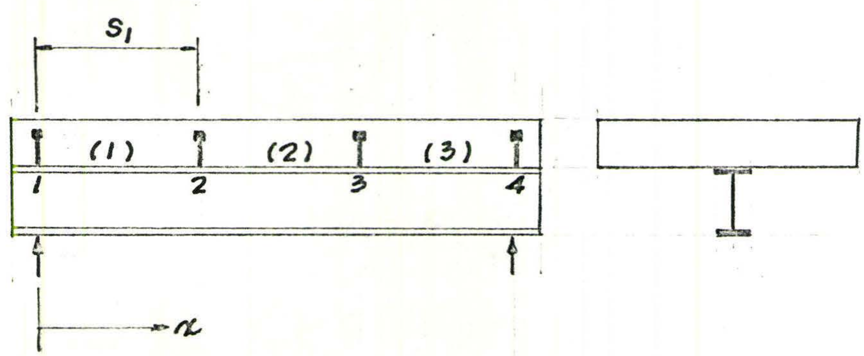

$$\left(as_1 + \frac{1}{k_1} + \frac{1}{k_2}\right) F_{(1)} - \frac{1}{k_2} F_{(2)} = \frac{z}{\Sigma EI} \int_{s_1} M(x)\, dx$$

$$-\frac{1}{k_2} F_{(1)} + \left(as_2 + \frac{1}{k_2} + \frac{1}{k_3}\right) F_{(2)} - \frac{1}{k_3} F_{(3)} = \frac{z}{\Sigma EI} \int_{s_2} M(x)\, dx$$

$$-\frac{1}{k_3} F_{(2)} + \left(as_3 + \frac{1}{k_3} + \frac{1}{k_4}\right) F_{(3)} = \frac{z}{\Sigma EI} \int_{s_3} M(x)\, dx$$

ELASTIC FINITE DIFFERENCE EQUATIONS
FOR 3-INTERVAL BEAM

FIG. 5.6

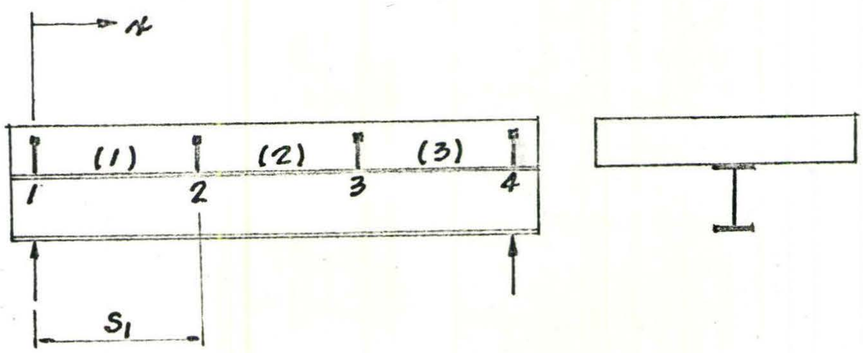

$$\left(as_1 + \frac{1}{k_1'} + \frac{1}{k_2}\right) F_{(1)} \quad - \frac{1}{k_2} F_{(2)} \qquad = A$$

$$-\frac{1}{k_2} F_{(1)} + \left(as_2 + \frac{1}{k_2} + \frac{1}{k_3}\right) F_{(2)} \quad - \frac{1}{k_3} F_{(3)} \quad = B$$

$$-\frac{1}{k_3} F_{(2)} + \left(as_3 + \frac{1}{k_3} + \frac{1}{k_4'}\right) F_{(3)} = C$$

$$A = \frac{z}{\Sigma EI} \int_{s_1} M(x)\,dx + \left(\frac{Q_P}{k_1'} - \gamma_P\right)_1$$

$$B = \frac{z}{\Sigma EI} \int_{s_2} M(x)\,dx$$

$$C = \frac{z}{\Sigma EI} \int_{s_3} M(x)\,dx + \left(\frac{Q_P}{k_4'} - \gamma_P\right)_4$$

ELASTIC FINITE DIFFERENCE EQUATIONS FOR 3-INTERVAL BEAM — CORRECTED FOR YIELDING OF END CONNECTORS

FIG. 5.7

5.3 The Inelastic Finite Difference Method of Analysis

The elastic finite difference computations described in part 5.2 above are capable of analysing a composite beam up to a load at which the steel becomes inelastic. The steel beam will become inelastic in only one interval initially. For all the other elastic intervals, difference equations such as equation 5.3 will be applicable. For the interval(s) in which the steel has begun to yield, Dai and Siess suggest using a difference equation derived from the equation of compatibility (equation 5.2). The finite difference equation to be used for an interval in which the steel has begun to yield is called the inelastic finite difference equation, and is (for the i^{th} interval)

$$-\frac{F_{(i+1)}}{k_{i+1}} + \left(\frac{1}{k_{i+1}} + \frac{1}{k_i}\right) F_{(i)} - \frac{F_{(i-1)}}{k_i} = -\int_{S_i} (\epsilon_b - \epsilon_s)\, dx \qquad 5.5$$

The term on the right-hand side of equation 5.5 is not known. This term must be arrived at by a trial and error procedure which will be described below.

The assumptions for the inelastic analysis are:

1. All the assumptions relevant to the elastic finite difference analysis apply except that the steel beam has an elasto-plastic (Fig. 5.8) stress-strain curve. The concrete remains linearly elastic as in the elastic analysis.

2. If at the end of a certain loading stage, the stress at the bottom fibre of the steel beam is found to have reached the yield point for one interval, the state of stress is considered to be in the inelastic range for all higher load levels in this interval.

3. The distributions of strain E_s and E_b are still linear along the length of the intervals.

From assumption 3, above, the unknown term on the right-hand side of equation 5.5 reduces to

$$\int_{S_i} (\epsilon_b - \epsilon_s) = (\epsilon_b - \epsilon_s)_{(i)} \cdot S_i \qquad 5.6$$

The basic unknown in the inelastic analysis is the value of $(\epsilon_b - \epsilon_s)$ at the mid-point of the inelastic intervals.

For example, the middle interval of the four-connector, three-interval beam of Fig. 5.6 is just at the point of yielding for a load of P kips. For a load of P + Δ P kips, the middle interval will have yielded. At a load of P + Δ P kips, the three finite difference equations of Fig. 5.9 can be written. Note that the two equations written for the outside (elastic) intervals are of the form of equation 5.3. The middle equation is of the form of equation 5.5 because the middle interval has yielded.

The equations shown in Fig. 5.9 are written as if all the connector forces were below Q_p of Fig. 5.5. Dai and Siess recommend that if some connectors' forces have become greater than Q_p or Q_y, then corrections to the relevant equations must be made. These corrections take the same form as those described in section 5.2 for the elastic finite difference equations(9).

The set of elastic and inelastic finite difference equations such as those of Fig. 5.9 cannot be solved until all the terms

$$(\epsilon_b - \epsilon_s)_{(i)} \cdot S_i \qquad 5.6$$

have been found. To determine the correct numerical value of the term 5.6 requires a trial and error procedure.

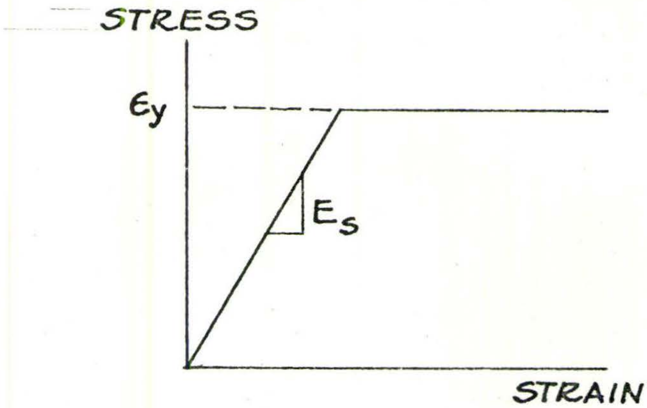

ELASTO-PLASTIC STRESS-STRAIN CURVE
FOR STEEL

FIG. 5.8

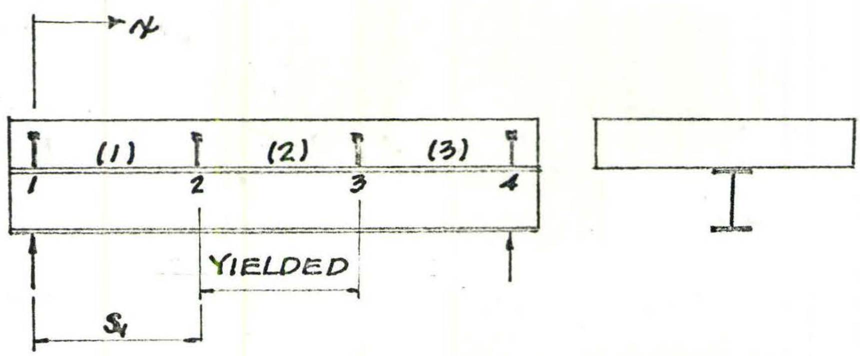

$$\left(a s_1 + \frac{1}{k_1} + \frac{1}{k_2}\right) F_{(1)} - \frac{1}{k_2} F_{(2)} = \frac{z}{\Sigma EI} \int_{S_1} M(x)\, dx$$

$$-\frac{1}{k_2} F_{(1)} + \left(\frac{1}{k_2} + \frac{1}{k_3}\right) F_{(2)} - \frac{1}{k_3} F_{(3)} = -\int_{S_2} (\epsilon_b - \epsilon_s)\, dx$$

$$-\frac{1}{k_3} F_{(2)} + \left(\frac{1}{k_3} + \frac{1}{k_4}\right) F_{(3)} = \frac{z}{\Sigma EI} \int_{S_3} M(x)\, dx$$

ELASTIC-INELASTIC FINITE DIFFERENCE EQUATIONS
FOR 3-INTERVAL BEAM

FIG. 5.9

The dependence of F (interaction force), M (applied moment), ϕ (curvature), and ϵ_{bb} (bottom fibre steel strain) for one interval can be shown in schematic form by Fig. 5.10. This was first shown by Dai and Siess, and was proven to be true by calculations made for this report. One point on Fig. 5.10 represents one possible solution satisfying equilibrium for one interval.

Not all the solutions on Fig. 5.10 will apply to an interval of one particular composite beam at one particular loading level.

To the left of the sloping straight line labelled $\epsilon_{bb} = \epsilon_Y$ on Fig. 5.10, the strains are elastic. This is the domain of the elastic finite difference solution. To the right of the same line is the domain of the trial and error inelastic finite difference solution.

It should be pointed out that for each point on Fig. 5.10, there is not only an F, M, ϕ, and ϵ_{bb} as shown, but also M_s, and M_b which are not shown.

Point O' on Fig. 5.10 represents the state of stress of an interval under applied moment M_1. At O' the bottom fibre steel strain is ϵ_y, the interaction force is F*, and the curvature in the concrete slab and steel beam is equal to ϕ_2.

Point B on Fig. 5.10 represents the state of stress of an interval under applied moment $M_2 = M_1 + \Delta M$ at which the interaction force is equal to F* also. Point A on Fig. 5.10 represents the state of stress of an interval under applied moment M_2 at which the curvature is equal to ϕ_2. The curvature at point B is ϕ_3 which is greater than ϕ_2. The interaction force at point A is F** which is greater than F*.

Dai and Siess show that the correct state of stress for an

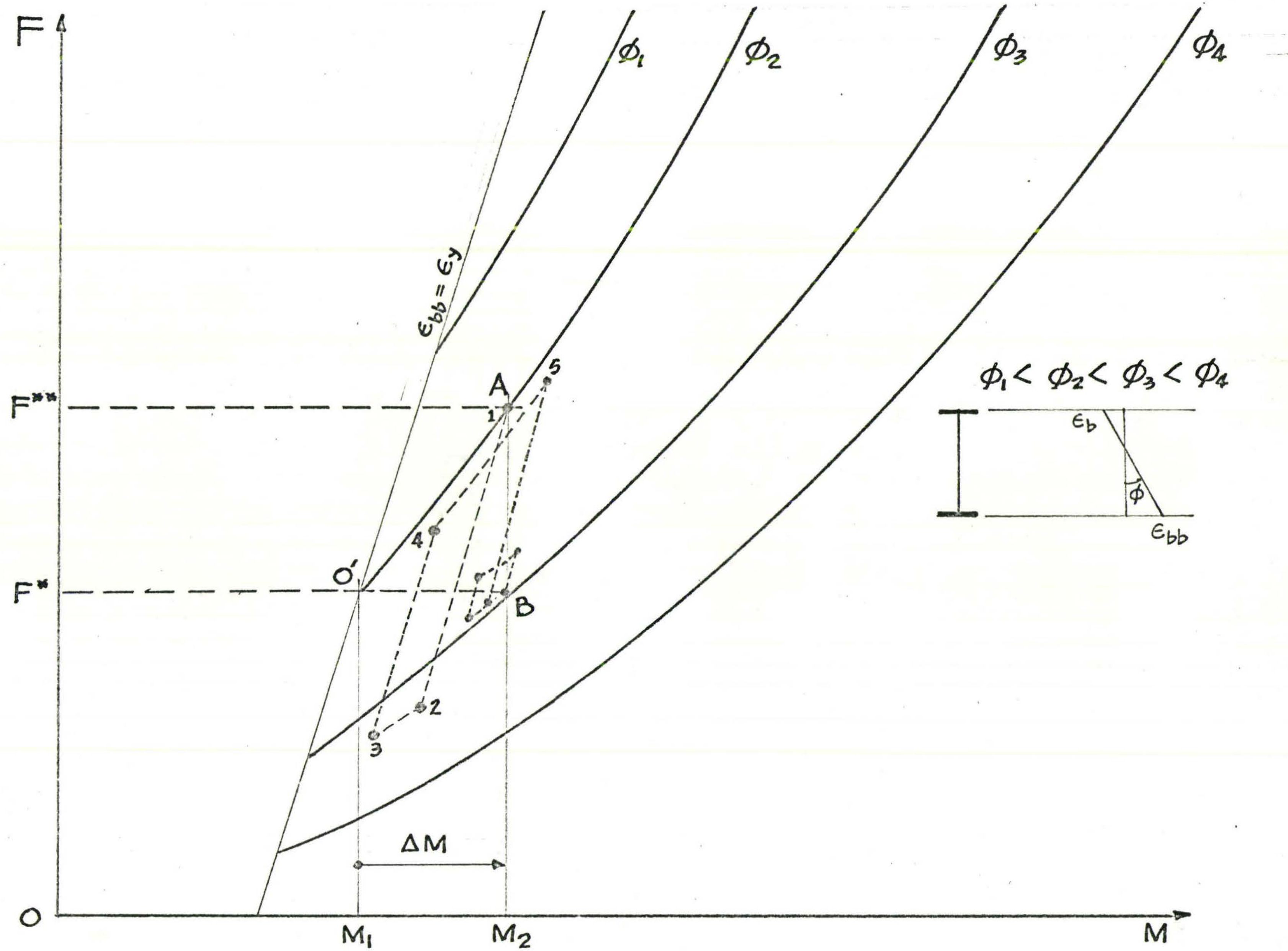

SCHEMATIC REPRESENTATION OF EQUILIBRIUM RELATION OF $F, M, \phi, \epsilon_{bb}$

FIG. 5.10

interval under applied moment M_2 (Fig. 5.10) must lie on the vertical line between points A and B. To find the correct point on line AB of Fig. 5.10, Dai and Siess indicate that point A should be taken as a first approximation.

The trial and error procedure subsequent to finding point A as the first approximation is as follows:

1. Substitute the $(\epsilon_b - \epsilon_s)_i$ associated with point A of Fig. 5.10 into the set of elastic and inelastic equations. Since the first trial value of $(\epsilon_b - \epsilon_s)$ is associated with a point on Fig. 5.10, it represents an equilibrium condition.

2. Repeat step 1 for every interval that is to become inelastic.

3. Solve the set of inelastic and elastic finite difference equations. The F generated by this solution represents an F that satisfies compatibility.

4. Compare the equilibrium F initially tried with the compatible F generated. If they are equal or reasonably close, the iteration procedure goes to step 9. If they are not equal, step 5 is used next.

5. If the equilibrium F and the compatible F do not agree, choose another $(\epsilon_b - \epsilon_s)$. The new $(\epsilon_b - \epsilon_s)$ is chosen at the point on line AB of Fig. 5.10 that is associated with the compatible F generated.

6. Repeat steps 4 and 5 for every interval which is inelastic.

7. Substitute the $(\epsilon_b - \epsilon_s)$ associated with the newly chosen equilibrium F into the set of elastic and inelastic finite difference equations and solve.

8. Compare the compatible F generated with the equilibrium F chosen. If they are equal or reasonably close, the iteration procedure goes to step 9. If not, steps 5 to 8 are repeated.

9. The beam is checked for new yielding in some other intervals. If it has yielded, suitable corrections must be made to the set of elastic and inelastic equations. More trial and error steps must be done.

By using this laborious trial and error procedure, the correct strains and interaction forces can be found along the length of the beam for one load increment. The load increment in the elastic range can be as large or as small as convenient, because every new applied load is solved as a new problem. In the inelastic range, the correct solution at one loading stage is used as a beginning point for the next loading stage. Therefore, each loading step must be as accurately solved as possible.

It was found by this researcher that the largest loading increment that could be used was a ΔM corresponding to about 200 lbs. applied to the beam. If a larger increment were used, point A of Fig. 5.10 was too crude an approximation to the true solution.

Dai and Siess computed equilibrium points on Fig. 5.10 by systematically varying ϵ_{bb} and ϕ, and calculating ϵ_b, F, M_b, M_s, ϵ_s and ϵ_{ss} from ϵ_{bb} and ϕ. Dai and Siess constructed a table of possible equilibrium solutions and selected from the table to arrive at their trial values of $(\epsilon_b - \epsilon_s)$. The computations of Dai and Siess were more comprehensive than the computations of this report in that they used an elasto-plastic stress-strain curve for the concrete slab as well as for the steel beam. For the computations of this report, the concrete was assumed linearly elastic.

5.4 Work Done in This Report Towards Duplicating the Inelastic Moment-Curvature Curve

5.4a Finding Possible Equilibrium Solutions

Using the assumptions and theory outlined in Part 5.3 above, a computer programme was written to calculate ϵ_b, F, M_b, M_s, ϵ_s, ϵ_{ss} and M from a given ϵ_{bb} and $\emptyset$. The calculation of all these parameters at one point of Fig. 5.10 constitutes a definition of the state of stress at the point. By varying ϵ_{bb} and $\emptyset$, the state of stress at any point on Fig. 5.10 could be computed.

Depending on how far into the steel beam yielding had progressed, F and M_b were computed from the equations shown in Appendix (e). M_s, ϵ_s, ϵ_{ss}, and finally M were computed from F and M_b.

The computer programme that executed these computations was called ITER, and is presented in Appendix (f). ITER deals with only one interval at a time. Referring to Fig. 5.10, ITER has the ability to go from point O' (incipient yielding of one interval) to point A (given M_2). ITER is furthermore capable of finding the state of stress at point B or any point between A and B on Fig. 5.10. The programme ITER was used every time the trial and error procedure called for a new equilibrium point in Fig. 5.10. This obviated setting up a table of possible equilibrium solutions as Dai and Siess did. Furthermore, use of the programme ITER obviated extrapolation and interpolation between values in a table of possible equilibrium solutions.

A typical sequence of iterative steps in ITER can be pictured by following the numbered node points on the dotted line of Fig. 5.10.

To get from point A. of Fig. 5.10 to (say) point B of Fig. 5.11, the following steps were necessary:

1. Point 1 to point 2 - increase $\emptyset$ by $a.\Delta\emptyset$ until F (calculated after every increase in $\emptyset$) was less than F*.

2. Point 2 to point 3 - decrease ϵ_{bb} by $b.\Delta\epsilon_{bb}$ until M (calculated after every decrease in ϵ_{bb}) was less than M_2.

(At this point the interval multipliers a and b were decreased so the iteration became finer.)

3. Point 3 to point 4 - decrease $\emptyset$ by $a.\Delta\emptyset$ until F (calculated after every decrease in $\emptyset$) was greater than F*.

4. Point 4 to point 5 - increase ϵ_{bb} by $b.\Delta\epsilon_{bb}$ until M (calculated after every increase in ϵ_{bb}) was greater than M_2.

Similar steps repeated many times finally converged on point B.

In conclusion, programme ITER was constructed to find possible equilibrium solutions schematically shown as any point in the plane of the axes of Fig. 5.11. ITER used the assumptions of section 5.3 above and the equations of Appendix (e).

5.4b Checking Compatibility

A programme called INELAS was constructed which accepted values of $(\epsilon_b - \epsilon_s)$ for certain inelastic intervals, and solved the set of elastic and inelastic finite difference equations. INELAS thereby calculated the F for the inelastic interval which was compatible with the $(\epsilon_b - \epsilon_s)$ fed in as a trial value. INELAS is listed in Appendix (g).

5.4c Inelastic Computations

To test the above theory and programmes, beam 1 was taken from a total live load of 35,000 lbs. to 35,400 lbs. in two increments of 200 lb. ϵ_y was made equal to 1186×10^{-6} in/in.

Only the seventh interval (and because of symmetry, the ninth interval) was expected to become inelastic under an applied load greater than 35,000 lb. This was because at 35,000 lb. the bottom fibre steel strain in the seventh interval was just below 1186×10^{-6} in/in.

ITER and INELAS were used three times each to get an acceptable solution at 35,200 lb. satisfying both equilibrium and compatibility. That is, three cycles of iteration were required. No other intervals became inelastic at 35,200 lb.

From 35,200 lb. to 35,400 lb., three complete cycles of iteration were required. No other intervals became inelastic at 35,400 lb.

The computational results of these six iterative steps are shown in Fig. 5.12. Fig. 5.12 represents the numerical results of the calculations made on the one interval only.

Column 1 of Fig. 5.12 lists the applied load on the beam (35,000 lb), the results of the elastic finite difference analysis (ELAS), and the moment applied to the mid-interval of interval No. 7 (M = 1,155,000 in-kips). Column 2 of Fig. 5.12 lists the state of stress of the first trial equilibrium solution at a moment of 1,161,700 in-kips found by ITER. The $(\epsilon_b - \epsilon_s)$ term of column 2 (-418×10^{-6} in/in), when used in INELAS, resulted in a computed F of 77,214 lbs. listed in column 3. Columns 4 and 5, and 6 and 7 are two other similar iterations. The equilibrium F arrived at in column 7 (77,335 lbs.) and the compatible F arrived at in column 7 (77,249 lbs.) were judged to be close enough.

Columns 8 to 13 of Fig. 5.12 represent three similar iterations relevant to interval 7 in taking the beam from a load of 35,200 lbs. to a load of 35,400 lbs. The agreement between the last equilibrium F tried (column 12, 77,509 lbs.) and the compatible F produced by it (column 13, 77,502 lbs.) was very good.

Column 14 of Fig. 5.12 shows the state of stress that would have been calculated by the elastic finite difference method of analysis (ELAS) at 35,400 lbs.

The final state of stress at 35,400 lbs. is listed in column 12 of Fig. 5.12. Comparing column 12 with column 14, it can be seen that the F calculated by the inelastic method (77,509 lbs.) is considerably greater than the F that would have been computed had no inelasticity been taken into account (77,183 lbs., column 14). This is contrary to what would be expected because any inelasticity in the steel beam should tend to reduce the interaction force compared to an elastic computation at the same load.

The reason that the inelastic computations did not yield answers as expected was very likely due to inaccuracies accumulated from the use

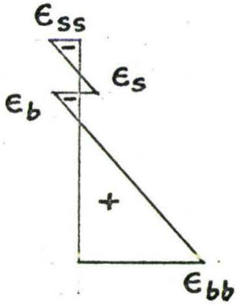

FIG. 5.11

Intermediate and End Results of Taking Interval 7 of Beam 1 from a Load of 35,000 lb. to a Load of 35,400 lb.

$\epsilon_y = +1186.0 \times 10^{-6}$ in/in

Adjacent Intervals Remain Elastic

35,000 lb. = M of 1,155,000 in-lb.
35,200 lb. = M of 1,161,600 in-lb.
35,400 lb. = M of 1,168,200 in-lb.

M = Applied Moment at Mid-Interval

	1	2	3	4	5	6	7	8	9	10	11	12	13	14	
Load	35,000 ELAS	35,200 ITER	35,200 INELAS	35,200 ITER	35,200 INELAS	35,200 ITER	35,200 INELAS	35,400 ITER	35,400 INELAS	35,400 ITER	35,400 INELAS	35,400 ITER	35,400 INELAS	35,400 ELAS	
ϵ_{bb}	+1185.9	1190.7		1191.2		1190.7		1196.7		1204.7		1202.9		1203.	ϵ_{bb}
ϵ_b	- 243.	-238.3		-242.6		-241.6		-236.3		-253.8		-250.		-256.	ϵ_b
ϵ_s	+ 176.	+180.0		+181.7		+181.3		+180.0		+187.3		+185.6		-188.	ϵ_s
$(\epsilon_b-\epsilon_s)$	- 419.	-418.		-424.		-423.		-416.		-441.		-435.7		-444.	$(\epsilon_b-\epsilon_s)$
ϵ_{ss}	- 288.6	-290.		-290.3		-291.7		-291.5		-292.7		-294.4		-292.	ϵ_{ss}
F	76,837	77,600	77,214	77,283	77,260	77,335	77,249	78,206	77,313	77,318	77,470	77,509	77,502	77,183	F
M	1,155,000	1,161,700	1,161,600	1,160,500	1,161,600	1,160,500	1,161,600	1,168,100	1,168,200	1,168,100	1,168,200	1,168,100	1,168,200	1,168,200	M
		First Trial	Yields	Second Trial	Yields	Third Trial	Yields	First Trial	Yields	Second Trial	Yields	Third Trial	Yields		
							Iteration Terminated						Iteration Terminated		

of programme ITER. ITER was capable of finding locations on Fig. 5.10 to accuracies of $\pm$ .001 of the moment M and to within $\pm$ .001 of the interaction force F. To make ITER more accurate would have required more time, and very likely would have made ITER unuseable in a general inelastic finite difference analysis programme.

In conclusion, the theoretical investigation of this report studying the inelastic finite difference method of analysing composite beams showed that the theory was correct. This was not a new finding because Dai and Siess(9) had concluded this before. However, a clear understanding of the theory was obtained by this researcher.

In the opinion of this researcher, the inelastic finite difference method is apparently workable as a research tool even though it is extremely sensitive. It is unlikely to be used for design because of its complexity. Simpler methods are being studied(27) by other researchers which are capable of generating the complete moment-curvature curve.

It was intended to combine the elastic finite difference programme (ELAS, App. (d)), ITER (App. (f)), and INELAS (App. (g)) into a general analytical programme for composite beams. However, due to anticipated programming difficulties and lack of time, this was not done.

CONCLUSIONS

The conclusions are listed as they appear throughout this report. There are, however, a few overall conclusions that should be noted.

1. Push-Out Tests:

The mode of failure of the shear connection in a push-out specimen is very different from that observed in composite beams. However, the ultimate strength of the shear connection as measured in a push-out test can be used to calculate the ultimate strength of a composite beam. The modulus of the shear connection as measured in a push-out test appears to be different than the modulus of the composite beam's shear connection. However, on the basis of the elastic finite difference method of analysis, the performance of the beams tested was not sensitive to what shear force vs. slip relation was chosen for the shear connection. Therefore, for the composite beams of this report, the push-out test can be used as an indicator of the performance of the shear connection in the composite beam. This conclusion may not apply to other composite beams.

2. Analysis of composite beams:

For the beams of this report, up to working load, analysis based on complete interaction yielded strains which were approximately correct and deflections which were conservative. Analysis based on the C.S.S.B.I. Composite Beam Manual, for loads up to working load, yielded strains close to those measured and deflections which were conservatively high. The calculations based on the C.S.S.B.I. Composite Beam Manual yielded results which were a better approximation to the measured values of strain and deflection at working load compared to the complete interaction calculations.

3. Arrangement of shear connectors:

Grouping of shear connectors appeared to make very little difference in beam performance.

4. Thickness of slab:

The ultimate load and elastic stiffness improved markedly with a deeper slab. However, due to higher dead load strains, the working load of the beam with the 5" slab was not appreciably higher than the working loads of the other beams with the 4" slab.

5. The inadequate connection model yields conservative results for the ultimate strengths of the composite beams. This calculation is simple and could be recommended for use by designers for calculation of ultimate strength of composite beams with cellular steel floor.

The following results of the ultimate strengths of the composite beams were obtained:

Beam	q_u	$\frac{\Sigma q_u}{\text{Shear Span}}$	Slab Thickness	$M_u(\text{meas.})/M'_u$
1	11.3	67.8	4	1.03
2	17.0	102.0	4	1.06
3	11.3	101.7	4	1.08
4	17.0	102.0	4	1.07
5	25.4	152.4	5	1.11

6. The inelastic finite difference method of composite beam analysis is too complicated for use by designers.

BIBLIOGRAPHY

(1) Robinson, H., "Preliminary Investigation of a Composite Beam with Ribbed Slab Formed by Cellular Steel Decking", Engineering Dept. Report No. 35, McMaster University, October 1961.

(2) Robinson, H., "Tests on Composite Beams with Cellular Deck", Journal of the Structural Division, Proceedings of the ASCE, Vol. 93, No. ST4, August 1967, pp. 139-164.

(3) Robinson, H., "Composite Beams Incorporating Cellular Steel Decking", paper given at the ASCE National Meeting on Transportation Engineering, Structural Division, San Diego, California, USA, February 1968.

(4) Robinson, H., "Tests of Composite Push-Out Specimens with Stud Connectors and Metal Deck", Engineering Dept. Report, McMaster University, October 1967.

(5) Slutter, R.G., Driscoll, G.C., "Flexural Strength of Steel-Concrete Composite Beams", Journal of the Structural Division, Proceedings of the ASCE, Vol. 91, No. ST2, Proc. Paper 4292, April 1965, pp. 71-99.

(6) British Standard Code of Practice, CP 117:Part 1: 1965, "Composite Construction in Structural Steel and Concrete; Part I: Simply-Supported Beams in Buildings", The Council for Codes of Practice, British Standards Institution.

(7) American Association of State Highway Officials, "Code for Highway Bridges", Section 1.7, Composite Girders, Standard Specifications for Highway Bridges, 1965, Washington D.C.

(8) American Institute of Steel Construction, "Specification for the Design, Fabrication, and Erection of Structural Steel for Buildings", 1961. Also proposed revisions to same.

(9) Dai, P.K.H., Siess, C.P., "Analytical Study of Composite Beams with Inelastic Shear Connection", Dept. of Civil Engineering Study, Structural Research Series No. 267, University of Illinois, Urbana Illinois, USA, June 1963.

(10) Canadian Sheet Steel Building Institute, "Composite Beam Manual", Crestview Plaza, South Service Road, Port Credit Ontario, March 1969.

(11) Fisher, J.W., Kim, S., Slutter, R.G., "Tests of Lightweight Concrete Composite Beams and Pushout Specimens with Cellular Steel Deck", Fritz Engineering Laboratory Report No. 200.67.438.1, Lehigh University Institute of Research, July 1967.

(12) Siess, C.P., Viest, I.M., Newmark, N.M., "Studies of Slab and Beam Highway Bridges: Part III, Small-Scale Tests of Shear Connectors and Composite T-Beams", University of Illinois Bulletin No. 396, February 1952.

(13) Viest, I.M., Siess, C.P., Appleton, J.H., Newmark, N.M., "Studies of Slab and Beam Highway Bridges, Part IV, Full-Scale Tests of Channel Shear Connectors and Composite T-Beams", University of Illinois Bulletin No. 405, December 1952.

(14) Galambos, T.V., Lay, M.G., "Studies of the Ductility of Steel Structures", Journal of the Structural Division, ASCE, August 1965, p. 125.

(15) Lay, M.G., Galambos, T.V., "Inelastic Beams under Moment Gradient", Journal of the Structural Division, ASCE, February 1967, p. 381.

(16) Lay, M.G., "Flange Local Buckling in Wide-Flange Shapes", Journal of the Structural Division, ASCE, December 1965, p. 95.

(17) Viest, I.M., "Review of Research on Composite Steel-Concrete Beams", Journal of the Structural Division, ASCE, June 1960, p. 1.

(18) Spillers, W.R., "On Composite Beams", Journal of the Structural Division, ASCE, August 1965, p. 17.

(19) Chapman, J.C., "Composite Construction in Steel and Concrete - The Behaviour of Composite Beams", The Structural Engineer, April 1964.

(20) Chapman, J.C., Balakrishnan, S., "Experiments on Composite Beams", The Structural Engineer, November 1964, p. 369.

(21) Barnard, P.R., Johnson, R.P., "Ultimate Strength of Composite Beams", Proceedings of the Institute of Civil Engineers, October 1965, p. 161.

(22) Barnard, P.R., Johnson, R.P., "Plastic Behaviour of Continuous Composite Beams", Proceedings of the Institute of Civil Engineers, October 1965, p. 180.

(23) Johnson, R.P., Finlinson, J.C.H., Heyman, J., "A Plastic Composite Design", Proceedings of the Institute of Civil Engineers, October 1965, p. 198.

(24) Discussion on the above 3 references, Proceedings of the Institute of Civil Engineers, August 1966, p. 562.

(25) Stüssi, F., "Zusammengesetzte Vollwandträger", Publications, Inter-National Association for Bridge and Structural Engineering, Vol. VIII, p. 249, 1947.

(26) Archer, I.H., "The Behaviour of Composite Beams with Flexible Connections", M. of Eng. Thesis, McMaster University, Dept. of Civil Engineering, Hamilton, February 1966.

(27) Yam, L.C.P., Chapman, J.C., "The Inelastic Behaviour of Simply-Supported Composite Beams of Steel and Concrete", paper 7111, Proceedings I.C.E., Vol. 41, pp. 651, 653, December 1968.

APPENDIX (a)

WORKING LOAD BASED ON COMPLETE INTERACTION

TRANSFORMED MOMENTS OF INERTIA

	Beams 1-4	Beam 5
	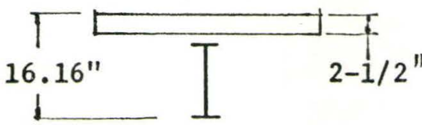	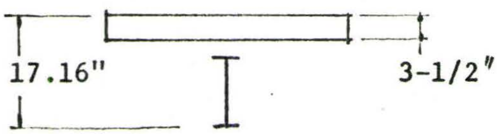
A_c/n	$\frac{68 \times 2.5}{9} = 18.9$	$\frac{68 \times 3.5}{9} = 26.4$
Moments of area	$18.9 \times 1.25 + 5.62 \times 10.08 = 80.3$	$26.4 \times 1.75 + 5.62 \times 11.08 = 108.4$
Transformed area	$18.9 + 5.62 = 24.52$	$26.4 + 5.62 = 32.02$
Centroid	$\bar{y} = \frac{80.3}{24.52} = 3.29''$	$\bar{y} = \frac{108.4}{32.02} = 3.37''$
Moment of inertia slab	$18.9 \times 2.5^2/12 = 10$ $18.9 \times 2.14^2 = 86$	$26.4 \times 3.5^2/12 = 27$ $26.4 \times 1.62^2 = 69$
beam	130 $5.62 \times 6.79^2 = 259$ 485	130 $5.62 \times 7.71^2 = 335$ 561
Section modulus bottom steel fibre	$\frac{485}{12.87} = 36.9 \text{ in}^3$	$\frac{561}{13.79} = 40.7 \text{ in}^3$

<u>Allowable Strain Difference for Live Load</u>

	Beams 1-4	Beam 5
Dead load, uniform moment, d.l. $\frac{WL^2}{8}$	259 plf. 172 in-k	329 plf. 218 in-k
Bottom fibre stress from dead load $\frac{M}{S_b}$ (S_b = 21.4)	8040 p.s.i.	10,200 p.s.i.
Bottom fibre strain from dead load $\frac{\sigma}{E}$ ($E = 29 \times 10^6$)	277 M "/"	351 M "/"
Yield stress, minimum	44,000	44,000
Yield strain $\frac{44,000}{29 \times 10^6}$	1510 M"/"	1510 M "/"
0.66 f_y	1000	1000
Lower fibre strain from dead load at 1/4 span = 3/4 x 277, etc.	208	264
Allowable live load strain difference	792	736

<u>Working Load</u>

Allowable live load stress = allowable strain x E	23.0 ksi	21.4 ksi
Live load bending moment = stress x S_s	845 in-k	870 in-k
Total allowable 2-pt live load = $\frac{M}{33}$	25.6 kips	26.4

APPENDIX (b)

WORKING LOAD BASED ON C.S.S.B.I. COMPOSITE DESIGN MANUAL

From table 6.2 of Manual, record properties of transformed section,

	Beams 1-4	Beam 5
b'	68.	68.
$b'/_n = \frac{68}{9}$	7.55	7.55
S_s	37.0	40.7
I'_f	476.7	559.5
Y_b	12.85	13.75
D'	.1629	.1384
From table 6.3 of Manual,		
L	21'	21'
$'/CL^2$	.020	.020
$(1/L^2) \times 10^9$	1.234	0.994
(ALPHA) $\times 10^9$	125.77	119.27
BETA	1.612	1.623
GAMMA	0.612	0.622
From F/F' nomograph Fig. 6.1 of Manual,		
F/F' deflection	0.95	0.95
From Fig. 6.2 of Manual,		
C_d	0.82	0.79
From F/F' nomograph Fig. 6.1 of manual,		
F/F' stress	0.79	0.79
From Fig. 6.3 of Manual,		
C_s	0.88	0.88

	Beams 1-4	Beam 5
C.S.S.B.I. effective section modulus		
for stress = C_s x S_s =	32.5 in^3	35.8 in^3
C.S.S.B.I. effective moment of inertia		
for deflection = C_d x I'_f =	391. in^4	443. in^4
Allowable live load strain		
difference (from App.(a))	792.	736.
Allowable live load stress		
= allowable strain x E	23.0 ksi	21.4 ksi
Live load bending moment		
M = stress x S_s x C_s =	748 in-k	766 in-k
Total allowable 2-pt. live load		
= $\frac{M}{33}$ =	22.6 kips	23.2 kips

APPENDIX (c)

WORKING LOAD BASED ON A.I.S.C. EFFECTIVE SECTION MODULUS

$$S_{eff} = S_s + \frac{V_h'}{V_h}(S_b - S_s)$$

Where V_h is the total horizontal shear to be resisted between the point of maximum positive moment and points of zero moment, and is the smaller value of

$$V_h = \frac{0.85\, f_c' bt}{2}, \quad V_h = \frac{A_s F_y}{2}$$

V_h' is the horizontal shear determined by multiplying the number of connectors between the point of maximum moment and the point of zero moment by q, the allowable connector load for working stress design.

There are no published allowable working loads for stud connectors in a composite beam with cellular steel floor. Therefore, on the basis of the push-out tests done in this report, V_h' and V_h can be redefined as:

$V_h' = \sum q_u$, sum of the ultimate shear forces on the connectors between the load point and the end support of the beam.

$V_h = 0.85\ f_c'bt$ or A_sF_y, whichever is smaller.

	Beam 1	2	3	4	5
$V_h' = \sum q_u$, kips	67.8	102	101.7	102	153
V_h, kips	247.	247.	247.	247.	247.
S_b, in^3	36.9	36.9	36.9	36.9	40.7
$\frac{V_h'}{V_h}$	.28	.41	.41	.41	.62
S_s, in^3	21.4	21.4	21.4	21.4	21.4
$\frac{V_h'}{V_h}(S_b - S_s)$	4.3	6.3	6.3	6.3	9.6
S_{eff}, in^3	25.7	27.7	27.7	27.7	31.0
Allowable live load stress, App. (a)	23.0	23.0	23.0	23.0	21.4
S_{eff} x stress = M	592	638	638	638	663
allowable load $= \frac{M}{33}$	18.0	19.3	19.3	19.3	20.1

```
C                              A P P E N D I X   D
C
C                              ------------------
C
C       GENERAL PROGRAM TO ANALYSE COMPOSITE BEAM WITH FLEXIBLE SHEAR
C       CONNECTION, UP TO THE POINT WHERE INELASTICITY OCCURS IN STEEL.
C       A MAXIMUM OF 301 GROUPS OF STUDS ARE ALLOWED (ONE STUD CAN BE
C       CALLED A GROUP, OR MORE THAN ONE, IF THEY ARE ADDED TOGETHER AT
C       EACH CROSS-SECTION), AND ALL STUDS MAY BE DIFFERENT.
C
C       TRI-LINEAR MODULUS IS USED FOR THE STUD FORCE-SLIP CHARACTERISTIC.
C
C
RUN(S,,,,,,22100)
LGO.
'          6400 END RECORD
        PROGRAM TST (INPUT,OUTPUT,TAPE5=INPUT,TAPE6=OUTPUT)
C
C
C       M= NO OF STUDS (OR GROUPS OF STUDS )
C       N= NO OF INTERVALS BETWEEN STUDS
C       ES= E OF SLAB
C       EB= E OF BEAM
C       CS= DISTANCE INTERFACE TO CENTROID SLAB
C       CB= DISTANCE INTERFACE TO CENTROID BEAM
C       Z = SUM OF CS AND CB
C       AB = AREA BEAM
C       AS = AREA SLAB
C       BI = I OF BEAM ALONE
C       SI = I OF SLAB ALONE
C       ZL = SPAN OF BEAM
C       P  = TOTAL LOAD ON COMPOSITE BEAM DISTRIBUTED TO 2 POINTS
C       PZERO = INITIAL TOTAL LOAD
C       DELTAP= LOAD INCREMENT
C       PMAX = MAXIMUM TOTAL LOAD
C       CONST = Z OVER SIGMA EI
C       COUNT = COUNTER OF LOOPS REQ,D TO STABILIZE STUD FORCES
C       BURP = INDICATOR WHICH = 0 IF PO IS CHOSEN LOW ENOUGH,=1 IF NOT
C       OKAY  = 1.0 IF STUD FORCES ARE STABILIZED, =0.0 IF NOT
C       B(I,J) = STUSSI MULTIPLIER ARRAY
C       B1,B2,B3,B4(I,J) =SEPARATELY-GENERATED ARRAYS, WHICH WHEN ADDED,
C                          SUM TO B(I,J) WITH CORRECTED ELEMENTS
C       CK,CKP,CKPP(I) =  STUD MODULUS ARRAYS
C       QP,QY,QU(I) = LIMITS OF APPLICABILITY OF CK,CKP,CKPP ARRAYS
C       SLIP,SLIPP,SLIPY(I) = SLIP AND SLIP LIMITS ARRAYS. (AND SLIPU(I))
C       BENMOM(I) = IMPRESSED MOMENT ON BEAM, CAUSED BY PO ONLY.
C       BADMOM(I) = BENMOM(I) * P/PO
C       AVGMOM,SUMMOM,DUMMOM(I) = ARRAYS OF IMPRESSED MOMENTS
C       BMOM2,BMOM3(I) = ARRAYS OF CORRECTIONS TO RHS OF STUSSI MATRIX
C                         EQUATION
C       BENSLB,BENBEM(I) = ARRAYS OF MOMENTS IN SLAB,BEAM
C       FORCEF,FORCEQ(I) = ARRAYS OF FORCES IN SLAB AND ON STUDS
C       FORCPR(I) = FORCE IN SLAB ASSUMING COMPLETE INTERACTION
C       STRANS,STRANB(I) = STRAIN IN SLAB AND BEAM ARRAYS.
C       SPACE(I) = ARRAY OF SPACES BETWEEN STUDS AND/OR SUPPORTS
C       TRACE(I) = TRACES STATE OF CORRECTIONS IN STUSSI MATRIX EQUATION
```

```
C     RANGE(I) = INDICATES RANGE OF STUD FORCE COMPUTED
C           STUD FORCES ARE STABILIZED WHEN TRACE(I) = RANGE I)
      COMMON/BLOK1/B(3,300),B1(3,300),B2(3,300),B3(3,300),B4(3,300)
      COMMON/BLOK2/CK(301),CKP(301),CKPP(301)
      COMMON/BLOK3/QP(301),QY(301),QU(301)
      COMMON/BLOK4/SLIP(301),SLIPP(301),SLIPY(301),SLIPU(301)
      COMMON/BLOK5/BENMOM(301),AVGMOM(300),BADMOM(301)
      COMMON/BLOK6/SUMMOM(300),BMOM2(300),BMOM3(300)
      COMMON/BLOK7/FORCEF(300),FORCEQ(301)
      COMMON/BLOK8/SPACE(300)
      COMMON/BLOK9/TRACE(301),RANGE(301)
      DIMENSION BENSLB(300),BENBEM(300),FORCPR(300),STRANS(300)
      DIMENSION STRANB(300),EQUILM(300)
      DIMENSION FORCRA(300)
      DIMENSION TITLE(13)
      DIMENSION STRASS(300),STRABB(300)
      DD = 1.25
      READ(5,4)TITLE
    4 FORMAT(13A6)
      READ(5,5)M,N,ES,EB,CS,CB,AB,AS,BI,SI
    5 FORMAT(2I5,2E10.4,4F7.3,2F10.4)
      READ(5,10)PZERO,DELTAP,PMAX
   10 FORMAT(3E10.3)
      P=PZERO
      DO 25 I=1,M
      READ(5,15)QP(I),SLIPP I),QY(I),SLIPY(I),QU(I),SLIPU(I)
   15 FORMAT(6E12.4)
      CK(I) = QP(I)/SLIPP(I)
      CKP(I)=(QY(I)-QP(I))/(SLIPY(I)-SLIPP(I))
      CKPP(I)= (QU(I)-QY(I))/(SLIPU(I)-SLIPY(I))
   25 CONTINUE
      READ(5,30)(BENMOM(I),I=1,M)
      READ(5,35)(SPACE(I),I=1,N)
   30 FORMAT(8F10.0)
   35 FORMAT(8F10.2)
      WRITE(6,58)(TITLE(I),I = 1,13)
   58 FORMAT(1H1,13A6)
      WRITE(6,60)M,N
   60 FORMAT(16H COMPOSITE BEAM,,I5,7H STUDS,,I5,10H INTERVALS///)
      WRITE(6,65)
   65 FORMAT(50X,19H SECTION PROPERTIES)
      WRITE(6,66)
   66 FORMAT(40X,41H -----------------------------------------///)
      WRITE(6,67)
   67 FORMAT(111H      ES          EB          CS          CB          AS
     1AB        IS          IB          PO      DELTA P    P MAX        /)
      WRITE(6,68)ES,EB,CS,CB,AS,AB,SI,BI,PZERO,DELTAP,PMAX
   68 FORMAT(E10.3,1X,E10.3,F8.3,3F10.3,2F10.4,3E10.3//)
      WRITE(6,69)
   69 FORMAT(48X,22H CONNECTION PROPERTIES)
      WRITE(6,66)
      WRITE(6,70)
   70 FORMAT (82H   STUD NO          K              K'              K''        PRECEDE
     1S SPACE (IN)   ZERO MOMENT /)
      IF(PZERO.EQ.5000.0)GO TO 73
      DO 72 I = 1,M
      BENMOM(I) = (PZERO/5000.0)*BENMOM(I)
   72 CONTINUE
```

```
 73 DO 75 I = 1,N
    WRITE(6,74)I,CK(I),CKP(I),CKPP(I),SPACE(I),BENMOM(I)
 74 FORMAT(4X,I3,3X,3E12.4,6X,F10.2,10X,F10.0)
 75 CONTINUE
    WRITE(6,77)M,CK(M),CKP(M),CKPP(M),BENMOM(M)
 77 FORMAT 4X,I3,3X,3E12.4,26X,F10.0///)
    WRITE(6,80)
 80 FORMAT(84H    STUD NO          QP           GAMMA P          QY          GAMMA
   1 Y          QU          GAMMA U  )
    DO 85 I = 1,M
    WRITE(6,83)I,QP(I),SLIPP(I),QY(I),SLIPY(I),QU(I),SLIPU(I)
 83 FORMAT(4X,I3,4X,6E12.4)
 85 CONTINUE
    WRITE(6,992)
    WRITE(6,66)
    WRITE(6,992)
    Z = CS + CB
    SUMEI = EB*BI + ES*SI
    EABAR = (EB*AB*ES*AS)/(ES*AS + EB*AB)
    EIBAR = SUMEI + EABAR*Z**2.0
    AA = EIBAR/(EABAR*SUMEI)
    CONST = Z/SUMEI
    WRITE(6,86)Z,SUMEI,EABAR,EIBAR,AA,CONST
 86 FORMAT(3H Z=,E10.4,5X,7H SUMEI=,E10.4,5X,7H EABAR=,E10.4,7H EIBAR=
   1,E10.4,5X,4H AA=,E10.4,5X,7H CONST=,E10.4)
    BURP = 0.0
    OKAY = 1.0
    DO 90 I = 1,3
    DO 90 J = 1,N
    B(I,J) = 0.0
 90 CONTINUE
    DO 95 I = 1,M
    RANGE(I) = 0.0
 95 CONTINUE
    COUNT = 0.0
499 DO 50 I = 1,3
    DO 50 J = 1,N
    B1(I,J) = 0.0
    B2 I,J) = 0.0
    B3(I,J) = 0.0
    B4(I,J) = 0.0
 50 CONTINUE
502 DO 55 J = 1,N
    BMOM2(J) = 0.0
    BMOM3(J) = 0.0
 55 CONTINUE
500 CALL ARAMOM(M,N,PZERO,P,CONST)
501 CALL ALTER(M,N,AA)
    WRITE(6,505)
505 FORMAT(30X,7H SUMMOM,13X,6H BMOM2,14X,6H BMOM3)
    DO 510 I = 1,N
    WRITE(6,508)SUMMOM(I),BMOM2(I),BMOM3(I)
508 FORMAT(29X,E11.4,9X,E11.4, 8X,E11.4)
510 CONTINUE
    DO 515 I = 1,N
514 SUMMOM(I) = SUMMOM(I) + BMOM2(I) + BMOM3(I)
515 CONTINUE
    DO 517 J = 1,N
```

```
      WRITE(6,516)J,B(1,J),B(2,J),B(3,J),SUMMOM(J),J
  516 FORMAT(20X,I5,3E12.4,10X,E12.4,I5)
  517 CONTINUE
      CALL DIAG3(B,SUMMOM,N)
      DO 520 J = 1,N
      FORCEF(J) = SUMMOM(J)
  520 CONTINUE
      CALL CALSTD(M)
      CALL RANGER(M)
      IF(P.GT.PZERO)GO TO 599
      CALL CHECK1(M,BURP)
      IF(BURP.GT.0.0) GO TO 9999
  599 COUNT = COUNT + 1.0
  600 CALL COMPAT(M,OKAY)
      IF(OKAY.GT.0.0) GO TO 900
      GO TO 502
  900 DO 950 I = 1,N
      BENSLB(I) = ((ES*SI)*(AVGMOM(I) - FORCEF(I)*Z))/SUMEI
      BENBEM(I) = ((EB*BI)*(AVGMOM(I) - FORCEF(I)*Z))/SUMEI
      STRANS(I) =-FORCEF(I)/(ES*AS) - BENSLB(I)*DD/(ES*SI)
      STRASS(I) =-FORCEF(I)/(ES*AS) + BENSLB(I)*DD/(ES*SI)
      STRANB(I) = FORCEF(I)/(EB*AB) + BENBEM(I)*CB/(EB*BI)
      STRABB(I) = FORCEF(I)/(EB*AB) - BENBEM(I)*CB/(EB*BI)
      FORCPR(I) = (EABAR/EIBAR)*Z*AVGMOM(I)
      FORCRA(I) = FORCEF(I)/FORCPR(I)
      EQUILM(I) = BENSLB(I) + BENBEM(I) + FORCEF(I)*Z
  950 CONTINUE
      PP = 2.0*P
      WRITE(6,975)PP,COUNT
  975 FORMAT(1H1,39X,9HTOTAL LD=,E10.3,4H LBS,5X,8H COUNT =,F6.0)
      WRITE(6,66)
      WRITE(6,985)
  985 FORMAT(125H INTERVAL      F         F/F'     BEAM MOM       SLAB MOM    TO
     1P STR SLB  BOT STR SLB  TOP STR BM    BOT STR BM      AVGMOM      MS+MB
     1+F*Z//)
      DO 990 I = 1,N
      WRITE(6,987)I,FORCEF(I),FORCRA(I),BENBEM(I),BENSLB(I),STRANS(I),ST
     1RASS(I),STRABB(I),STRANB(I),AVGMOM(I),EQUILM(I)
  987 FORMAT(2X,I3,3X,E12.4,F5.2,1X,2E12.4,1X,E12.4,1X,E12.4,1X,E12.4,1X
     1,2E12.4,1X,E12.4/)
  990 CONTINUE
      WRITE(6,992)
  992 FORMAT(2X,////)
      DO 1100 I = 1,M
      IF(ABS(FORCEQ(I)).GT.QP(I)) GO TO 1020
      SLIP(I) = FORCEQ(I)/CK(I)
      GO TO 1100
 1020 IF(ABS(FORCEQ(I)).GT.QY(I)) GO TO 1040
      SLIP(I) = SLIPP(I) + (FORCEQ(I) - QP(I))/CKP(I)
      GO TO 1100
 1040 SLIP(I) = SLIPY(I) + (FORCEQ(I) -QY(I))/CKPP(I)
 1100 CONTINUE
      WRITE(6,995)
  995 FORMAT(48X,29H STUD    FORCE         SLIP     //)
      DO 997 I = 1,M
      WRITE(6,996)I,FORCEQ(I),SLIP(I)
  996 FORMAT(47X,I3,2E12.4/)
  997 CONTINUE
```

```
      WRITE(6,66)
      WRITE(6,992)
      IF(P.EQ.PMAX)GO TO 9997
      P = P + DELTAP
      WRITE(6,1000)
 1000 FORMAT(24H LOAD HAS BEEN INCREASED)
      WRITE(6,992)
      GO TO 499
 9997 WRITE(6,9998)
 9998 FORMAT(40H SAY MAN, YOU EVER HEARD OF AN ABACCUS ?)
 9999 STOP
      END
$IBFTC ALTER
C     ALTER SETS UP ALL ELEMENTS IN THE MATRIX EQUATION DEPENDING ON
C     THE RANGE OF STUD FORCE CURRENT.  THIS IS TAKEN INITIALLY AT ZERO.
C     THE VECTOR OF INTEGRATED IMPRESSED MOMENTS IS SET UP IN ARAMOM.
      SUBROUTINE ALTER(M,N,AA)
      COMMON/BLOK1/B(3,300),B1(3,300),B2(3,300),B3(3,300),B4(3,300)
      COMMON/BLOK2/CK(301),CKP(301),CKPP(301)
      COMMON/BLOK3/QP(301),QY(301),QU(301)
      COMMON/BLOK4/SLIP(301),SLIPP(301),SLIPY(301),SLIPU(301)
      COMMON/BLOK5/BENMOM(301),AVGMOM(300),BADMOM(301)
      COMMON/BLOK6/SUMMOM(300),BMOM2(300),BMOM3(300)
       COMMON/BLOK7/FORCEF(300),FORCEQ(301)
      COMMON/BLOK8/SPACE(300)
      COMMON/BLOK9/TRACE(301),RANGE(301)
      DO 500 J = 1,N
      IF(RANGE(J).GT.0.0) GO TO 100
      IF(J.GT.1) GO TO 20
      B1(2,J) = 1.0/CK(J)
      TRACE(J) = 0.0
      GO TO 500
   20 B1(2,J) = 1.0/CK(J)
      B2(2,J-1) = 1.0/CK(J)
      B4(1,J) = -1.0/CK(J)
      B4(3,J-1) = B4(1,J)
      TRACE(J) = 0.0
      GO TO 500
  100 IF(RANGE(J).GT.1.0) GO TO 200
      IF(J.GT.1) GO TO 120
      B1(2,J) = 1.0/CKP(J)
      TRACE(J) = 1.0
      IF(FORCEQ(J).GE.0.0) GO TO 110
      DC = -1.0
      GO TO 111
  110 DC = +1.0
  111 BMOM2(J) = DC*(QP(J)/CKP(J) - SLIPP(J))
      GO TO 500
  120 B1(2,J) = 1.0/CKP(J)
      B2(2,J-1) = 1.0/CKP(J)
      B4(1,J) = -1.0/CKP(J)
      B4(3,J-1) = B4(1,J)
      TRACE(J) = 1.0
      IF(FORCEQ(J).GE.0.0) GO TO 130
      DC = -1.0
      GO TO 131
  130 DC = +1.0
  131 BMOM2(J-1) = -DC*(QP(J)/CKP(J) - SLIPP(J)) + BMOM2(J-1)
```

```
  132 BMOM2(J) = DC*(QP(J)/CKP(J) - SLIPP(J))
      GO TO 500
  200 IF(RANGE(J).GT.2.0) GO TO 500
      IF(J.GT.1) GO TO 220
      B1(2,J) = 1.0/CKPP(J)
      TRACE(J) = 2.0
      IF(FORCEQ(J).GE.0.0) GO TO 210
      DC = -1.0
      GO TO 211
  210 DC = +1.0
  211 BMOM3(J) = DC*(QY(J)/CKPP(J) - SLIPY(J))
      GO TO 500
  220 B1(2,J) = 1.0/CKPP(J)
      B2(2,J-1) = 1.0/CKPP(J)
      B4(1,J) = -1.0/CKPP(J)
      B4(3,J-1) = B4(1,J)
      TRACE(J) = 2.0
      IF(FORCEQ(J).GE.0.0) GO TO 230
      DC = -1.0
      GO TO 231
  230 DC = +1.0
  231 BMOM3(J-1) = -DC*(QY(J)/CKPP(J) - SLIPY(J)) + BMOM3(J-1)
  232 BMOM3(J) = DC*(QY(J)/CKPP(J) - SLIPY(J))
  500 CONTINUE
      IF(RANGE(M).GT.0.0) GO TO 550
      B2(2,N) = 1.0/CK(M)
      TRACE(M) = 0.0
      GO TO 610
  550 IF(RANGE(M).GT.1.0) GO TO 575
      B2(2,N) = 1.0/CKP(M)
      TRACE(M) = 1.0
      IF(FORCEQ(M).GE.0.0) GO TO 560
      DC = -1.0
      GO TO 561
  560 DC = +1.0
  561 BMOM2(N) = -DC*(QP(M)/CKP(M) - SLIPP(M)) + BMOM2(N)
      GO TO 610
  575 IF(RANGE(M).GT.2.0) GO TO 610
      B2(2,N) = 1.0/CKPP(M)
      TRACE(M) = 2.0
      IF(FORCEQ(M).GE.0.0) GO TO 580
      DC = -1.0
      GO TO 581
  580 DC = +1.0
  581 BMOM3(N) = -DC*(QY(M)/CKPP(M) - SLIPY(M))+ BMOM3(N)
  610 DO 620 I = 1,N
      B3(2,I)= AA*SPACE(I)
  620 CONTINUE
      DO 650 I = 1,3
      DO 650 J = 1,N
      B(I,J) = B1(I,J) + B2(I,J) + B3(I,J) + B4(I,J)
  650 CONTINUE
      RETURN
      END
$IBFTC ARAMOM
C     ARAMOM INTEGRATES IMPRESSED MOMENTS AND SETS UP RHS OF UNCORRECTED
C     STUSSI MATRIX EQUATION.
      SUBROUTINE ARAMOM(M,N,PZERO,P,CONST)
```

```
      COMMON/BLOK5/BENMOM(301),AVGMOM(300),BADMOM(301)
      COMMON/BLOK6/SUMMOM(300),BMOM2(300),BMOM3(300)
      COMMON/BLOK8/SPACE(300)
      IF(P.GT.PZERO) GO TO 100
      DO 50 I = 1,N
      AVGMOM(I) = (BENMOM(I) + BENMOM(I+1))/2.0
      SUMMOM(I) = CONST* AVGMOM(I) * SPACE(I)
   50 CONTINUE
      GO TO 150
  100 DO 120 I = 1,M
      BADMOM(I) = (P/PZERO)*BENMOM(I)
  120 CONTINUE
      DO 130 I = 1,N
      AVGMOM(I) = (BADMOM(I) + BADMOM(I+1 )/2.0
      SUMMOM(I) = CONST*AVGMOM(I)*SPACE(I)
  130 CONTINUE
  150 RETURN
      END
$IBFTC CALSTD
C     CALSTD CALCULATES THE FORCES ON THE STUDS
      SUBROUTINE CALSTD(M)
      COMMON/BLOK7/FORCEF(300),FORCEQ(301)
      DO 50 I = 1,M
      IF(I-1.GT.0) GO TO 40
   20 FORCEQ(I) = FORCEF(I)
      GO TO 50
   40 IF(I.EQ.M) GO TO 45
      FORCEQ(I) = FORCEF(I) - FORCEF(I-1)
      GO TO 50
   45 FORCEQ(I) = -FORCEF(I-1)
   50 CONTINUE
      RETURN
      END
$IBFTC RANGER
C     RANGER KEEPS TRACK OF THE RANGE OF STUD FORCES CALCULATED
      SUBROUTINE RANGER(M)
      COMMON/BLOK3/QP(301),QY(301),QU(301)
      COMMON/BLOK7/FORCEF(300),FORCEQ(301)
      COMMON/BLOK9/TRACE(301),RANGE(301)
      DO 200 I = 1,M
      IF(ABS(FORCEQ(I)).GT.QP(I)) GO TO 25
      RANGE(I) = 0.0
      GO TO 200
   25 IF(ABS(FORCEQ(I)).GT.QY(I)) GO TO 35
      RANGE(I) = 1.0
      GO TO 200
   35 IF(ABS(FORCEQ(I)).GE.QU(I)) GO TO 45
      RANGE(I) = 2.0
      GO TO 200
   45 RANGE(I) = 3.0
      WRITE(6,50) I
   50 FORMAT(8H STUD NO,I3,27H HAS REACHED ULTIMATE SHEAR//)
  200 CONTINUE
      RETURN
      END
$IBFTC CHECK1
C     CHECK1 MAKES SURE THAT THE FIRST APPLIED MOMENT IS LOW ENOUGH TO
C     YIELD STUD FORCES IN THE ZERO RANGE.
```

```
      SUBROUTINE CHECK1(M,BURP)
      COMMON/BLOK9/TRACE(301),RANGE(301)
      BURP = 0.0
      DO 100 I = 1,M
      IF(RANGE(I).EQ.0.0) GO TO 100
      BURP = BURP + 1.0
  100 CONTINUE
      IF(BURP.EQ.0.0) GO TO 200
      WRITE(6,150)
  150 FORMAT(25H INITIAL LOAD IS TOO HIGH//)
  200 RETURN
      END
$IBFTC COMPAT
C     COMPAT COMPARES STUD FORCES CALCULATED AND LEVEL OF CORRECTIONS
      SUBROUTINE COMPAT(M,OKAY)
      COMMON/BLOK9/TRACE(301),RANGE(301)
      OKAY = 1.0
      DO 100 I = 1,M
      IF(RANGE(I).EQ.TRACE(I)) GO TO 100
      OKAY = 0.0
  100 CONTINUE
      WRITE(6,125)
  125 FORMAT(21H RANGE OF STUD FORCES/)
      WRITE(6,150)(RANGE(I),I=1,M)
      WRITE(6,135)
  135 FORMAT(28H STATE OF CORRECTIONS SO FAR/)
      WRITE(6,150)(TRACE(I),I=1,M)
  150 FORMAT(30F4.0)
      WRITE(6,160)
  160 FORMAT(2X,///)
      RETURN
      END
'        6400 END RECORD
1968 MCMASTER TESTS -- BEAM NO 1( SIX SINGLE STUDS IN SHEAR SPAN )
  16    15 .3190E+07 .2900E+08  2.750  6.080  5.620170.000  130.1000    88
  .100E+04  .500E+03  .200E+05
   .6000E+04   .2000E-02   .1100E+05   .2000E-01   .1200E+05   .1000E+00
   .6000E+04   .2000E-02   .1100E+05   .2000E-01   .1200E+05   .1000E+00
   .6000E+04   .2000E-02   .1100E+05   .2000E-01   .1200E+05   .1000E+00
   .6000E+04   .2000E-02   .1100E+05   .2000E-01   .1200E+05   .1000E+00
   .6000E+04   .2000E-02   .1100E+05   .2000E-01   .1200E+05   .1000E+00
   .6000E+04   .2000E-02   .1100E+05   .2000E-01   .1200E+05   .1000E+00
   .6000E+04   .2000E-02   .1100E+05   .2000E-01   .1200E+05   .1000E+00
   .6000E+04   .2000E-02   .1100E+05   .2000E-01   .1200E+05   .1000E+00
   .6000E+04   .2000E-02   .1100E+05   .2000E-01   .1200E+05   .1000E+00
   .6000E+04   .2000E-02   .1100E+05   .2000E-01   .1200E+05   .1000E+00
   .6000E+04   .2000E-02   .1100E+05   .2000E-01   .1200E+05   .1000E+00
   .6000E+04   .2000E-02   .1100E+05   .2000E-01   .1200E+05   .1000E+00
   .6000E+04   .2000E-02   .1100E+05   .2000E-01   .1200E+05   .1000E+00
   .6000E+04   .2000E-02   .1100E+05   .2000E-01   .1200E+05   .1000E+00
   .6000E+04   .2000E-02   .1100E+05   .2000E-01   .1200E+05   .1000E+00
   .6000E+04   .2000E-02   .1100E+05   .2000E-01   .1200E+05   .1000E+00
        0.     60000.    120000.    180000.    240000.    300000.    330000.
   330000.    330000.    300000.    240000.    180000.    120000.     60000.
     12.00      12.00      12.00      12.00      12.00      24.00      24.00
     24.00      24.00      12.00      12.00      12.00      12.00      12.00
'        6400 END FILE
```

APPENDIX (e)

BOTTOM FLANGE PARTIALLY YIELDED

$\epsilon_{bb} > \epsilon_y$
$|\epsilon_b| \leq \epsilon_y$

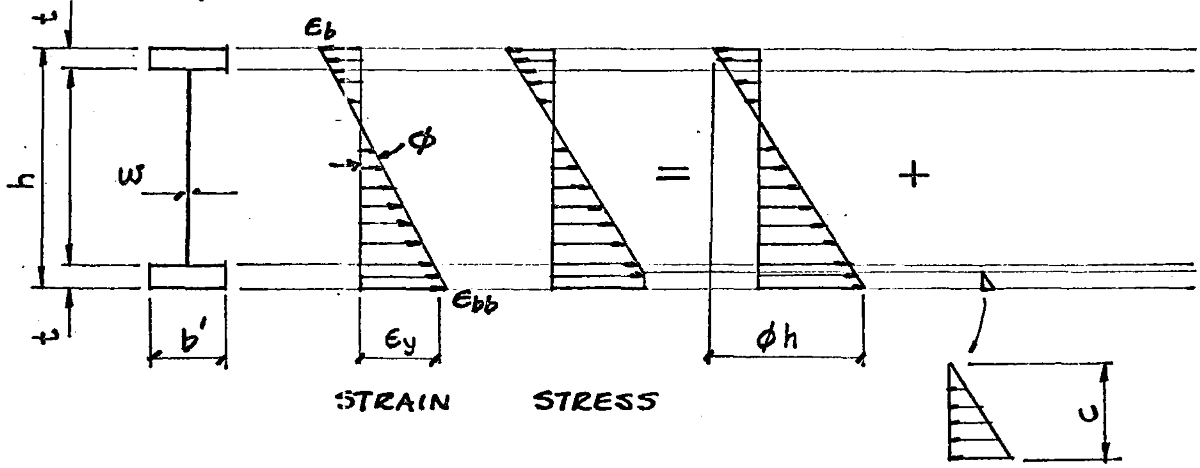

$$\frac{\phi h}{h} = \frac{\epsilon_{bb} - \epsilon_y}{c}$$

$$c = \frac{\epsilon_{bb} - \epsilon_y}{\phi}$$

$$F = \frac{E_b A}{2}\left[(\epsilon_{bb} + \epsilon_b) - \frac{b'}{\phi A}(\epsilon_{bb} - \epsilon_y)^2\right]$$

$$M_b = E_b I_b\left[\phi - \frac{b'}{12\phi^2 I_b}(3\phi h - 2\epsilon_{bb} + 2\epsilon_y)(\epsilon_{bb} - \epsilon_y)^2\right]$$

BOTTOM FLANGE AND PART OF WEB YIELDED

$\epsilon_{bb} > \epsilon_y$
$|\epsilon_b| \leq \epsilon_y$

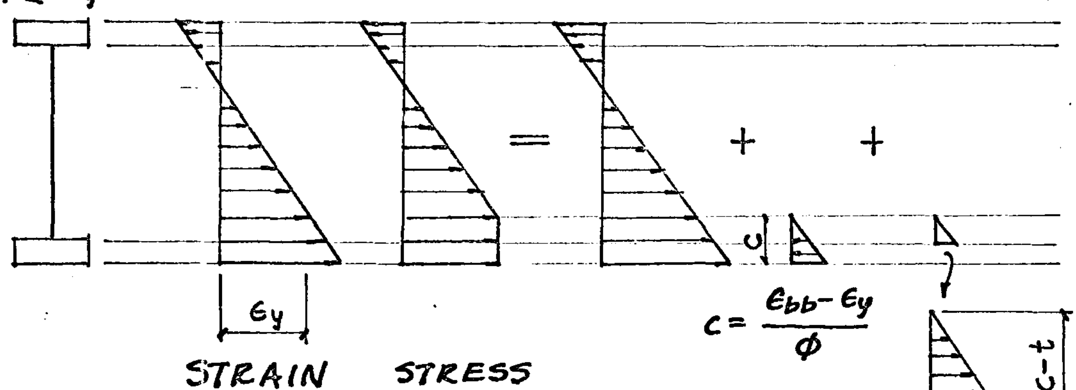

C'

$c' = \phi(c-t)$

$$F = \frac{E_b A}{2}\left[(\epsilon_{bb} + \epsilon_b) - \frac{b'}{A\phi}(\epsilon_{bb} - \epsilon_y)^2 + \frac{b'-w}{A\phi}(\epsilon_{bb} - \epsilon_y - \phi t)^2\right]$$

$$M_b = \frac{E_b I_b \phi}{12}\left[12 - \frac{(3\phi h - 2\epsilon_{bb} + 2\epsilon_y)}{\phi^2}(\epsilon_{bb} - \epsilon_y)^2 \cdot \frac{b'}{\phi I_b} + \frac{(3\phi h - 4\phi t - 2\epsilon_{bb} + 2\epsilon_y)}{\phi^2}(\epsilon_{bb} - \epsilon_y - \phi t)^2 \cdot \frac{(b'-w)}{\phi I_b}\right]$$

BOTTOM FLANGE ENTIRELY YIELDED AND PART OF TOP FLANGE

$|\epsilon_b| > \epsilon_y \qquad |\epsilon_b| \leq \epsilon_y + \phi t$

$\epsilon_{bb} > \epsilon_y + \phi t$

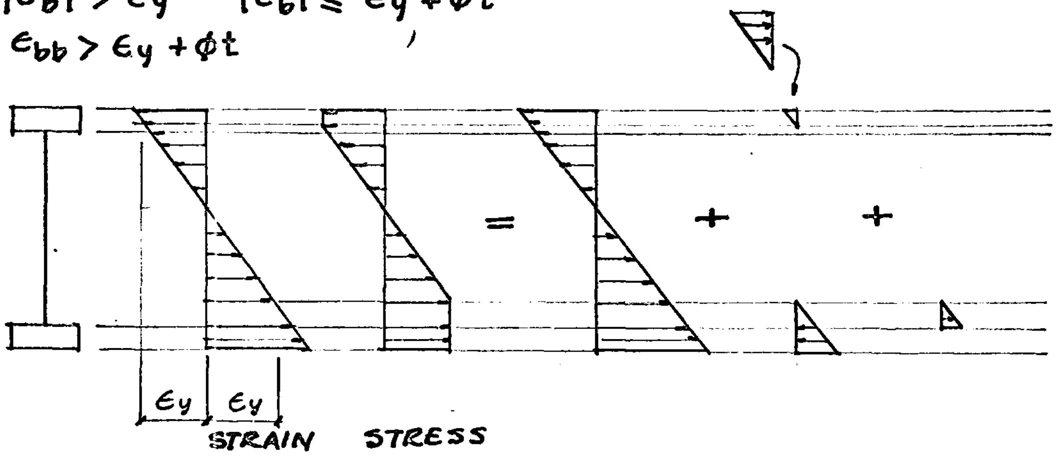

$$F = \frac{E_b A}{2}\left[(\epsilon_{bb} + \epsilon_b) - \frac{b'}{\phi A}(\epsilon_{bb} - \epsilon_y)^2 + \frac{b'-w}{\phi A}(\epsilon_{bb} - \epsilon_y - \phi t)^2 + \frac{b'}{\phi A}(-\epsilon_b - \epsilon_y)^2\right]$$

$$M_b = E_b I_b\left[\phi - \frac{b'}{12\phi^2 I_b}(\epsilon_{bb} - \epsilon_y)^2(3\phi h + 2\epsilon_y - 2\epsilon_{bb}) + \frac{(b'-w)}{12\phi^2 I_b}(\epsilon_{bb} - \epsilon_y - \phi t)^2(3\phi h - 4\phi t + 2\epsilon_y - 2\epsilon_{bb}) - \frac{b'}{12\phi^2 I_b}(-\epsilon_b - \epsilon_y)^2(3\phi h + 2\epsilon_y - 2\epsilon_b)\right]$$

BOTTOM FLANGE ENTIRELY YIELDED AND ALL OF TOP FLANGE

$|\epsilon_b| > \epsilon_y \qquad |\epsilon_b| > \epsilon_y + \phi t \qquad \epsilon_{bb} > \epsilon_y + \phi t$

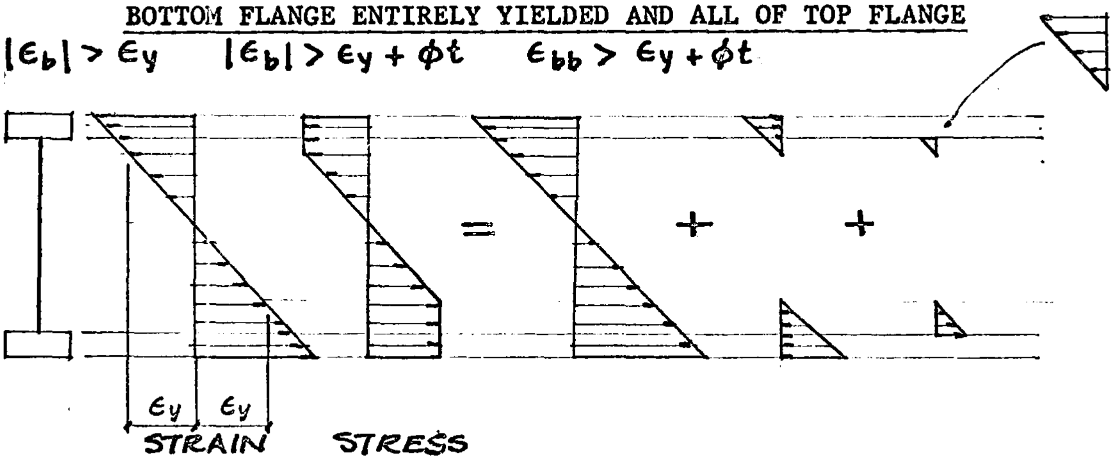

$$F = \text{AS ABOVE} + \frac{E_b A}{2}\left[-\frac{b'-w}{\phi A}(-\epsilon_y - \epsilon_b - \phi t)^2\right]$$

$$M = \text{AS ABOVE} - \frac{E_b(b'-w)}{12\phi^2}(-\epsilon_y - \epsilon_b - \phi t)^2(3\phi h - 4\phi t + 2\epsilon_y - 2\epsilon_b)$$

```
C                            A P P E N D I X   F
C
C                            -------------------
C
C     PROGRAM TO COMPUTE TRIAL SOLUTIONS SATISFYING EQUILIBRIUM ..
C
C
RUN(S,,,,,,6200)
REDUCE.
LGO.
'       6400 END RECORD
      PROGRAM TST (INPUT,OUTPUT,TAPE5=INPUT,TAPE6=OUTPUT)
$JOB            003402 WALLACE I W      100   010   030
$IBJOB          NODECK
$IBFTC
C
C      BEAM 1 -- INTERVAL 7
      DIMENSION AVGMOM(2)
      A = 1.0
      B = 5.0
      ES = 3190000.
      SI = 88.500
      H = 12.16 $ D = 2.50 $ BPR = 4.01 $ Z = 8.83 $T = 0.35 $W = 0.24
      AB = 5.620 $ EB = 29000000. $ BI = 130.10
      AS = 170.
      EPSBB = .0012029
      EPSB = -.000250
      EPSY = .001186
      AVGMOM(1) = 1168200.
      AVGMOM(2) = 1188000.
      FSTAR = 77461.
      DELEPS = ((AVGMOM(2)/AVGMOM(1)) - 1.0) * EPSBB
      DELPHI = .000005
      COUNT  = 1.0
      COUNT1 = 1.0
      COUNT2 = 1.0
      COUNT3 = 1.0
      COUNT4 = 1.0
   20 PHI = (EPSBB - EPSB)/H
   22 IF(EPSBB.LT.EPSY) GO TO 50
      IF(EPSBB.LE.(EPSY + PHI*T))GO TO  40
   30 F = (EB*AB/2.) * ( EPSBB+EPSB -((EPSBB-EPSY)**2.0)*BPR/(PHI*AB) +(
     1(BPR-W)*(EPSBB-EPSY-PHI*T)**2.0)/(PHI*AB))
   31 BMB = EB*BI*PHI - (EB*BPR/(12.0*PHI**2.0)) * ((EPSBB-EPSY)**2.0)*
     1(3.0*PHI*H - 2.0*EPSBB + 2.0*EPSY) +  (BPR-W)*EB/(12.0*PHI**2.0) *
     2 ((EPSBB - EPSY - PHI*T)**2.0)* (3.0*PHI*H - 4.0*PHI*T - 2.0*EPSBB
     3+ 2.0*EPSY)
      GO TO 60
   40 F = (EB*AB/2.0) * ((EPSBB+EPSB) -(BPR/(AB*PHI))*(EPSBB-EPSY)**2.0
   41 BMB =  EB*BI*PHI -((EB*BPR/PHI)*(EPSBB-EPSY)**2.0)*(H/4.0 - (EPSBB
     1-EPSY)/(6.0*PHI))
      GO TO 60
   50 F = EB*AB*(EPSBB + EPSB)/2.0
   51 BMB = EB*BI*PHI
   60 WRITE(6,61)F,BMB
   61 FORMAT(3H F=,E12.4,4H MB=,E12.4)
```

1172

```
      EPSSS = -F/(ES*AS) - PHI*D/2.0
      BMS = ES*SI*PHI
      EPSS = EPSSS + PHI*4.00
   65 BM = BMB + BMS + F*Z
      STRDIF = EPSB - EPSS
      WRITE(6,70)BM,EPSBB,PHI,EPSSS,STRDIF,EPSB,EPSS
   70 FORMAT( 8H MOMENT=,E12.4,4HEBB=,E12.4,5H PHI=,E12.4,5H ESS=,E12.4,
     17H EB-ES=,E12.4,4H EB=,E12.4,4H ES=,E12.4)
      IF(BM.LE.(1.0001*AVGMOM(2))) GO TO 101
      A = 0.70*A
      EPSBB = EPSBB - DELEPS*A
      EPSB = EPSBB - PHI*H
      COUNT = COUNT + 1.0
      IF(COUNT .GT.40.0) GO TO 636
      GO TO 22
  101 IF(BM.GE.(0.9999*AVGMOM(2))) GO TO 200
  110 EPSBB = EPSBB + DELEPS*A
      EPSB = EPSBB - PHI*H
      COUNT  = COUNT  + 1.0
      IF(COUNT .GT.40.0) GO TO 636
      GO TO 22
  200 A = 1.0
  210 PHI = PHI + DELPHI*B
      EPSB = EPSBB - PHI*H
      IF((ABS(EPSB)).GT.EPSY) GO TO 251
      IF(EPSBB.LT.EPSY) GO TO 250
      IF(EPSBB.LE.(EPSY + PHI*T))GO TO 240
  230 F = (EB*AB/2.  * ( EPSBB+EPSB -((EPSBB-EPSY)**2.0)*BPR/(PHI*AB) +(
     1(BPR-W)*(EPSBB-EPSY-PHI*T)**2.0)/(PHI*AB))
      GO TO 260
  240 F = (EB*AB/2.0) * ((EPSBB+EPSB) -(BPR/(AB*PHI))*(EPSBB-EPSY)**2.0
      GO TO 260
  250 F = EB*AB*(EPSBB + EPSB)/2.0
      GO TO 260
  251 IF(EPSBB.LT.(EPSY + PHI*T)) GO TO 640
  252 IF((ABS(EPSB)).LE.(EPSY + PHI*T)) GO TO 258
  253 F = (EB*AB/2.0) *(EPSBB + EPSB - (BPR/(PHI*AB))*((EPSBB-EPSY)**2.0
     1 - (EPSB-EPSY)**2.0) + ((BPR-W)/(PHI*AB)) * ((EPSBB-EPSY-PHI*T)**2
     2.0 - (EPSY-EPSB-PHI*T)**2.0))
      GO TO 260
  258 F = (EB*AB/2.0) *(EPSBB + EPSB - (BPR/(PHI*AB))*((EPSBB-EPSY)**2.0
     1 - (EPSB-EPSY)**2.0) + ((BPR-W)/(PHI*AB)) * ((EPSBB-EPSY-PHI*T)**2
     2.0 ))
  260 WRITE(6,261)F,PHI
  261 FORMAT(3H F=,E12.4,5H PHI=,E12.4)
      IF(F.LE.FSTAR) GO TO 310
      COUNT1 = COUNT1 + 1.0
      IF(COUNT1.GT.40.0) GO TO 636
      GO TO 210
  310 EPSBB = EPSBB - DELEPS*A
      EPSB = EPSBB - PHI*H
      IF((ABS(EPSB)).GT.EPSY) GO TO 351
      IF(EPSBB.LT.EPSY) GO TO 350
      IF(EPSBB.LE.(EPSY + PHI*T))GO TO 340
  330 F = (EB*AB/2.) * ( EPSBB+EPSB -((EPSBB-EPSY)**2.0)*BPR/(PHI*AB) +(
     1(BPR-W)*(EPSBB-EPSY-PHI*T)**2.0)/(PHI*AB))
  331 BMB = EB*BI*PHI - (EB*BPR/(12.0*PHI**2.0)) * ((EPSBB-EPSY)**2.0)*
     1(3.0*PHI*H - 2.0*EPSBB + 2.0*EPSY) +  (BPR-W)*EB/(12.0*PHI**2.0) *
```

```
   2 ((EPSBB - EPSY - PHI*T)**2.0)* (3.0*PHI*H - 4.0*PHI*T - 2.0*EPSBB
   3+ 2.0*EPSY)
    GO TO 360
340 F = (EB*AB/2.0) * ((EPSBB+EPSB) -(BPR/(AB*PHI))*(EPSBB-EPSY)**2.0)
341 BMB =  EB*BI*PHI -((EB*BPR/PHI)*(EPSBB-EPSY)**2.0)*(H/4.0 - (EPSBB
   1-EPSY)/(6.0*PHI))
    GO TO 360
350 F = EB*AB*(EPSBB + EPSB)/2.0
    BMB = EB*BI*PHI
    GO TO 360
351 IF(EPSBB.LT.(EPSY + PHI*T)) GO TO 358
352 IF((ABS(EPSB)).LE.(EPSY + PHI*T)) GO TO 358
353 F = (EB*AB/2.0) *(EPSBB + EPSB - (BPR/(PHI*AB))*((EPSBB-EPSY)**2.0
   1 - (EPSB-EPSY)**2.0) + ((BPR-W)/(PHI*AB)) * ((EPSBB-EPSY-PHI*T)**2
   2.0 - (EPSY-EPSB-PHI*T)**2.0))
355 BMB= EB*BI*PHI - (EB*BPR/(12.0*PHI**2.0)) * (((EPSBB-EPSY)**2.0)*
   1(3.0*PHI*H - 2.0*EPSBB + 2.0*EPSY) +((EPSB-EPSY)**2.0)*(3.0*PHI*H
   2- 2.0*EPSY + 2.0*EPSB)) + ((BPR-W)*EB/(12.0*PHI**2.0)) *(((EPSBB
   3 - EPSY - PHI*T)**2.0) * (3.0*PHI*H - 4.0*PHI*T - 2.0*EPSBB + 2.0
   4 * EPSY)  +  ((EPSY-EPSB-PHI*T)**2.0)*(3.0*PHI*H - 4.0*PHI*T
   5 -2.0*EPSY + 2.0*EPSB))
    GO TO 360
358 F = (EB*AB/2.0) *(EPSBB + EPSB - (BPR/(PHI*AB))*((EPSBB-EPSY)**2.0
   1 - (EPSB-EPSY)**2.0) + ((BPR-W)/(PHI*AB)) * ((EPSBB-EPSY-PHI*T)**2
   2.0 ))
359 BMB= EB*BI*PHI - (EB*BPR/(12.0*PHI**2.0)) * (((EPSBB-EPSY)**2.0)*
   1(3.0*PHI*H - 2.0*EPSBB + 2.0*EPSY) +((EPSB-EPSY)**2.0)*(3.0*PHI*H
   2- 2.0*EPSY + 2.0*EPSB)) + ((BPR-W)*EB/(12.0*PHI**2.0)) *(((EPSBB
   3 - EPSY - PHI*T)**2.0) * (3.0*PHI*H - 4.0*PHI*T - 2.0*EPSBB + 2.0
   4 * EPSY))
360 EPSSS = -F/(ES*AS) - PHI*D/2.0
    BMS = ES*SI*PHI
    EPSS = EPSSS + PHI*4.00
365 BM = BMB + BMS + F*Z
    WRITE(6,370)F,BM,EPSBB
370 FORMAT(8H FORCE =,E12.4,9H MOMENT =,E12.4,5H EBB=,E12.4)
    IF(BM.LE.(1.0001*AVGMOM(2))) GO TO 375
    GO TO 390
375 IF(BM.GE.(0.9999*AVGMOM(2))) GO TO 376
    GO TO 390
376 IF(F.GT.(0.9999*FSTAR)) GO TO 377
    GO TO 390
377 IF(F.LE.(1.0001*FSTAR)) GO TO 630
390 IF(BM.LE.AVGMOM(2)) GO TO 410
    COUNT2 = COUNT2 + 1.0
    IF(COUNT2.GT.40.0) GO TO 636
    GO TO 310
410 B = 0.80*B
411 PHI = PHI - DELPHI*B
    EPSB = EPSBB - PHI*H
    IF((ABS(EPSB)).GT.EPSY) GO TO 451
    IF(EPSBB.LT.EPSY) GO TO 450
    IF(EPSBB.LE.(EPSY + PHI*T))GO TO 440
430 F = (EB*AB/2.) * ( EPSBB+EPSB -((EPSBB-EPSY)**2.0)*BPR/(PHI*AB) +
   1(BPR-W)*(EPSBB-EPSY-PHI*T)**2.0)/(PHI*AB))
    GO TO 460
440 F = (EB*AB/2.0) * ((EPSBB+EPSB) -(BPR/(AB*PHI))*(EPSBB-EPSY)**2.0)
    GO TO 460
```

1176

```
450 F = EB*AB*(EPSBB + EPSB)/2.0
    GO TO 460
451 IF(EPSBB.LT.(EPSY + PHI*T)) GO TO 458
453 F = (EB*AB/2.0) *(EPSBB + EPSB - (BPR/(PHI*AB))*((EPSBB-EPSY **2.0
   1 - (EPSB-EPSY)**2.0) + ((BPR-W)/(PHI*AB)) * ((EPSBB-EPSY-PHI*T)**2
   2.0 - (EPSY-EPSB-PHI*T)**2.0))
    GO TO 460
458 F = (EB*AB/2.0) *(EPSBB + EPSB - (BPR/(PHI*AB))*((EPSBB-EPSY)**2.0
   1 - (EPSB-EPSY)**2.0) + ((BPR-W)/(PHI*AB)) * ((EPSBB-EPSY-PHI*T)**2
   2.0 ))
460 WRITE(6,461)F,PHI
461 FORMAT(3H F=,E12.4,6H PHII=,E12.4)
    IF(F.GE.FSTAR) GO TO 510
    COUNT3 = COUNT3 + 1.0
    IF(COUNT3.GT.40.0) GO TO 636
    GO TO 411
510 A = A
511 EPSBB = EPSBB + DELEPS*A
    EPSB = EPSBB - PHI*H
    IF((ABS(EPSB)).GT.EPSY) GO TO 551
    IF(EPSBB.LT.EPSY) GO TO 550
    IF(EPSBB.LE.(EPSY + PHI*T))GO TO 540
530 F = (EB*AB/2.) * ( EPSBB+EPSB -((EPSBB-EPSY)**2.0)*BPR/(PHI*AB) +
   1(BPR-W)*(EPSBB-EPSY-PHI*T)**2.0)/(PHI*AB))
531 BMB = EB*BI*PHI - (EB*BPR/(12.0*PHI**2.0)) * ((EPSBB-EPSY)**2.0)*
   1(3.0*PHI*H - 2.0*EPSBB + 2.0*EPSY) +  (BPR-W)*EB/(12.0*PHI**2.0) *
   2 ((EPSBB - EPSY - PHI*T)**2.0)* (3.0*PHI*H - 4.0*PHI*T - 2.0*EPSBB
   3+ 2.0*EPSY)
    GO TO 560
540 F = (EB*AB/2.0) * ((EPSBB+EPSB) -(BPR/(AB*PHI))*(EPSBB-EPSY)**2.0
541 BMB =  EB*BI*PHI -((EB*BPR/PHI)*(EPSBB-EPSY)**2.0)*(H/4.0 - (EPSBB
   1-EPSY)/(6.0*PHI))
    GO TO 560
550 F = EB*AB*(EPSBB + EPSB)/2.0
    BMB = EB*BI*PHI
    GO TO 560
551 IF(EPSBB.LT.(EPSY + PHI*T))GO TO 640
552 IF((ABS(EPSB)).LE.(EPSY + PHI*T)) GO TO 558
553 F = (EB*AB/2.0) *(EPSBB + EPSB - (BPR/(PHI*AB))*((EPSBB-EPSY)**2.0
   1 - (EPSB-EPSY)**2.0) + ((BPR-W)/(PHI*AB)) * ((EPSBB-EPSY-PHI*T)**2
   2.0 - (EPSY-EPSB-PHI*T)**2.0))
555 BMB= EB*BI*PHI - (EB*BPR/(12.0*PHI**2.0)) * (((EPSBB-EPSY)**2.0)*
   1(3.0*PHI*H - 2.0*EPSBB + 2.0*EPSY) +((EPSB-EPSY)**2.0)*(3.0*PHI*H
   2- 2.0*EPSY + 2.0*EPSB)) + ((BPR-W)*EB/(12.0*PHI**2.0)) *(((EPSBB
   3 - EPSY - PHI*T)**2.0) * (3.0*PHI*H - 4.0*PHI*T - 2.0*EPSBB + 2.0
   4 * EPSY)  +  ((EPSY-EPSB-PHI*T)**2.0)*(3.0*PHI*H - 4.0*PHI*T
   5 -2.0*EPSY + 2.0*EPSB))
    GO TO 560
558 F = (EB*AB/2.0) *(EPSBB + EPSB - (BPR/(PHI*AB))*((EPSBB-EPSY)**2.0
   1 - (EPSB-EPSY)**2.0) + ((BPR-W)/(PHI*AB)) * ((EPSBB-EPSY-PHI*T)**2
   2.0 ))
559 BMB= EB*BI*PH8 - (EB*BPR/(12.0*PHI**2.0)) * (((EPSBB-EPSY)**2.0)*
   1(3.0*PHI*H - 2.0*EPSBB + 2.0*EPSY) +((EPSB-EPSY)**2.0)*(3.0*PHI*H
   2- 2.0*EPSY + 2.0*EPSB)) + ((BPR-W)*EB/(12.0*PHI**2.0)) *(((EPSBB
   3 - EPSY - PHI*T)**2.0) * (3.0*PHI*H - 4.0*PHI*T - 2.0*EPSBB + 2.0
   4 * EPSY))
560 EPSSS = -F/(ES*AS) - PHI*D/2.0
    BMS = ES*SI*PHI
```

```
      EPSS = EPSSS + PHI*4.00
  565 BM = BMB + BMS + F*Z
      STRDIF = EPSB - EPSS
      WRITE(6,570 F,BM,EPSBB,EPSB,EPSS,STRDIF
  570 FORMAT(8H FORCE =,E12.4,9H MOMENT =,E12.4,6H EBBB=,E12.4,4H EB=,
     1E12.4,4H ES=,E12.4,7H EB-ES=,E12.4)
      IF(BM.GE.(0.9999*AVGMOM(2))) GO TO 610
      COUNT4 = COUNT4 + 1.0
      IF(COUNT4.GT.40.0) GO TO 636
      GO TO 511
  610 A = 0.80*A
      COUNT1 = 0.0
      COUNT2 = 0.0
      COUNT3 = 0.0
      COUNT4 = 0.0
      IF(F.LE.(1.0001*FSTAR)) GO TO 611
      GO TO 210
  611 IF(F.GE.(0.9999*FSTAR)) GO TO 620
      GO TO 210
  620 IF(BM.LE.(1.0001*AVGMOM(2))) GO TO 630
      GO TO 210
  630 WRITE(6,635)
  635 FORMAT(47H HERE ARE YOUR COTTON-PICKING CONVERGED ANSWERS)
      GO TO 690
  636 WRITE(6,637)
  637 FORMAT(13H RATS-A-FRATS)
      GO TO 690
  640 WRITE(6,641)
  641 FORMAT(11H SMARTEN UP)
  690 CONTINUE
      STOP
      END
$ENTRY
'        6400 END RECORD
'        6400 END FILE
```

```
C                              A P P E N D I X   G
C
C                              -------------------
C
C      PROGRAM TO CHECK COMPATIBILITY OF TRIAL SOLUTIONS ..
C
C
RUN(S)
LGO.
'          6400 END RECORD
      PROGRAM TST (INPUT,OUTPUT,TAPE5=INPUT,TAPE6=OUTPUT)
C
C     301 GROUPS OF STUDS ARE ALLOWED
C
C          MULTILINEAR MODULUS PERMITTED
C
C
C     M= NO OF STUDS (OR GROUPS OF STUDS )
C     N= NO OF INTERVALS BETWEEN STUDS
C     ES= E OF SLAB
C     EB= E OF BEAM
C     CS= DISTANCE INTERFACE TO CENTROID SLAB
C     CB= DISTANCE INTERFACE TO CENTROID BEAM
C     Z = SUM OF CS AND CB
C     AB = AREA BEAM
C     AS = AREA SLAB
C     BI = I OF BEAM ALONE
C     SI = I OF SLAB ALONE
C     ZL = SPAN OF BEAM
C     P  = TOTAL LOAD ON COMPOSITE BEAM DISTRIBUTED TO 2 POINTS
C     PZERO = INITIAL TOTAL LOAD
C     DELTAP= LOAD INCREMENT
C     PMAX = MAXIMUM TOTAL LOAD
C     CONST = Z OVER SIGMA EI
C     COUNT = COUNTER OF LOOPS REQ,D TO STABILIZE STUD FORCES
C     BURP = INDICATOR WHICH = 0 IF PO IS CHOSEN LOW ENOUGH,=1 IF NOT
C     OKAY  = 1.0 IF STUD FORCES ARE STABILIZED, =0.0 IF NOT
C     B(I,J) = STUSSI MULTIPLIER ARRAY
C     B1,B2,B3,B4(I,J) =SEPARATELY-GENERATED ARRAYS, WHICH WHEN ADDED,
C                          SUM TO B(I,J) WITH CORRECTED ELEMENTS
C     CK,CKP,CKPP I) =  STUD MODULUS ARRAYS
C     QP,QY,QU(I) = LIMITS OF APPLICABILITY OF CK,CKP,CKPP ARRAYS
C     SLIP,SLIPP,SLIPY(I) = SLIP AND SLIP LIMITS ARRAYS. (AND SLIPU I))
C     BENMOM(I) = IMPRESSED MOMENT ON BEAM,ONE FOR EVERY STUD(GROUP
C                  LOCATION  OR  SUPPORT LOCATION, FOR PO ONLY
C     BADMOM(I) = BENMOM(I) * P/PO
C     AVGMOM,SUMMOM,DUMMOM(I  = ARRAYS OF IMPRESSED MOMENTS
C     BMOM2,BMOM3(I) = ARRAYS OF CORRECTIONS TO RHS OF STUSSI MATRIX
C                       EQUATION
C     BENSLB,BENBEM(I) = ARRAYS OF MOMENTS IN SLAB,BEAM
C     FORCEF,FORCEQ(I) = ARRAYS OF FORCES IN SLAB AND ON STUDS
C     FORCPR(I  = FORCE IN SLAB ASSUMING COMPLETE INTERACTION
C     STRANS,STRANB I) = STRAIN IN SLAB AND BEAM ARRAYS.
C     SPACE(I) = ARRAY OF SPACES BETWEEN STUDS AND/OR SUPPORTS
C     TRACE(I  = TRACES STATE OF CORRECTIONS IN STUSSI MATRIX EQUATION
```

```
C      RANGE(I) = INDICATES RANGE OF STUD FORCE COMPUTED
C            STUD FORCES ARE STABILIZED WHEN TRACE(I  = RANGE(I)
C      EQUILM=MS+MB+F*Z
       COMMON/BLOK1/B(3,300),B1 3,300 ,B2(3,300),B3(3,300),B4 3,300
       COMMON/BLOK2/CK(301),CKP(301 ,CKPP(301)
       COMMON/BLOK3/QP(301),QY(301),QU 301)
       COMMON/BLOK4/SLIP(301),SLIPP(3 1),SLIPY 301 ,SLIPU(301)
       COMMON/BLOK5/BENMOM(301),AVGMOM(300),BADMOM(301
       COMMON/BLOK6/SUMMO (300),BMOM2(300),BMOM3(300
       COMMON/BLOK7/FORCEF(300),FORCEQ(301)
       COMMON/BLOK8/SPACE(300)
       COMMON/BLOK9/TRACE(301),RANGE(301)
       COMMON/BLOK10/EXTENT(300),STRDIF(300)
       DIMENSION BENSLB(300),BENBEM(300),FORCPR 300),STRANS(300)
       DIMENSION STRANB(300 ,EQUILM(300)
       DIMENSION FORCRA(300)
       DIMENSION TITLE(13)
       DIMENSION STRASS(300 ,STRABB(300)
       DD = 1.25
       READ(5,4 TITLE
     4 FORMAT(13A6)
       READ(5,5)M,N,ES,EB,CS,CB,AB,AS,BI,SI
     5 FORMAT(2I5,2E10.4,4F7.3,2F10.4
       READ(5,10)PZERO
    10 FORMAT(E10.3)
       P=PZERO
       DO 25 I=1,M
       READ(5,15)QP(I),SLIPP(I),QY(I),SLIPY(I),QU(I),SLIPU(I)
    15 FORMAT(6E12.4)
       CK(I) = QP(I)/SLIPP(I)
       CKP(I)=(QY(I)-QP(I))/(SLIPY(I)-SLIPP(I))
       CKPP(I)= (QU(I)-QY(I))/(SLIPU(I)-SLIPY(I))
    25 CONTINUE
       READ(5,30)(BENMOM(I),I=1,M)
       READ(5,35)(SPACE(I),I=1,N)
    30 FORMAT(8F10.0)
    35 FORMAT(8F10.2)
       WRITE(6,58)(TITLE(I),I = 1,13)
    58 FORMAT(1H1,13A6)
       WRITE(6,60)M,N
    60 FORMAT(16H COMPOSITE BEAM,,I5,7H STUDS,,I5,10H INTERVALS///)
       WRITE(6,65)
    65 FORMAT(50X,19H SECTION PROPERTIES)
       WRITE(6,66)
    66 FORMAT(40X,41H -----------------------------------------///)
       WRITE(6,67)
    67 FORMAT(111H      ES           EB          CS           CB           AS
      1AB      IS           IB          PO      DELTA P    P MAX         /)
       WRITE(6,68)ES,EB,CS,CB,AS,AB,SI,BI,PZERO,DELTAP,PMAX
    68 FORMAT(E10.3,1X,E10.3,F8.3,3F10.3,2F10.4,3E10.3//)
       WRITE(6,69)
    69 FORMAT(48X,22H CONNECTION PROPERTIES)
       WRITE(6,66)
       WRITE 6,70)
    70 FORMAT (82H   STUD NO        K               K'             K''       PRECEDE
      1S SPACE (IN)    ZERO MOMENT /)
       IF(PZERO.EQ.5000.0)GO TO 73
```

```
      DO 72 I = 1,M
      BENMOM(I  = (PZERO/5000.0)*BENMOM(I)
   72 CONTINUE
   73 DO 75 I = 1,N
      WRITE(6,74)I,CK(I ,CKP(I ,CKPP(I),SPACE(I),BENMOM(I)
   74 FORMAT(4X,I3,3X,3E12.4,6X,F10.2,10X,F10.0)
   75 CONTINUE
      WRITE(6,77)M,CK(M ,CKP(M),CKPP(M),BENMOM M)
   77 FORMAT(4X,I3,3X,3E12.4,26X,F10.0///)
      WRITE(6,80)
   80 FORMAT(84H   STUD NO         QP           GAMMA P         QY           GAMMA
     1 Y          QU          GAMMA U  )
      DO 85 I = 1,M
      WRITE(6,83)I,QP(I),SLIPP(I),QY(I),SLIPY(I),QU(I),SLIPU(I)
   83 FORMAT(4X,I3,4X,6E12.4)
   85 CONTINUE
      WRITE 6,992)
      WRITE(6,66)
      WRITE(6,992)
      Z = CS + CB
      SUMEI = EB*BI + ES*SI
      EABAR = (EB*AB*ES*AS)/(ES*AS + EB*AB)
      EIBAR = SUMEI + EABAR*Z**2.0
      AA = EIBAR/(EABAR*SUMEI)
      CONST = Z/SUMEI
      WRITE(6,86)Z,SUMEI,EABAR,EIBAR,AA,CONST
   86 FORMAT(3H Z=,E10.4,5X,7H SUMEI=,E10.4,5X,7H EABAR=,E10.4,7H EIBAR=
     1,E10.4,5X,4H AA=,E10.4,5X,7H CONST=,E10.4)
      BURP = 0.0
      OKAY = 1.0
      DO 90 I = 1,3
      DO 90 J = 1,N
      B(I,J) = 0.0
   90 CONTINUE
      DO 95 I = 1,M
      RANGE(I) = 0.0
   95 CONTINUE
      COUNT = 0.0
  499 DO 50 I = 1,3
      DO 50 J = 1,N
      B1(I,J) = 0.0
      B2(I,J) = 0.0
      B3(I,J) = 0.0
      B4(I,J) = 0.0
   50 CONTINUE
      READ(5,97)(EXTENT(I),I = 1,N)
   97 FORMAT(40I2)
      READ 5,96)(STRDIF(I),I = 1,N)
   96 FORMAT(6E12.5)
  502 DO 55 J = 1,N
      BMOM2(J) = 0.0
      BMOM3(J  = 0.0
   55 CONTINUE
  500 CALL ARAMOM(M,N,PZERO,P,CONST)
  501 CALL ALTER(M,N,AA)
      CALL INELAS(N,AA,CONST)
      WRITE(6,505)
```

```
505 FORMAT(30X,7H SUMMOM,13X,6H BMOM2,14X,6H BMOM3)
    DO 510 I = 1,N
    WRITE 6,508 SUMMOM(I ,BMOM2(I),BMOM3(I)
508 FORMAT(29X,E11.4,9X,E11.4, 8X,E11.4)
510 CONTINUE
    DO 515 I = 1,N
514 SUMMOM(I) = SUMMOM(I  + BMOM2(I) + BMOM3(I)
515 CONTINUE
    DO 650 I = 1,3
    DO 650 J = 1,N
    B(I,J  = B1(I,J) + B2(I,J) + B3(I,J) + B4(I,J)
650 CONTINUE
    DO 517 J = 1,N
    WRITE(6,516)J,B(1,J),B(2,J),B(3,J),SUMMOM(J),J,EXTENT(J),STRDIF(J)
516 FORMAT(20X,I5,3E12.4,10X,E12.4,2I5,2X,E12.4)
517 CONTINUE
    CALL DIAG3(B,SUMMOM,N)
    DO 520 J = 1,N
    FORCEF(J) = SUMMOM(J)
520 CONTINUE
    CALL CALSTD(M)
    CALL RANGER(M)
599 COUNT = COUNT + 1.0
    IF(COUNT.GT.5.0) GO TO 9997
600 CALL COMPAT( ,OKAY)
    IF(OKAY.GT.0.0) GO TO 900
    GO TO 502
900 DO 950 I = 1,N
    IF((EXTENT(I)).GT.0.0) GO TO 950
    BENSLB(I) = ((ES*SI)*(AVGMOM(I) - FORCEF I)*Z) /SUMEI
    BENBEM(I) = ((EB*BI)*(AVGMOM(I  - FORCEF(I)*Z))/SUMEI
    STRANS(I) =-FORCEF(I)/(ES*AS) - BENSLB(I *DD/(ES*SI
    STRASS(I) =-FORCEF(I)/(ES*AS) + BENSLB(I)*DD/(ES*SI)
    STRANB(I) = FORCEF(I /(EB*AB) + BENBEM(I)*CB/(EB*BI)
    STRABB(I) = FORCEF(I)/ EB*AB) - BENBEM I)*CB/(EB*BI)
    FORCPR(I) = (EABAR/EIBAR)*Z*AVGMOM(I)
    FORCRA(I) = FORCEF(I)/FORCPR(I)
    EQUILM(I) = BENSLB(I) + BENBEM I) + FORCEF(I)*Z
950 CONTINUE
    PP = 2.0*P
    WRITE(6,975)PP,COUNT
975 FORMAT(1H1,39X,9HTOTAL LD=,E10.3,4H LBS,5X,8H COUNT =,F6.0)
    WRITE(6,66)
    WRITE(6,985)
985 FORMAT(115H INTERVAL     F        F/F'     BEAM MOM      SLAB MOM    TO
   1P STR SLB  BOT STR SLB  TOP STR BM   BOT STR BM    AVGMOM     MS+MB
   1+F*Z//)
    DO 990 I = 1,N
    WRITE(6,987)I,FORCEF(I),FORCRA I),BENBEM(I),BENSLB(I ,STRANS(I),ST
   1RASS(I),STRABB(I),STRANB(I),AVGMOM(I),EQUILM(I)
987 FORMAT(2X,I3,3X,E12.4,F5.2,1X,2E12.4,1X,E12.4,1X,E12.4,1X,E12.4,1X
   1,2E12.4,1X,E12.4/)
990 CONTINUE
    WRITE(6,992)
992 FORMAT(2X,////)
    DO 1100 I = 1,M
    IF(ABS(FORCEQ(I)).GT.QP(I)  GO TO 1020
```

```
      SLIP(I) = FORCEQ(I)/CK(I)
      GO TO 1100
 1020 IF(ABS(FORCEQ(I)).GT.QY(I)) GO TO 1040
      SLIP(I) = SLIPP(I  + (FORCEQ(I  - QP(I))/CKP(I)
      GO TO 1100
 1040 SLIP I) = SLIPY(I  + (FORCEQ(I) -QY(I))/CKPP(I)
 1100 CONTINUE
      WRITE(6,995)
  995 FORMAT(48X,29H STUD    FORCE        SLIP     //)
      DO 997 I = 1,M
      WRITE(6,996)I,FORCEQ(I ,SLIP(I)
  996 FORMAT(47X,I3,2E12.4/)
  997 CONTINUE
 9997 WRITE(6,9998)
 9998 FORMAT(40H SAY MAN, YOU EVER HEARD OF AN ABACCUS 2)
 9999 STOP
      END
$IBFTC ALTER
      SUBROUTINE ALTER(M,N,AA)
      COMMON/BLOK1/B(3,300),B1(3,300),B2(3,300),B3(3,300),B4(3,300)
      COMMON/BLOK2/CK(301),CKP(301 ,CKPP(301
      COMMON/BLOK3/QP(301),QY(301),QU 301)
      COMMON/BLOK4/SLIP(301),SLIPP(301),SLIPY(301),SLIPU(301)
      COMMON/BLOK5/BENMOM(301),AVGMOM(300),BADMOM(301)
      COMMON/BLOK6/SUMMOM(300),BMOM2(300 ,BMOM3(300)
       COMMON/BLOK7/FORCEF(300),FORCEQ(301)
      COMMON/BLOK8/SPACE(300)
      COMMON/BLOK9/TRACE(301),RANGE(301)
      DO 500 J = 1,N
      IF(RANGE(J).GT.0.0) GO TO 100
      IF(J.GT.1) GO TO 20
      B1(2,J) = 1.0/CK(J
      TRACE(J) = 0.0
      GO TO 500
   20 B1(2,J) = 1.0/CK(J)
      B2(2,J-1) = 1.0/CK(J)
      B4(1,J) = -1.0/CK(J)
      B4(3,J-1) = B4(1,J)
      TRACE(J) = 0.0
      GO TO 500
  100 IF(RANGE(J).GT.1.0) GO TO 200
      IF(J.GT.1) GO TO 120
      B1(2,J) = 1.0/CKP(J)
      TRACE(J) = 1.0
      IF(FORCEQ(J .GE.0.0) GO TO 110
      DC = -1.0
      GO TO 111
  110 DC = +1.0
  111 BMOM2(J) = DC*(QP(J)/CKP(J) - SLIPP(J))
      GO TO 500
  120 B1(2,J) = 1.0/CKP(J)
      B2(2,J-1) = 1.0/CKP(J)
      B4(1,J) = -1.0/CKP(J)
      B4(3,J-1) = B4(1,J)
      TRACE(J) = 1.0
      IF(FORCEQ(J).GE.0.0  GO TO 130
      DC = -1.0
```

```
      GO TO 131
  130 DC = +1.0
  131 BMOM2(J-1) = -DC*(QP J)/CKP(J) - SLIPP(J)) + B OM2(J-1
  132 BMOM2(J) = DC*(QP(J)/CKP J) - SLIPP(J )
      GO TO 500
  200 IF(RANGE(J).GT.2.0) GO TO 500
      IF(J.GT.1) GO TO 220
      B1(2,J) = 1.0/CKPP(J)
      TRACE(J) = 2.0
      IF(FORCEQ(J).GE.0.0) GO TO 210
      DC = -1.0
      GO TO 211
  210 DC = +1.0
  211 BMOM3(J) = DC*(QY(J)/CKPP(J) - SLIPY(J))
      GO TO 500
  220 B1(2,J) = 1.0/CKPP(J)
      B2(2,J-1) = 1.0/CKPP(J)
      B4(1,J) = -1.0/CKPP(J)
      B4(3,J-1) = B4(1,J)
      TRACE(J) = 2.0
      IF(FORCEQ(J).GE.0.0) GO TO 230
      DC = -1.0
      GO TO 231
  230 DC = +1.0
  231 BMOM3(J-1) = -DC*(QY J)/CKPP(J) - SLIPY(J)) + BMOM3(J-1
  232 BMOM3 J) = DC*(QY(J)/CKPP(J) - SLIPY(J))
  500 CONTINUE
      IF(RANGE(M).GT.0.0) GO TO 550
      B2(2,N) = 1.0/CK(M)
      TRACE(M) = 0.0
      GO TO 610
  550 IF(RANGE(M).GT.1.0) GO TO 575
      B2(2,N) = 1.0/CKP(M)
      TRACE(M) = 1.0
      IF(FORCEQ(M).GE.0.0) GO TO 560
      DC = -1.0
      GO TO 561
  560 DC = +1.0
  561 BMOM2(N) = -DC*(QP(M)/CKP(M) - SLIPP(M)  + BMOM2(N
      GO TO 610
  575 IF(RANGE(M).GT.2.0) GO TO 610
      B2(2,N  = 1.0/CKPP(M)
      TRACE(M) = 2.0
      IF(FORCEQ(M).GE.0.0) GO TO 580
      DC = -1.0
      GO TO 581
  580 DC = +1.0
  581 BMOM3(N) = -DC*(QY(M)/CKPP(M) - SLIPY(M))+ BMOM3(N)
  610 DO 620 I = 1,N
      B3(2,I)= AA*SPACE(I)
  620 CONTINUE
      RETURN
      END
$IBFTC ARAMOM
      SUBROUTINE ARAMOM(M,N,PZERO,P,CONST)
      COMMON/BLOK5/BENMOM(301),AVGMOM(300 ,BADMOM(301)
      COMMON/BLOK6/SUMMOM(300),BMOM2(300 ,BMOM3(300
```

```
      COMMON/BLOK8/SPACE(300
      IF(P.GT.PZERO) GO TO 100
      DO 50 I = 1,N
      AVGMOM I) = (BENMOM(I) + BENMOM(I+1 )/2.0
      SUMMOM(I) = CONST* AVGMOM(I) * SPACE(I)
   50 CONTINUE
      GO TO 150
  100 DO 120 I = 1,M
      BADMOM(I) = (P/PZERO)*BENMOM(I)
  120 CONTINUE
      DO 130 I = 1,N
      AVGMOM(I) = (BADMOM(I) + BADMOM(I+1))/2.0
      SUMMOM(I  = CONST*AVGMOM(I)*SPACE(I
  130 CONTINUE
  150 RETURN
      END
$IBFTC CALSTD
      SUBROUTINE CALSTD(M
      COMMON/BLOK7/FORCEF(300),FORCEQ(301)
      DO 50 I = 1,M
      IF(I-1.GT.0) GO TO 40
   20 FORCEQ(I) = FORCEF(I)
      GO TO 50
   40 IF(I.EQ.M) GO TO 45
      FORCEQ(I) = FORCEF(I) - FORCEF I-1)
      GO TO 50
   45 FORCEQ(I) = -FORCEF(I-1)
   50 CONTINUE
      RETURN
      END
$IBFTC RANGER
      SUBROUTINE RANGER(M
      COMMON/BLOK3/QP(301 ,QY(301),QU(301)
      COMMON/BLOK7/FORCEF(300 ,FORCEQ(301)
      COMMON/BLOK9/TRACE(301),RANGE(301
      DO 200 I = 1,M
      IF(ABS(FORCEQ(I) .GT.QP(I)) GO TO 25
      RANGE(I) = 0.0
      GO TO 200
   25 IF(ABS(FORCEQ(I) .GT.QY(I ) GO TO 35
      RANGE(I) = 1.0
      GO TO 200
   35 IF(ABS(FORCEQ(I)).GE.QU(I)) GO TO 45
      RANGE(I) = 2.0
      GO TO 200
   45 RANGE(I) = 3.0
      WRITE(6,50) I
   50 FORMAT(8H STUD NO,I3,27H HAS REACHED ULTIMATE SHEAR//
  200 CONTINUE
      RETURN
      END
$IBFTC COMPAT
      SUBROUTINE COMPAT M,OKAY)
      COMMON/BLOK9/TRACE(301),RANGE(301)
      OKAY = 1.0
      DO 100 I = 1,M
      IF(RANGE(I).EQ.TRACE(I)) GO TO 100
```

```
      OKAY = 0.0
  100 CONTINUE
      WRITE 6,125)
  125 FORMAT(21H RANGE OF STUD FORCES/)
      WRITE(6,150 (RANGE I),I=1,M)
      WRITE(6,135)
  135 FORMAT(28H STATE OF CORRECTIONS SO FAR/)
      WRITE(6,150 (TRACE(I ,I=1,M)
  150 FORMAT(30F4.0)
      WRITE(6,160)
  160 FORMAT(2X,///)
      RETURN
      END
$IBFTC INELAS
      SUBROUTINE INELAS(N,AA,CONST)
      COMMON/BLOK1/B(3,300),B1(3,300 ,B2(3,300),B3(3,300),B4 3,300)
      COMMON/BLOK5/BENMOM(301),AVGMOM(300 ,BADMOM(301)
      COMMON/BLOK6/SUMMOM(300),BMOM2(300),BMOM3(300)
      COMMON/BLOK8/SPACE(300)
      COMMON/BLOK10/EXTENT(300),STRDIF(300)
      DO 200 I = 1,N
      IF((EXTENT(I)).EQ.0.0) GO TO 200
      B3(2,I) = B3(2,I) - AA*SPACE I
      SUMMOM(I) = - SPACE(I)*STRDIF(I
  200 CONTINUE
      RETURN
      END
$ENTRY
'       6400 END RECORD
1968 MCMASTER TESTS -- BEAM NO 1( SIX SINGLE STUDS IN SHEAR SPAN )
  16   15 .3190E+07 .2900E+08  2.750   6.080   5.620170.000  130.1000   88.
 .180E+05
   .6000E+04   .2000E-02   .1100E+05   .2000E-01   .3500E+05   .1500E+01
   .6000E+04   .2000E-02   .1100E+05   .2000E-01   .3500E+05   .1500E+01
   .6000E+04   .2000E-02   .1100E+05   .2000E-01   .3500E+05   .1500E+01
   .6000E+04   .2000E-02   .1100E+05   .2000E-01   .3500E+05   .1500E+01
   .6000E+04   .2000E-02   .1100E+05   .2000E-01   .3500E+05   .1500E+01
   .6000E+04   .2000E-02   .1100E+05   .2000E-01   .3500E+05   .1500E+01
   .6000E+04   .2000E-02   .1100E+05   .2000E-01   .3500E+05   .1500E+01
   .6000E+04   .2000E-02   .1100E+05   .2000E-01   .3500E+05   .1500E+01
   .6000E+04   .2000E-02   .1100E+05   .2000E-01   .3500E+05   .1500E+01
   .6000E+04   .2000E-02   .1100E+05   .2000E-01   .3500E+05   .1500E+01
   .6000E+04   .2000E-02   .1100E+05   .2000E-01   .3500E+05   .1500E+01
   .6000E+04   .2000E-02   .1100E+05   .2000E-01   .3500E+05   .1500E+01
   .6000E+04   .2000E-02   .1100E+05   .2000E-01   .3500E+05   .1500E+01
   .6000E+04   .2000E-02   .1100E+05   .2000E-01   .3500E+05   .1500E+01
   .6000E+04   .2000E-02   .1100E+05   .2000E-01   .3500E+05   .1500E+01
   .6000E+04   .2000E-02   .1100E+05   .2000E-01   .3500E+05   .1500E+01
        0.      60000.     120000.     180000.     240000.     300000.     330000.
   330000.     330000.     300000.     240000.     180000.     120000.      60000.
     12.00       12.00       12.00       12.00       12.00       24.00       24.00
     24.00       24.00       12.00       12.00       12.00       12.00       12.00
 0 0 0 0 0 1 1 0 1 1 0 0 0 0 0
-0.00000E+00-0.00000E+00-0.00000E+00-0.00000E+00+0.00000E+00-0.59639E-03
-0.36334E-03+0.00000E+00-0.36334E-03-0.59639E-03+0.00000E+00+0.00000E+00
-0.00000E+00-0.00000E+00-0.00000E-00
'       6400 END FILE
```